UNIVERSIDAD AUTÓNOMA DE MADRID

Programa de Doctorado en Biociencias Moleculares

Defining novel physiological roles for cardiac-resident macrophages

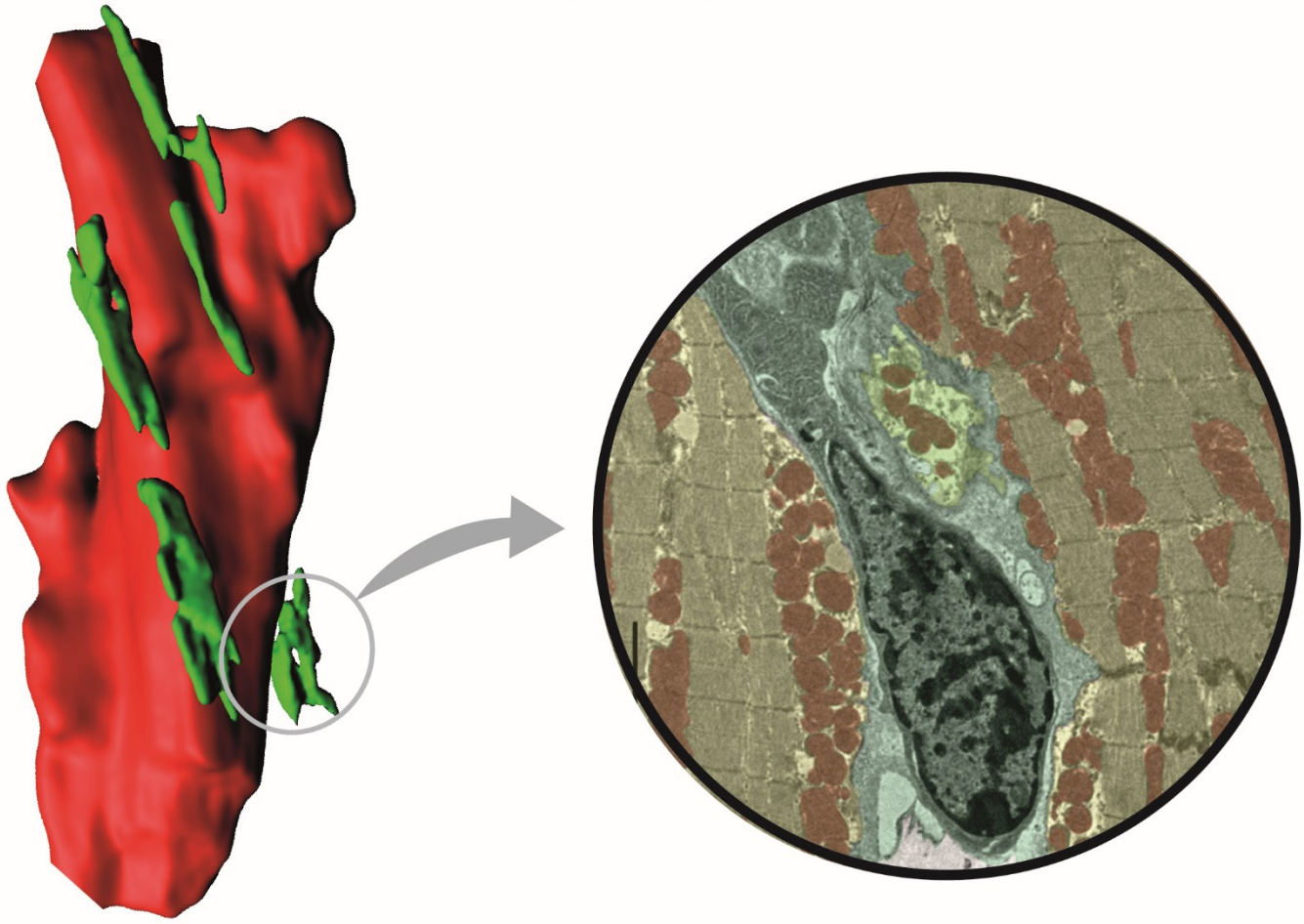

José Ángel Nicolás Ávila

DIRECTED BY ANDRÉS HIDALGO ALONSO (PHD)

Madrid, 2019

GOBIERNO DE ESPAÑA
MINISTERIO DE CIENCIA, INNOVACIÓN Y UNIVERSIDADES
Instituto de Salud Carlos III
cnic

Tesis Doctoral:

Doctorado en Biociencias Moleculares

Departamento de Bioquímica

Facultad de Medicina

Universidad Autónoma de Madrid (UAM)

"Defining novel physiological roles for cardiac-resident Macrophages"

José Ángel Nicolás Ávila

Licenciado en Biología por la Universidad de Santiago de Compostela

Dirigida por:

Dr. Andrés Hidalgo Alonso

Realizada en el Centro Nacional de Investigaciones Cardiovasculares (CNIC)

Financiada por el Ministerio de Ciencia Innovación y Universidades (MICINN)

Madrid, Septiembre 2019

Dr. Andrés Hidalgo Alonso CERTIFICA:

Que la presente memoria de tesis titulada “Defining novel physiological roles for cardiac-resident Macrophages”, que presenta D. José Ángel Nicolás Ávila para obtener el grado de Doctor, ha sido realizada bajo mi dirección, autorizándola para su presentación al Tribunal Calificador.

Madrid, 15 Agosto de 2019

Fdo. Dr. Andrés Hidalgo Alonso

Director de la presente Tesis Doctoral

Éste trabajo se ha realizado en el laboratorio del Dr. Andrés Hidalgo Alonso, “Imagen de la Inflamación Cardiovascular y la Respuesta Inmune”, englobado en el Área de Biología Celular y del Desarrollo del Centro Nacional de Investigaciones Cardiovasculares (CNIC), en Madrid.

El estudio ha sido financiado por los proyectos (120/C/2015-20153032) y SAF2015-65607-R otorgados al Dr. Andrés Hidalgo por la Fundació La Marató de TV3 y el Ministerio de Economía, Industria y Competitividad (MEIC), respectivamente. Por su parte, D. José Ángel Nicolás Ávila ha sido beneficiario de una beca FPI Severo Ochoa (SVP-2014-068595; MEIC). El CNIC recibe financiación del MEIC y la Fundación Pro-CNIC, y es un Centro de excelencia Severo Ochoa (SEV-2015-0505; MEIC).

A mis padres…

Agradecimientos

¡Ya estoy aquí!, en el final del corredor… a puntito de defender mi tesis doctoral. Aún recuerdo lo lejano que me parecía éste momento cuando empecé en el laboratorio, como un horizonte hacia el que caminar sin la convicción real de alcanzarlo eventualmente. Ahora que me acerco a la meta, parece que éstos años han pasado en un suspiro. Aunque no ha sido un camino fácil (creo que ninguna tesis lo es), me considero afortunado ya que mucha gente ha contribuido a hacerlo más placentero. Sería imposible hacerles justicia a todos ellos en un puñado de páginas, así que me disculpo por adelantado. Quién me conoce sabe que me caracterizo más por el humor que por un gran sentimentalismo, pero como no creo que tenga otra oportunidad de hacer algo similar (al menos hasta la escritura de mis memorias ☺), intentaré ablandar un poco mi corazoncito.

En primer lugar, me enorgullece dedicar éste trabajo a mis padres. "Madre/ Mamá" y "Padre/Papá", son muchas las cosas que tengo que agradeceros y muy pocas las veces que lo he hecho (al menos de forma explícita). Por todas las veces que habéis celebrado mis logros como si fueran vuestros y habéis creído en mí cuando yo no he sido capaz… **GRACIAS**. Soy lo que soy gracias a vosotros, tanto a nivel genético como a nivel personal, y no podría haber pedido mejor suerte. ¿Que podría haber tenido ojos verdes y menos tendencia al engorde?, sí; pero hay que dejar algo para los demás. Bromas aparte, me haría falta un "tocho" el doble de gordo que éste para recoger todo lo que os debo y aun así me quedaría corto.

De ti mamá, he aprendido lo que es el valor del esfuerzo y la capacidad de sacrificio. Me he pasado años viendo como llegabas a casa "derrengada" después de todo el día trabajando, y sacabas fuerzas de aún no sé dónde para poner orden en casa y hacer esas comidas tan ricas que tanto echo en falta. No sólo eso, sino que además te sobraba tiempo para devorar libros, aprender idiomas o diseñar la próxima reforma. De ti también he aprendido lo que es el amor, en forma de besos y abrazos, y la rectitud, materializada en forma de "pinoques" cuando la situación lo requería. De ti papá, he aprendido lo que es la empatía y el respeto hacia los demás, ambas cualidades difíciles de encontrar hoy en día. Siempre poniendo cordura donde se había perdido y anteponiendo el bien común, aunque a veces te perjudique a ti mismo. Pero sobre todo, de ti he aprendido a vivir la vida con humor, relativizar los problemas y ser positivo. Aun cuando los problemas (físicos o mentales) intentan amargarte el día, tú me has enseñado a esperar los "Days like this" prometidos por Van. Porque para quién no lo sepa, mi pasión por la música también te la debo a ti.

Tampoco me olvido de ti “Bego/Goñita/Hermanita”. ¡La única y mejor hermana que tengo! A ti te doy las gracias por aguantarme durante toda una vida y te pido perdón por tres cuartos de lo mismo. Espero que recuerdes tanto como yo esos momentos en casa riéndonos por la última ocurrencia de papá o intercambiando miradas cómplices cuando mamá buscaba al culpable de algún infortunio. Estoy muy orgulloso de tener una hermana física (de profesión me refiero, no vayáis a pensar que tengo parientes imaginarios) y se lo cuento a todo el mundo siempre que se tercia, como quien ha visto al monstruo del Lago Ness. Estoy seguro de que pronto tendremos otra tesis que celebrar, ¡La tuya!

Y mención especial para Mª Jesús, porque me has criado como si fuera un hijo y eres mi mayor fuente de alabanzas. Gracias por tu amabilidad y humildad. Aunque no tengamos lazos genéticos, sabes que tanto Bego como yo te consideramos nuestra segunda madre.

En lo académico, hay que resaltar que ésta tesis no podría haber visto la luz si no fuese por Andrés (el Doctor Hidalgo), a quien le agradezco el haberme acogido en su laboratorio. Él es el director de ésta tesis y mentor en mi otra vida, la laboral. Ha sido un placer y un orgullo poder formar parte de su equipo. Creo que poca gente reúne tantas cualidades necesarias en un buen científico: juicio crítico, curiosidad, implicación en los proyectos y agudeza mental. Gracias por tener la puerta abierta para recibirme cada vez que tengo una duda, un resultado que celebrar o uno que lamentar. Al igual que los que me han precedido, solo espero estar a la altura y dejar el escudo de este laboratorio bien alto en las etapas que estén por venir.

Dicho esto, la familia Hidalgo la compone mucha más gente, sin la cual sería imposible haber presentado este trabajo. Tras aterrizar aquí en el 2013, actualmente soy el miembro más antiguo del laboratorio (Galardón compartido con Geo), lo significa que visto a mucha gente incorporarse y marcharse del grupo. En algún momento hemos sido 4 gatos, pero a día de hoy necesitamos un tablón de 15 metros para poder sentarnos juntos a comer… Gracias a todos los que estaban cuando llegué (Noelia, Paola, María, Linnea, Magda, Chris, Vinatha) por haberme recibido con los brazos abiertos; especialmente a Noelia, por haber enseñado a éste primate a desenvolverse en un laboratorio y a Paola, por compartir conmigo una amistad de las que rompen los muros del CNIC (Ricardo, ¡cuídamela bien!). Gracias también a todos aquellos que han compartido conmigo períodos más o menos largo, especialmente a Elena, Juan, Diego y Arturo que marcaron un antes y un después en esta institución.

The Lab.

2014-2019

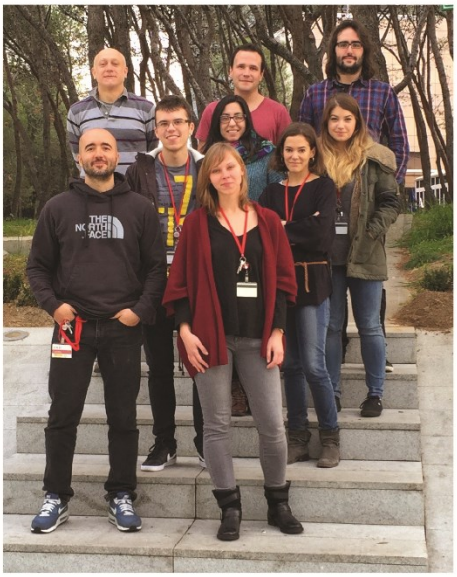

Y, por último, gracias al grueso del laboratorio actual: José María, que me ha marcado el camino a seguir (y ha puesto el listón muy alto, por cierto); Geo y Sandra, que aportan la alegría al laboratorio (algún día os echarán por el escándalo ☺) y nos hacen la vida más fácil gracias a su apoyo en el bench (sois el pulmón del laboratorio, y más ahora que no está Juan); A Iván, Jackson y Kanako, que son la voz de la experiencia y con los que uno siempre puede contar cuando no tiene ni idea de cómo diseñar un experimento; Itziar, Andrea, Ale y María, gente tremendamente válida que se queda a defender el fortín y espero que me sigan en éste paso más pronto que tarde (mucho ánimo). A María y a Elena quiero hacerles una mención

especial, ya que ellas trabajaron directamente conmigo y me han sufrido más. Gracias a las dos por vuestra ayuda y paciencia. Me alegra ver que, después de todo, ambas conserváis el espíritu científico e incluso habéis tenido la osadía de embarcaros en una tesis doctoral. ¡Espero que os vaya muy bien y toda la chapa que os he dado os sirva para algo!

Asimismo, agradezco enormemente a todo el personal del CNIC el apoyo recibido. A Inés Ortega, Laura Cabezuela, Eva Santos y todo el pool de animalario por cuidar tan cariñosamente de nuestro bien más preciado, los ratoncillos. Gracias a ellos también porque han dado (involuntariamente) su vida por un fin egoísta (Nos veremos en el infierno). A las magníficas unidades del CNIC, porque los caminos de la ciencia son inescrutables y me han llevado a trabajar con casi todas ellas. A Elena, Mariano, Jose y Raquel que me han acompañado en largas horas de sorting y han estado ahí para domar los citómetros cada vez que intentaban revelarse. A Vero y Elvira por enseñarme los entresijos de los microscopios y acudir en mi auxilio cada vez que estos entraban en barrena. A Lorena, Ana y Eva por amenizarme con su alegría y conversación el enésimo experimento de ecocardiografía a las 8 de la mañana. A las Unidades de Proteómica, Genómica, Bioinformática y Vectores Virales que me han ayudado con su magia exotérica a separar el grano de la paja. A Cristina Giménez, porque sin sus alertas de todos los plazos relativos a la burocracia del Ministerio y la Universidad, estaría en la calle hace ya tiempo.

No puedo olvidar la inestimable ayuda de los diversos grupos con los que hemos colaborado para hacer realidad este trabajo. Especialmente a Ana victoria Lechuga (quién ha realizado importantes experimentos, necesarios para que ésta tesis tenga sentido) y a Jose Antonio Enríquez. Ambos han contribuido a la calidad de éste trabajo con su visión mitocondrio-céntrica y aguzado ingenio. Gracias también a: Akhila Balachander y Lai Guan Ng (Singapore Immunology Network, A*Star); Lorena Esteban y Miguel Torres (CNIC); Mario Cordero (INEBIR); Andrés Pun y Borja Ibañez (CNIC); Elías Herrero y Jorge Alegre (CNIC); Pura Muñoz (CNIC); Hector Bueno (CNIC); Guillermo Reyes (Hospital La Princesa); Demetrio J. Santiago y Silvia Priori (CNIC); que nos ha permitido darle un salto de calidad sustancial a nuestro trabajo. Y, por supuesto, a todos los colaboradores que han contribuido con animales o reactivos esenciales para este trabajo: Paqui y Greg Lemke (Salk Institute); Antonio Castrillo (IIB) y Carla Rothlin (Yale university).

Gracias a Susana Alemany de la Peña, mi tutora académica de la Universidad Autónoma de Madrid, por atender mis demandas burocráticas con tan buena disposición y por sus continuas alabanzas. No se merecen.

Agradezco también al MINECO, al recientemente formado MICINN y al CNIC el apoyo económico que me ha permitido realizar mi labor investigadora durante todos estos años. Espero que algún día el Gobierno comprenda la importancia del trabajo desempeñado por nuestro colectivo e invierta más fondos para asegurar muchos más estudiantes puedan formarse como lo he hecho yo. Y puestos a pedir, sería GENIAL que éstas becas aseguraran unas condiciones laborales acordes al nivel curricular que la adjudicación de estos contratos-becas exige.

En lo personal hay mucha gente que ha influido de un modo u otro en esta historia, porque para tener la cabeza despejada en el trabajo hay que disfrutar del tiempo fuera de él. Por ello, doy gracias a mis amigos de Carballo, que siempre me reciben con los brazos abiertos pese a los largos períodos que pasamos sin vernos. Han sido muchísimos los momentos que hemos compartido y, aunque el grupo esté desperdigado últimamente, siempre nos las apañamos para aumentar la retahíla de historias cada vez que nos juntamos. No sabéis la rabia que da estar a 600 km cuando os veo escribir en el grupo de whatsapp que quedáis a tomar una en el Ágora… o dos, o las que hagan falta. ¡Espero que la próxima sea a mi salud!

A mis compañeros de Vegan Wolves, que me han animado a retomar uno de mis mayores hobbies, la música. He vivido cada concierto juntos con la ilusión de un adolescente y lo mejor es que esto no para de crecer. Como aún no nos han puesto los millones encima de la mesa, me temo que en algún momento tendré que abandonar Madrid para seguir con mi carrera científica. En caso de que llegue ese momento, espero que podáis seguir dando forma a éste proyecto en mi ausencia. Yo os seguiré desde la distancia y fardaré de haber sido miembro fundador. ¡Viva Vegan Wolves!

A mis antiguos compañeros de piso en la residencia Aralar (aka Pisomoncho) y asociados (team xONGA). Porque la vida te sorprende y, al igual que puedes encontrarte una croqueta al fondo de unas natillas, yo he encontrado a un puñado de buena gente en una residencia nefasta. Al maravilloso grupo de la Cicerone 2013, gente fascinante que ha compartido buena parte de este trayecto conmigo. También al núcleo duro de natación de la Vicente del Bosque por esos 8 larguitos entre caña y caña.

Y finalmente, muchísimas gracias a Laura (y a Gandalf por extensión). Gracias por haber decidido compartir tu vida con este cabezón: alegrías, penas y todas esas cosas que no se pueden poner aquí… Porque ya hace mucho tiempo que mi casa está allí donde tú te encuentras. Sin ti aquí, estos años en Madrid hubiesen sido muy duros. Espero contar con tu ayuda en mi (nuestra) próxima etapa, ¡Y en todas aquellas que estén por venir!

Index

1. Resumen / Abstract

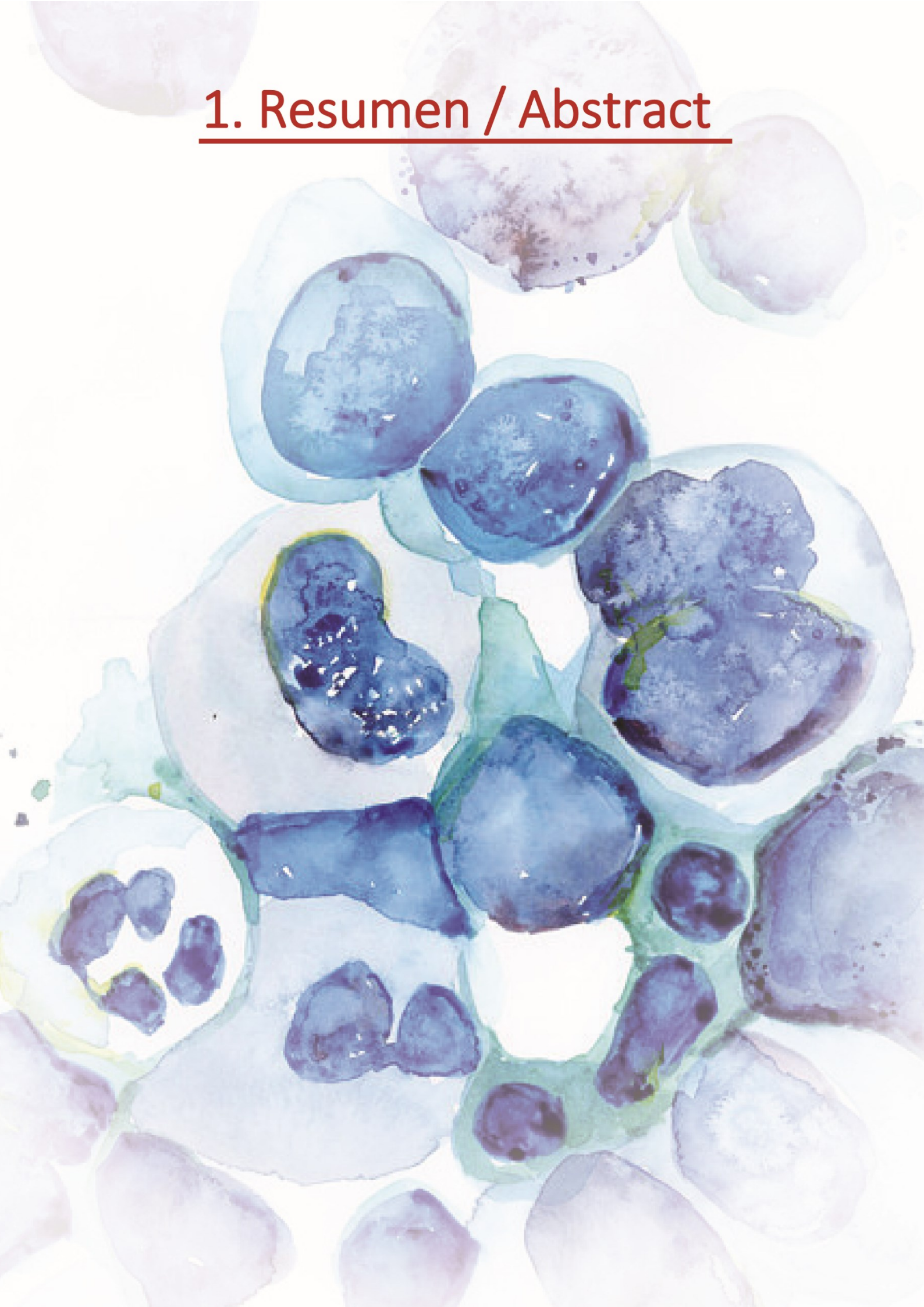

1. Resumen / Abstract

1.1. Resumen

Aunque clásicamente se les ha definido como células inmunes, sabemos ahora que los macrófagos también desempeñan otras funciones necesarias para mantener la homeostasis en aquellos tejidos en los que residen (Davies et al., 2013). Éstas funciones son prominentes en el corazón, donde se ha descrito que los macrófagos previenen la formación de fibrosis (Chakarov et al., 2019) y favorecen la recuperación del tejido tras un daño (Dick et al., 2019; Nahrendorf and Swirski, 2013). Asimismo, una población de macrófagos residentes en el nodo atrioventricular modula la conducción eléctrica en el corazón (Hulsmans et al., 2017). No obstante, hay un gran número de macrófagos residentes en otras regiones del corazón sano, incluyendo el miocardio ventricular, (Pinto et al., 2012) sugiriendo funciones aún desconocidas.

En la presente tesis, hemos analizado distintos aspectos de los macrófagos ubicados en el miocardio de ratones sanos. Hemos encontrado que estas células tienen una amplia distribución en el tejido y fagocitan material procedente de cardiomiocitos de forma activa. Los cardiomiocitos expelen mitocondrias dentro de unas estructuras rodeadas de membrana dedicadas a tal fin, a través de un proceso regulado por su maquinaria de autofagia. Éstas estructuras se asemejan a exoferas descritas en neuronas, y su producción se incrementa al inducir estrés celular. Las mitocondrias eyectadas a través de éste proceso están en su mayoría dañadas y son eficientemente eliminadas por los macrófagos cardíacos. El receptor de membrana Mertk en los macrófagos cardiacos permite el reconocimiento y eliminación eficiente de las exoferas, evitando una activación del inflamasoma y alteraciones en el tejido cardíaco. Por otra parte, la eliminación de macrófagos con herramientas genéticas resulta en una cardiopatía severa. Nuestros descubrimientos identifican un par celular inmune-parenquimal en el corazón necesario para preservar la estabilidad metabólica de los cardiomiocitos mediante la eliminación subrogada de componentes celulares dañados a los macrófagos circundantes.

1.2. Abstract

Classically defined as defensive cells, macrophages are now known to be endowed with tissue-specific tasks unrelated to immunity (Davies et al., 2013). These pleiotropic functions are prominent in the heart, where tissue-resident macrophages have been shown to prevent fibrosis (Chakarov et al., 2019), facilitate electrical conduction in the atrioventricular node (Hulsmans et al., 2017), or to favour healing in injured areas (Dick et al., 2019; Nahrendorf and Swirski, 2013). Notwithstanding these observations, large numbers of macrophages of unknown functions populate other regions of the healthy heart, including the ventricular myocardium (Pinto et al., 2012), suggesting broader homeostatic functions for heart-resident macrophages.

In this work, we have analysed macrophages lodged within the healthy murine myocardium, and find that they are broadly distributed and actively took cellular material derived from cardiomyocytes. Cardiomyocytes ejected mitochondria in dedicated membranous particles reminiscent of neural exophers, through a process driven by the cardiomyocyte's autophagy machinery that was enhanced during cardiac stress. Mitochondria disposed through exophers were largely dysfunctional, and were efficiently eliminated by adjacent macrophages. Recognition of cardiac exophers by the phagocytic receptor Mertk prevented inflammasome activation, mitochondrial dysfunction and proteostatic defects, while elimination of macrophages with genetic tools results in a severe cardiomyopathy. Our findings identify an immune-parenchymal pair in the murine heart that allows material transfer to preserve metabolic stability and cell homeostasis.

2. Introduction

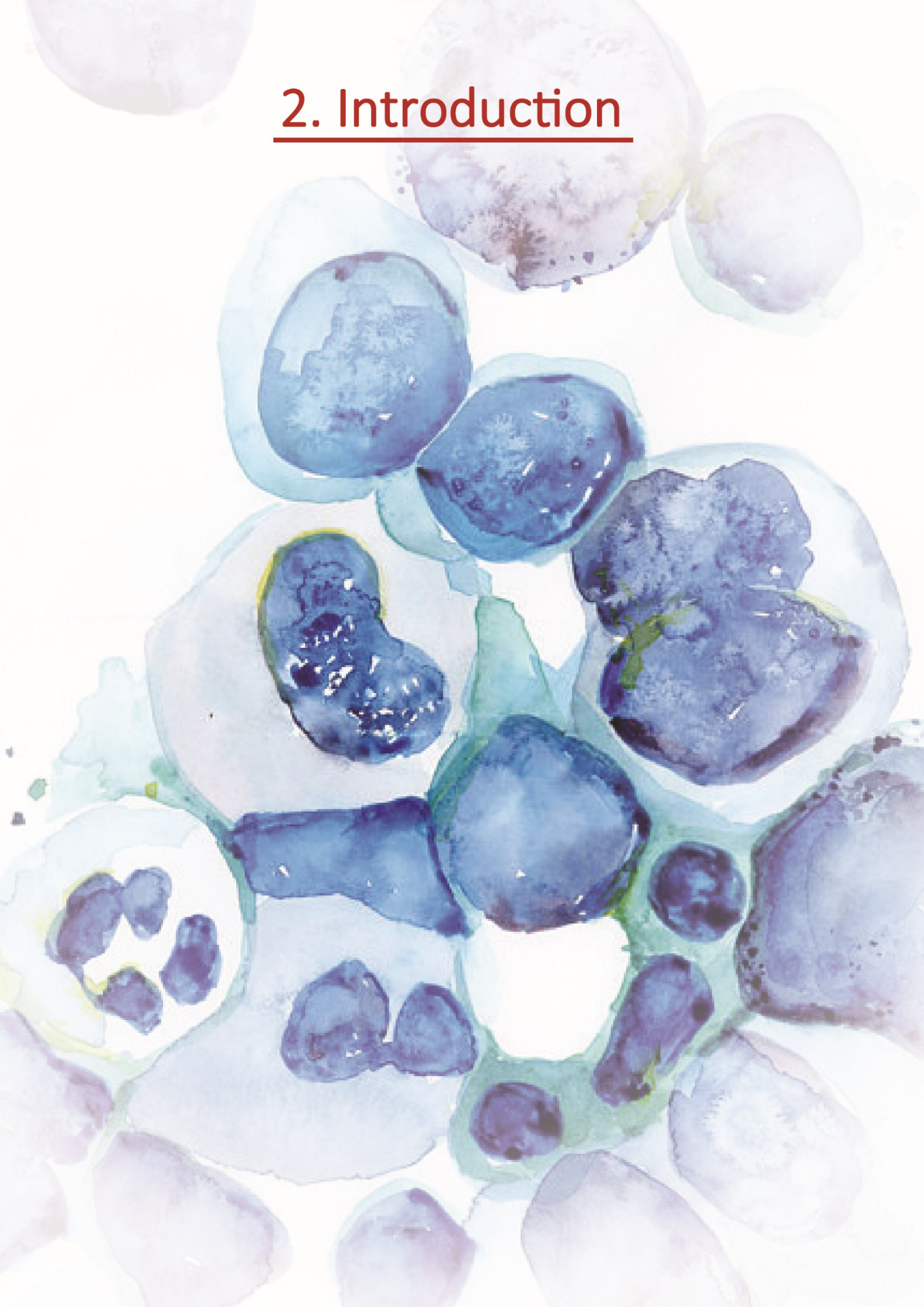

2. Introduction

2.1 Immune system in Immunity & Homeostasis

2.1.1. Immunity

In Biology, **Immunity** is the capacity of organisms to fight off and resist the attack of external agents. It comprehends physical barriers, tissues, as well as specialized cells and physiological processes dedicated to this aim that collectively are referred to as the **Immune System**. The importance of Immunity is reflected in its ancient evolutionary origin (Medzhitov, 2008), from sentinel cells in social amoebas, at the interface between uni- and multicellularity (Chen et al., 2007), to the so called "superior organisms". In the latter, the Immune system acquires a higher level of complexity with two different but interconnected branches: Adaptive and Innate Immunity.

Adaptive Immunity is a more sophisticated Immune strategy; it is mainly present in vertebrates (Cooper and Alder, 2006), but is not exclusive to them (Kaufman, 2010). It has a slow response to the primary insult, which can take up to several days (Janeway, 2005), yet is able to generate immunological memory thanks to antibodies, which are specialized proteins that recognize specific antigens with high affinity. In this way, adaptive immunity guarantees a more efficient response in a second encounter, which represents the basis of vaccinations. Under some conditions, antibodies against endogenous proteins (autoimmune diseases) or non-pathogenic proteins (allergy) can be generated that cause pathologies. The main mediators of adaptive immunity are T and B cells, with the latter being the responsible for antibody production. Importantly, innate immunity activation is necessary for the activation of adaptive immunity (Abbas et al.).

Innate Immunity is highly conserved in evolution (Medzhitov, 2008). It is not antigen specific, however it is very fast (from minutes to hours), and constitutes the first line of defence against pathogens (Janeway, 2005). In this case, pathogen recognition is generally mediated by **PRRs** (for Pattern Recognition Receptors) (Janeway, 1989), which recognise conserved structures present in infectious agents, called **PAMPs** (from Pathogen Associated Molecular Patterns), or in damaged own cells, called **DAMPS** (from

Damage Associated Molecular Patterns). The known cellular mediators of innate immunity are macrophages, monocytes, dendritic cells, neutrophils, basophils, eosinophils, mastocytes, natural killer cells (NK), and innate lymphoid cells (Spits and Di Santo, 2011).

In the late 1800s Ilya Ilyich Mechnikov (1845-1916) first studied the behaviour of **macrophages** and **neutrophils** (which he termed microphages), and found that they are essential for phagocytosis of exogenous microorganisms and that this was a programmed response crucial for the maintenance of Immunity. Thus Mechnikov concluded that the accumulation of inflammatory cells (or inflammation) is not a pathologic state, but rather an organismal response against an external insult, whose goal is the restoration of homeostasis (Mechnikov, 1892).

2.1.2. Homeostasis

Homeostasis is a key concept in biology. It is the process by which an organism or a cell keeps constant internal conditions even in the face of environmental changes. This mechanism ensures that fundamental parameters, for example glucose or oxygen levels, are maintained within a range that is acceptable for the organism. Alterations in this equilibrium result in transient or permanent adaptations to the new conditions. This concept is important because the immune system is one of the key mechanisms that enables organismal homeostasis. In fact, the inflammatory response is envisioned as a transient process that attempts to restore the baseline physiological state after an insult (Nathan and Ding, 2010). When this fails, the organism enters into a state of chronic inflammation, as seen during atherosclerosis, obesity or cancer.

However, excessive activation of the immune cells can cause damage to tissues and therefore the innate immune system has developed programs that try to minimize the amplitude and duration of the inflammatory response (Soehnlein and Lindbom, 2010). Organisms are continuously exposed to changes in their environment, some of which cause inflammatory responses which are resolved without appreciable changes in organismal homeostasis. Only when the insult is sufficiently strong or persistent, a series of events are triggered in response to the stress, resulting in **inflammation** (Chovatiya and Medzhitov, 2014).

An **inflammatory response** starts when the tissue parenchyma, endothelial cells or resident immune cells detect the presence of a pathogen (through PAMPs) or tissue damage (through DAMPs). Upon detection, these stimuli elicit an orchestrated production of cytokines and chemokines which recruit immune cells such as neutrophils and monocytes (Schiwon et al., 2014). Once they reach their destination, neutrophils release cytotoxic compounds from its granules, produce ROS and release Neutrophil Extracellular Traps (NETs), which enable frontline defence against pathogens. The release of these compounds, however, is a double-edge sword as they can also damage neighbouring host cells (Adrover et al., 2016; Nicolas-Avila et al., 2017). Finally, once the inflammatory stimulus is under control, infiltrated immune cells die *in situ* and are removed by macrophages or other phagocytes through a process called **phagocytosis**, a process that ultimately leads to the release of anti-inflammatory cytokines like IL-10 or TGFβ, or lipids such as lipoxins, resolvins and protectins (Serhan et al., 2008; Soehnlein and Lindbom, 2010; Watanabe et al., 2019). At the same time apoptotic neutrophils release mediators that may dampen further inflammatory recruitment (Soehnlein and Lindbom, 2010), overall contributing to the resolution of inflammation and restoration of homeostasis.

2.2. Macrophages

Macrophages are a type of white blood cells which belong to the innate immune system. It has long been appreciated that macrophages are present in virtually every tissue, in each of which they receive different names (Microglia, Osteoclasts, Kupffer cells or Langherhans cells; (Ovchinnikov, 2008)). Although macrophages may vary in morphology and other properties throughout the body (Krombach et al., 1997), they can be identified by expression of specific proteins and transcription factors, such as F4/80 or PU.1, respectively (Gordon et al., 2014; Gosselin et al., 2014; Hoeksema and Glass, 2019).

Macrophages perform a plethora of functions. The most prominent of these is the recognition, engulfment and degradation of pathogens and damaged cells through a process called **phagocytosis**. In order to fulfil their phagocytic role, those cells contain a series of receptors in their membrane to capture the target material as well as large

amounts of lysosomes in their cytoplasm to degrade it (Gordon, 2016). They are also one of the first lines of defence against infections in tissues where they integrate signals from their environment and orchestrate early inflammatory responses (Davies et al., 2013). Finally, they also perform important functions in organ development and in maintaining tissue homeostasis (Davies et al., 2013). Below I introduce the cardinal features of macrophages.

2.2.1. Phagocytosis

The word **"macrophage"** derives from the Greek "makros" (large) and "phagein" (eater). Macrophages are immune cells defined by their high phagocytic capacity and this PhD thesis is focused on their study. Macrophages perform important functions by eliminating unwanted material during embryonic development (Gordon, 2016; Henson and Hume, 2006), microbial infection (Dockrell et al., 2001; Kosmider et al., 2012; Martin et al., 2012), tissue injury (DeBerge et al., 2017) or during normal tissue function (Arandjelovic and Ravichandran, 2015), thereby preserving homeostasis. In most of these cases, the eliminated material consists of **apoptotic** or **necrotic cells**, i.e. cells that become irreversibly damaged as a consequence of external aggression or programmed cell death, as is the case for neutrophils and other blood cells that display a short lifespan (Pillay et al., 2010; Tak et al., 2013). Indeed, billions of cells are eliminated every day from a healthy organism in a manner that does not trigger an inflammatory response but is instead part of a homeostatic clearance program that involves their engulfment by macrophages and other cells types (Arandjelovic and Ravichandran, 2015; Gordon, 2016).

The efficiency of this clearance process is ensured by a series of soluble or cell-bound molecules that mediate the attraction, recognition, and engulfment of the target cells by macrophages (Hochreiter-Hufford and Ravichandran, 2013). Attraction of macrophages is mediated by the so called "find me" signals, and relies on gradients of molecules like lisophosphatidilcholine (LPC), sphingosine-1-phosphate (S1P), fractalkine (CX3CL1) or nucleosides (i.e. ATP) (Hochreiter-Hufford and Ravichandran, 2013). Once macrophages enter in contact with the apoptotic cell a series of molecules called "eat me" signals trigger the initiation of phagocytosis. Among these **Phosphatidylserine (PS)**,

a phospholipid normally restricted to the inner layer of the plasma membrane by the flippase enzyme, is the best characterized. In apoptotic cells scramblases catalyse the rapid transfer of PS to the outer layer (Verhoven et al., 1995) allowing its specific recognition and silent elimination of the cell (Bose et al., 2004; Fadok et al., 1992; Huynh et al., 2002). Opsonin proteins like Growth arrest-specific 6 (Gas6), Annexin A1, S-protein or milk-fat globule EGF factor 8 (Mfge8) recognize PS (Dalli et al., 2012; Hanayama et al., 2004) and interact directly or indirectly with receptors on the surface of macrophages, including T cell immunoglobulin- and mucin-domain–containing molecule 4 (Tim4) (Miyanishi et al., 2007), the receptor tyrosine kinases Mer (Scott et al., 2001), Axl and Tyro3 (Lemke, 2013). Tyro3, Axl and Mer constitute the **TAM receptor family** and are essential for tissue homeostasis (Rothlin et al., 2015).

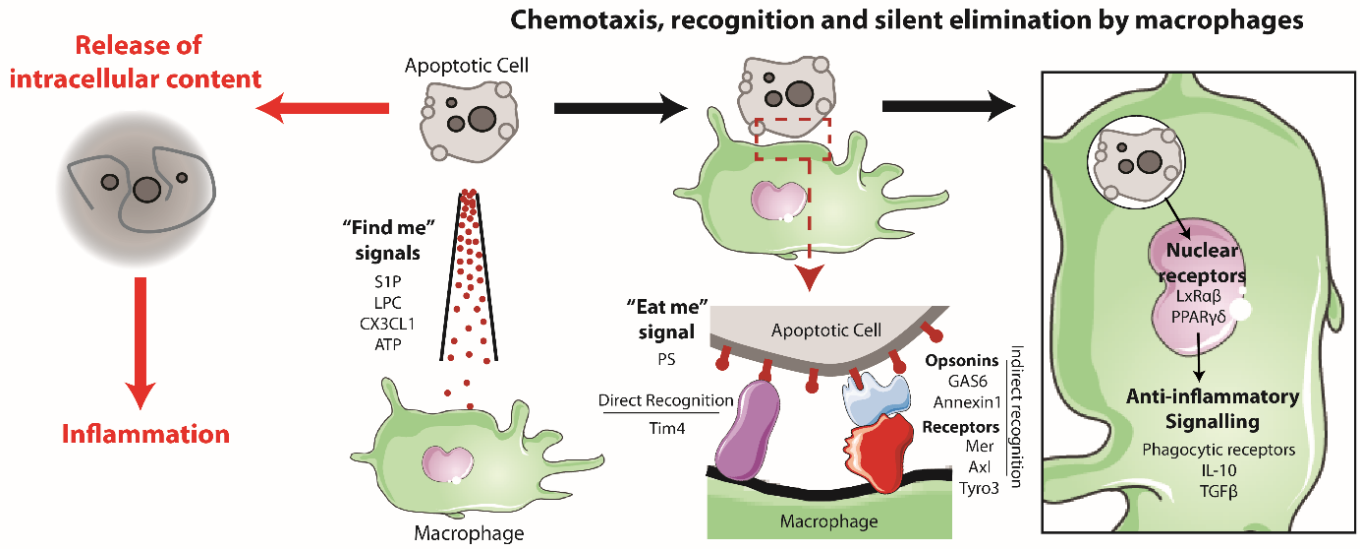

Introduction Figure 1. Apoptotic cell phagocytosis by macrophages.

(Right) Apoptotic cells are recognized by macrophages through "Find me" and "Eat me" signals. Once macrophages phagocytose the apoptotic cells, they upregulate the expression of Phagocytic receptors and anti-inflammatory cytokines, favoring the silent removal of apoptotic cells. (Left) When macrophages fail to recognize apoptotic cells, intracellular content is released to the interstitium causing inflammation.

Importantly, phagocytosis often influences the transcriptional profile of macrophages by activation of nuclear receptors in macrophages, including LXRα and β or PPARδ and γ (encoded by *Nr1h3, Nr1h2, Nr1c2 and Nr1c3,* respectively) (A-Gonzalez et al., 2009; Roszer et al., 2011)), which results in transcriptional expression of genes involved in the phagocytic cascade and anti-inflammatory signalling, such as IL-10 and

TGF-β (Fadok et al., 1998; Huynh et al., 2002; Notley et al., 2015), while at the same time repressing inflammatory mediators, like IL1-β (A-Gonzalez et al., 2017). Thus, macrophages mediate silent removal of apoptotic cells through phagocytosis (Introduction Figure 1) thereby avoiding pathologies associated with chronic inflammation or autoimmune diseases (A-Gonzalez et al., 2009; Griffith and Ferguson, 2011; Hanayama et al., 2004; Mukundan et al., 2009; Nagata, 2007; Roszer et al., 2011; Scott et al., 2001).

2.2.2. Tissue Resident macrophages

The majority of tissues in the body contain **tissue-resident macrophages** andoften several phenotypically distinct subsets are evident in discrete micro-anatomical niches of the same tissue. As a result of the varying tissue environments and their micro-anatomical disposition, tissue-resident macrophages are extremely heterogeneous and perform functions that are integral to tissue function and homeostasis (Davies et al., 2013; Hashimoto et al., 2011).

Apart of their important role in maintaining immune quiescence (Davies et al., 2013), some tissue-resident macrophages were found to perform major tissue-specific functions, directly related or not with their phagocytic activity (Hochreiter-Hufford and Ravichandran, 2013), and typically of non-immune nature. A summary including well-defined examples of these functions is available in Introduction Figure 2. Importantly, animals in which these tissue-resident populations of macrophages are absent or have an impaired function manifest severe diseases. For instance, human mutations affecting cytokines important for macrophage differentiation and survival (like GM-CSF or M-CSF) lead to alveolar macrophage and osteoclast loss, resulting in pulmonary alveolar proteinosis (Carey and Trapnell, 2010) or osteopetrosis (Yoshida et al., 1990), thus highlighting their importance in maintaining homeostasis (Davies et al., 2013).

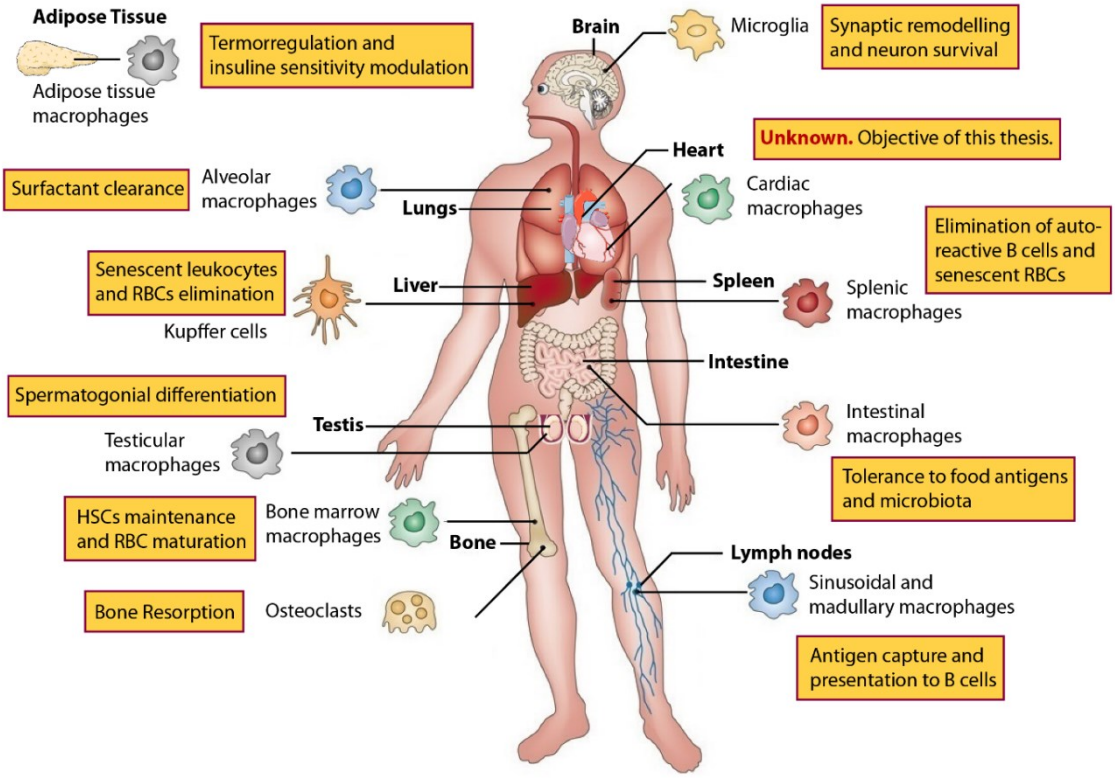

Introduction Figure 2. Tissue-resident macrophages perform tissue-specific functions.

Figure adapted from (Murray and Wynn, 2011), highlighting tissue-resident macrophage populations and their roles in different tissues, including: Brain (London et al., 2013; Paolicelli et al., 2011), Spleen (Kohyama et al., 2009; MacLennan, 1994), Intestine (Bain et al., 2013; Zigmond and Jung, 2013), Lymph nodes (Gray and Cyster, 2012), Bone (Edwards and Mundy, 2011; Pollard, 2009), Bone marrow (Casanova-Acebes et al., 2013; Chow et al., 2013; Chow et al., 2011; Nagata, 2007), Testis (DeFalco et al., 2015), Liver (Ganz, 2012; Klein et al., 2007), Lungs (Carey and Trapnell, 2010; Gautier et al., 2012), Adipose tissue (Nguyen et al., 2011; Odegaard and Chawla, 2008; Odegaard et al., 2007). RBC (Red Blood Cells) and HSC (Hematopoietic Stem Cell).

2.2.3. Origin of tissue resident macrophages

As indicated above, macrophages are present in many tissues at very early embryonic stages, indicating that this cell type is not only critical during inflammation and homeostasis in the adult, but also for development, maintenance and repair of growing tissues. After their discovery by Mechnikov, macrophages were eventually incorporated in early 1900s into the reticulo-endothelial system, a tissue system comprised of reticuloendothelia (phagocytes) and endothelial cells, which were proposed to have a common tissue origin. Thus, implying that macrophages originated from, resided and renewed within that tissue. Later, the mononuclear phagocyte system (MPS) model was

formulated postulating that the origin of all macrophages is the terminal differentiation from blood monocytes (Davies and Taylor, 2015). Still today the origin of tissue-resident macrophages remains controversial and is known to vary depending on the organ.

Until the early 2000s it was generally assumed that all macrophages shared the same monocytic/myeloid progenitor in the bone marrow, as postulated by the MPS model (Davies and Taylor, 2015). Indeed, **monocytes** are myeloid leukocytes produced in the bone marrow with potential to differentiate into macrophages and dendritic cells in response to inflammatory stimuli (Geissmann et al., 2003). **Myeloid,** derived from the Greek *"muelós"* (marrow) and *"oid"* (derived from), is a term used to refer cells produced in the bone marrow, which include monocytes but also granulocytes, erythrocytes, megakaryocytes and platelets, all of which are now known to derive from a **common myeloid progenitor (CMP)** (Ema et al., 2014). However, many of these cells including monocytes have been described to be produced in extramedullary tissues like spleen or liver under certain conditions, both during development and adulthood (Tomczyk et al., 2017). Two subsets of monocytes can be distinguished in mice and humans based on the expression of different markers (Geissmann et al., 2003; Nahrendorf et al., 2007; Ziegler-Heitbrock, 2007). In mice, the "classic" or "pro-inflammatory" monocytes are characterized by Ly6C^{hi} CX3CR1^{low} CCR2^{hi} surface phenotype, and are recruited rapidly from blood into inflamed tissues, where they differentiate into macrophages. On the other hand, the "patrolling" or "anti-inflammatory" monocytes feature a Ly6C^{low} CX3CR1^{hi} CCR2^{low} phenotype, and have housekeeping functions such as clearing endothelial debris (Auffray et al., 2007; Geissmann et al., 2003).

The appearance of new tools in the last decade has challenged the theory of monocytic origin for tissue resident macrophages (Hoeffel and Ginhoux, 2018; Nicolas-Avila et al., 2018). Thanks to genetic engineering and fate-mapping studies in the mouse, it was demonstrated that a significant number of macrophages are derived from primitive **erythromyeloid precursors (EMPs)**, cells with potential to give rise to both erythroid and myeloid lineages, that arise in the yolk sac early in development (Kierdorf et al., 2013; Schulz et al., 2012; Yona et al., 2013). These macrophages or their progenitors seed tissues before birth and proliferate to populate the growing tissues,

with negligible or only minimal dependence on circulating monocytes (Perdiguero et al., 2015; Schulz et al., 2012). During adult life, they maintain their numbers mainly by proliferation inside the tissue (Hashimoto et al., 2013).

However, the system of macrophage formation is not binary, as tissue-macrophage origin and reliance on monocyte precursors largely depends on the tissue of residence. For example, microglia (macrophages from the CNS) are considered a prototypical example of yolk sac-derived macrophage with minimal dependence on adult haematopoiesis, and display very low rates of replacement in steady-state in adult animals as evidenced by transplantation, parabiosis and lineage-tracing studies (Ginhoux et al., 2010; Kierdorf et al., 2013; Schulz et al., 2012; Yona et al., 2013). Similar results have been obtained for macrophages in the spleen, peritoneum, liver, and lung, which appear to be maintained independently of adult haematopoiesis (Hashimoto et al., 2013; Schulz et al., 2012; Yona et al., 2013). On the contrary, other adult tissues including regions of the skin and intestine continue to be colonized by monocytes through adulthood, such that these tissue-resident macrophage populations in aged mice are largely derived from adult haematopoiesis (Bain et al., 2014; Hoeffel et al., 2012). Thus, macrophage origins are different among tissues and their reliance on monocytes may vary in the presence of inflammatory stimuli (Dey et al., 2014).

2.2.4. Cardiac-resident macrophages

The heart is composed of multiple cell types including cardiomyocytes, fibroblasts, endothelial cells, smooth muscle cells, and immune cells, which constitute around 10% of non-myocytic cells in the heart (Pinto et al., 2016). **Cardiac tissue-resident macrophages (cMacs)** constitute a large fraction (around 70%) of all immune cells in the mouse myocardium (Pinto et al., 2012). They are located in perivascular areas, interspersed between cardiomyocytes (Pinto et al., 2012), the epicardium (Pinto et al., 2014) and the atrioventricular node (Hulsmans et al., 2017). cMacs were also reported in normal human hearts as defined by expression of CD68, a myeloid-specific protein (Azzawi et al., 1997). A more comprehensive study on hearts from patients subjected to surgical procedures was published recently (Bajpai et al., 2018), however those may be

not *bona fide* resident cMacs but inflammatory macrophages that appear due to the pathological state of the tissue.

After the original description of cMacs in 2012, work from several laboratories defined heterogeneity in their origin and in the expression of different markers. Although the extent of cMacs heterogeneity remains incomplete, most of these cells express *bona fide* markers of tissue macrophages, such as F4/80, CX3CR1, CD68, and CD64 (Epelman et al., 2014a; Pinto et al., 2012; Skelly et al., 2018). Like in other tissues, various populations of macrophages can be distinguished in the myocardium based on the differential expression of specific surface markers by flow cytometry and tissue immunostaining, single cell RNAseq (Dick et al., 2019; Skelly et al., 2018), and genetic lineage tracing (Molawi et al., 2014). Surface markers that differ in expression between cMacs include CX3CR1, MHCII, Ly6C, Lyve-1 and CCR2, which define different populations in adult and embryonic mice (Dick et al., 2019; Epelman et al., 2014a; Leid et al., 2016; Molawi et al., 2014), and in humans (Bajpai et al., 2018).

Different studies using genetic fate mapping and parabiosis (Epelman et al., 2014a; Heidt et al., 2014; Molawi et al., 2014) have addressed the ontogeny of cMacs. Lineage-tracing analysis revealed that primitive macrophages originating from yolk sac progenitors entered the heart as early as E9.5–E10.5 (Epelman et al., 2014a). In addition, part of the embryonic macrophages seems to be derived from the haemogenic endocardium (Shigeta et al., 2019). Genetic labelling at E8.5 in mice expressing the Cre recombinase gene under the control of one of the endogenous promoters including the runt-related transcription factor 1 ($Runx1^{CreER}$) or the receptor for M-CSF ($Csf1r^{CreER}$), which label yolk-sac derived macrophages at this point (Epelman et al., 2014b), showed that significant numbers of these cells persisted well into adult life (Epelman et al., 2014a). The initial seeding of foetal yolk-sac-derived macrophages to the developing heart is through the mesothelium, a structure within and just below the epicardium. Accordingly, epicardial ablation results in defective macrophage settlement in the heart (Stevens et al., 2016). After E10.5, the foetal liver becomes the major haematopoietic organ, with the budding of the first definitive haematopoietic stem cells (HSCs) (Hoeffel and Ginhoux, 2018), HSCs express FLT3, a tyrosine kinase receptor, (Boyer et al., 2011). By using $Flt3^{Cre}$ mediated lineage tracing a second wave of macrophages originating from

foetal liver hematopoietic progenitors was identified at later developmental stages (Epelman et al., 2014a). Similar results were obtained labelling cells by Cre recombinase expression under the control of theCX3CR1 gene ($Cx3cr1^{CreER}$), which labels yolk-sac or HSC-derived macrophages, depending on the time of induction (Molawi et al., 2014). These studies showed that early yolk-sac-derived macrophages persist longer in the heart than in other tissues, suggesting a largely embryonic origin for these cells in the adult. After birth, cMacs expand and are maintained by local proliferation (Epelman et al., 2014a; Heidt et al., 2014; Pinto et al., 2014), which is consistent with studies showing that the contribution of blood monocytes to the cMacs pool is minimal even after 4–8 weeks in parabiosis (Epelman et al., 2014a; Heidt et al., 2014; Molawi et al., 2014). However, the interpretation of these results varies between groups: some consider the cMac pool as a closed, embryonically-derived system with low contribution of adult haematopoiesis (Epelman et al., 2014a; Molawi et al., 2014), while others interpret it as a progressive substitution of embryonic derived macrophages by monocyte-derived macrophages with age (Heidt et al., 2014). Supporting the latter, both circulating monocytes as well as residual cMacs repopulate the heart after severe inflammation (Heidt et al., 2014), angiotensin II infusion, sub-lethal irradiation, or cMac depletion (Epelman et al., 2014a). Interestingly, self-renewal of the embryo-derived macrophage pool declines with age, and may allow progressive replenishment by circulating monocytes, even in the absence of injury (Heidt et al., 2014). Together, these data argue that cMacs exist independently from blood monocytes in the steady state and self-renew through in situ proliferation with low monocyte input, with an estimated turnover rate of about one month based in BrdU incorporation experiments (Heidt et al., 2014). When cMacs are depleted, they are preferentially replenished through both local expansion and monocyte replacement to differing degrees (Epelman et al., 2014a; Heidt et al., 2014). This shift in the source of cardiac macrophages through development, disease, and aging is biologically intriguing but of unknown significance.

Contrary to other tissue resident populations, little is known about the role of cMacs in the steady-state heart, perhaps because they discovery was relatively recent (Pinto et al., 2012). However, gene expression profiling and recent functional experiments reveal various roles for cMacs in the healthy heart. These processes include general

macrophage functions like Immune defence (Heidt et al., 2014; Mylonas et al., 2015) and maintenance of immune quiescence through the elimination of debris deposited in the cardiac tissue (DeBerge et al., 2017; Pinto et al., 2014; Pinto et al., 2012), but also unexpected roles such as the modulation of electrical conduction in the auricular-ventricular node (Hulsmans et al., 2017), or developmental roles in coronary plexus (Leid et al., 2016) and valve formation (Shigeta et al., 2019). A more detailed description of cMacs heterogeneity, ontogeny and functions can be found in our recent review (Nicolas-Avila et al., 2018) (see Annex 9.3.).

2.3. Cardiac physiology

The **heart** is the main component of the circulatory system and functions as a pump that moves blood through the body. **Blood** is a fluid tissue that transport nutrients and oxygen to tissues while, at the same time, collects metabolic waste by-products away. To understand how cMacs influence cardiac function, which is the central goal of this thesis, it is important to introduce important concepts in cardiac biology and metabolism.

2.3.1. Heart: energy and mitochondria

In order to fulfil its function, the heart needs massive amounts of energy: it consumes 3.5 to 5 kg of ATP per day (in humans) (Neubauer, 2007), at a rate of around 1 mM ATP consumed per second (Piquereau and Ventura-Clapier, 2018). Even at rest, the consumption of ATP per minute exceeds the size of the ATP and Phosphocreatine (PCr) storage pool, which allows for only a few seconds of activity (Piquereau and Ventura-Clapier, 2018). This exorbitant energy consumption demands for a complex and efficient machinery that supplies with high-energy phosphates. In the healthy adult heart, energy is largely provided by oxidative phosphorylation that takes place in mitochondria (>90%), with minor contribution of glycolysis, as evidenced by the linear correlation between oxygen consumption and cardiac work (Stepanov et al., 1997). **Mitochondria**, the key energy-producing organelle in cells, are mainly fuelled by fatty Acetyl-CoA and pyruvate, which are the primary metabolites of fatty acids, and carbohydrates, respectively (Lopaschuk and Jaswal, 2010). Typically, substrates for oxidative phosphorylation consist of 60% to 90% fatty acids and 10% to 40% glucose (Lopaschuk

and Jaswal, 2010; Saddik and Lopaschuk, 1991). Nonetheless, healthy hearts present metabolic flexibility and reverse coupling between fatty acid and glucose metabolism (the Randle cycle) (Hue and Taegtmeyer, 2009), which allows for rapid replenishment of consumed ATP under different physiological conditions. This strict energetic demand explains why about one third of the cardiomyocyte's volume is occupied by mitochondria, making cardiomyocytes the cells with the highest mitochondria content in the body (Schaper et al., 1985), and the heart one of the tissues with highest mitochondrial gene expression (Herbers et al., 2019).

2.3.2. Mitochondria and Autophagy

Mitochondria are vital for key cellular processes including oxidative metabolism, calcium buffering, and production of reactive oxygen species (ROS). Damaged mitochondria can additionally activate death signals (Green and Kroemer, 2004; Saelens et al., 2004) and contribute to cardiac dysfunction via loss of metabolic capacity and excessive ROS production (Dai et al., 2014a). Thus, quality control mechanism that mediate the elimination of senescent mitochondria, such as **mitophagy** and **macro-autophagy**, are critical for energy and oxidative homeostasis.

Autophagy, or "eating of the self", is an evolutionarily conserved mechanism for degradation of intracellular components and recycling of metabolites (Levine and Kroemer, 2008; Rubinsztein et al., 2011). In most contexts, autophagy denotes macro-autophagy, a process in which various intracellular materials and organelles are recruited into auto-phagosomes, which can be observed in adult mouse hearts by electron microscopic (Ikeda et al., 2015), and are targeted for degradation via fusion with lysosomes. Mitochondria can also be degraded through mitophagy, which consists in the selective formation of phagophores that mature into auto-phagosomes which only contain mitochondria and the membrane-associated protein MAP1 light chain 3 (LC3), that fuses to lysosomes for degradation (Kim et al., 2007). Alternative mechanisms of mitochondria degradation, such as mitochondrial derived vesicles, have also been described (Sugiura et al., 2014).

Organelle replacement is partly accomplished during cell division. Although the adult mammalian heart is largely post-mitotic, cardiomyocytes retain some proliferative

capacity in response to stress. However, this is very inefficient and does not allow for significant replacement of myocytes or dilution of damaged proteins or organelles in daughter cells (Bergmann et al., 2009; Senyo et al., 2014). Hence, the adult heart heavily relies on quality control mechanisms that ensure cell function and tissue homeostasis throughout life (Delbridge et al., 2017; Nakai et al., 2007; Taneike et al., 2010; Wang et al., 2008).

2.3.3. Autophagy and Mitochondria in Cardiac Aging

Aging is the progressive accumulation of changes with time. In the heart, aging causes gradual loss of tissue homeostasis and organ failure (Boengler et al., 2009), leading to increased incidence of cardiovascular disease in humans (Mozaffarian et al., 2016) and mice (Taffet et al., 1997). At the cellular level, aging results in the accumulation of damaged proteins, organelles, DNA and oxidized lipids in cardiomyocytes, concomitant to reduction in mitochondrial function, gene expression and loss of endogenous protective components. Altogether, this contributes to structural and functional defects, cardiomyocyte degeneration, loss of protection against injury, and overall cardiac dysfunction (Biala et al., 2015; Boengler et al., 2009; Chen et al., 2012; Dai et al., 2014b; Li et al., 2018). Since autophagy plays a crucial role in the degradation of long-lived proteins and organelles, part of these features are attributable to a decline in the maintenance of protein quality control systems (e.g., autophagy) with age (Cuervo et al., 2005; Rubinsztein et al., 2011; Shirakabe et al., 2016; Yamaguchi and Otsu, 2012). An age-related decline in autophagic activity may exacerbate the accumulation of harmful cellular debris (Cuervo et al., 2005; Cuervo and Dice, 2000). Accumulation of biological debris is relatively slow and therefore typical of long-lived post-mitotic cells such as cardiomyocytes, neurons, skeletal muscle fibbers or retinal pigment epithelial cells relative to short-lived or renewable cells (Terman et al., 2003). Thus, the dependence of cardiomyocytes on autophagy is profound; even more so if one considers that the human heart can remain disease free and functionally viable for 70 years or more.

There is increasing evidence that disrupted autophagy underlies age-related cardiomyopathy (Cuervo, 2008; Linton et al., 2015; Shirakabe et al., 2016; Zhou et al., 2017). First, genetic inhibition of autophagy genes induce an age-like phenotype in the

heart. For example, cardiac-specific depletion of the Autophagy Related Gene 5 (*Atg5*) develop an aged-like phenotype with accumulation of ubiquitinilated proteins, p62 and damaged mitochondria, resulting in cardiac dysfunction and premature death, (Nakai et al., 2007; Taneike et al., 2010). Second, pharmacological or genetic enhancement of autophagy delays cardiac deterioration. Systemic overexpression of Atg5 improved mitochondrial morphology, respiratory rates and autophagy flux in the mouse heart, thus extending organismal lifespan (Pyo et al., 2013). Autophagy activation with rapamycin (an mTOR inhibitor) or reduced mTOR expression increased clearance of damaged mitochondria, delayed aging and extended lifespan (Anisimov et al., 2011; Dai et al., 2014b; Flynn et al., 2013; Harrison et al., 2009; Wu et al., 2013). Long-term caloric restriction, a potent inducer of autophagy (Blagosklonny, 2010), increases autophagy flux and preserves cardiac function in aged rodents and monkeys (Colman et al., 2009; Dai et al., 2014b; Han et al., 2012; Maeda et al., 1985; Niemann et al., 2010; Shinmura et al., 2011; Taffet et al., 1997; Wohlgemuth et al., 2007). Further, changes in the expression of autophagy related proteins (e.g., Atg9, LC3-II and LAMP-1) have been reported in parallel with a decline in cardiac function in aged rats and mice (Boyle et al., 2011; Hua et al., 2011; Taneike et al., 2010; Wohlgemuth et al., 2007). However, those changes at the protein level are difficult to interpret without autophagy flux experiments (Klionsky et al., 2016) and are subjected to great variability in experimental design (e.g., age choice).

Another feature of cardiac aging is the accumulation of damaged mitochondria. Age correlates with a general decline in mitochondrial function, clonal expansion of dysfunctional mitochondria (Khaidakov et al., 2003; Piko et al., 1988; Wanagat et al., 2002), suppressed degradation of mitochondria through autophagy (Ikeda et al., 2014), dysregulation of fusion/fission (Dorn et al., 2011; Sebastian et al., 2016; Stotland and Gottlieb, 2016; Zhao et al., 2014) and increased production of ROS (Perez et al., 2009). ROS are generated in the cell as a by-product of mitochondrial respiration. Under normal conditions, low ROS levels regulate biological processes including autophagy (Scherz-Shouval et al., 2007; Sciarretta et al., 2013; Song et al., 2014). However, dysfunctional mitochondria produce excess ROS that can modify nuclear and mitochondrial DNA (mtDNA), proteins, lipids and organelles generating a positive feedback loop that

progressively aggravates oxidative stress and mitochondrial dysfunction (Dai et al., 2014a; Das and Muniyappa, 2013; Judge et al., 2005; Perez et al., 2009; Terman et al., 2003).

The simultaneous increase of damaged mitochondria and reduced autophagy with age suggested possible mechanistic connection of both phenomena. Indeed, activation of autophagy increases expression of proteins involved in mitochondrial energy metabolism and restores a more youthful proteomic signature (Dai et al., 2014b), reduces mitochondrial H_2O_2 production and mtDNA damage (Gredilla et al., 2001), restores oxidative phosphorylation and beta-oxidation (Dai et al., 2014b; Dhahbi et al., 2006) and improves diastolic function (Dai et al., 2014b; Dhahbi et al., 2006; Flynn et al., 2013; Spaulding et al., 1997) in old hearts. The link between autophagy and mitochondria damage is bidirectional, since mitochondria-derived ROS production, increased DNA damage and defective DNA repair can inhibit autophagy (Aumailley et al., 2015; Hariharan et al., 2011; Li-Harms et al., 2015; Scherz-Shouval et al., 2007; Sciarretta et al., 2013; Song et al., 2014). Thus, it is conceivable that excessive ROS production and mitochondria damage with age impairs autophagy in cardiomyocytes, but this has not yet been unambiguously demonstrated.

In summary, accumulation of damaged mitochondria and consequent dysfunction of cardiomyocytes with age is likely the consequence of defective quality control systems. This thesis deals with the identification of one such control mechanism that preserves mitochondrial quality in cardiomyocytes.

2.3.4. Mitochondria quality control and inflammation

Along with mitochondrial dysfunction, sterile chronic inflammation is a hallmark of aging, a process termed **inflammaging** (Baylis et al., 2013; Picca et al., 2017; Salminen et al., 2012) that also affects the cardiac tissue (Wang and Shah, 2015). The two phenomena may be causally linked since damaged mitochondria and mitochondria derived-compounds are strong activators of inflammation (Weinberg et al., 2015). In this context, free mtDNA, extracellular ATP, ROS, N-formyl peptides, Mitochondrial transcription Factor A (TFAM) and cardiolipin can function as DAMPs that are released

in response to cell stress (Krysko et al., 2011; Little et al., 2014; Nakahira et al., 2011; Shimada et al., 2012; Tschopp, 2011; Zhou et al., 2011). DAMPs activate inflammation through different mechanism leading to caspase-1 activation and the release of proinflammatory cytokines such as Il-1β and TNFα (Baylis et al., 2013; Krysko et al., 2011), both of which are increased with age (Baylis et al., 2013; Green and Kroemer, 2004; Salminen et al., 2012). mtDNA is one of the best studied mitochondrial DAMPs. In response to cell insults it can be released into the extracellular space or cytoplasm, where it can function as an agonist for Toll-like receptors (TLRs) and Nod-like receptors (NLRs), (Collins et al., 2004; Oka et al., 2012) or for DNA sensing pathways, such as cGAS-cGAMP-STING, in which cyclic guanosine monophosphate (GMP)–adenosine monophosphate (AMP) synthase (cGAS) acts as a DNA sensor that triggers innate immune responses through the activation of STING (from Stimulator of IFN Gene) (Cai et al., 2014). In the heart, lysosomal mtDNA that escapes from autophagy in DNAse-deficient cardiomyocytes has been shown to activate TLR 9 and to cause severe myocarditis and dilated cardiomyopathy upon pressure overload (Oka et al., 2012). In contrast, autophagy prevents the release of mitochondrial-derived compounds to the extracellular space (Nakahira et al., 2011) and autophagy activation through caloric restriction or rapamycin treatment suppresses inflammation (Flynn et al., 2013; Spaulding et al., 1997). Further, caspase-1 produced upon inflammasome activation damages mitochondria and induces degradation of the key mitophagy regulator Parkin, resulting in mitophagy block (Yu et al., 2014). These series of findings provide a connection between the mitochondrial quality control machinery and inflammasome activation in the heart.

Accumulation of DAMPs has been shown to activate tissue resident macrophages and to favour leukocyte infiltration (Goldberg and Dixit, 2015). As pointed at the beginning of this introduction (points 2.1 and 2.2), heterogeneous populations of tissue-resident macrophages are now known to safeguard tissue homeostasis and to favour resolution of local inflammation (Davies et al., 2013). Reduced phagocytosis of macrophage subsets with age (Aprahamian et al., 2008; De La Fuente, 1985; Linehan et al., 2014) or phagocytic receptor mutant mice (DeBerge et al., 2017; Howangyin et al., 2016; Wan et al., 2013) may compromise disposal of cellular debris and accumulation of DAMPs in the

myocardium, which contribute to inflammasome activation and heart dysfunction. This mechanism would explain the striking protection of hearts seen in Nlrp3-deficient mice (Pavillard et al., 2017), and further provide a link between immune and cardiac dysfunctions in aged individuals.

2.4. Assisted phagocytosis and surrogated disposal of mitochondria.

2.4.1. Assisted phagocytosis

In the canonical view of phagocytosis (introduced in Point 2.2.1.), professional phagocytes engulf apoptotic cells. However, there are some examples in biology of **assisted phagocytosis**, a process in which macrophages or other specialized phagocytic cells incorporate and eliminate material coming from healthy, intact cells. Indeed, although most of the cells recycle their damaged or unwanted components through autophagy (see Point 2.3.2. and 2.3.3.), some specialized cells may require assisted phagocytosis for various reasons, as seen during erythroid and sperm maturation, neuronal health maintenance and tissue function as described below.

Primitive erythroblasts circulate as nucleated cells in mammals until embryonic day E14.5-16.5, at which point they interact witch foetal liver macrophages and start to enucleate (Kingsley et al., 2004). Upon this period of gestation and later in the adult life, a specialized unit formed by macrophages and erythroid progenitors, the erythroblastic islands, can be found in haematopoietic organs. These islands are where erythroid precursors proliferate and differentiate aided by macrophages, which provide trophic factors and eliminate the nucleus of erythroblasts to form the mature enucleated erythrocytes (Chasis and Mohandas, 2008; Chow et al., 2013). In testis, male germ cells that finalize their differentiation process shed most of their cytoplasmic components as residual bodies that are eliminated by Sertoli cells via phagocytosis, thereby removing autoantigens that may induce an autoimmune response and recycling the material as an energy source (Carr et al., 1968; Sun et al., 2010).

Interestingly, processes of transcellular degradation have also been observed in different types of neurons. For example, retinal ganglion cells of mice expel axonal protrusions containing mitochondria at the optic nerve head, which are degraded by

neighbouring astrocytes (glial cells) (Davis et al., 2014). In the nematode *C. elegans*, touch neurons produce sub-particles of 3-4 µm diameter at neural soma containing mitochondria and protein aggregates which are captured by distant coelomocytes (Melentijevic et al., 2017). A similar assisted phagocytosis is involved in the turnover of photoreceptor outer segments by retinal pigment epithelial cells in the retina, which is crucial for maintain photoreceptor cells alive (Kim et al., 2013). Finally, astrocytes can specifically phagocytose synapses in the CNS, maintaining the rest of the cells intact, in a process termed synaptic pruning (Chung and Barres, 2012; Chung et al., 2013; Paolicelli et al., 2011).

Similar to canonical phagocytosis, many of these phagocytic events have been shown to be dependent on PS exposure in the phagocytosed material (Gyorffy et al., 2018; Lu et al., 1999; Ruggiero et al., 2012; Yoshida et al., 2005) and multiple receptors and specialized proteins in the phagocytic cells are required for PS recognition and uptake of the material. Among these receptors and protein mediators are Mertk, Emp and CD163 in macrophages from erythroid islands (Fabriek et al., 2007; Soni et al., 2006; Toda et al., 2014); Tyro3, Axl, Mertk and Bal1 in Sertoli cells (Lu et al., 1999; Sun et al., 2010); Mertk, Mfge8 and Itgb5 in Retinal pigment epithelial cells (Feng et al., 2002; Gal et al., 2000; Ruggiero et al., 2012); and Mertk, Mefg10 and Complement receptor 1 in astrocytes for synaptic pruning (Chung et al., 2013; Gyorffy et al., 2018). Failure of these processes, e.g. by genetic defects in one of these receptors, leads to major disturbances in tissue function such as anaemia (Soni et al., 2006), autoimmune disease (Nagata, 2007), male infertility (Lu et al., 1999); blindness (Gal et al., 2000) and altered brain development (Paolicelli et al., 2011).

2.4.2. Surrogated transfer of mitochondria

In the last few years, mitochondria have been shown to be horizontally transferred between mammalian cells. In some cases, this transfer promotes the incorporation of exogenous mitochondria into the mitochondrial network of recipient cells, contributing to changes in their bioenergetic profile and in other functional properties of recipient cells (Ahmad et al., 2014; Hayakawa et al., 2016; Islam et al., 2012; Moschoi et al., 2016; Tan et al., 2015; Torralba et al., 2016). In other rare cases, transferred mitochondria have

been reported to be degraded by recipient cells, thus resulting in surrogated disposal of mitochondria. Indeed, transcellular degradation of mitochondria (a process termed **"transmitophagy"**) has been observed in retinal ganglion cells at the optic nerve head (Davis et al., 2014). For retinal ganglion cells this process accounts for the majority of mitochondrial turnover, rather than mitochondria degradation by autophagy in the ganglion cell soma. The most likely reason for this mechanism is that it is energetically beneficial to transfer mitochondria to neighbouring astrocytes, which have high phagocytic activity, rather than to transport axonal mitochondria back to the soma for degradation (Davis and Marsh-Armstrong, 2014). Interestingly, mesenchymal stem cells (MSCs) have been shown to be able to transfer mitochondria to other cells both *in vitro* and *in vivo* (Rodriguez et al., 2018; Torralba et al., 2016) and damaged MSCs are able to transfer deleterious mitochondria to macrophages, which could in principle improve their own survival (Phinney et al., 2015). Finally, similar transcellular degradation of mitochondria occurs in gametes upon fertilization, in which sperm mitochondria are actively degraded by oocytes by the same molecular machinery used in autophagy (Al Rawi et al., 2011; Sato and Sato, 2011). Despite these examples, surrogated disposal of mitochondria remains a poorly explored process of unknown significance. In this thesis, we uncover a phenomenon of surrogated mitophagy in the adult mammalian heart that suggests a stronger reliance of tissue homeostasis on this mechanism than previously anticipated.

3. Objectives

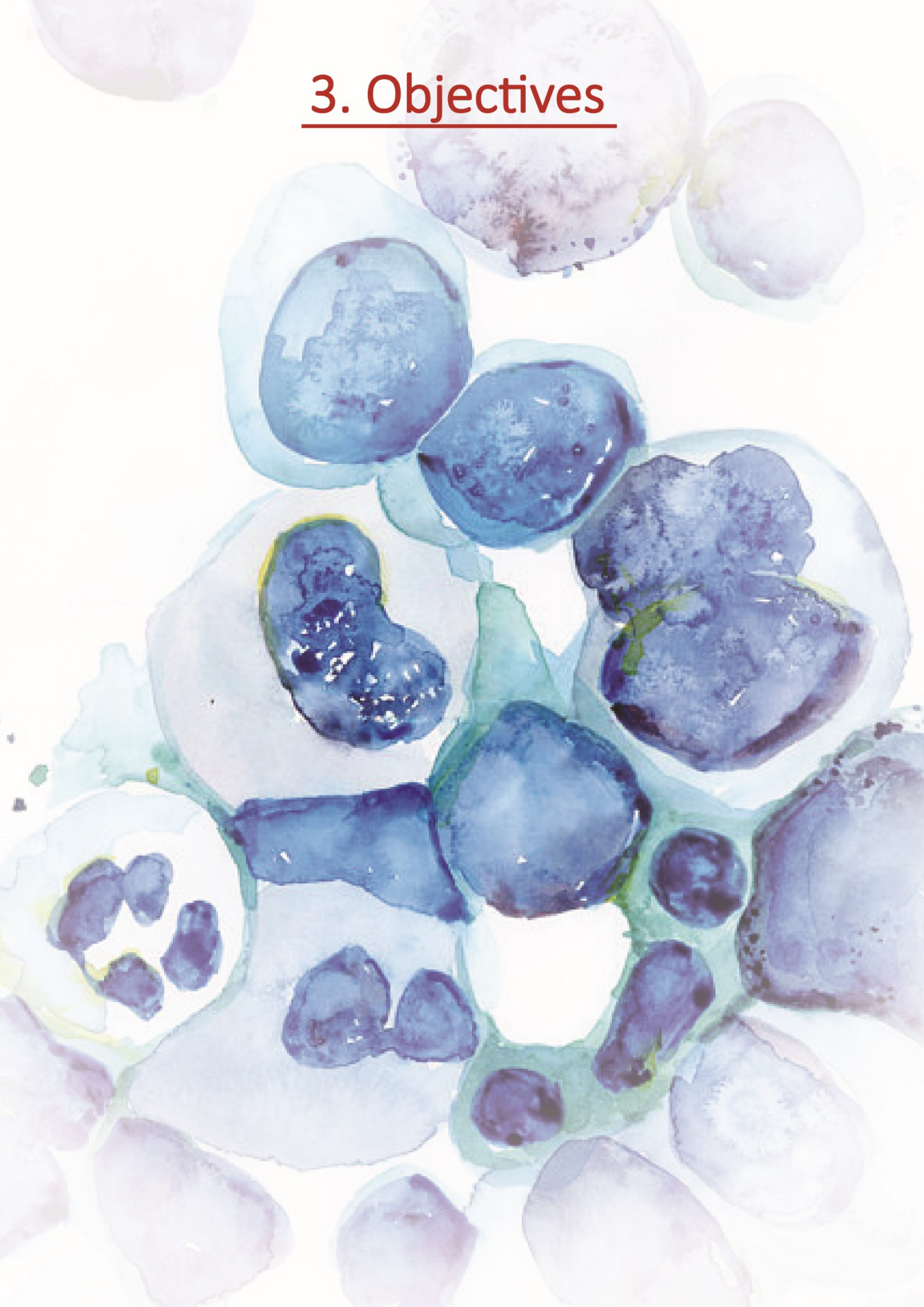

3. Objectives

In 2012, a population of tissue-resident macrophages was described in cardiac tissue of mice. Although much work has been done by other laboratories in addressing their origins and heterogeneity during the course of this thesis, the general contribution of cardiac tissue-resident macrophages to tissue function remains elusive.

Initially, the main aim of this thesis was the characterization of cardiac tissue-resident macrophages and their contribution to general tissue function. In the process, we found an intriguing process by which cardiomyocytes produce large particles, which we named *cardiac exophers*, that are phagocytosed by surrounding macrophages. Thus, we also focused in the definition of this process, identification of the cargo in cardiac exophers, mechanism of exopher production as well as their recognition and elimination by cardiac tissue-resident macrophages.

The specific objectives are the following ones:

1. Characterize tissue-resident macrophages in adult hearts at the phenotypic level, as well as their distribution patterns and phagocytic activity.

2. Define the content and production mechanism of particles produced by cardiomyocytes and phagocytosed by cardiac-resident macrophages.

3. Analyse the functional significance of this process in models with defective cardiac tissue-resident macrophages.

4. Resuts

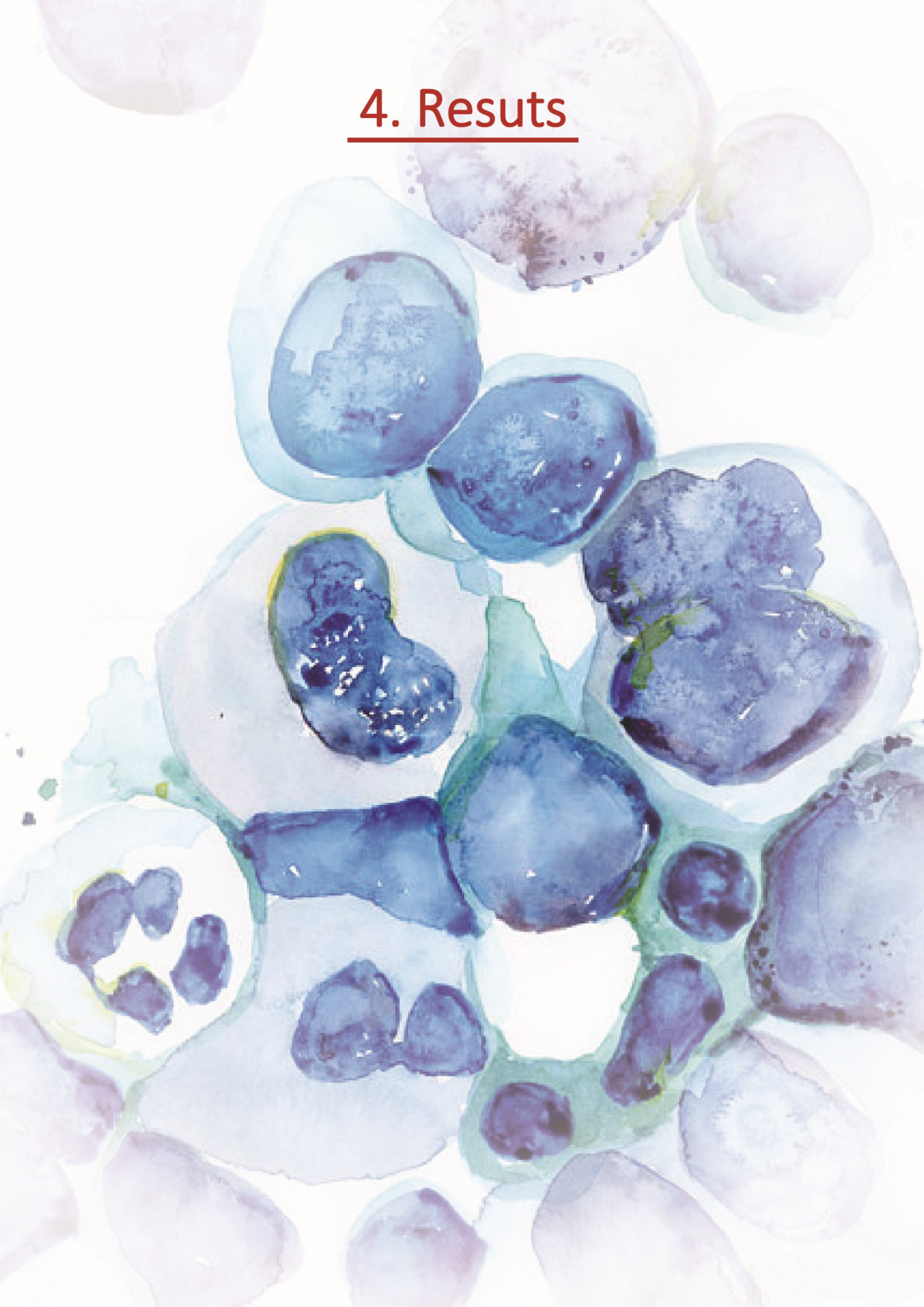

4. Results

4.1. Characterization of tissue-resident macrophages in adult hearts (cMacs).

Macrophages display high heterogeneity among different tissues and even within a single tissue. A population of macrophages was described in the murine heart in 2012, the cardiac tissue-resident macrophages (cMacs). However, many aspects of cMac biology and their function in healthy myocardia are still unknown. In order to clarify the function of these cells we aimed to assess different properties of those cells.

4.1.1. Definition and phenotypic characterization.

Initial characterization of cMacs was done based on GFP expression in CX3CR1$^{GFP/+}$ mice (Pinto et al., 2012). However, this is a gene also expressed by other immune cells including monocytes and dendritic cells (Jung et al., 2000). Thus, after the initial description of cMacs other laboratories tried to optimize a gating strategy using auto-fluorescence and alternative surface markers in order to avoid the use of reporter mice to define those cells by FACS (Epelman et al., 2014a; Molawi et al., 2014).

Following previous reports (Epelman et al., 2014a), we defined macrophages as CD45, CD11b, F4/80 and MHCII positive cells in the myocardium, with 3 main subsets characterized by differential expression of MHCII and Ly6C: MHCII^{hi} Ly6C^{NEG} (hereafter **cMac1**), MHCII^{lo} Ly6C^{NEG} (hereafter **cMac2**), and **Ly6C+** macrophages (Fig.1a). Consistent with their macrophage identity, these cells featured large phagolysosome-like vacuoles indicative of active phagocytosis (Fig.1b). Combined, the three cMacs subsets account for 49.7 ± 2.6% of total leukocytes (CD45+ cells) in the heart. Within total cMacs, cMac1 subset is the most abundant (59.5 ± 1.8% of total cMacs), followed by cMac2 (24.9 ± 1.1% of total cMacs) and then the Ly6C+ subset (12.2 ± 1.2% of total cMacs). We confirmed that cMacs have myeloid origin as determined by GFP expression in

Cx3cr1^{GFP}, MAFIA (a Csf1r-GFP reporter) and LysM^{GFP} reporter mice (Burnett et al., 2004; Faust et al., 2000; Hulsmans et al., 2017; Jung et al., 2000) (Fig.1c).

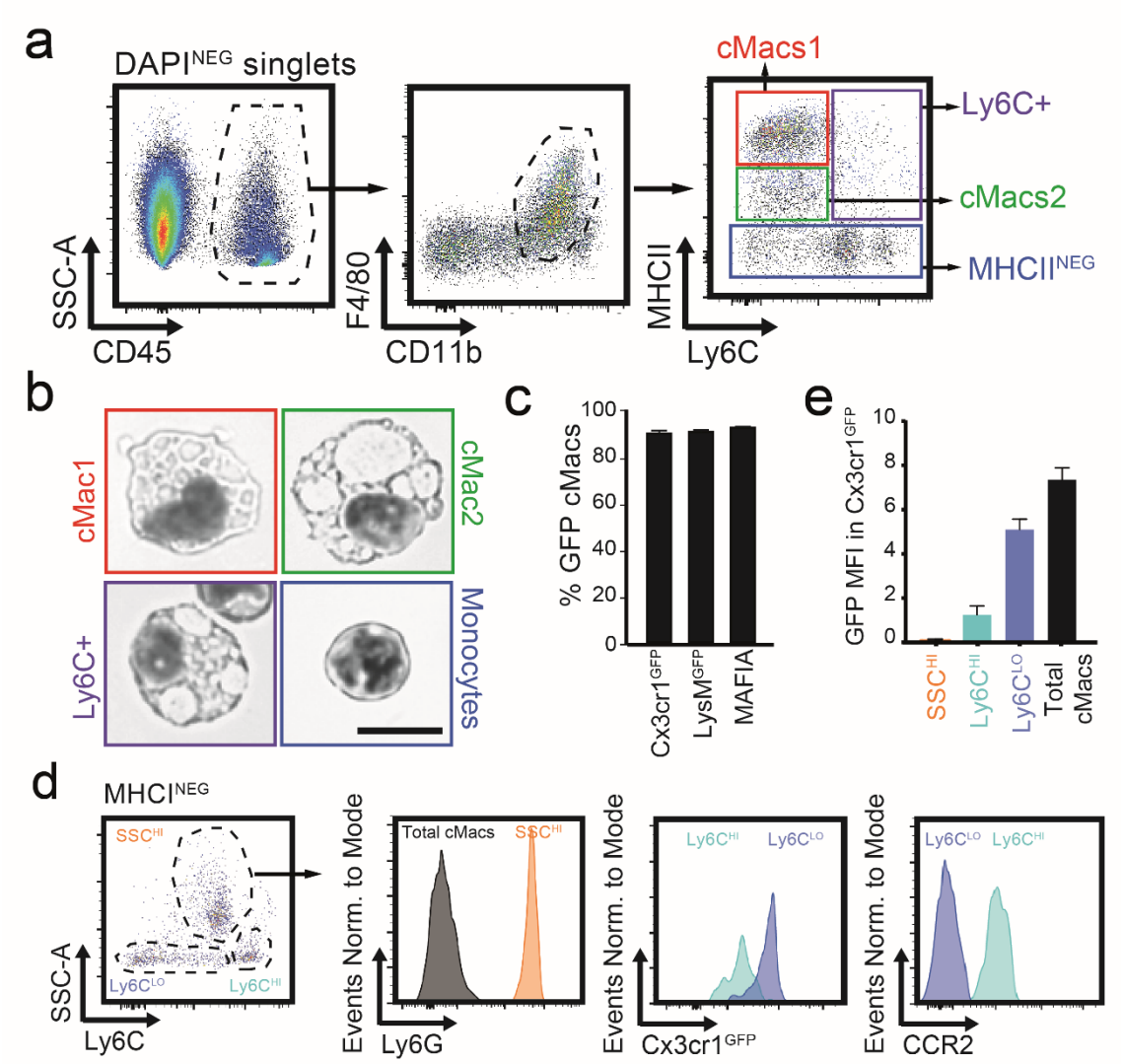

Figure 1. cMacs definition by flow cytometry and myeloid origin.

(a) Gating strategy used to identify cardiac macrophage subsets by flow cytometry. **(b)** Bright-field images of sorted and cytospined cardiac leukocytes corresponding to the subsets in (a), and stained with Giemsa. Note the presence of large phagolysosomes-like vacuoles in cMacs that are absent in monocytes. **(c)** Percentage of GFP+ within total cMacs in CX3CR1^{GFP}, LysM^{GFP} and MAFIA reporter mice. Bars are mean ± SEM from 3-6 mice per group. **(d)** Dot plot (Left) and Histograms (Right) for MHCII^{NEG} cells identified in panel (a). **(e)** GFP mean fluorescence intensity (MFI) for different leukocyte subsets in CX3CR1^{GFP} mice as defined in (a) and (d).

In order to better define our gating strategy, we examined if other myeloid cell types (e.g., monocytes and neutrophils) might be present in the myocardium under steady-state conditions, potentially contaminating our cytometric strategy. Epelman and colleagues found that very few CD11c+ CD103+ dendritic cells (DC) populate the

myocardium (Epelman et al., 2014a), and thus we discarded DCs. We found some MHCII^{NEG} cells in our CD45+ CD11b+ F4/80+ gate that were not present in their report (Fig.1a). We identified a fraction of SSC^{hi} cells within this gate with Ly6G expression, which is characteristic of neutrophils (Fig1.d). However Ly6G+ neutrophils in the steady state were scarce (6.9 ± 0.5% of total leukocytes) indicating little contribution to our cMacs population. We could also identify within this MHCII^{NEG} population the two monocyte subsets that were previously characterized in inflamed heart: the "pro-inflammatory" (Ly6C^{hi} CX3CR1^{low} CCR2^{hi}), and the "patrolling" or "anti-inflammatory" (Ly6C^{low} CX3CR1^{hi} CCR2^{low}) (Fig1.d) and (Nahrendorf et al., 2007). The latter are more abundant in steady state (around 64.1 ± 4.6% of total monocytes) while the first are present in low numbers (35.9 ± 4.6% of total monocytes) (Fig1.d). The abundance of monocytes in the steady-state was low (8.1 ± 0.7% of total monocytes) in comparison to cMacs, and they have lower GFP expression in Cx3cr1^{GFP} model (Fig1.e).

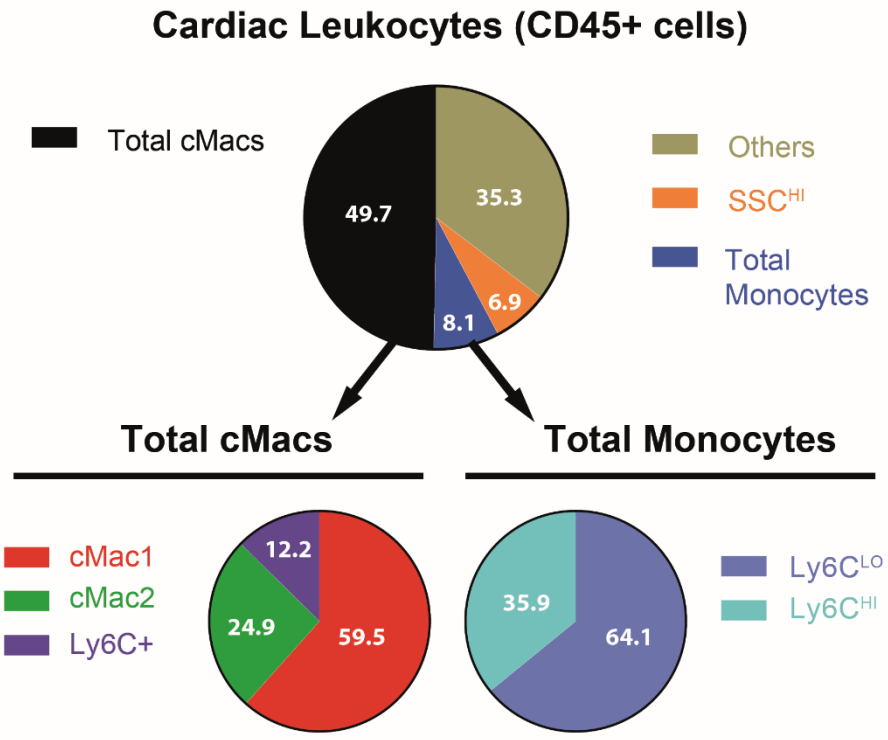

Figure 2. Distribution of cardiac leukocyte cell types.

Relative cell numbers of cardiac leukocyte as determined by flow cytometry. Note that cMacs subsets combined (Total cMacs) constitute almost 50% of all leukocytes present in the steady-state myocardium.

Thus, there is a measurable population of macrophages in the heart that accounts for about half of the total leukocytes present in the heart in steady-state (Fig.2) and can be defined by their F4/80 and MHCII expression. Although some neutrophils and monocytes are present in the heart, they are in low numbers in the steady-state and can be easily discriminated from cMacs using antibodies against MHCII or GFP expression in $Cx3cr1^{GFP}$ mice (Fig.1a and Fig.1e).

4.1.2. Distribution in cardiac tissue

Because histology studies on murine cMacs in steady state are largely missing, we decided to examine macrophage distribution in the hearts of $CX3CR1^{GFP/+}$ mice. The easy discrimination of macrophages form other cells in this model made $CX3CR1^{GFP/+}$ mice a preferred tool for our analyses when compared to the LysM-GFP strain, in which other myeloid cells are also GFP+ (Casanova-Acebes et al., 2018), or the MAFIA strain, in which monocytes have higher GFP expression than Macrophages (Evrard et al., 2015).

To examine the global distribution of cMacs in detail, we optically cleared hearts from healthy $CX3CR1^{GFP/+}$ mice and performed whole-organ imaging. GFP+ cMacs were ubiquitously distributed (Fig.3a, and Movies S1-2), with an estimate of about 3×10^5 cells per heart, an estimation that was comparable to those obtained by FACS. Although a previous work reported higher density of cMacs in the atrio-ventricular node (Hulsmans et al., 2017), we did not find increased accumulation in that area or any other area in the heart. Contrary, cMacs displayed an even distribution in the myocardium around both ventricles and the septum (Fig.3b).

To analyse the micro anatomical distribution of macrophages in wild type (WT) mice, we used antibodies against CD68 (Gordon et al., 2014). Macrophages were typically located between cardiomyocytes, but also in proximity to blood vessels and in the pericardium (Fig.3c). These cells were aligned to the fibers and showed spindled or round shapes, depending on the orientation of the myocardial fibers (Fig.3c).

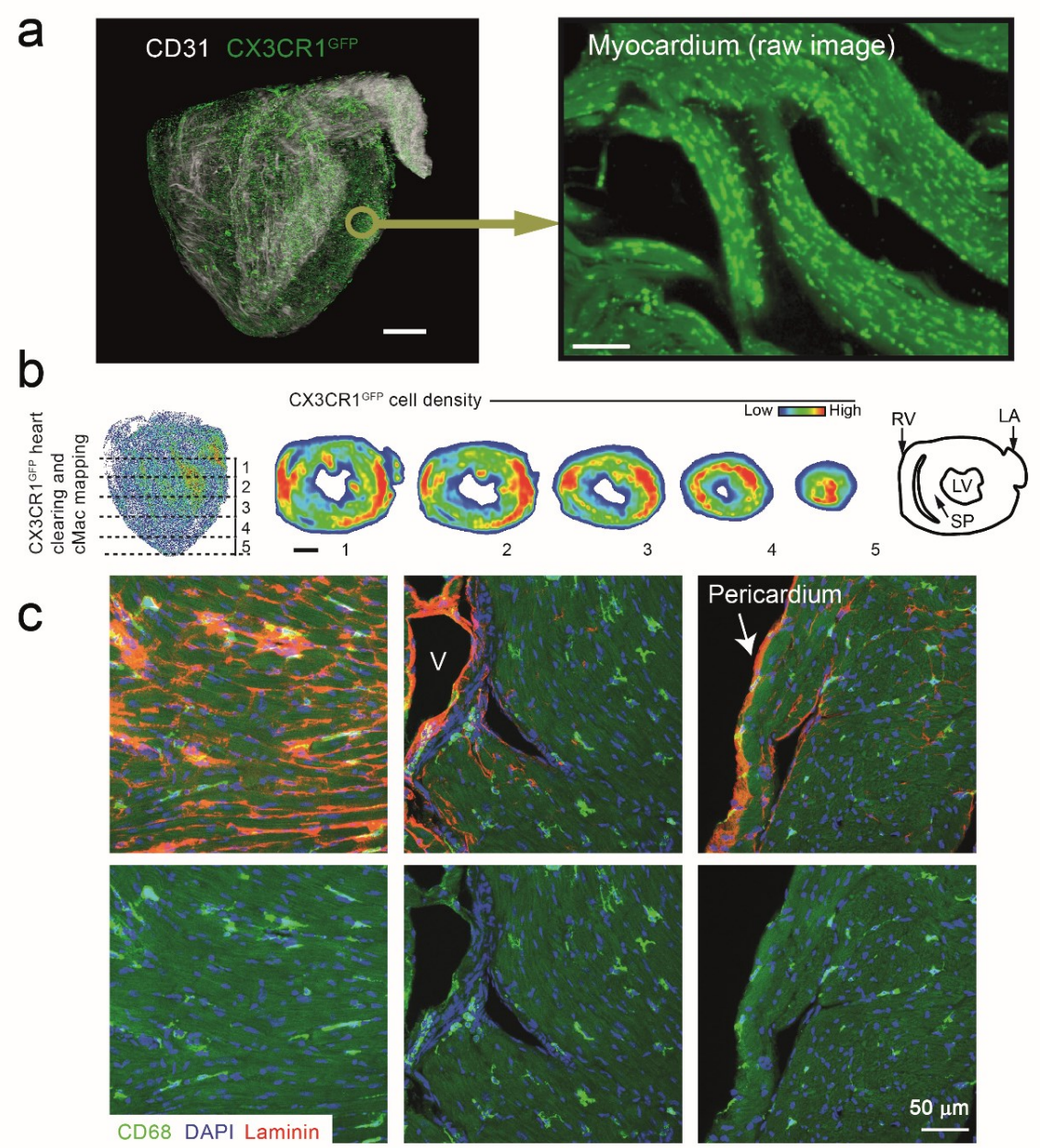

Figure 3. cMac distribution in the healthy myocardium.

(a) Heart imaging. 3D reconstruction of a whole optically-cleared heart from a CX3CR1^{GFP} mouse imaging by light sheet microscopy, showing the distribution of cMacs (CX3CR1^{GFP}+ cells), and green vessels (CD31, white). Inset at right is a high-magnification raw image of the myocardium showing the distribution of cMacs over the autofluorescent tissue. Scale bars, 1 mm (left panel) and 100 µm (inset). **(b)** Distribution of cMacs in same hearts in (a). Left, whole heart with each dot representing one CX3CR1^{GFP}+ cMac. Right, optical transversal sections (655 µm thick, indicated with numbers 1-5) pseudo-colored to display cMac densities. Far right, scheme showing the position of the left atrium (LA), left ventricle (LV), right ventricle (RV) and Septum (SP). Scale bar, 1 mm. See also Movies 1-2. **(c)** Micrographs of WT mice showing the different micro-anatomical distribution of cMacs (CD68, green): between cardiomyocytes (Left), in perivascular regions (Middle. Vessel indicated by (V)) and in the pericardium (Right. Arrow indicates Pericardium). Nuclei (DAPI, blue) and Laminin (Grey) are also shown. Scale bar, 50 µm.

Imaging analyses of thick heart sections of CX3CR1$^{GFP/+}$ mice at higher spatial resolution revealed that, on average, each cardiomyocyte is surrounded by about five cMacs, and in turn each cMac establishes contacts with five cardiomyocytes through long cellular processes (Fig.4a-c).

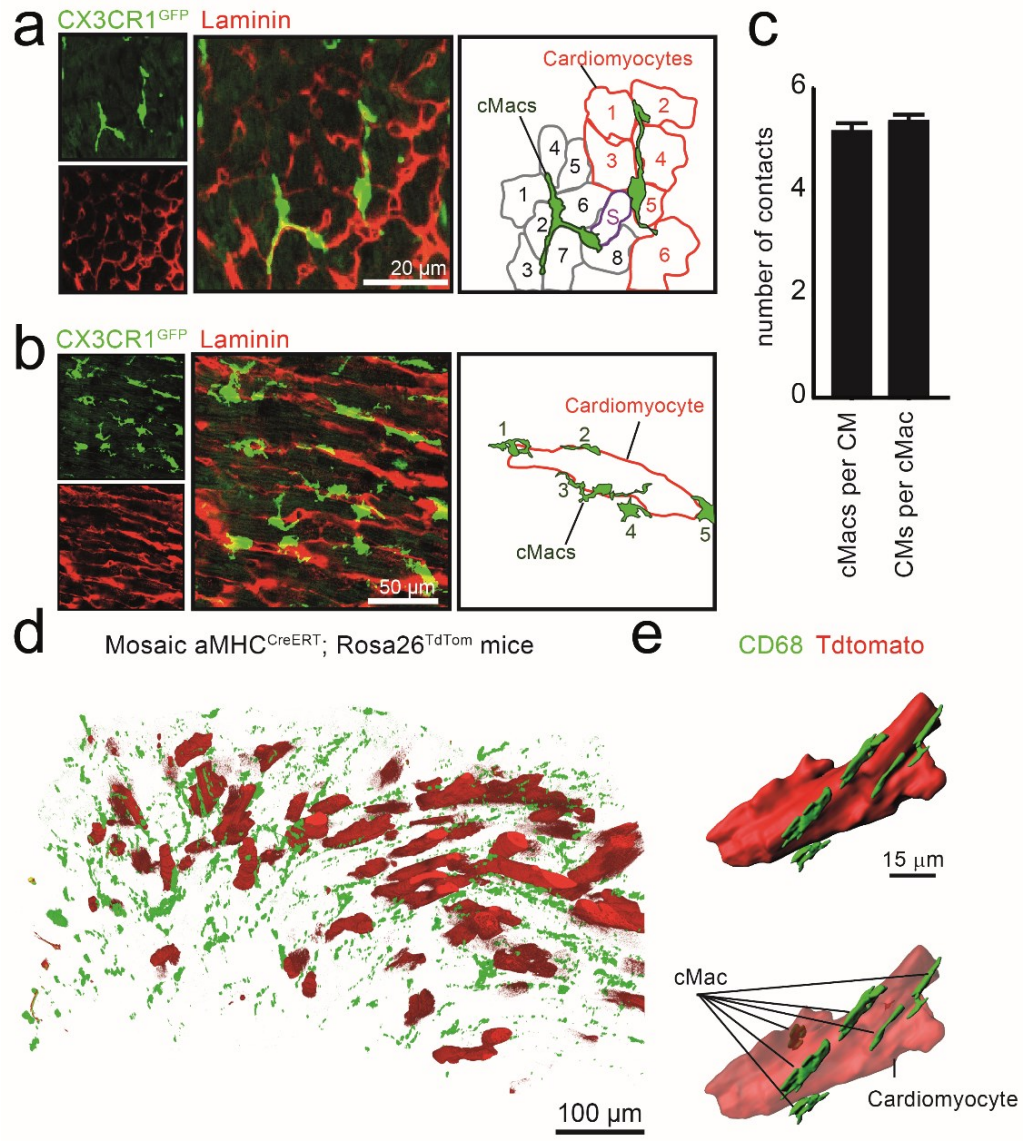

Figure 4. cMac interactions with cardiomyocytes.

(a-b) Micrographs of hearts from CX3CR1^{GFP} mice and matched schemes (right panels) illustrating contacts between cardiomyocytes, which are defined by the staining of their basal lamina with laminin (red) and cMacs (CX3CR1^{GFP}+, green) in transversal (a) or longitudinal sections (d). Scale bars, 20 µm (panel a) and 50 µm (panel b). **(d)** Quantification of the number of interactions as indicated in panels (a-b). Bar graphs show mean ± SEM, from 3 mice. **(d-e)** 3D reconstruction of a large field in the left ventricle of a αMHC^{CreERT} Rosa26^{TdTom} mouse one week after low tamoxifen administration (d) and an inset (e) showing contacts between one cardiomyocyte (tdTomato, red) and six cMacs (CD68, green). Scale bars, 100 µm (d) and 15 µm (e). Images are representative of hearts from 4 mice. See also Movie S3.

We find similar ratios in hearts of αMHC^{CreERT} R26^{Tdtom} reporter mice injected with low doses of Tamoxifen, which allows generation of Tomato+ mosaics for high resolution imaging of individual cardiomyocytes (Fig.4d-e and Movie S3). Altogether these results suggest intimate parenchymal-immune interactions in the heart, and potential housekeeping functions for cMacs.

4.1.3. Phagocytic activity of cMacs

Because the myocardial tissue is subjected to constant mechanical stress, we speculated that cMacs might facilitate removal of naturally damaged or dead cells. Consistent with this possibility, isolated cMacs, but not cardiac monocytes, featured large phagolysosome-like vacuoles indicative of active phagocytosis (Fig.1b). To explore the phagocytic activity of cMacs, we first used bone marrow transplantation to generate mice in which parenchymal cells expressed the DsRed fluorescent protein but cMacs did not, thus allowing quantification of material transfer into macrophages by gain of red fluorescence (as in (A-Gonzalez et al., 2017)). cMacs from these mice presented marked increases in fluorescence, indicating phagocytosis of material from neighbouring DsRed+ cells (Fig.5a).

To define the origin of the phagocytosed material, we generated various mouse models in which only circulating leukocytes (using parabiosis Fig.5b; (A-Gonzalez et al., 2017)), endothelial cells (Fig.5c; using Cadh5^{CreERT}; Rosa26^{TdTom} mice) or cardiomyocytes (Fig.5d αMHC^{Cre}; Rosa26^{TdTom} mice, hereafter referred to as Card^{RED} mice) expressed fluorescent proteins, and examined fluorescence gain by cMacs by flow cytometry. cMacs took up abundant fluorescent material from circulating cells as well as from cardiomyocytes and, to a lesser extent, endothelial cells (Fig.5b-d). Phagocytosis was homogenous among the different subsets of cMacs, except for endothelial cells which preferentially transfer fluorescence to Ly6C+ macrophages. Monocytes, in contrast,

incorporated little fluorescence in all the models tested (Fig.5a-d), altogether revealing that cMacs actively and specifically take up cellular material in healthy hearts.

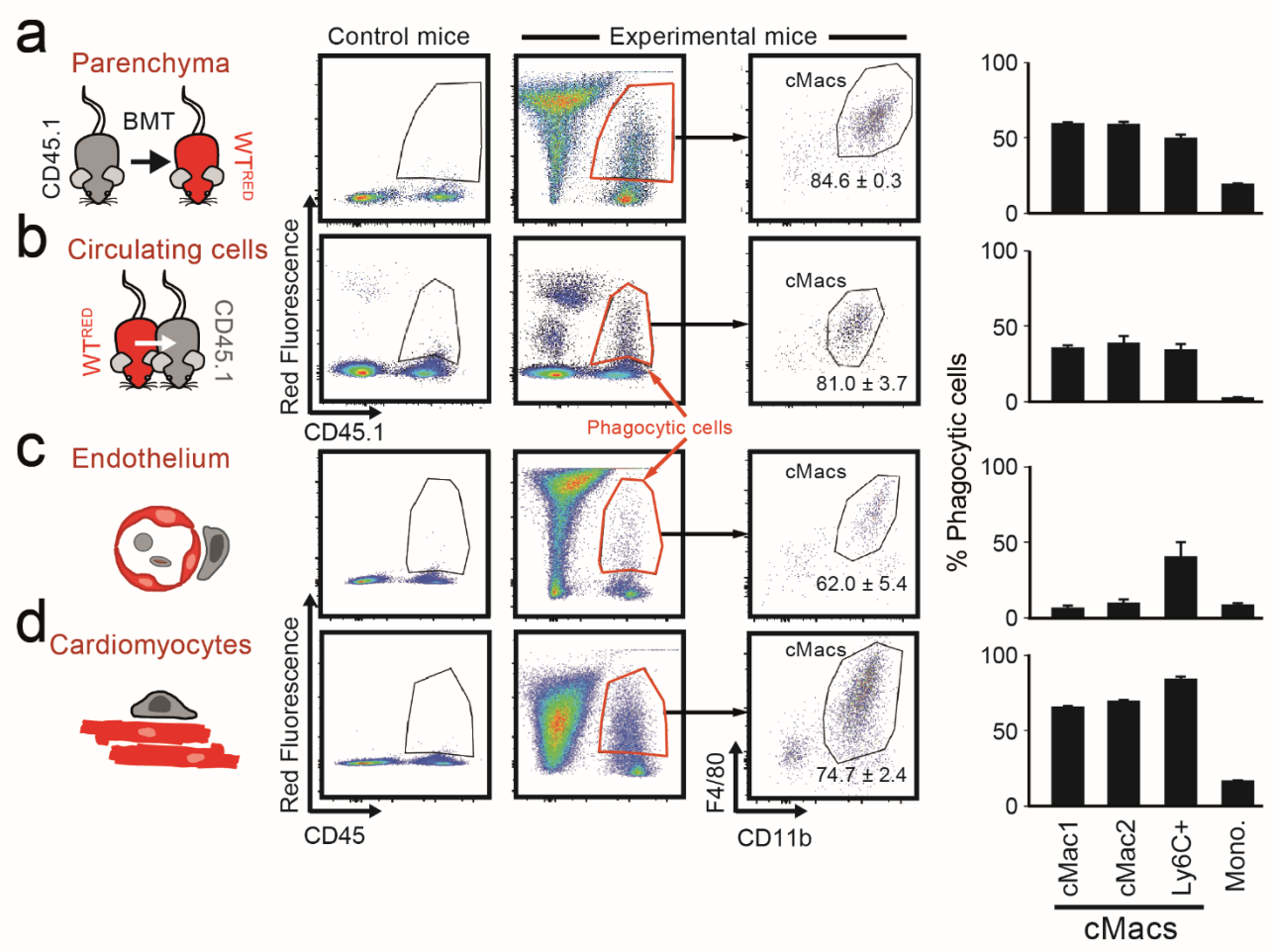

Figure 5. cMacs are highly phagocytic in the steady state.

(a-d) Cytometric identification of phagocytic cells in the heart of the indicated mouse models. Numbers in right Bar plots show mean ± SEM of phagocytic cMacs in each model, from 3-6 mice per experiment. Dot Plots show the percentage of F4/80+CD11b+ macrophages (right plots) within CD45.1+ or total CD45+ leukocytes that engulf DsRed+/Tomato+ material (middle plots) from parenchymal cells (CD45.1 BM transplanted into WT^{RED} mice) **(a)**, circulating cells (WT^{RED} x CD45.1 parabionts) **(b)**, endothelial cells ($Cadh5^{CreERT}$ $Rosa26^{TdTom}$) **(c)**, or cardiomyocytes (αMHC^{Cre} $Rosa26^{TdTom}$; $Card^{RED}$) **(d)**, respectively.

4.2. Identification and characterization of cardiac exophers.

4.2.1. Definition of cardiac exophers

Uptake of cardiomyocyte-derived material was surprising given the low death rates of these cells in the steady-state (Bergmann et al., 2009). We therefore examined the source of cardiomyocyte-derived material by confocal imaging of ventricular myocardium from Card^{RED} mice. We found, unexpectedly, numerous subcellular particles (11.5 ± 1.3 particles per 100 µm^2 tissue; Fig.6a and Movie S4) whose bright fluorescence indicated a cardiomyocyte origin; we referred to these particles as **cardiac exophers**, in analogy to similar structures recently described in *C. elegans* neurons (Melentijevic et al., 2017).

Cardiac exophers were relatively homogenous in size, with dimensions similar to those produced by neurons (mean diameter 3.5 ± 0.1 µm; mean volume 31.0 ± 2.5 µm^3), but markedly smaller than cMacs (Fig.6b) and were often found associated with or inside them (Fig.6c-d and Movie S5), indicating that exophers were part of the phagocytosed material. The proximity of exophers to cMacs could not be explained by random distribution when comparing distances from macrophages to exophers or to random dots in the same images (Fig.6e). The particulate pattern of Tomato signal inside cMacs (Fig.6d) and absence of Tomato expression in FACS isolated cMacs from Card^{RED} mice allowed us to rule out horizontal transfer of DsRed-encoding mRNA as a mechanism of fluorescence acquisition (Fig.6f). Altogether these results demonstrated active uptake of cardiomyocyte-derived exophers by cMacs in the healthy myocardium.

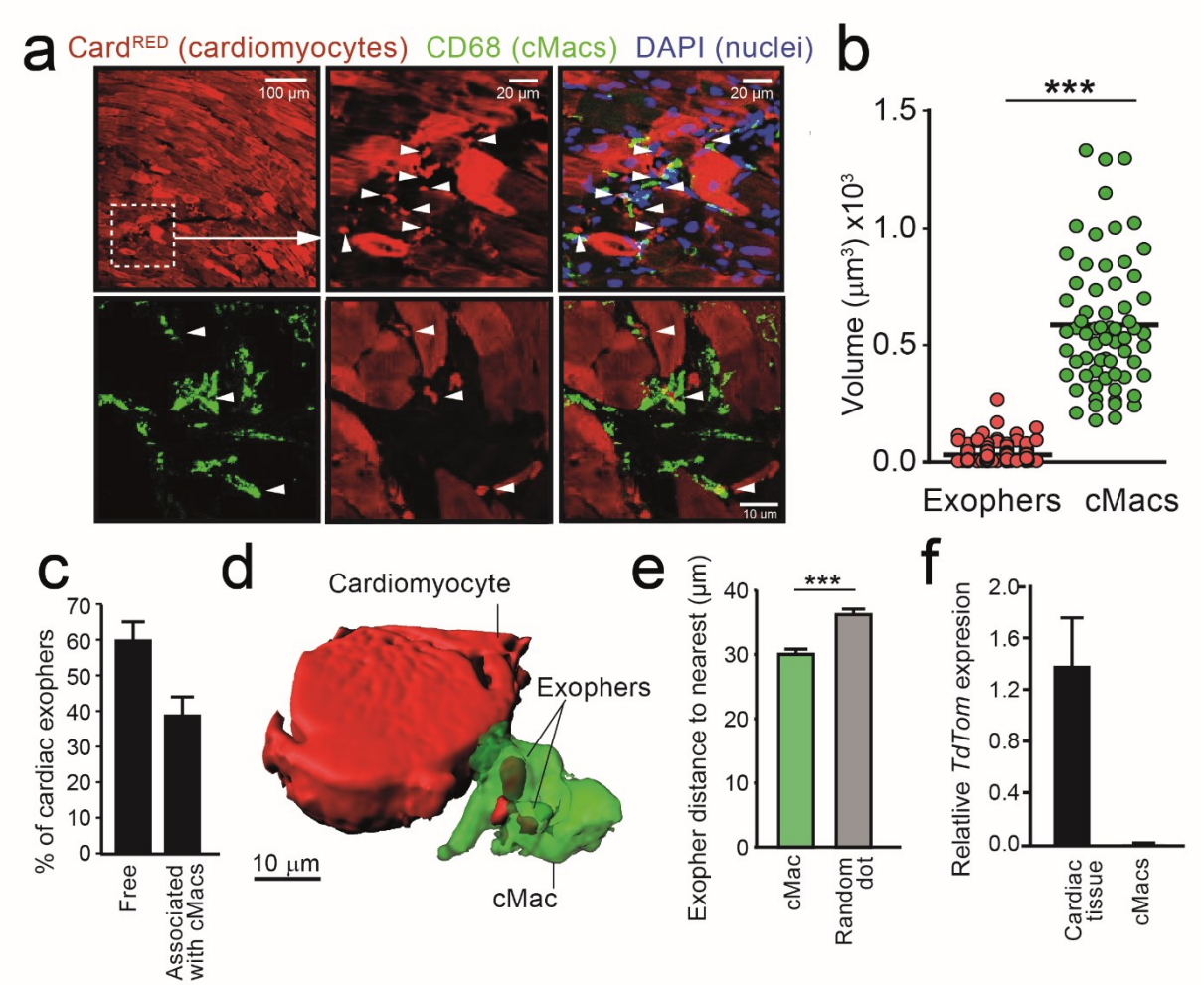

Figure 6. cMacs phagocytose cardiomyocyte-derived material through cardiac exophers.

(**a**) Low and high magnification micrographs of hearts from Card^{RED} mice illustrating the presence of cardiomyocytes and cardiomyocyte-derived exophers (white arrowheads) proximal to cMacs (green). Nuclei are shown in blue (DAPI). **(b)** Volumes of cardiac exophers and cMacs reconstructed by confocal imaging of hearts from Card^{RED} stained with anti-CD68. Data are mean volumes, from 8 mice per group. ***, p<0.001 as determined by nonparametric Mann-Whitney test. **(c)** Percentage of cardiac exophers that were associated or not-associated ("Free") with cMacs. The bar graph shows mean ± SEM, from 40 images from 4 mice. (**d**) 3D reconstructions from confocal images showing cardiomyocyte-derived exophers (red), some of which appear inside a cMac. See also Movies 4-5. Images are representative of 8 mice. **(e)** Bars indicate distance of Cardiac exophers (green) or Random spots (grey) to the closest cMac in images. Data is mean ± SEM distances for each group. Data from 30 images from 3 mice. P-value was obtained by nonparametric Mann-Whitney test. **(n)** Expression of *tdTomato* transcript in total cardiac tissue but not cMacs in Card^{RED} mice, as determined by qPCR. Bars shows mean ± SEM from 10-11 mice per group of 2 independent experiments. ***, p<0.01 as determined by Student´s t-test.

4.2.2. Cargo of cardiac exophers

Because *C. elegans* neurons use exophers as a means to dispose of protein aggregates and organelles (Melentijevic et al., 2017), we examined whether cardiac exophers accumulated similar cargo. Transmission electron microscopy (TEM) of mouse murine heart sections revealed the prominent presence of mitochondria (Fig.7a) and in rare instances sarcomere fragments inside extravascular vesicles similar in size to exophers (Fig.7b). Notably, we could find similar structures and cMacs in human samples from papillary muscles removed during surgery interventions (Fig.7c-d).

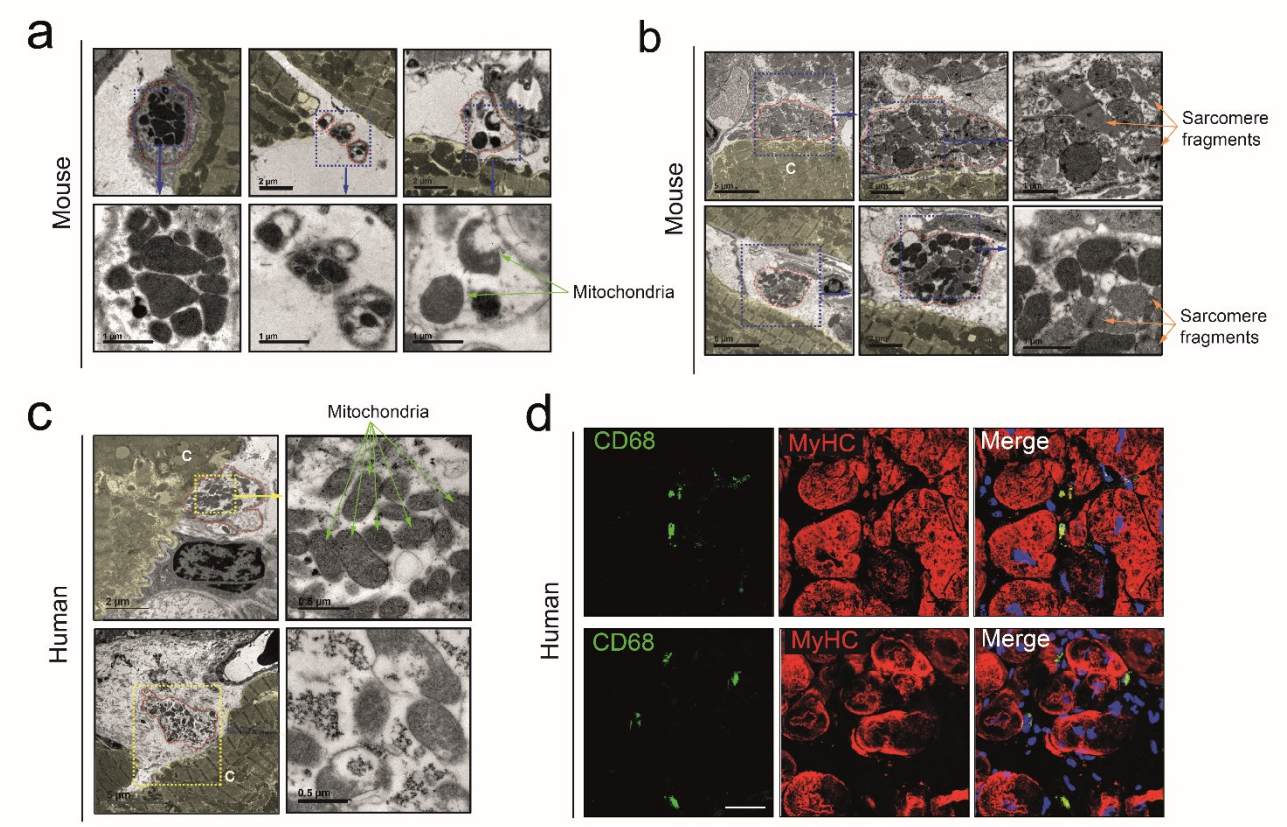

Figure 7. Visualization of cardiac exophers by TEM in mice and humans.

(a-b) Representative TEM images of mitochondria- **(a)** and sarcomere- **(b)** containing structures surrounded by membranes from murine hearts. Scale bars are 2 (top) and 1 µm (bottom) in **(a)** and 5, 2 and 1 µm (left to right) in **(b).** Images are representative of 5 hearts. **(c)** TEM imaging of similar structures in human hearts. Scale bars (left to right) are 2 and 0.5 µm. Exophers are highlighted by a red dotted line, and adjacent cardiomyocytes by a yellow mask. Mitochondria and sarcomere are pointed to with green and orange arrows. Images are representative of at least 5 hearts. **(d)** Immunofluorescence micrographs of human myocardium obtained from surgical resections of papillary muscles. Stained are macrophages (CD68, green), nuclei (DAPI, blue) and sarcomere /cardiomyocytes (MyHC; red). Images are representative of 5 samples. Scale bar, 20 µm.

To obtain a thorough characterization of the cargo contained within these particles, we purified exophers from the myocardia of healthy mice for cytometric and proteomic analyses. We used a strategy of serial precipitation and centrifugation combined with fluorescence activated cell sorting (FACS) to isolate small tdTomato^{bright} particles from pools of hearts of Card^{RED} mice (Fig.8a-b). This strategy was adapted from previous reports for the isolation of apoptotic bodies, which are in the same size-range than cardiac exophers (around 4 µm diameter; (Atkin-Smith et al., 2017)). Following this strategy, we could discard cardiomyocytes and small cardiac cells in the first two steps (50g and 300g respectively; Fig.8a and c). Subsequently, we centrifuged at 1000g to obtain pellets enriched in small TdTomato+ particles devoid of nuclei and negative for the endothelial marker CD31, that we purified by FACS sorting (Fig.8a-c).

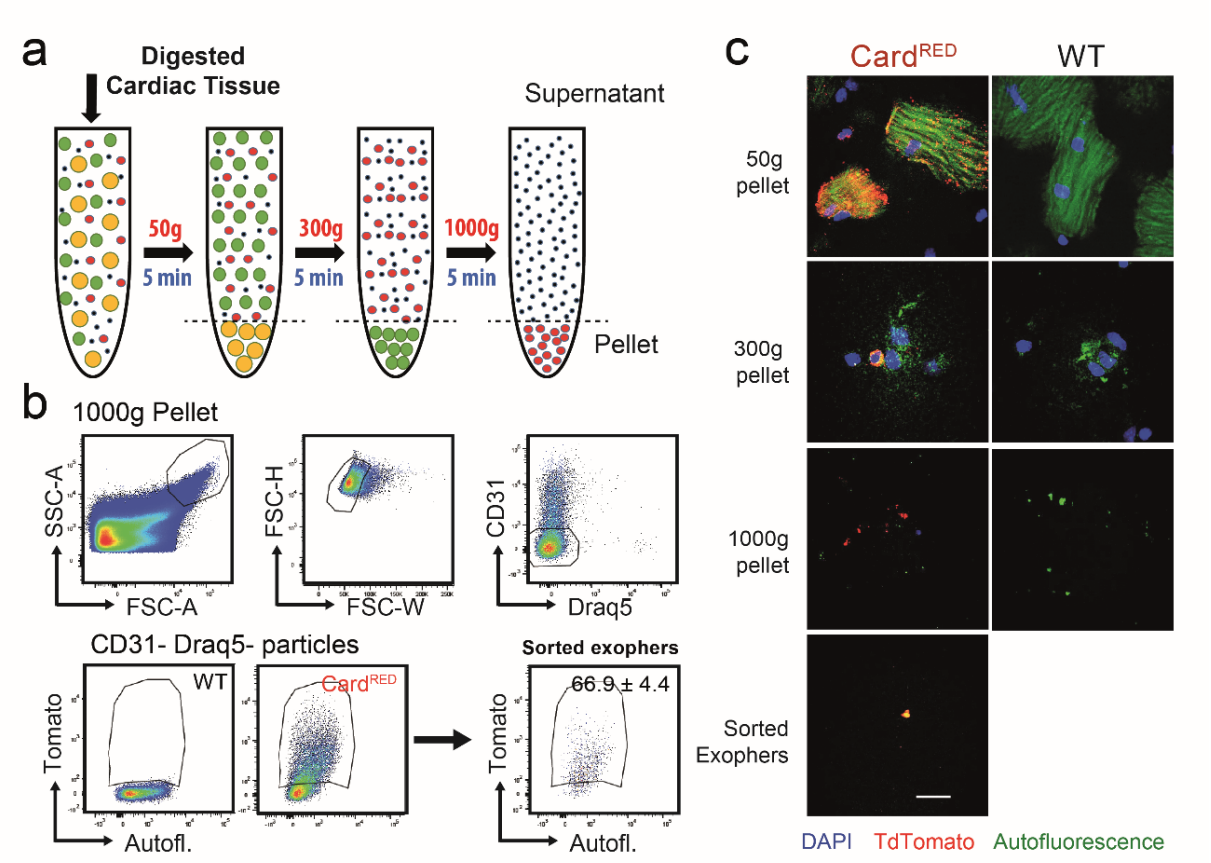

Figure 8. Isolation of cardiac exophers.

(a) Strategy for enrichment and purification of cardiac exophers by serial sedimentation and centrifugation, as indicated in the Methods. **(b)** Gating strategy used to define exophers by FACS in the 1000g pellet of Card^{RED} mice (see Methods). **(c)** tdTomato (Red) immunofluorescence in the pellet of the 50, 300 and 1000g fractions (as defined in (a)) and isolated cardiac exophers (as defined in (b)). Nuclei (DAPI, blue) and autofluorescence (green) are also shown. Scale bar 15 µm. Images are representative of 3 mice per group.

Importantly, proteomic analyses comparing the proteome of purified exophers with that of total cardiac tissue revealed remarkable enrichment of mitochondrial proteins. This contrasted with a general reduction of proteins derived from all other organelles, the membrane and the cytosol (Fig.9a-b).

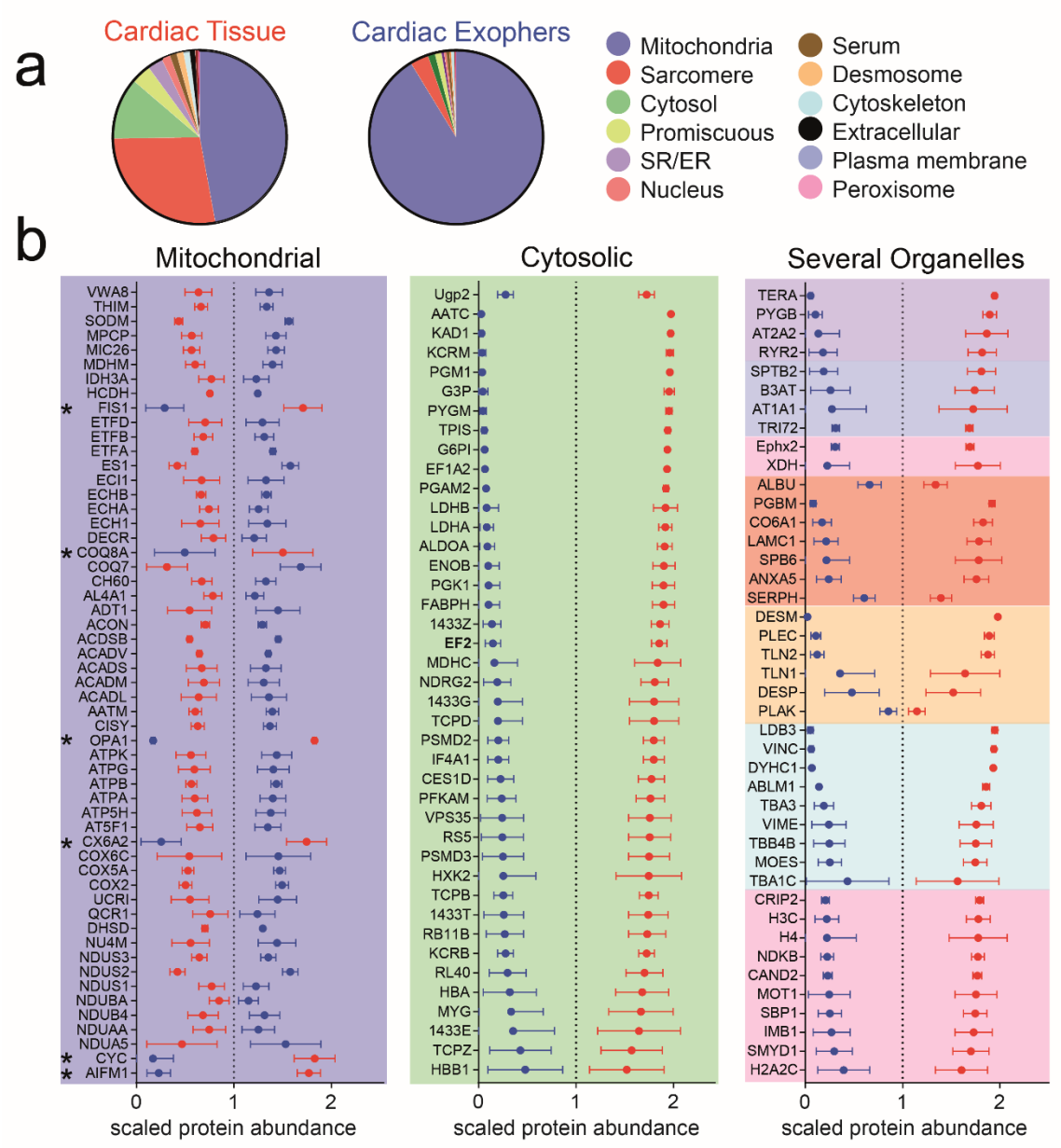

Figure 9. Proteomic analysis of cardiac exophers reveals preferential transport of mitochondria.

(a) Pie-charts showing the proteome composition of total cardiac tissue and cardiac exophers. Colors identify the cellular compartment from which the proteins originate, as shown in the legend. **(b)** List of selected proteins and their relative abundance in total heart and exopher proteomes annotated for each cellular compartment.

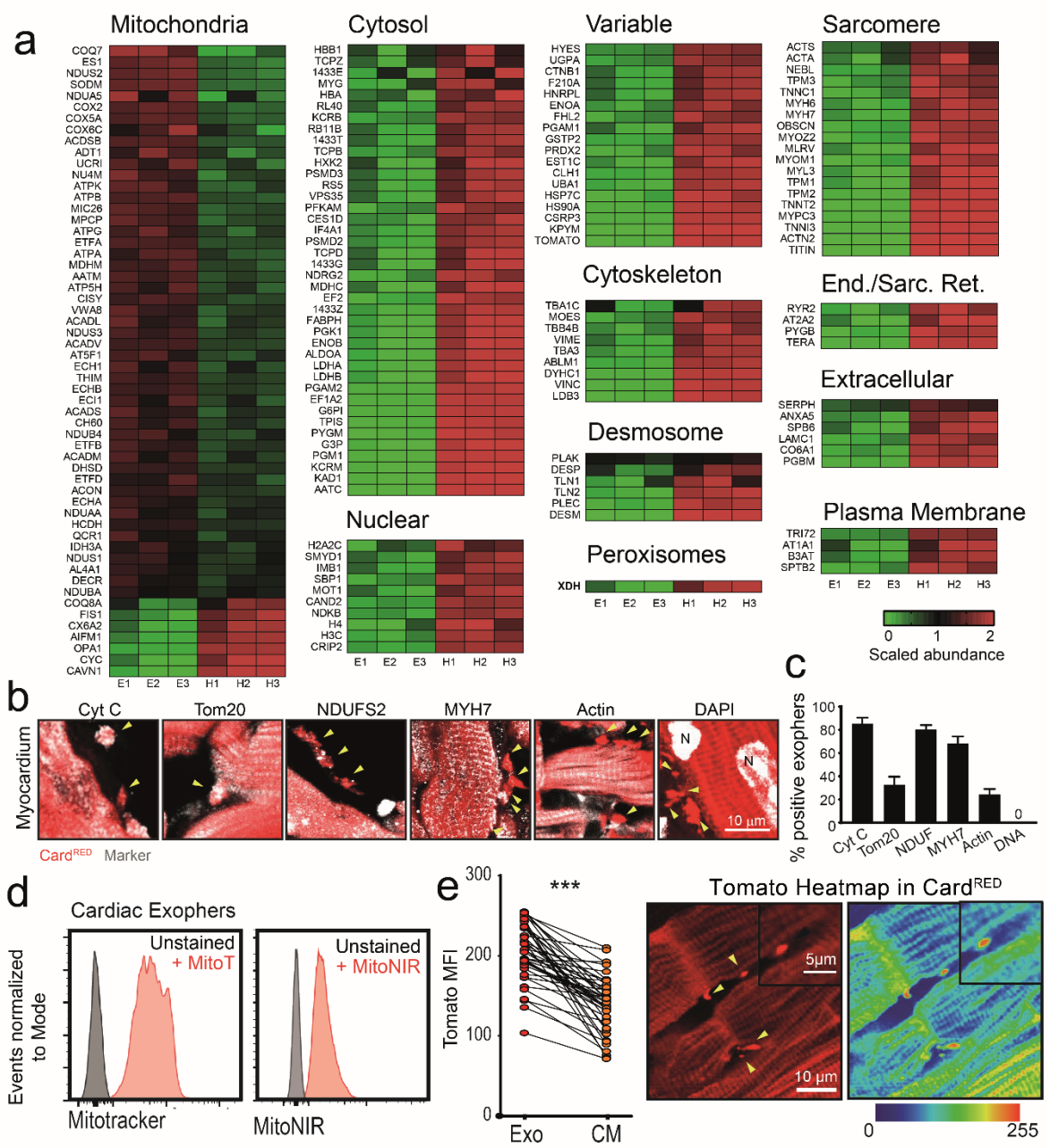

Figure 10. Validation of the exopher proteomic analysis.

(a) Full list of proteins that show statistically significant difference between exophers (E) and cardiac samples (H), as defined with adjusted p-value <0.05 for multiple Student´s t-test comparisons. **(b)** Representative sections of left ventricular sections in Card^{RED} mice (Tomato protein, red) stained for the indicated proteins (white) to score their presence in exophers (yellow arrowheads). **(c)** Fraction of exophers positive for the proteins shown in (b). Quantification from 3-6 mice. **(d)** Cytometric analyses of purified exophers stained with the mitochondria-specific probes MitoTracker and MitoNIR. Histograms are representative of 5 mice from 2 independent experiments. **(e)** Micrographs (Right) showing heatmap of tdTomato intensities in Card^{RED} mice by immunofluorescence, and dot polt (Left) showing tdTomato mean fluorescence intensities (MFI) in exophers and adjacent cardiomyocytes; data from 4 mice per group. ***, p<0.01 as determined by Student´s t-test.

It is important to highlight that, despite no enrichment in proteins other than those from mitochondria, this does imply complete absence. In fact, we were able to detect sarcomeric proteins myosin heavy chain 6 (MYH6) and 7 (MYH7) in cardiac exophers (Fig.10a), in agreement with sarcomere fragments presence in exophers analysed by TEM (Fig.7b). We confirmed the proteomic data by immunofluorescence staining of intact myocardial tissue, showing the consistent presence in exophers of the mitochondrial proteins TOM20 and NDUFS2, variable detection of CYTC, and low or no detection of myosin heavy chain 7 (MYH7), ACTIN and DNA (Fig.10b-c). Additionally, staining with two different mitochondria-specific probes confirmed the presence of mitochondria in isolated exophers by flow cytometry (Fig.10d). Finally, similar to neural exophers described in *C. Elegans* that accumulate fluorescent protein aggregates (Melentijevic et al., 2017), cardiac exophers were enriched in the fluorescent protein tdTomato, often presenting higher levels that surrounding cardiomyocytes (Fig.10e). Altogether, these data demonstrated that while exopher content is diverse, these structure are preferentially dedicated to the transport of mitochondria.

4.2.3. Cardiac exophers as a mechanism for disposal of mitochondria

Exophers were positive for the mitochondrial proteins NDUFS2 and Tom20 (Fig.10c and Fig.11a) and Tom20+ exophers could be identified inside CD68+ cMacs by immunofluorescence staining (Fig.11b and Movie S6), suggesting exopher-mediated intercellular transfer of mitochondria into cMacs. Accordingly, in our TEM analyses we could detect evidence of mitochondria-containing exophers in the periphery of cardiomyocytes taken up by adjacent cells that were akin in size and morphology with previously described cMacs (Fig.11c and (Hulsmans et al., 2017)).

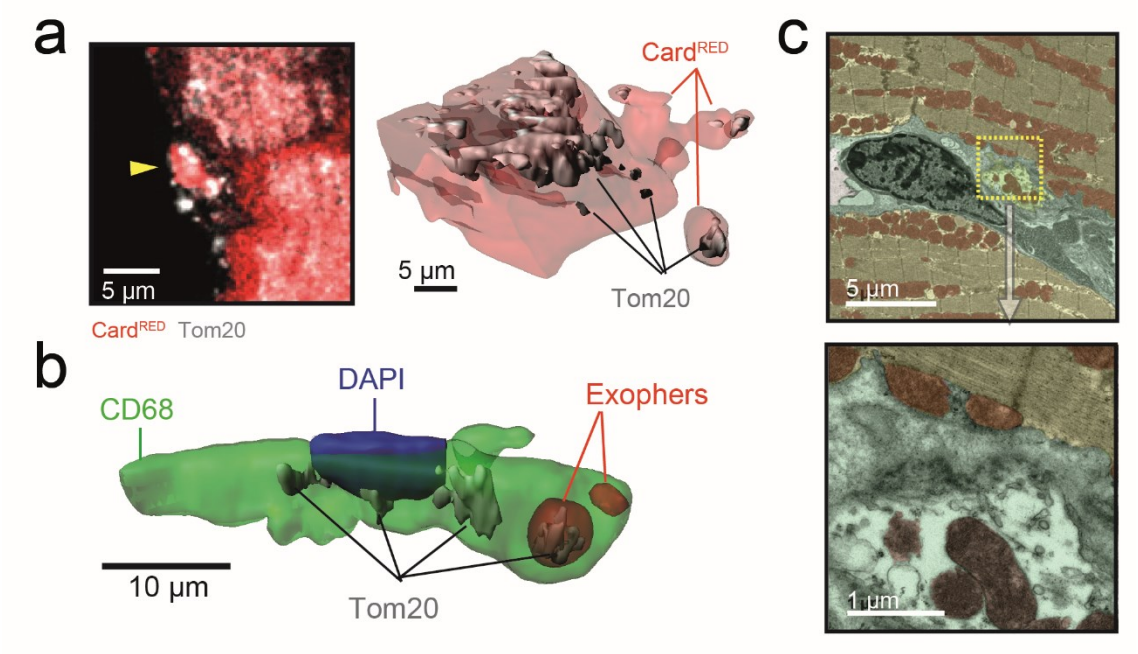

Figure 11. Cardiomyocyte-derived mitochondria are captured by cMacs.

(a) 2D micrograph of an exopher (arrowhead) containing Tom20+ material (white; left panel); right panel shows a 3D reconstruction from the heart of a Card^{RED} mouse, illustrating the presence of Tom20+ mitochondria (grey) inside cardiomyocytes and cardiac exophers (transparent red). Images are representative of hearts from 4 mice. **(b)** 3D reconstruction of a cMac from the heart of a Card^{RED} mouse containing cardiomyocyte-derived material, inside of which there are Tom20+ mitochondria. See also Movie S6. **(c)** Pseudo-colored TEM images of a mononuclear cell (green) taking up mitochondria (red) from a neighboring cardiomyocyte (yellow), at two different magnifications (dashed box).

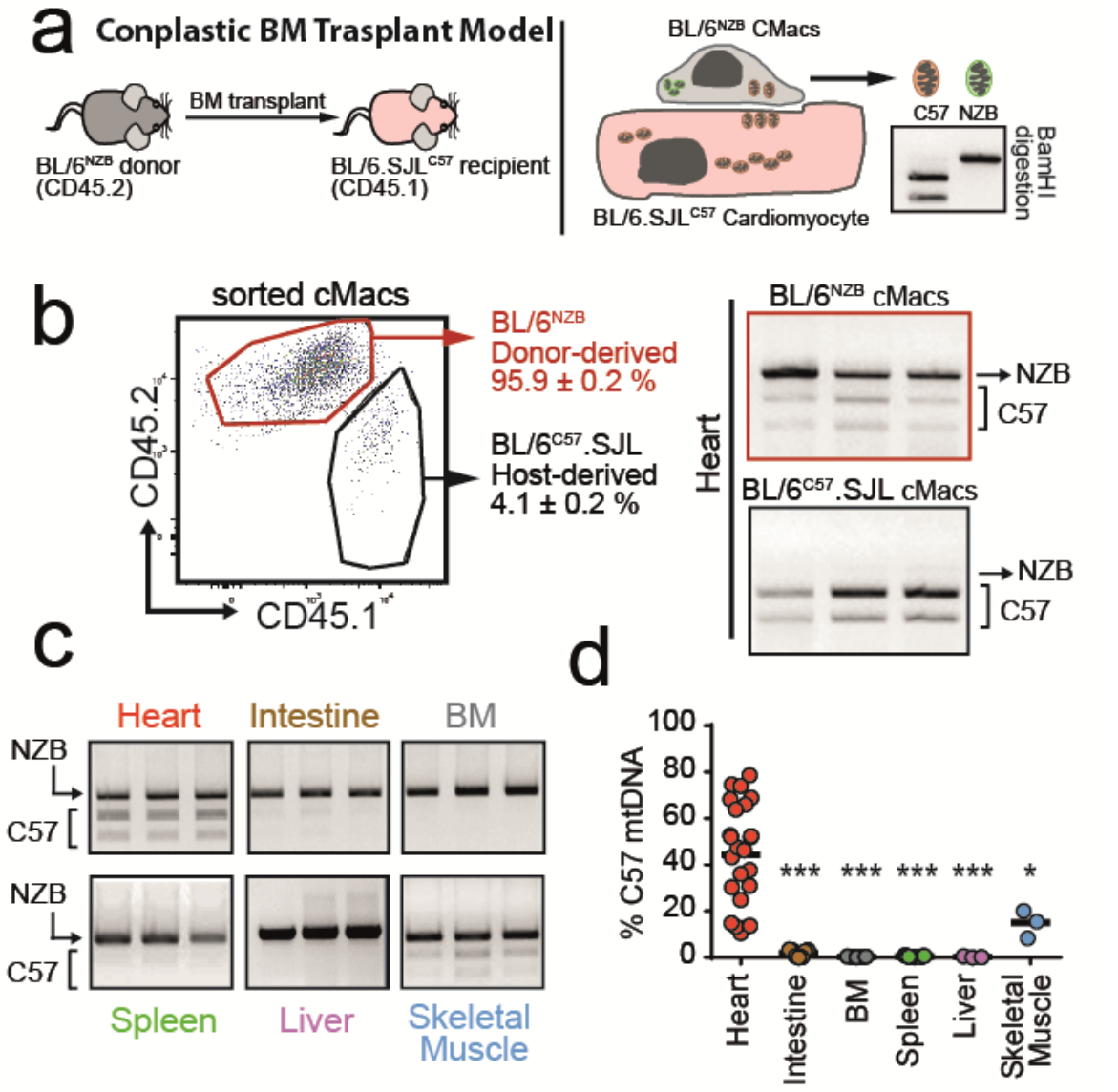

Figure 12. Mitochondrial transfer in the conplastic transplant model.

(a) Experimental strategy to track cardiomyocyte-derived mitochondrial DNA (mtDNA) in cMacs after bone marrow transplantation. cMacs from BL/6^{NZB} donors that take up mitochondria in BL/6.SJL^{C57} hearts (pink) can be sort-purified and analyzed to determine the amount of parenchymal C57-mtDNA by PCR and BamHI digestion. This allows discrimination of polymorphisms among the two mtDNA haplotypes. **(b)** Detection of C57-mtDNA in BL/6^{NZB}-derived cMacs. Note that while BL/6^{NZB}-derived cMacs contain both NZB and C57-mtDNA, BL/6.SJL^{C57}-derived cMacs only carry C57-mtDNA, indicating specificity and no cross-contamination during sorting. Percentages of donor- and host-derived cardiac macrophages are shown. Numbers are mean ± SEM, from 8 mice. **(c)** Representative PCR gels showing amplified C57 and NZB mtDNA, present in BL/6^{NZB}-derived macrophages isolated from the indicated tissues. **(d)** Plots at right show the percent amount of C57-derived mtDNA in BL/6^{NZB} macrophages sort-purified from the same tissues; BM, bone barrow. Each dot is one mouse and bars show means; n= 3-20 mice per group. **, p<0.01; ***, p<0.001; n.s., not significant as determined by kruskal-Wallis non-parametric test with multiple Dunn's comparison against Heart.

To rigorously assess transfer of cardiomyocyte mitochondria into adjacent cMacs, we used two complementary strategies. We first transplanted BL/6.SJL^{C57} mice with bone marrow from conplastic BL/6^{NZB} donors. These mouse strains have identical C57BL/6 nuclear genomes, but distinct mtDNA haplotypes, C57 and NZB respectively (Latorre-Pellicer et al., 2016). These mice also express different isoforms of *Ptprc* (which encodes CD45) that allow discrimination of donor from recipient-derived cMacs, thereby allowing identification of parenchyma-derived mitochondria in transplanted cMacs (Fig.12a-b). cMacs from BL/6^{NZB} donors purified from BL/6.SJL^{C57} hearts incorporated significant amounts of parenchymal C57 mtDNA, at much higher levels than the amount of mtDNA transferred in macrophages in multiple other tissues (Fig.12c-d), indicating tissue-specific transfer of mitochondria into cMacs.

Cardiomyocytes were a likely source of mitochondria taken up by cMacs given their contribution to the cardiac mass and high mitochondrial content (Goffart et al., 2004). To confirm that cardiomyocytes were indeed a source of transferred mitochondria, we analysed transfer of cardiomyocyte-derived mitochondrial protein. We enforced expression of a monomeric Keima fluorescent protein bearing a mitochondria-directing peptide (mt-Keima) in cardiomyocytes (Fig.13a and (Sun et al., 2015)). We ensured cell-specific transduction by using a cardiotrophic adeno-associated virus 9 (AAV9) combined with the cardiomyocyte-specific *Tnnt2* promoter to drive mt-Keima expression, and confirmed that Keima was expressed in cardiac tissue but not in cMacs (Fig.13b-c). Immunofluorescence staining of wild-type hearts five weeks after viral transduction revealed that a significant fraction of mt-Keima+ particles typically appeared inside CD68+ macrophages, indicating that cardiomyocyte-derived mitochondria were taken up by cMacs (Fig.13d and Movie S7).

The mt-Keima protein changes its excitation wavelength at different pH, displaying a bimodal excitation spectrum with peaks around 440 and 586 nm in neutral and acidic solutions, respectively (Sun et al., 2015). Thus, this strategy additionally allowed us to identify basic or acidic environments for individual mitochondria, such as those existing in the cytoplasm vs. phagolysosomes, respectively.

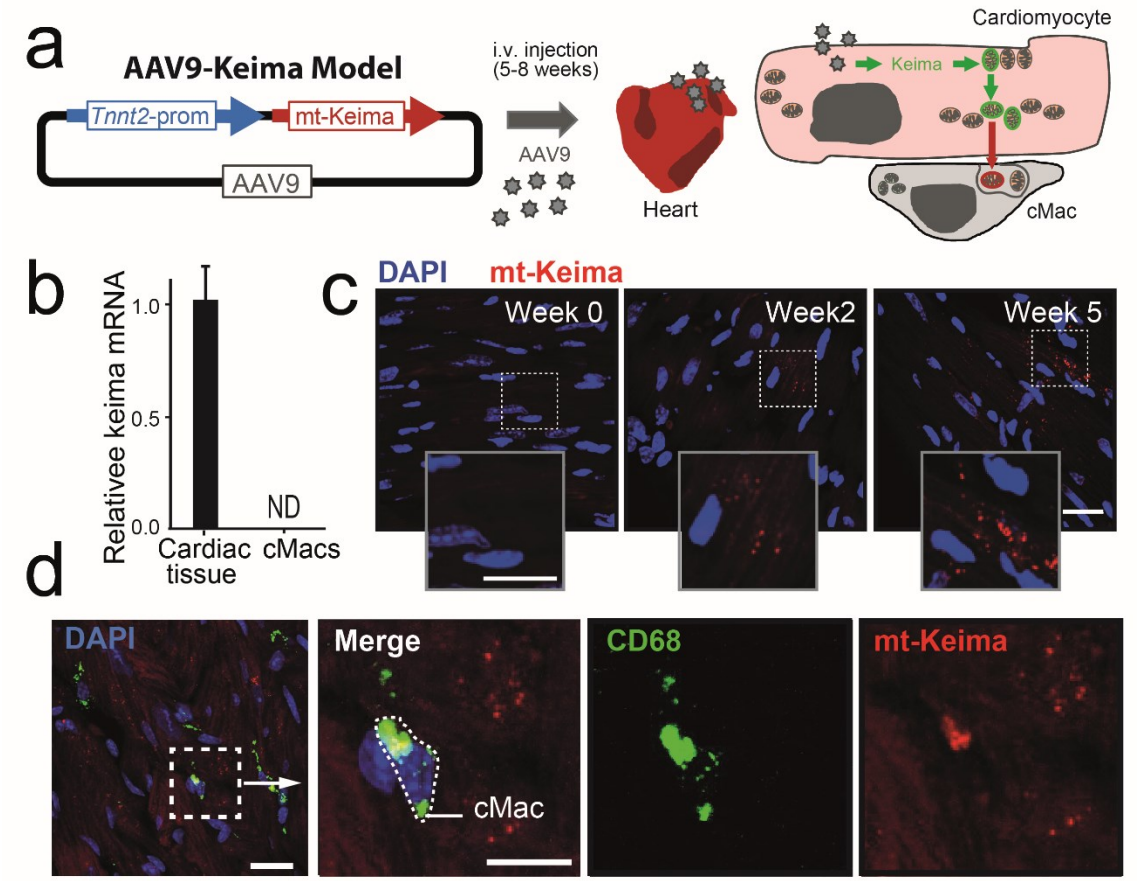

Figure 13. Mitochondria transfer in AAV9-mtKeima infected hearts.

(a) Experimental design to tag cardiomyocyte mitochondria with mt-Keima. Mice were injected with AAV9 encoding mitochondrial-targeted Keima fluorescent protein (mt-Keima) and expression driven by a cardiomyocyte-specific promoter (*Tnnt2*). **(b)** Expression of mt-Keima transcript in total cardiac tissue but not cMacs 6 weeks after infection, as determined by qPCR. Bars shows mean ± SEM from 4 mice per group. ND: Not detected. **(c)** Images illustrate the progressive acquisition of mt-Keima fluorescence in infected hearts at weeks 0, 2 and 5 post infection. Scale bars, 20 µm. **(d)** Micrographs from hearts infected with AAV9-mt-Keima, showing a cluster of cardiomyocyte-derived mitochondria (mt-Keima+, red) inside a cMac (CD68+, green). Scale bars, 20 µm (left) or 10µm (right panels).

Compared with mitochondria localized within cardiomyocytes, most Keima+ mitochondria within cMacs presented an mt-Keima fluorescence ratio indicative of an acidic environment (Fig.14a-b), suggesting that they were targeted for degradation within macrophage phagolysosomes. Consistent with this possibility, the majority of mt-Keima+ mitochondria were present in macrophage compartments positive for Lamp1, a marker of late phagolysosomes (Fig.14c and Movie S7). Importantly, cMacs isolated from mt-Keima-infected hearts or from BL/6^{NZB}-transplanted BL/6.SJL^{C57} mice lost most

of the mt-Keima fluorescence or BL/6^{NZB} mtDNA after 2-3 days of culture, respectively (Fig.14d), indicating that engulfed mitochondria are degraded in cMacs. Finally, quantitative analyses revealed that a sizable fraction of acidic mt-Keima+ particles (62.7 ± 9%) localized within cMacs, altogether revealing that a substantial fraction of cardiomyocyte mitochondria were eliminated by cMacs (Fig.14e). These data thus identify a population of resident macrophages that completes mitophagy of a neighbouring, highly-specialized parenchymal cell.

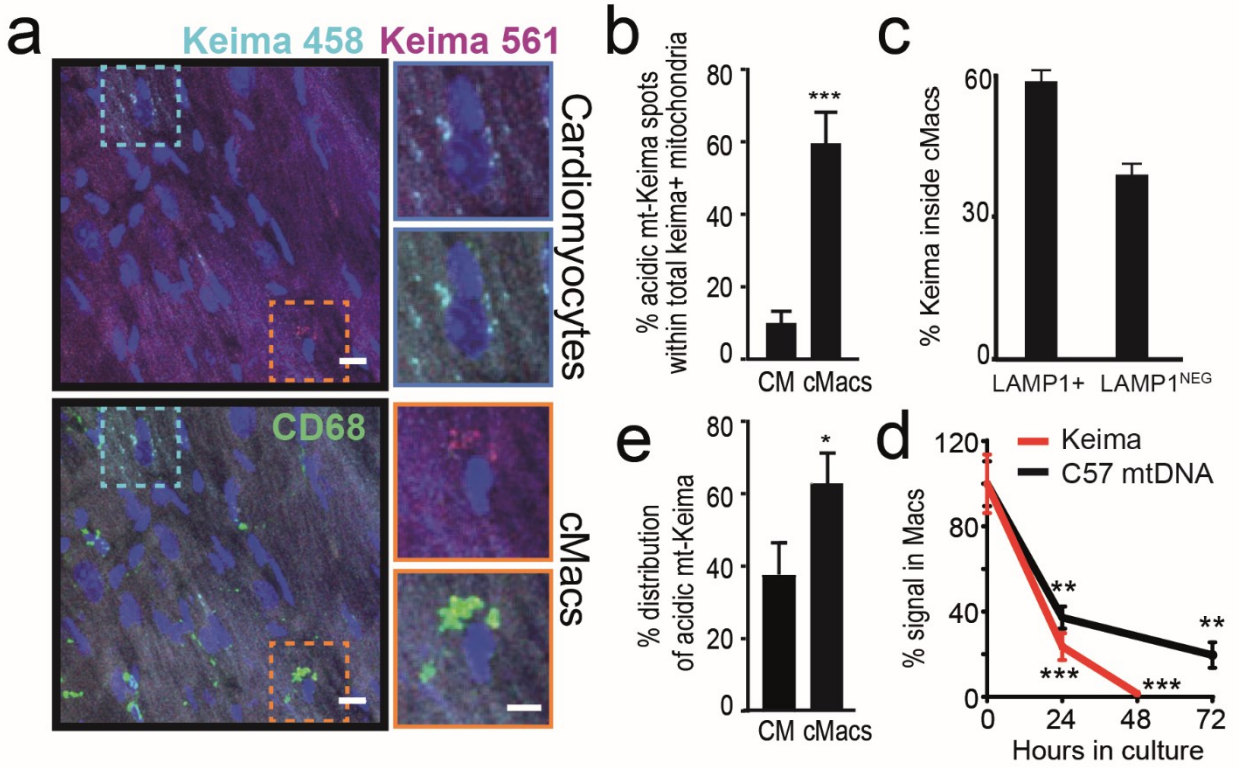

Figure 14. Transferred mitochondria are degraded by cMacs.

(a-b) Distribution of mt-Keima in infected hearts. **(a)** Micrographs illustrating pH-dependent mt-Keima fluorescence. Images show Keima-tagged mitochondria in non-acidic (Keima 458nm; Cyan) and acidic (Keima 561nm; red) environments. **(b)** The majority of mitochondria inside cMacs are "acidic" (high 561/456nm ratios) while most mitochondria inside cardiomyocytes (CM) are "non-acidic" (low 561/456nm ratios). **(c)** Percentage of mt-Keima signal localized inside LAMP1+ or LAMP^{NEG} compartments in cMacs. Bars show mean ± SEM from 45 images, from 3 mice. See also Movie S7. **(d)** Degradation of exogenous mitochondria by cMacs. The graph shows percentages of signal in cMacs isolated from transplanted (C57 recipient) mice or from wild-type mice infected with AAV9-mtKeimaat different times in culture., compared time 0; data from 1 (keima) and 2 (NzB transplants) independent experiments. **, $p<0.01$; ***, $p<0.001$, as determined by multiple nonparametric Mann-Whitney test, against time 0. **(e)** Percentage of total "acidic" keima+ mitochondria that are inside CM or inside cMacs. Bars shows the percentage of "acidic" Keima mitochondria (with 561nm signal>458nm signal) in CM or in cMacs. Data are mean ± SEM from 15 images and 3 mice per group. *, $p<0.05$, determined by a nonparametric Mann-Whitney test.

4.2.4. Mitochondria quality in exophers

While mitochondrial proteins were massively enriched in our proteomic analysis, we noticed that a few mitochondrial proteins were not enriched in exophers, including FIS1, OPA1, Cytochrome C (CYTC) and Apoptosis Inducing Factor Mitochondria Associated 1 (AIFM1; Fig9.b and Fig.15a), all of which were suggestive of dysfunctional mitochondria within exophers (Duvezin-Caubet et al., 2006; Joza et al., 2001; Mai et al., 2010). These results, along with the observation that cardiomyocyte-derived mitochondria captured by cMacs are degraded (Fig.14), suggested that dysfunctional mitochondria could be specifically routed to exophers. Complementing this findings, we found that damaged mitochondria often accumulated in budding vesicles in the periphery of cardiomyocytes (Fig.15b). Using a binary criteria to score mitochondrial fitness from TEM images as normal or abnormal (based on membrane integrity and cristae density), we found a progressive decline in fitness from perinuclear to border regions of the cardiomyocyte, with the highest frequency of morphologically aberrant mitochondria present in exophers (Fig.15c-d). This morphological criteria correlated with dramatic disruption of the membrane potential of mitochondria present in exophers (Fig.15e), suggesting that progressively damaged mitochondria accumulate in the periphery of cardiomyocytes and are ejected in exophers.

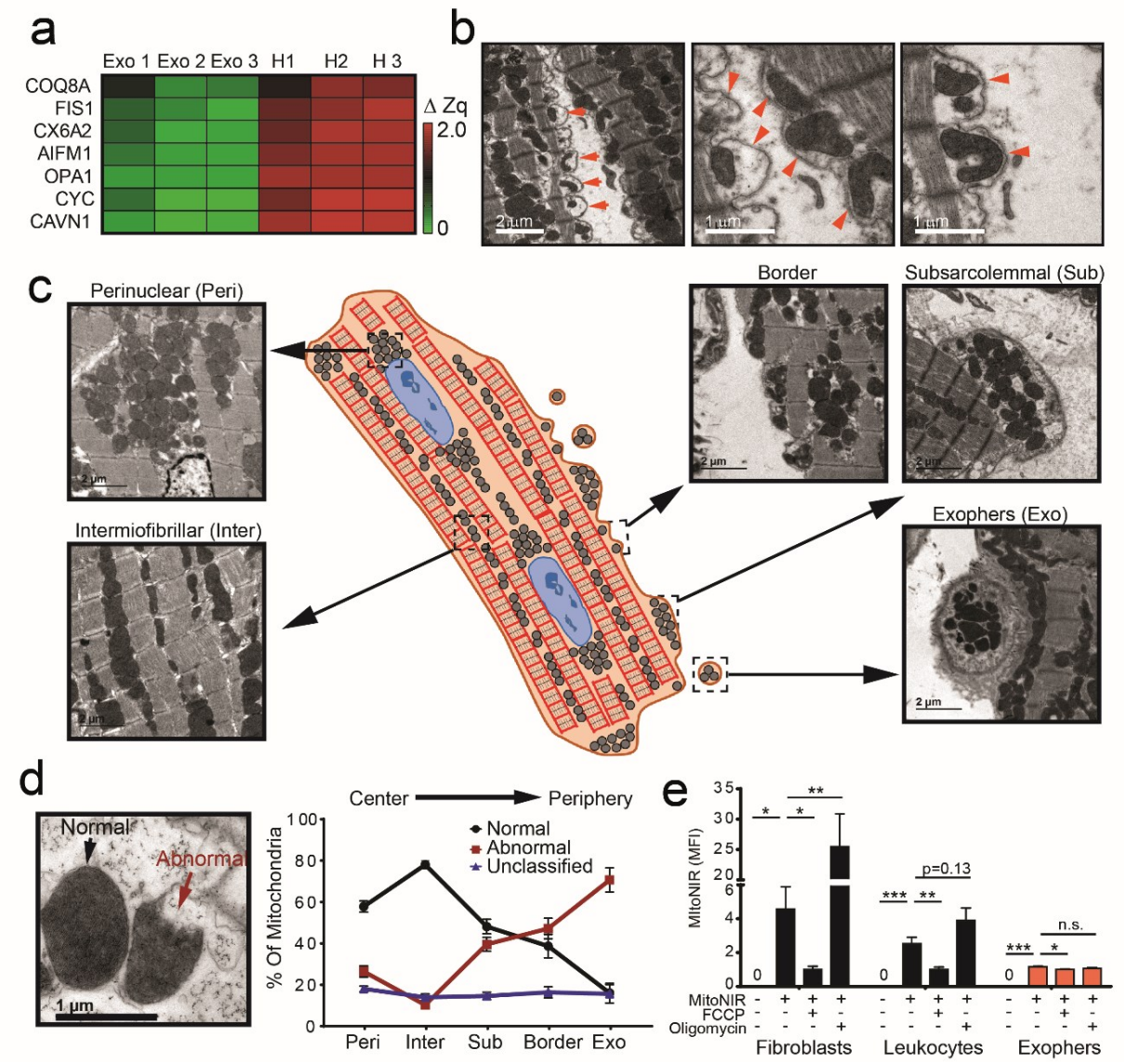

Figure 15. Exophers transport abnormal mitochondria.

(a) Proteins associated with mitochondrial fitness that show statistically significant decrease when compared to total cardiac tissue (see also Fig.10a). Adjusted p-value <0.05. **(b)** Representative TEM images of bubble-like structures containing mitochondria at the border zone (red arrowheads) of cardiomyocytes. Scale bars, 2 µm (Left) and 1 µm (Mid-right). **(c)** Scheme and representative images of mitochondria in different regions of cardiomyocytes (arrowheads). Scale bars, 2 µm. **(d)** (Left) TEM micrographs illustrating Normal (preserved integrity) and an Abnormal (damaged membranes, cristae or both) mitochondria criteria used for classification. (Right) Percentage of mitochondria classified as Normal, Abnormal or Unclassified (not obvious alterations at this resolution). Regions were defined as in panel (c); data from 3 mice **(e)** Membrane potential of mitochondria in cultured fibroblasts, cardiac leukocytes or cardiac exophers assessed by mitoNIR uptake in basal conditions or in the presence of depolarizing (FCCP) or hyperpolarizing (Oligomycin) agents. Bars show mean ± SEM from 4-5 samples per group, 2 independent experiments. *, p<0.05; **, p<0.01; ***, p<0.001; n.s., not significant as determined by Multiple t-test vs MitoNIR incubated sample without treatment in each group.

4.2.5. Production of cardiac exophers involves the cardiomyocyte autophagy machinery.

After exploring mitochondrial transfer into cMacs, we became interested in the mechanism underlying exopher formation by cardiomyocytes. The observation that exophers contained varied cargo and transported dysfunctional mitochondria raised the possibility that exopher production was related to autophagy, an ancient system that mediates disposal of damaged organelles, can be activated by Rapamycin (by inhibition of mTOR), or inhibited by genetic deletion of members of the *Atg* family, including *Atg7* (Garcia-Prat et al., 2016) (Fig.16a). Using a GFP reporter mouse for LC3, a marker of autophagosomes (Mizushima et al., 2004), we found positive puncta in the majority of exophers present in heart sections, and GFP was also detected by flow cytometry of isolated exophers (Fig.16b-c), suggesting that exophers were associated with autophagy pathways.

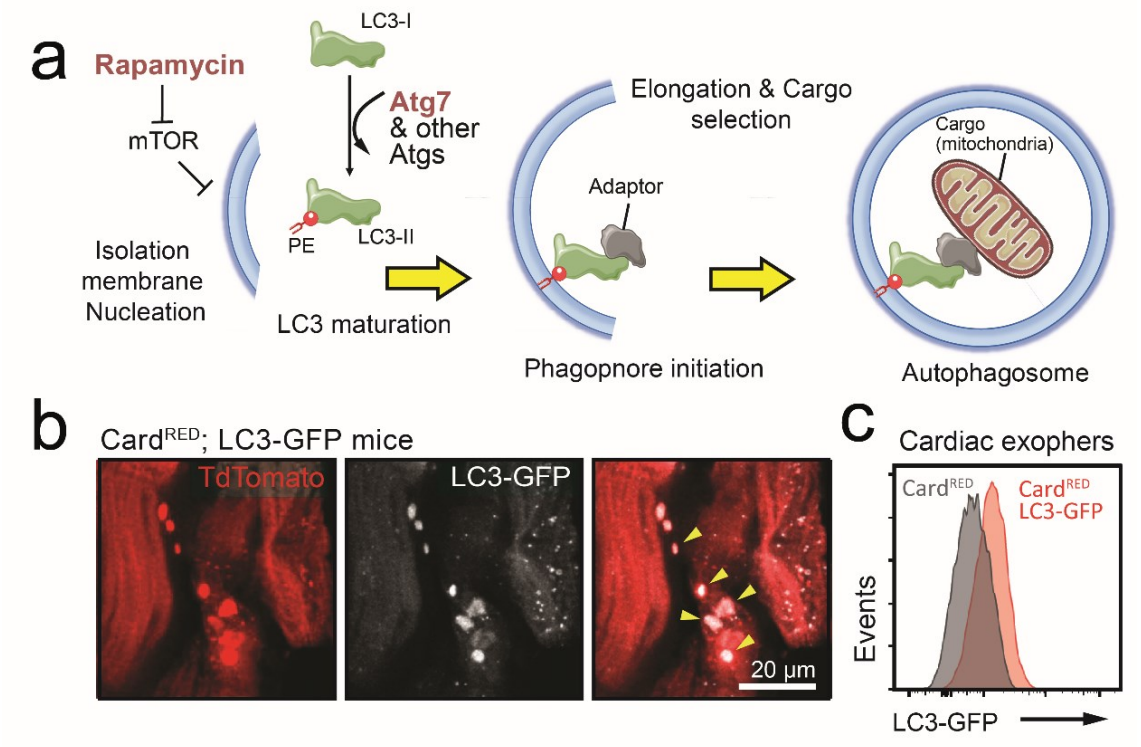

Figure 16. Cardiac exophers accumulate LC3.

(a) Scheme of pathways leading to packing mitochondria into autophagosomes, which can be modulated by the mTOR inhibitor rapamycin, and relies on Atg proteins, including Atg7. **(b)** Presence of GFP+ puncta revealing the presence of LC3 in exophers of Card^{RED} mice. **(c)** Detection of LC3-GFP in purified cardiac exophers by flow cytometry. representative of 1 experiment, n=3 animals.

We therefore treated Card^{RED} mice with rapamycin to stimulate autophagy, a treatment that resulted in elevated exopher numbers in the myocardium (Fig.17a). Consistent with the observation that exophers are captured by cMacs, rapamycin also caused increased uptake of cardiomyocyte-derived fluorescence and mt-Keima by cMacs (Fig.17b-c).

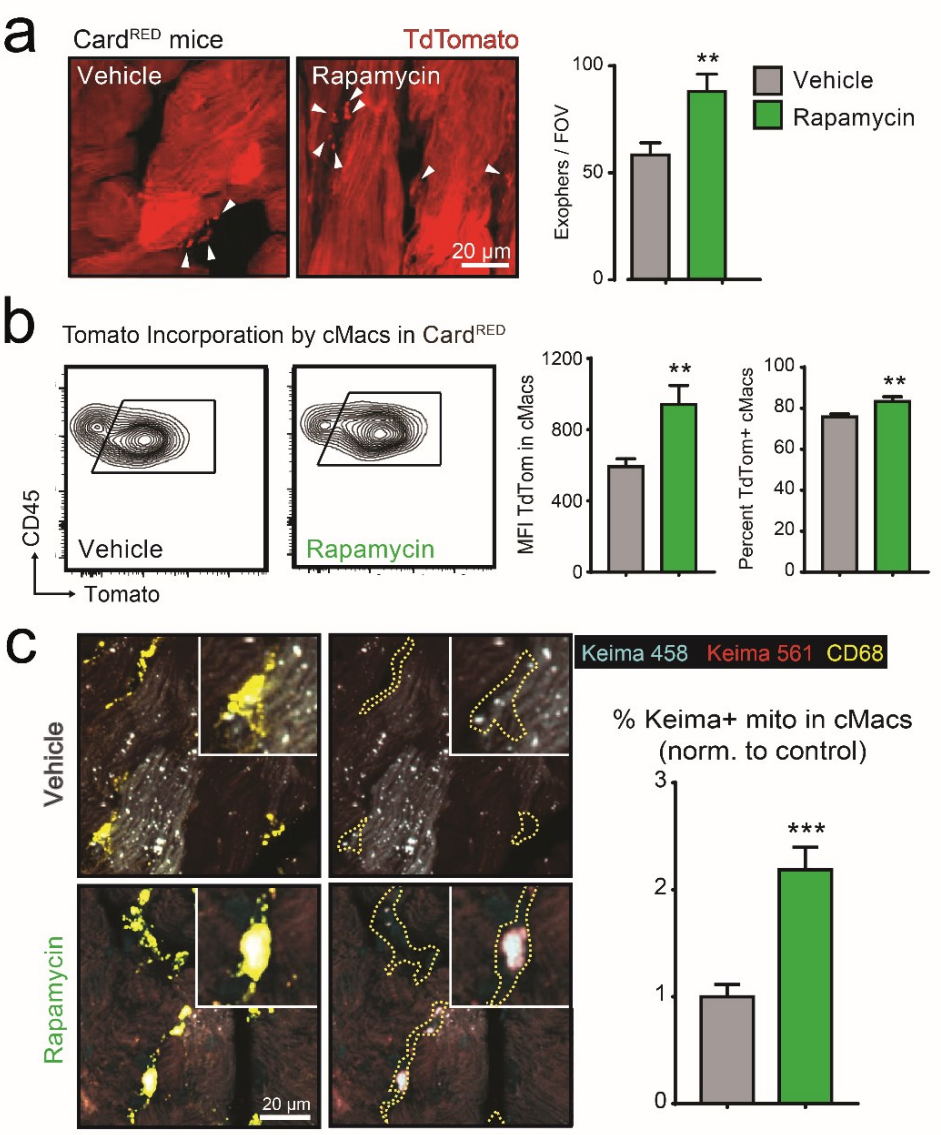

Figure 17. Rapamycin increases the production of cardiac exophers.

(a-c) Enhanced exopher production and mitochondria transfer in Rapamycin-treated mice compared with the vehicle group. **(a)** Micrographs showing increased exophers as detected by immunofluorescence in Card^{RED} mice, with bars showing the number of exophers per field of view (FOV); data from 4 mice per group. **(b)** Incorporation of cardiomyocyte-derived tdTomato signal into cMacs of vehicle or rapamycin-treated mice, as measured by flow cytometry (representative plots, left). Bars show mean fluorescence intensities (MFI) and percent of tdTomato+ cMacs; data from 4 mice per group. **(c)** Immunofluorescence images of AAV9-mt-Keima-transduced cardiomyocytes showing basic (458) or acidic (561) mt-Keima and macrophages, in control or rapamycin-treated mice; data from 5 mice per group.

We then induced cardiac-specific impairment of autophagy by constitutive (αMHC^{Cre}) or tamoxifen-inducible (αMHC^{CreERT}) deletion of only one Atg7 allele (Atg7$^{flox/+}$ mice) from cardiomyocytes, a manipulation that led to efficient suppression of autophagy flux in constitutive mice (Fig.18a-b) but better survival after tamoxifen administration to inducible mice (Fig.18c).

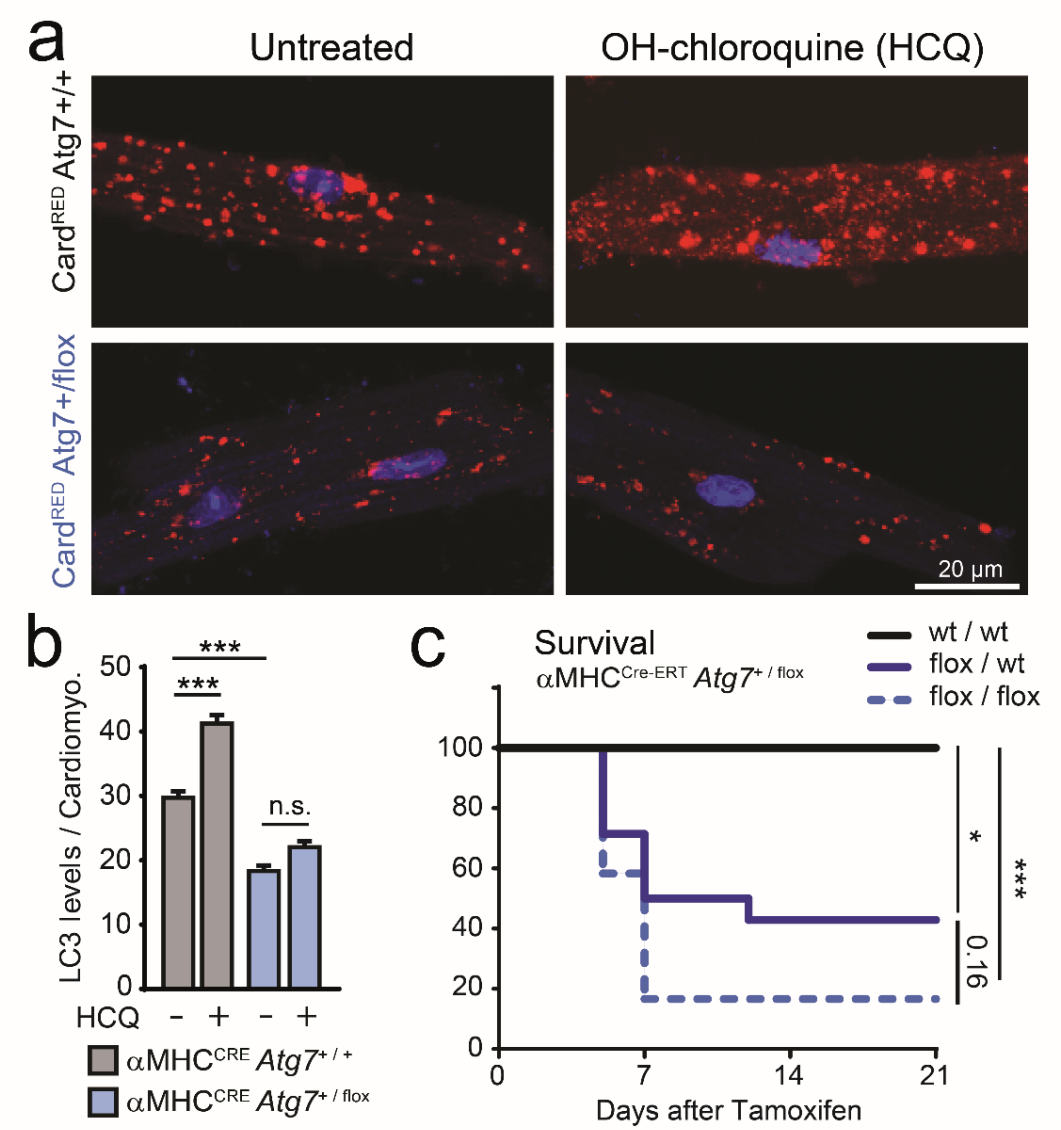

Figure 18. Autophagy block and mortality upon Atg7-deletion.

(a-b) Autophagy flux in αMHC^{CRE} Atg7$^{flox/+}$ and WT animals at baseline and 12 hours after incubation with Hydroxychloroquine (HCQ). **(a)** Immunofluorescence images of LC3 (red) and nuclei (DAPI, blue) in solated cardiomyocytes. **(b)** Bars show mean ± SEM of LC3 puncta per cardiomyocyte from 3 mice (300 cells) per group. Scale bar, 20 µm. ***, p<0.001; n.s., not significant as determined by Kruskal-Wallis with Dunn's multiple comparisons test against untreated. **(c)** Survival curves of αMHC^{CreERT} crossed with Atg7$^{+/+}$, Atg7$^{flox/+}$, Atg7$^{flox/flox}$ after Recombination induction with tamoxifen. *, p<0.05; ***, p<0.001 as determined by Log-rank for Mantel-Cox survival curves; data from 8-14 mice per group, 3 independent experiments.

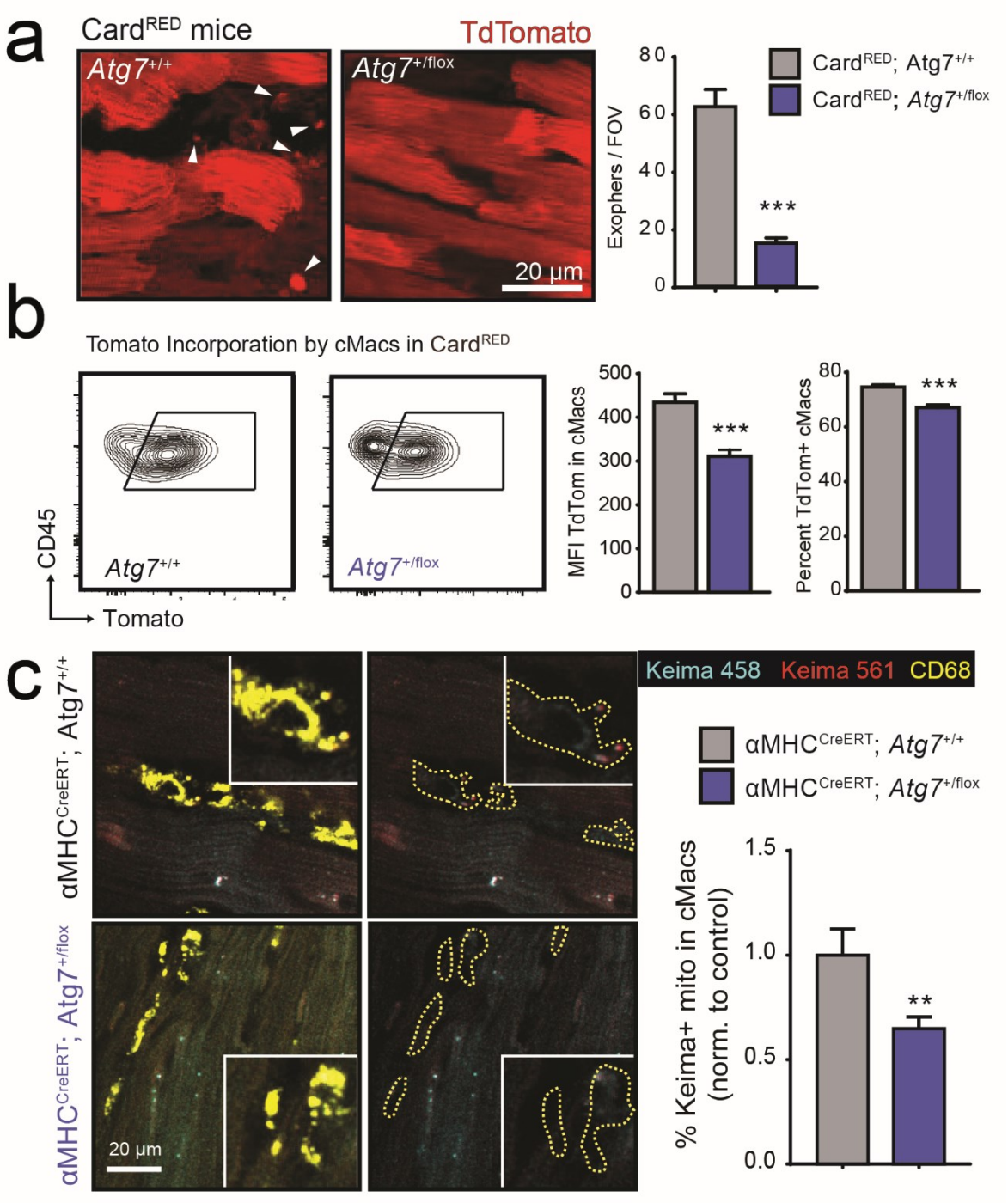

Figure 19. Production of cardiac exophers is mediated by cardiomyocyte autophagy.

(a-c) Impaired exopher production and mitochondria transfer in Card^{RED}; *Atg7*$^{+/flox}$ and αMHC^{CreERT}; *Atg7*$^{+/flox}$ mice. **(a)** Micrographs showing reduced exophers in Card^{RED}; *Atg7*$^{+/-}$ mice, with bars depicting the number of exophers by field of view (FOV). Data from 4 mice per group. **(b)** Incorporation of cardiomyocyte-derived tdTomato signal into cMacs of *Atg7*$^{+/+}$ or *Atg7*$^{+/-}$ mice, as measured by flow cytometry (representative plots, left). Bars show MFI and percent of tdTomato+ cMacs; data from 9-10 mice per group. **(c)** Immunofluorescence images of AAV9-transduced cardiomyocytes showing basic (458) or acidic (561) mt-Keima and macrophages, in control or αMHC^{CreERT}; *Atg7*$^{+/flox}$ mice 4 days after tamoxifen treatment; data from 4-5 mice per group. All bars show mean ± SEM, and statistical significance was determined using Student's t-test.

Atg7-heterozigous mice manifested a dramatic reduction of cardiac exophers (Fig.19a), which was consistently accompanied by reduced uptake of cardiomyocyte-derived fluorescent protein and mt-Keima by cMacs (Fig.19b-c). Altogether, these results support a causal connection between exopher production and the cardiomyocytes autophagy machinery.

4.2.6. Role of cMacs in the production of cardiac exophers.

Given the close proximity of macrophages to areas of exopher accumulation (Fig.6a), we initially hypothesized that cMacs might induce exopher release from adjacent cardiomyocytes. We found that, among heart cells, only cMacs expressed the sialoadhesin CD169 (Fig.20a) and therefore took advantage of mice expressing the diphtheria toxin receptor (DTR) under this locus (CD169^{DTR} mice; (Miyake et al., 2007)) to deplete cMacs from adult hearts upon diphtheria toxin (DT) injection (scheme in Fig.20b). A single injection of DT rapidly and efficiently depleted macrophages from the myocardium (Fig.20c), but not other close related leukocyte populations like monocytes or neutrophils. However, cMacs recovered their original numbers after only 4-7 days post- injection. Thus, to maintain cMac depletion for longer periods we used repeated injections of DT for up to 3 weeks, obtaining similar numbers (Fig.20d).

We then crossed Card^{RED} with CD169^{DTR} mice to explore the effect of cMac depletion in exopher production. Short-term depletion of cMacs (2 days) resulted in accumulation of exophers in the myocardial tissue, indicating that cMacs do not induce exopher production but instead are required for their removal from the tissue (Fig.21a). Interestingly, we noticed that depletion of cMacs for longer periods of time (up to 3 weeks) resulted in a progressive and strong reduction in exopher numbers (Fig.21a).

The lack of exophers in cMac-depleted mice was paralleled by a reduction of autophagy flux at day 21 but not at earlier points (Fig.21b-d), pointing to a link between both processes. Thus, the autophagy machinery of cardiomyocytes autonomously drives exopher formation, and their rate of release is matched by their uptake and elimination by cMacs. In addition, the data also suggests reciprocal regulation of cardiomyocyte autophagy and exopher formation by cMacs since their depletion for long periods results in blockade of cardiomyocyte autophagy.

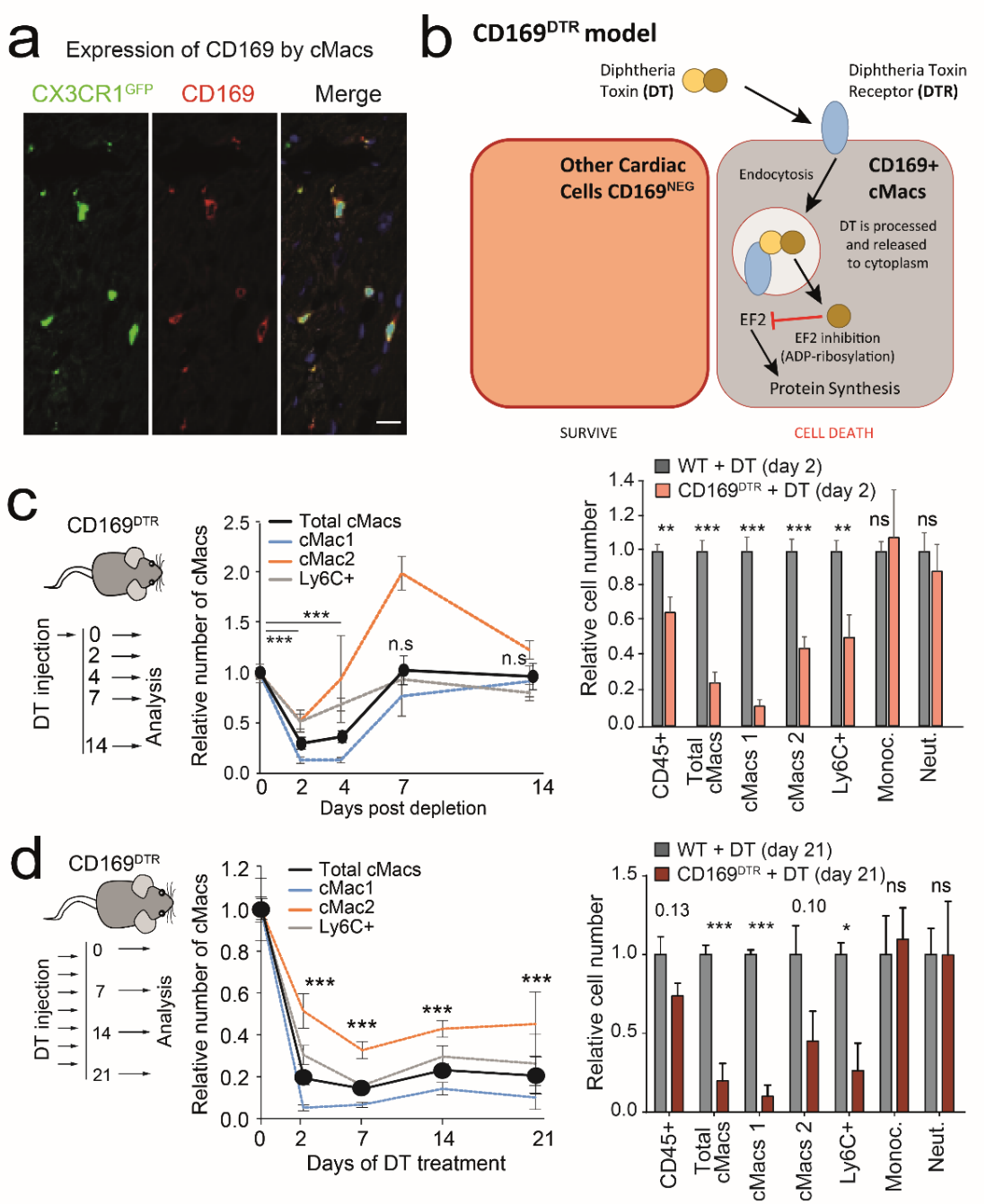

Figure 20. cMacs can be specifically depleted in the CD169^{DTR} model

(a) Expression of CD169 (red) only in CX3CR1^{GFP}+ cMacs (green). Nuclei (DAPI) are blue. Scale bar, 10 µm. **(b)** Scheme of DT mechanism of action leading to cell death of CD169 expressing cell, including cMacs. **(c)** Dynamics of cMacs populations after a single dose of DT (Left) and changes in cardiac leukocyte populations 2 days after a single injection in DT-treated CD169^{DTR} of relative to DT-treated wild-type mice (Right). Data are mean number of different leukocyte populations in the hearts at t=2 relative to t=0 ± SEM from 6-9 mice per group. **, p<0.1; ***, p<0.001; n.s., not significant, as determined by unpaired t-test against control. **(d)** Dynamics of cMacs populations in Long-term DT administration to CD169^{DTR} mice (DT administered thrice per week) and analysed at the indicated days (0, 7, 14 and 21 days; Left). (Right) Data are mean number of different leukocyte populations in the hearts at t=21 relative to t=0 ± SEM form 3 mice per group. ***, p<0.001, as determined by one-way ANOVA with Dunnett's multiple comparisons test against t= 0.

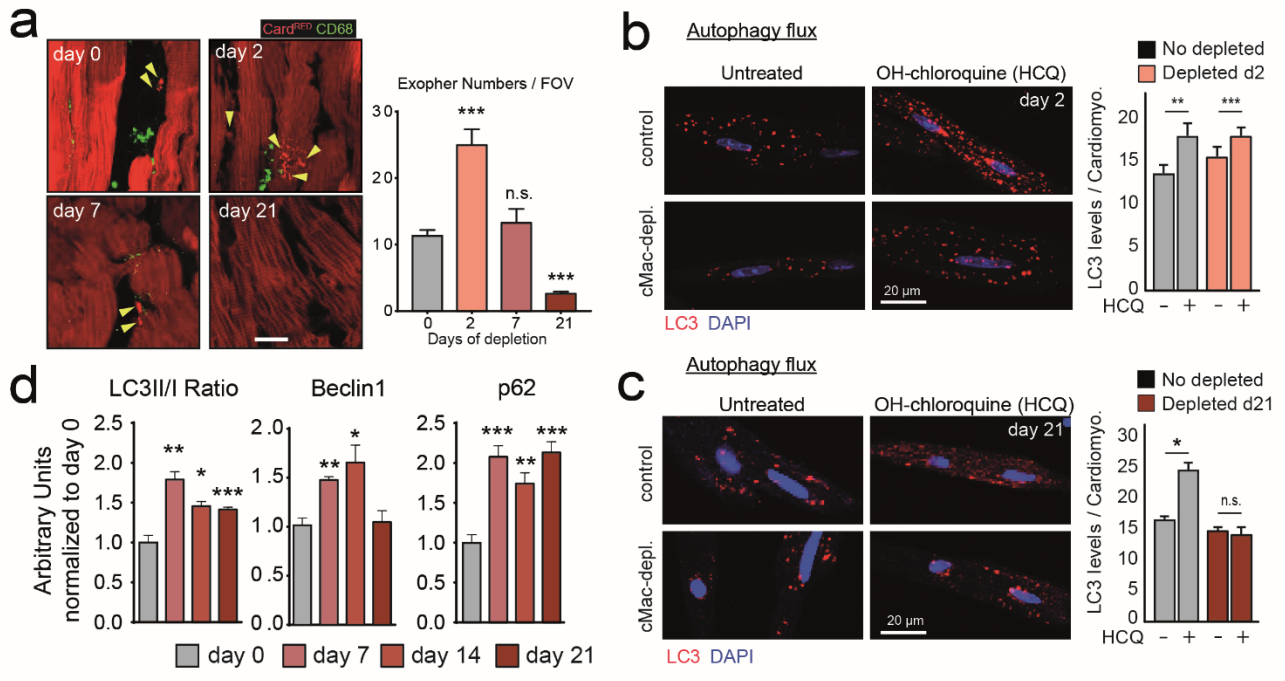

Figure 21. Long-term cMac depletion results in halted autophagy and cardiac exopher production.

(a) Left, Representative micrographs and exopher numbers in Card^{RED} CD169^{DTR} mice depleted of cMacs for the indicated days compared. Bars at right show mean ± SEM number of exophers per field of view (40000 µm^2). n = 4-8 mice per group. Scale bar, 20 µm. **, p<0.01; ***, p<0.001; n.s., not significant as determined by Kruskal-Wallis with Dunn's multiple comparisons test against day 0. **(b-c)** Autophagy flux in isolated cardiomyocytes from wild-type controls and cMac-depleted mice at day 2 **(b)** or 21 **(c)** in DT administration. Fluxes were measured by staining for LC3 (red) and nuclei (DAPI, blue) in basal and Hydroxychloroquine (HCQ)-treated cells. Bars show mean ± SEM of LC3+ particles per cardiomyocyte. n = 3 mice per group. Scale bar, 20 µm. *, p<0.05; **, p<0.01; ***, p<0.001; n.s., not significant, as determined by Student t-test test. **(d)** Changes in LC3II/I ratio and p62 measured by western blot in heart extracts of wild-type controls (day 0) and cMac-depleted mice for the indicated days. Bars shows mean ± SEM from 3-7 mice per group, two independent experiments. *, p<0.05; **, p<0.01; ***, p<0.001 as determined by unpaired t-test.

4.2.7. Cardiac stress induces exopher production.

To assess the capacity of exopher-mediated disposal of mitochondria to adapt to situations of cardiac stress, we treated Card^{RED} mice with Isoproterenol, a β-adrenergic receptor agonist that increases heart rate and induces tissue hypertrophy (Acin-Perez et al., 2018). Isoproterenol caused an increase in cardiac mass as expected, but no changes in cMac density after only one week of treatment (Fig.22a). Importantly, isoproterenol administration induced a decline in mitochondrial quality in cardiomyocytes as assessed by TEM (Fig.22b), which was paralleled by a marked increase in myocardial exophers (Fig.22c), elevated transfer of cardiomyocyte-derived fluorescence (Fig.22d), and dramatic increase of mt-Keima in cMacs (Fig.23a-c), thereby revealing exophers as a dynamic mechanism for elimination of damaged mitochondria under stress.

The presence of mitochondria in exophers and transfer into cMacs in healthy hearts suggested that this might represent a homeostatic mechanism for disposal of mitochondria regardless of organelle fitness. In contrast, the presence of dysfunctional mitochondria in border zones and exophers, suggested that exophers entailed active sorting of defective mitochondria for elimination, thus representing a mechanism of quality control. To discriminate between these possibilities, we analysed this process in Oma1-KO mice (deficient for a stress response protease that regulates different aspects of mitochondria biology) a condition known to preserve mitochondrial function under ISO stress (Acin-Perez et al., 2018). In line with these results, Oma1 deficiency (Fig.23a and Fig.23c) prevented mitochondrial transfer after isoproterenol treatment, indicating that exopher production is dependent of mitochondria quality.

To explore if this was the case under a different type of stress, we also analyzed this process in Card^{RED} mice after 1 week of permanent coronary artery ligation (Fig.24a). We found that areas within and around the infarcted myocardium became enriched in cardiomyocyte-derived particles that shared with exophers morphology, presence of mitochondria and lack of β-actin (Fig.24b-c). Altogether, the data suggested that mitochondrial disposal through exophers occurs in a range of pathophysiological conditions, and is enhanced under conditions of tissue stress.

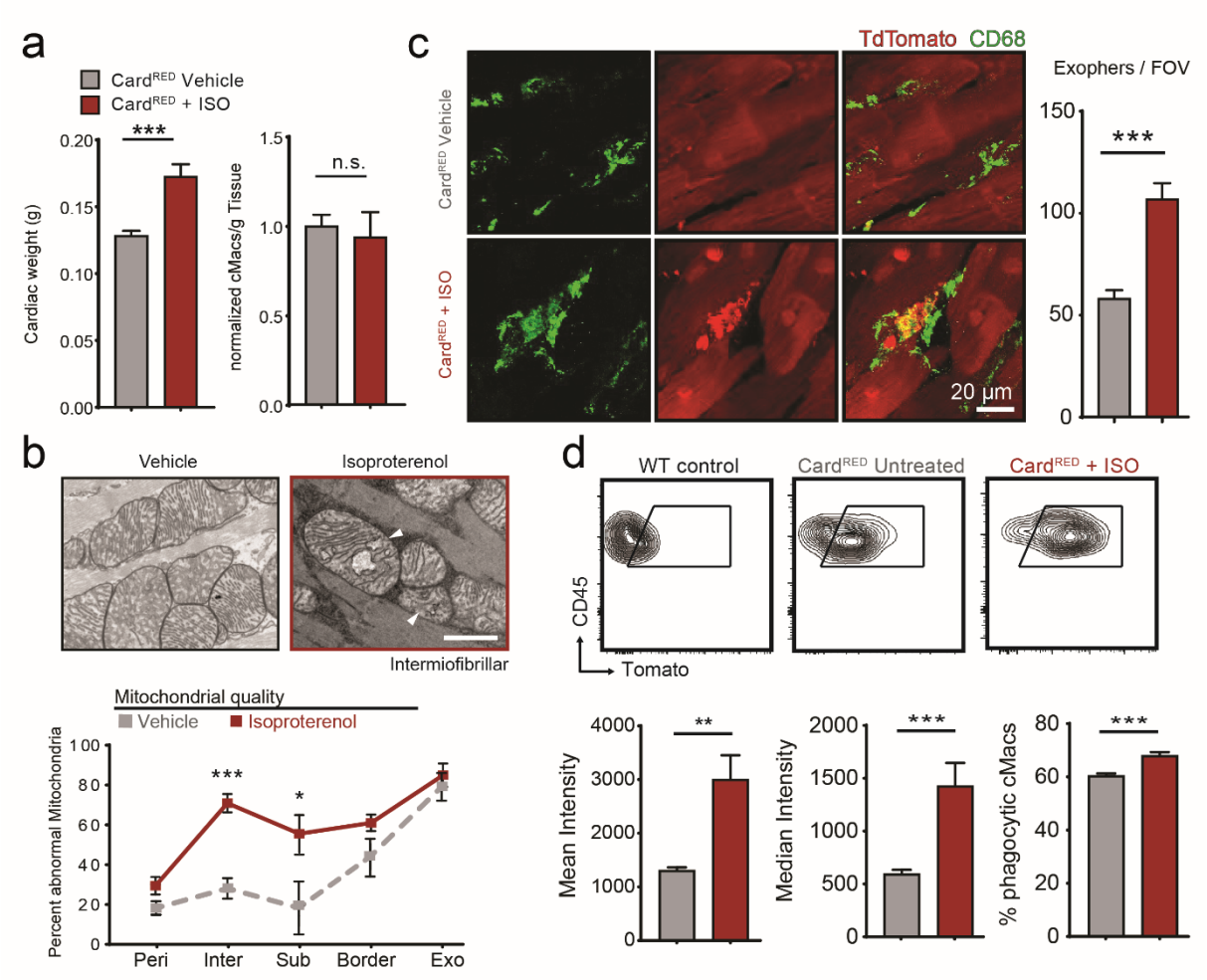

Figure 22. Cardiac stress induces exopher production.

(a-d) Card^{RED} mice treated with vehicle or isoproterenol (ISO) for one week. **(a)** Cardiac weight and cMacs numbers per gram of tissue. Bars shows mean ± SEM from 8 mice per group. ***, p<0.001; n.s., not significant, as determined by Student t-test test. **(b)** (Top) TEM images of mitochondria. Mitochondria from isoproterenol-treated mice often displayed reduced cristae density and vacuolations (arrowheads). Scale bar, 0.5 µm. Images representative of 5 mice per group. (Bottom) Percentage of mitochondria classified as Abnormal (damaged outer membrane, voids, cristae or both) in regions defined as in Fig.15; data from 5 mice per group. *, p<0.05; ***, p<0.001 as determined by two-way ANOVA with Sidak's multiple comparison test. **(c)** Representative micrographs and exopher numbers in Card^{RED} mice treated with vehicle or isoproterenol for one week. Bar graph show mean ± SEM of total exophers per field of view; data from 4 mice per group. **(d)** tdTomato incorporation in cMacs in same animals in panel **(c)**. Bars show mean ± SEM of tdTomato median fluorescence intensity (MFI) and percent of phagocytic cMacs (gated regions in plots); data from 4-8 mice per group.

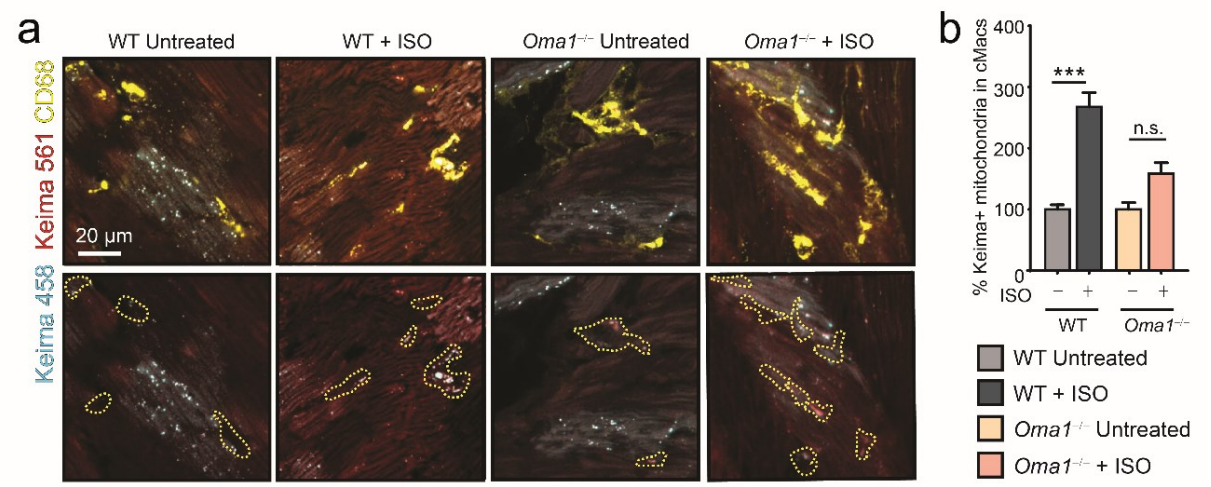

Figure 23. Cardiac stress induces mitochondria transfer.

(a) Representative micrographs and mt-Keima incorporation by cMacs in AAV9-infected WT or *Oma1*$^{-/-}$ mice treated with Isoproterenol or vehicle for one week. **(b)** Bars show mean ± SEM percent mt-Keima inside cMacs, normalized to untreated controls; data from 4-12 mice per group. ***, p<0.001; n.s., not significant as determined by ANOVA with Dunn´s multiple comparisons test.

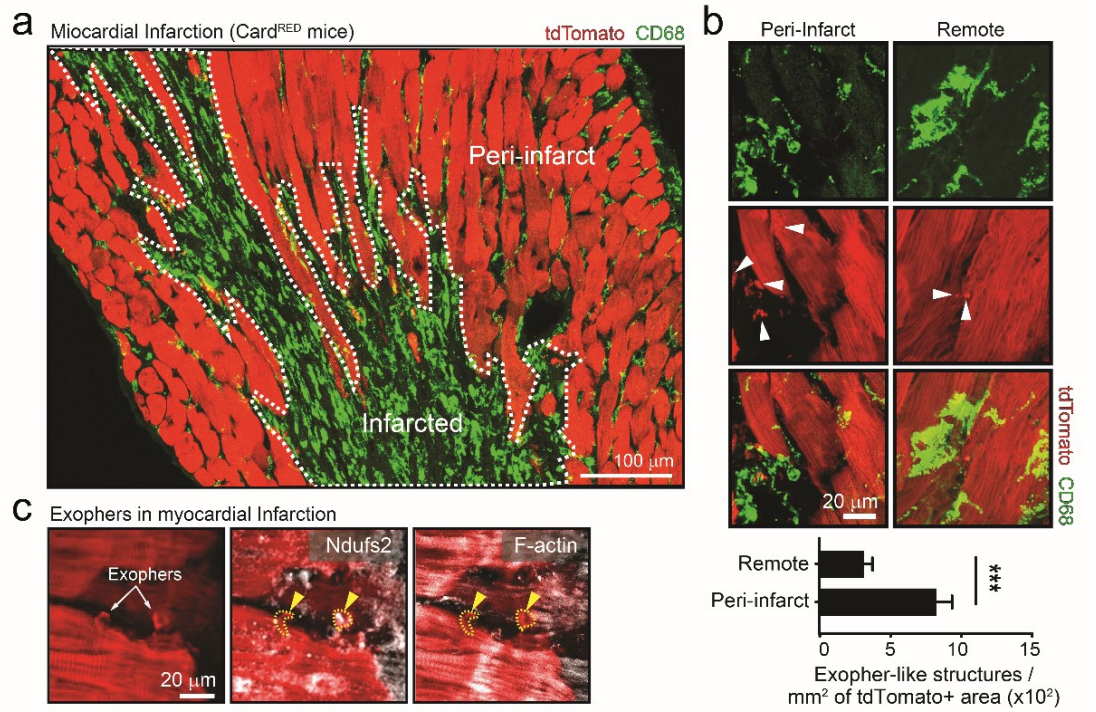

Figure 24. Exopher-like particles in infarcted hearts.

(a) Micrograph of infarcted areas in Card^{RED} mice after 7 days of permanent coronary artery ligation. Indicated are Infarct (inside dashed line) and Peri-infarct areas. Scale bar, 100 µm. **(b)** Representative micrographs of exopher-like structures (arrowheads) and cMacs in remote and peri-infarct areas of infarcted hearts. Bars show mean ± SEM number of exophers-like particles per mm^2 of cardiomyocyte-occupied area; data from 3 mice per group. ***, p<0.01, as determined by the Student´s t-test. Scale bar, 20 µm. **(c)** Micrographs of exopher-like particles (yellow arrowheads) in infarcted hearts positive for Ndufs2 and negative for Actin. Scale bar, 10 µm.

4.3. Effect of macrophage depletion in heart function.

We reasoned that if extrusion of particles and their elimination by cMacs was part of a proteostatic program that removes material from viable cells, then depletion of cMacs should affect cardiomyocyte homeostasis. We found in CD169^{DTR} mice a useful tool to assess this question.

4.3.1. Depletion of cMacs in CD169^{DTR} mice

As introduced in point 4.2.6., a single injection of DT to CD169^{DTR} mice allowed rapid and efficient depletion of macrophages from the myocardium (Fig20c). Contrary to other models previously used for the same purpose like Clodronate administration, CD11b^{DTR} or Cx3cr1^{DTR} mouse models (Dick et al., 2019; Epelman et al., 2014a; Heidt et al., 2014; Hulsmans et al., 2017), CD169^{DTR} is more specific since it does not affect other populations of leukocytes, such as monocytes or neutrophils (Fig.20c-d). However, as previously reported in other models (Epelman et al., 2014a), cMacs returned after 4-7 days of unique DT injection (Fig.20c), both due to in situ proliferation (analysed by BrdU incorporation in proliferating cells; Fig.25a) and incorporation of monocytes from the circulation (analysed in Parabiotic pairs; (Fig.25b)). Thus, to maintain cMac depletion for longer periods we used repeated injections of DT for up to 3 weeks (Fig.20d), as depletion beyond this time caused mortality (more than 5%; Fig.25c). Importantly, although this approach depletes macrophages in several tissues (e.g., liver and spleen; Fig.25d and (Gupta et al., 2016)), it did not cause overt inflammation (Table.1) or leukocyte recruitment to the myocardium (Fig.20c-d). Thus, upon continuous DT administration to CD169^{DTR} mice, we could maintain low numbers of cMacs for longer periods of time without directly affecting other cardiac populations (Fig.20c-d).

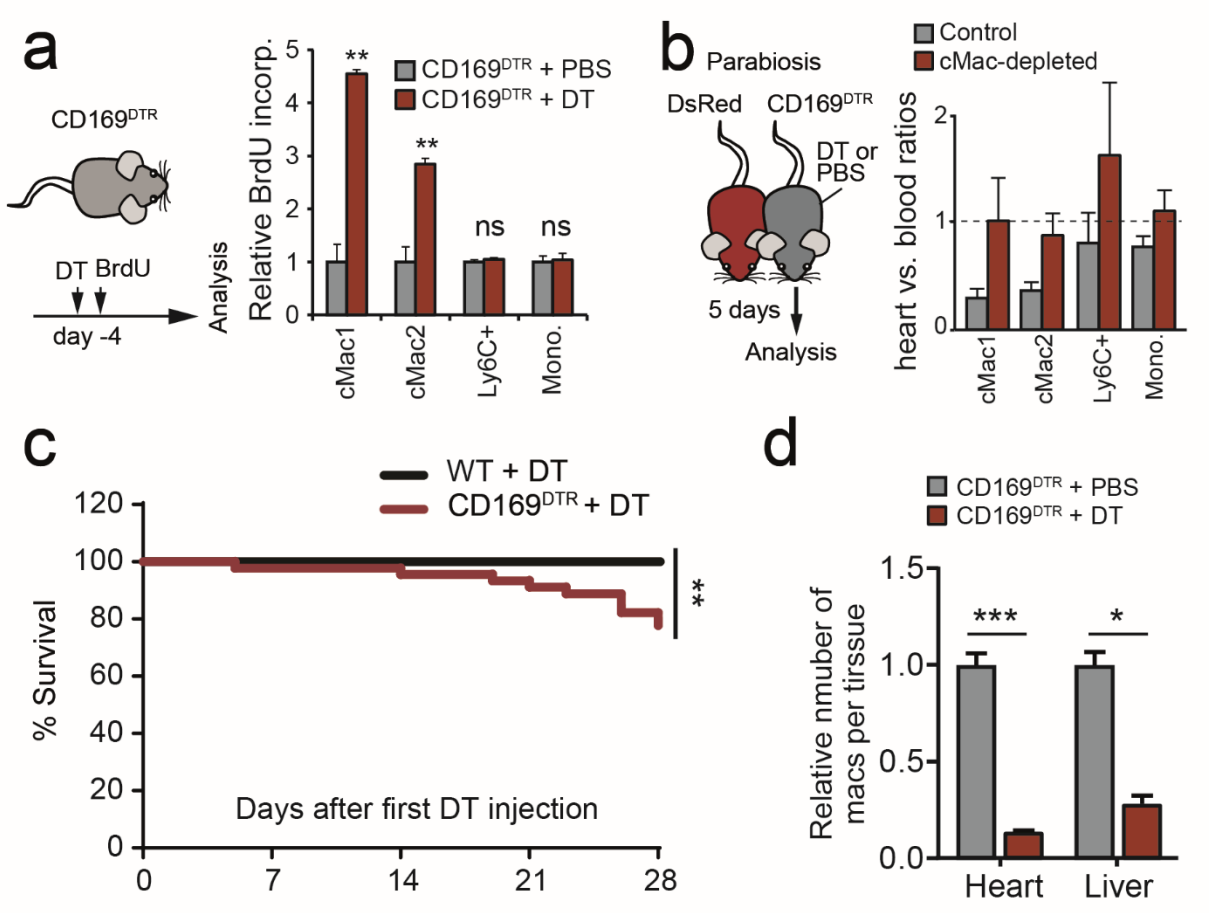

Figure 25. cMac repopulation after short-term depletion.

(a) cMacs proliferate after depletion. CD169-DTR animals injected with DT or saline were administered with BrdU. Bars show the percentage of BrdU+ cMacs normalized to the saline-treated group. Data are mean ± SEM from 3 mice per group. **, p<0.01; n.s., not significant, as determined by unpaired t-test. **(b)** cMacs rely on circulating monocytes for recovery after depletion. CD169^{DTR} were maintained in parabiosis with DsRed-transgenic mice for 1 month, and the chimerism of host vs. partner monocytes were measured in heart and blood 5 days after a single injection of saline or DT in the CD169^{DTR} partners. Chimerism in the heart only equilibrates with that in blood after depletion, indicating that circulating monocytes contribute to cMac repopulation. Data are mean ± SEM from 3 parabionts per group. **(c)** Survival curves of CD169^{DTR} or control (WT) mice treated with DT (thrice per week) for the indicated times. ***, p<0.001 as determined by Log-rank for Mantel-Cox survival curves; data from 30 mice per group, 3 independent experiments. **(d)** Macrophage numbers in the hearts and livers of CD169^{DTR} mice treated with saline or DT for 7 days. ***, p<0.001, as determined by unpaired t-test.

Table 1. Leukocyte counts in the blood and hearts of CD169DTR mice 21d after macrophage depletion. Values are mean ± SEM from 6-11 mice per group.

Parameter	Units	day 0	day 21	P value
Lymphocytes (Blood)	cells/mL	7457 ± 798	7656 ± 751	0.875
Neutrophils (Blood)	cells/mL	2347 ± 630	3653 ± 545	0.180
Monocytes (Blood)	cells/mL	338 ± 57	417 ± 102	0.615
Neutrophils (Heart)	cells/0.1 mg	16418 ± 3967	27610 ± 3951	0.086
Ly6C^{HI} Monocytes (Heart)	cells/0.1 mg	2734 ± 779	3895 ± 519	0.273
Ly6C^{LO} Monocytes (Heart)	cells/0.1 mg	5669 ± 1405	7413 ± 1621	0.466
cMacs (Heart)	cells/0.1 mg	37746 ± 1808	8329 ± 1754	<0.001***

4.3.2. Proteomic changes in cMac-depleted hearts

By analysing the hearts of DT-treated CD169^{DTR} mice by immunofluorescence we found, unexpectedly, that depletion of cMacs dramatically reduced the number of exophers in the myocardium (Fig.21a), in coincidence with autophagy block (Fig.21c) and de novo appearance of apoptotic TUNEL+ cardiomyocytes (Fig.26a), altogether suggesting that cMacs confer basal protection to cardiomyocytes.

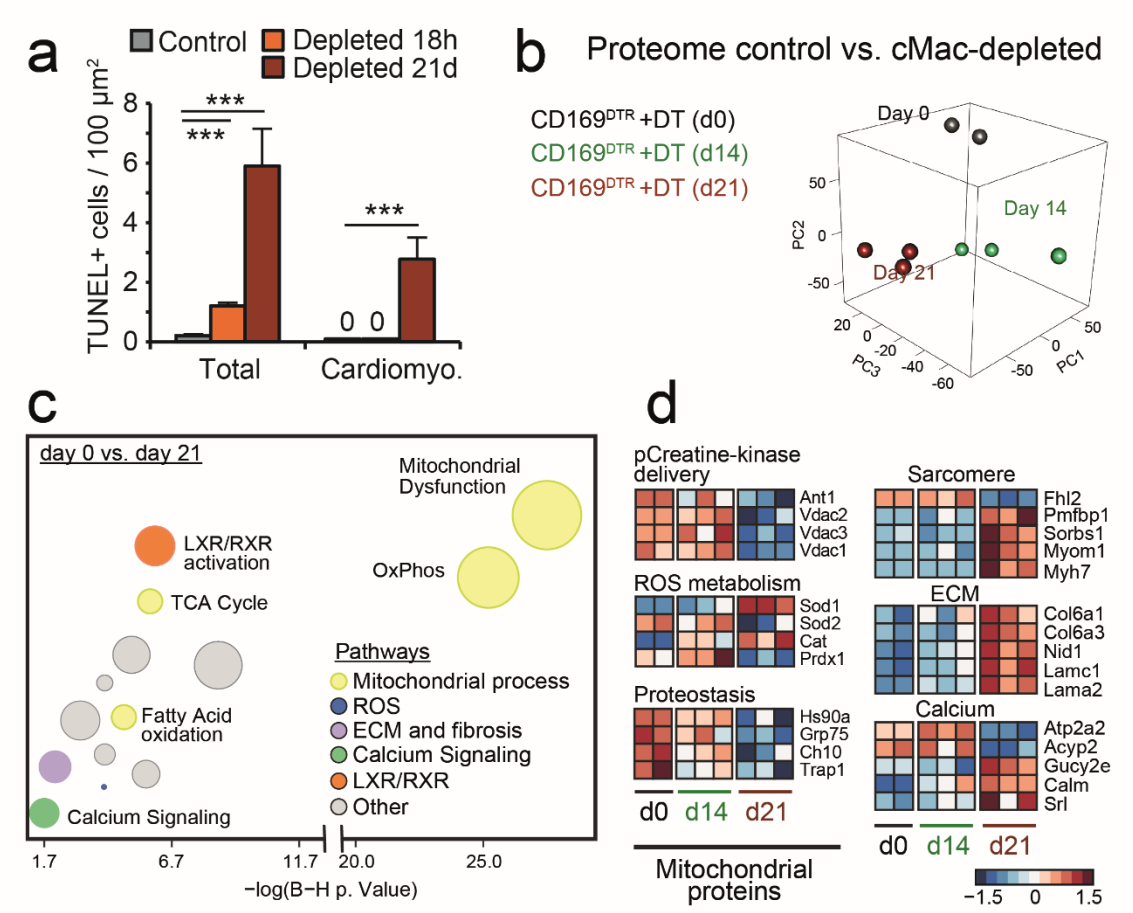

Figure 26. Proteomic changes in cMac-depleted hearts

(a) Number of total apoptotic cells or apoptotic cardiomyocytes in hearts of CD169^{DTR} mice after 18 h or 21 days of cMac depletion. Bars show the number of apoptotic cells identified by TUNEL staining. Data are mean ± SEM from 30 images and 3 mice per group. ***, p<0.001, as determined by nonparametric Mann-Whitney test against WT+DT. (**b-d**) Proteomic analyses of wild-type hearts at different times of cMac depletion. (**b**) Principal component analysis of control (day 0) and cMac-depleted mice (day 14 and 21). (**c**) Bubble plot representation of the most significant changed canonical pathways when comparing hearts at days 0 vs. 21, using the Ingenuity Pathway Analysis tool. (**d**) Heat map showing proteins differentially expressed between day 0 and 21, showing also the values for day 14, with z-score values shown according to the color scale. The proteins are grouped in categories according to their presence in mitochondria or other structures (sarcomere and ECM), and the functional pathway in which they are involved.

To understand how cMacs contributed to cardiac homeostasis, we performed proteomic analysis of the myocardium of cMac-depleted mice. We noticed remarkable changes in protein composition over time (Fig.26b-d), primarily affecting mitochondrial proteins involved in bioenergetic metabolism, ROS and proteostasis (Fig.26c-d), a finding that was consistent with the role of cMacs in promoting mitochondrial recycling. Those changes will be analysed with more detail in the following sections.

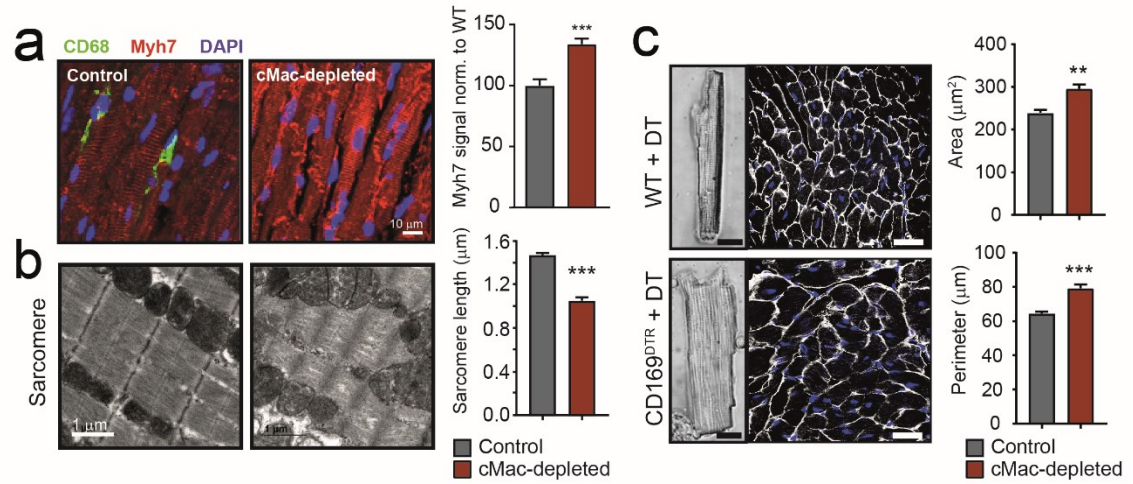

Figure 27. Structural changes of cardiomyocytes upon long-term cMac depletion.

Control (WT) and cMac-depleted mice ($CD169^{DTR}$) treated with DT for 3 weeks were analysed for different parameters. **(a)** Micrographs of heart sections showing the distribution and levels of Myh7 (red). Shown also are cMacs (green) and nuclei (blue). Scale bar, 10 µm. Bars show mean ± SEM from n= 5 mice per group; ***, p<0.001 as determined by unpaired t-test. **(b)** TEM images (left) illustrating sarcomere lengths (quantified in the right panel). Scale bar, 1 µm. Bars shows means ± SEM from n= 25-30 measures per mouse, 3 mice per group. ***, p<0.001 as determined by nonparametric Mann-Whitney test. **(c)** Representative images of isolated cardiomyocytes (bright field) and myocardium stained for laminin (white). Bar graphs show mean ± SEM areas and perimeters of individual cardiomyocytes measured in cardiac sections. Data are from 4-5 mice per group. **, p<0.01; ***, p<0.001 as determined from nonparametric Mann-Whitney test.

Other structures and proteins originally present in exophers, like the sarcomeric protein Myosin Heavy chain 7 (MYH7) (Fig26d and Fig.27a), were similarly altered in the absence of cMacs. TEM analyses revealed that these changes paralleled dramatic shortening of the sarcomeres (Fig.27b) and increase in cardiomyocyte size (Fig.27c) after cMac depletion. We also found changes in components of the extracellular matrix (ECM), and in proteins involved in the regulation of intracellular calcium (Fig.26d). Combined, these findings suggested that cMacs are needed for global cardiomyocyte homeostasis, from cell survival to proteostasis regulation.

4.3.3. cMacs preserve homeostasis of cardiomyocyte mitochondria

Exopher transfer from cardiomyocytes and the proteome alterations suggested global regulatory roles for cMacs in mitochondrial homeostasis, and proteomic analysis of CD169^{DTR} hearts confirmed mitochondrial alterations upon cMac-depletion. Although many mitochondrial proteins were less represented after cMac-depletion (Fig.26d), including those of the oxidative phosphorylation (OXPHOS) system (Fig.28a), transmission electron microscopy (TEM) imaging of cMac-depleted mice mice revealed a significant increase in the number of mitochondria within cardiomyocytes (Fig.28b), which we confirmed by immunostaining for the outer mitochondrial membrane protein Tom20 in heart sections (Fig.28c). Citrate synthase activity, another measure of mitochondrial mass, confirmed increased mitochondria content in the heart but not in the liver (Fig.28c), despite efficient depletion of macrophages in both tissues (Fig.25d and (Gupta et al., 2016)).

Increased mitochondria number could be due to both decrease in mitochondria degradation or increase in mitochondria production. The reduced number of exophers 21 days after depletion (Fig.21a) suggested that mitochondria increase could be due to mitochondria accumulation inside cardiomyocytes. However, we also found that markers of mitochondrial biogenesis were increased (Fig.28d), indicating that mitochondria accumulation in CD169^{DTR} mice might be the result of both processes. Interestingly, TEM imaging showed that mitochondria from cMac-depleted hearts were not only abundant but larger in size, had marked reductions in cristae density and overall morphological abnormalities (Fig.28e). These findings, together with changes in mitochondrial proteins were indicative of altered mitochondria function (Fig.26 and 28). Thus we explored the metabolic state of hearts 21 days after cMac depletion. First, the ratio between the mitochondrial-encoded Cytochrome c oxidase I (CoI) and the nuclear-encoded Cox IV, two components of the respiratory complex IV, was dramatically reduced (Fig.29a), which suggested defects in mitochondrial proteostasis and function in the absence of cMacs.

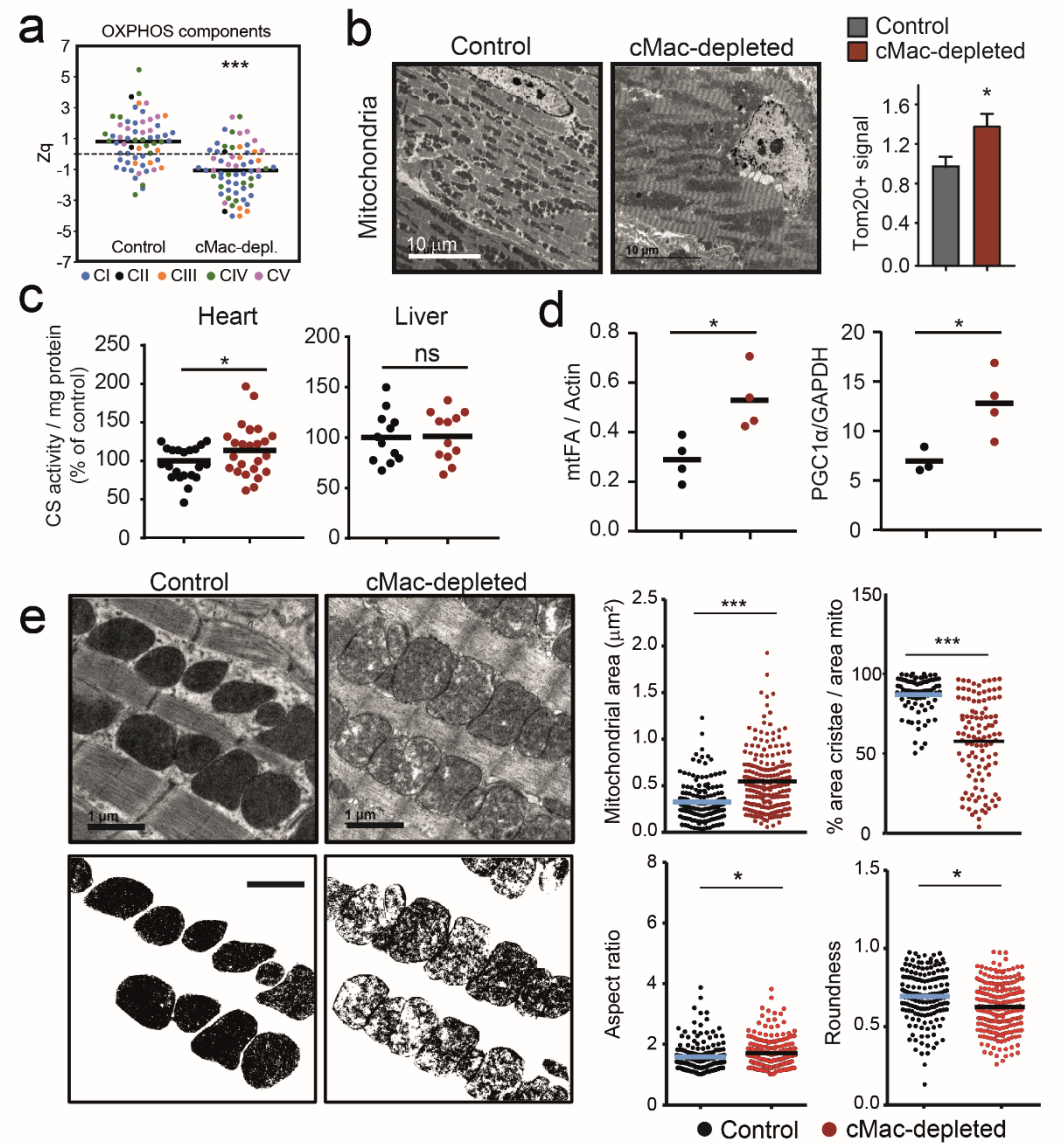

Figure 28. Accumulation of abnormal mitochondria in cMac-depleted mice.

Control (WT) and cMac-depleted mice (CD169^{DTR}) treated with DT for 3 weeks were analysed for different parameters. **(a)** Reduction in structural OXPHOS components identified from the proteomic analyses of hearts shown in Fig.25. Plots show mean Zq values for individual proteins in control and cMac-depleted mice and color-labeled according to the complex they form part of. ***, p<0.001 as determined by two-way ANOVA. (**b**) Representative TEM images (left) and mitochondrial content determined by Tom20 immunofluorescence analysis (right). Scale bar, 10 µm. Bars show mean ± SEM from n= 9-10 mice per group; *, p<0.05 as determined by unpaired t-test. **(c)** Citrate synthase activity. Graph shows enzymatic activity per mg of total protein from heart or liver, normalized to the control group. Each dot represents value with two technical duplicates per mouse, and black lines show means; n= 6-12 mice per group. *, p<0.05; n.s., not significant, as determined by unpaired t-test against the control groups. **(d)** mtFA and PGC1α protein levels measured by western blot, normalized to Actin or GADPH, respectively. from n= 4-3 mice per group; *, p<0.05 as determined by unpaired t-test. (**e**) Representative mitochondria from TEM images (Left). Scale bars, 1 µm. Morphometric parameters and quantification of mitochondrial area and cristae area per mitochondria. Each dot represents one mitochondria and bars show means, from 15-20 images from 3-4 mice per group. ***, p<0.001; *, p<0.05 as determined by nonparametric Mann-Whitney test.

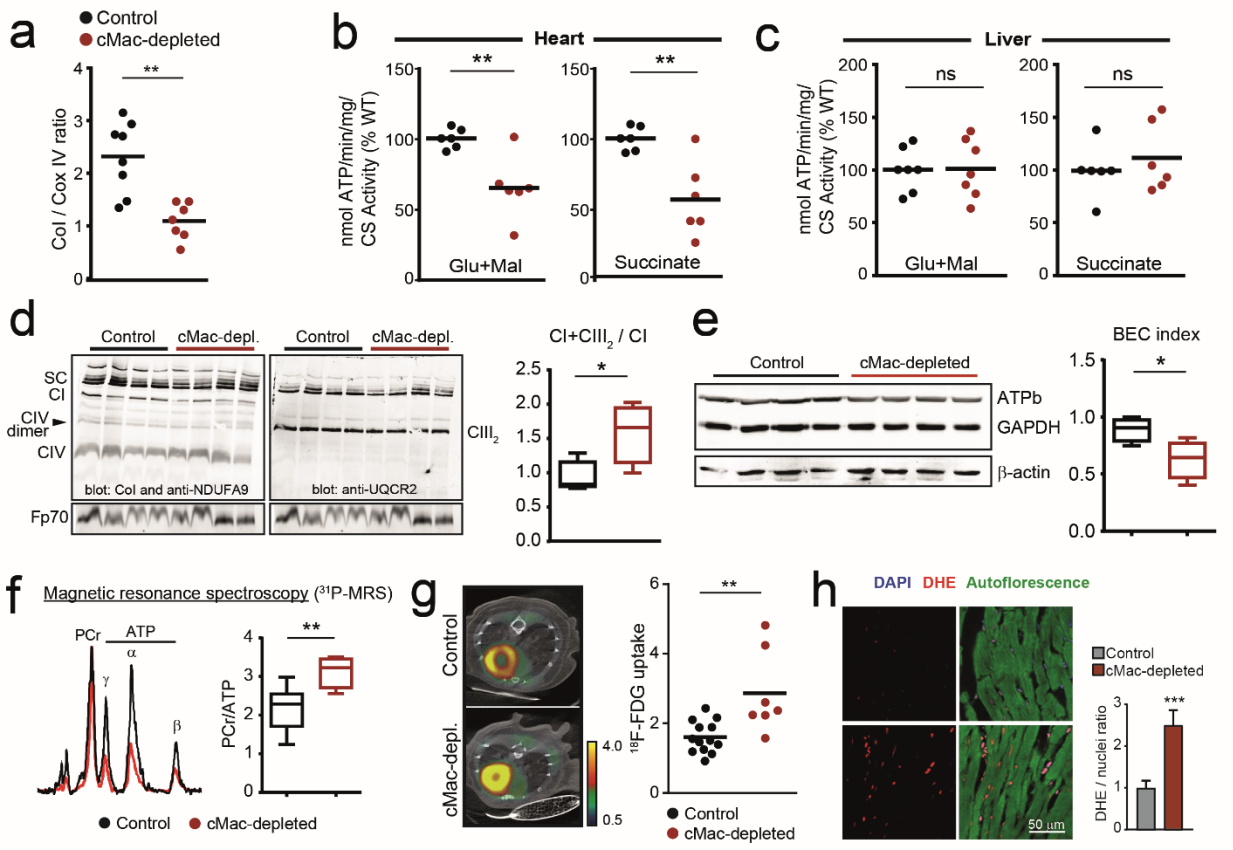

Figure 29. cMac depletion causes mitochondrial dysfunction in the heart

Control (WT) and cMac-depleted mice (CD169^{DTR}) treated with DT for 3 weeks were analysed for different parameters. **(a)** Ratios of CoI to Cox IV protein measured by western blot. Each dot is one mouse and bars show means, from 7 to 8 mice per group. **, p<0.01 as determined by nonparametric Mann-Whitney test. **(b-c)** Ex vivo ATP production rates in isolated mitochondria form heart **(b)** or liver **(c)**, in the presence of the indicated substrates. Values were obtained by kinetic luminescence assays and normalized to the control group. Each dot is the mean for 2 technical duplicates, from 6-7 mice per group. **, p<0.01; n.s, not significant as determined by unpaired t-test. **(d)** Supercomplex assembly assessed by blue native electrophoresis of isolated mitochondria from heart. Gels were sequentially stained for antibodies against CoI, NDUFA9, UQCR2 and Fp70 to identify complex IV (CIV), complex I (CI), complex III (CIII) and complex II (CII), respectively. SC, supercomplex. (Right) Graph shows the relative proportion of CI in complex with CIII dimers ($CIII_2$). Data presented as box and whiskers, from 4 mice per group. *, p<0.05; as determined by unpaired t-test. **(e)** Changes in ATPb/GADPH ratios (BEC index) measured by western blot in heart extracts. Western blot showing ATPb, GADPH and β-actin protein content. Data presented as box and whiskers, from 4 mice per group. *, p<0.05 as determined by unpaired t-test. **(f)** High-energy phosphate metabolites in mice hearts. The graph shows pCreatine (PCr)/ATP ratios measured in vivo by quantitative magnetic resonance spectroscopy (^{31}P-MRS). Data presented as box and whiskers, from 4-6 mice per group. **, p<0.01 as determined by unpaired t-test. **(g)** ^{18}F-FDG uptake analyses. Representative PET-CT images (left) and ^{18}F-FDG uptake quantification (standardized uptake values; right). Each dot represents a mouse and bars show means, from 7-13 mice per group. **, p<0.01 as determined by unpaired t-test. **(h)** Micrographs of heart sections, after staining with DAPI (nuclei, blue) and dihydroethidium (DHE, red) to identify superoxide production, which is quantified in the bar graph (right). Autofluorescence (green) identifies cardiomyocytes. Bars at right show mean ± SEM from 27-30 images in 9-10 mice per group. ***, p<0.001, as determined by unpaired t-test. Scale bar, 50 µm.

Consistent with this, analyses of isolated mitochondria revealed significant reductions in ATP production, both when the substrates were glutamate plus malate, or succinate (for which electrons are carried by NADH or FAD, respectively; Fig.29b). These reductions did not affect mitochondria obtained from livers of the same mice (Fig.29c), indicating that damage was tissue-specific. Direct examination of respiratory complexes in mitochondria from cMac-depleted mice revealed preferential association of complexes I and III into supercomplexes (Fig.29d), a conformation that favours glycolysis (Guaras et al., 2016; Lapuente-Brun et al., 2013). Extracts of cMac-depleted hearts showed reduced levels of the ATPase β-subunit relative to GAPDH (known as the bioenergetic cellular index or BEC (Cuezva et al., 2004), Fig.29e), which aligned with increased phosphocreatine (PCr)/ATP ratios in living hearts measured by magnetic resonance spectroscopy (^{31}P-MRS; Fig.29f). In functional terms, these findings suggested that depletion of cMacs promote a metabolic switch in the heart towards the use of glycolysis to compensate for defective oxidative phosphorylation and reduced ATP stores. Indeed, in vivo uptake of the glucose analogue 2-deoxy-2-(^{18}F)-fluoro-D-glucose (^{18}F-FDG) measured by PET-CT imaging confirmed elevated glycolysis in cMac-depleted hearts (Fig.29g). Finally, the proteomic analyses additionally revealed that cMac-depletion altered several proteins involved in ROS production by mitochondria (Fig.26c-d); accordingly, we found elevated ROS in sections of cMac-depleted hearts (Fig.29h). Thus, hearts depleted of cMacs accumulate defective mitochondria and are metabolically unstable.

4.3.4. Depletion of cMacs alters cardiac function.

The deficit in ATP production and constitutive shortening of sarcomeres predicted alterations in cardiac function in the absence of cMacs. In order to assess this point we performed longitudinal echocardiographic studies over three weeks (Fig.30a) followed by endpoint (day 21 of cMac depletion) intra-cardiac hemodynamic study in basal conditions or after Isoproterenol stimulation (Fig.32a).

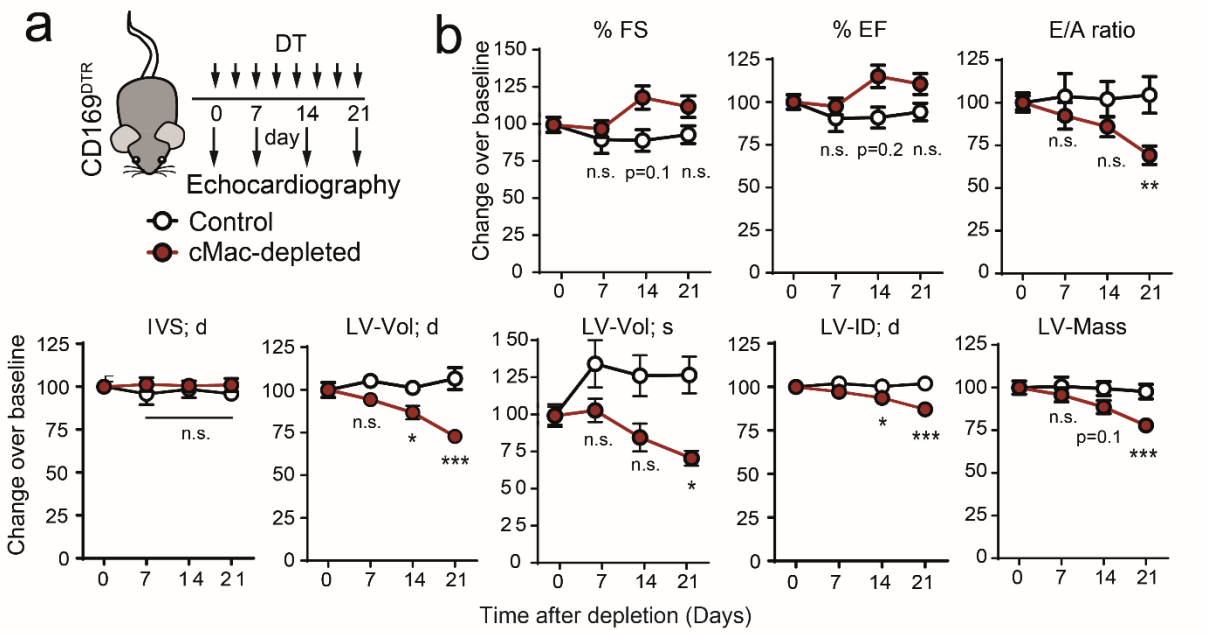

Figure 30. cMacs preserve cardiac function.

(a) Experimental scheme to analyze cardiac function by echocardiography, at different times of cMac depletion. **(b)** Selected cardiac parameters measured by echocardiography in control (WT+DT) and cMac-depleted mice ($CD169^{DTR}$+DT) at different times of DT treatment. See also Movie S8. % Fraction shortening (%FS), % Ejection Fraction (%EF), E/A mitral valve fluxes ratio (E/A ratio), interventricular septum thickness (IVS), left-ventricle volume (LV-Vol), left ventricular-internal diameter (LV-ID) and left ventricle mass (LV-Mass) are shown. In some cases, the same parameter is measured at systole (s) and diastole (d). n=15-21 mice per group

Echocardiographic analyses revealed progressive reduction in Left Ventricle (LV) diastolic and systolic volumes (Fig.30b), pointing to a reduction in LV mass which we confirmed by absolute and relative (to body size) measures of cardiac weight (Fig.31a-b). Functionally, this was accompanied by a reduction in stroke volume and cardiac output (Fig.31c), indicating that the amount of blood pumped by the heart was reduced.

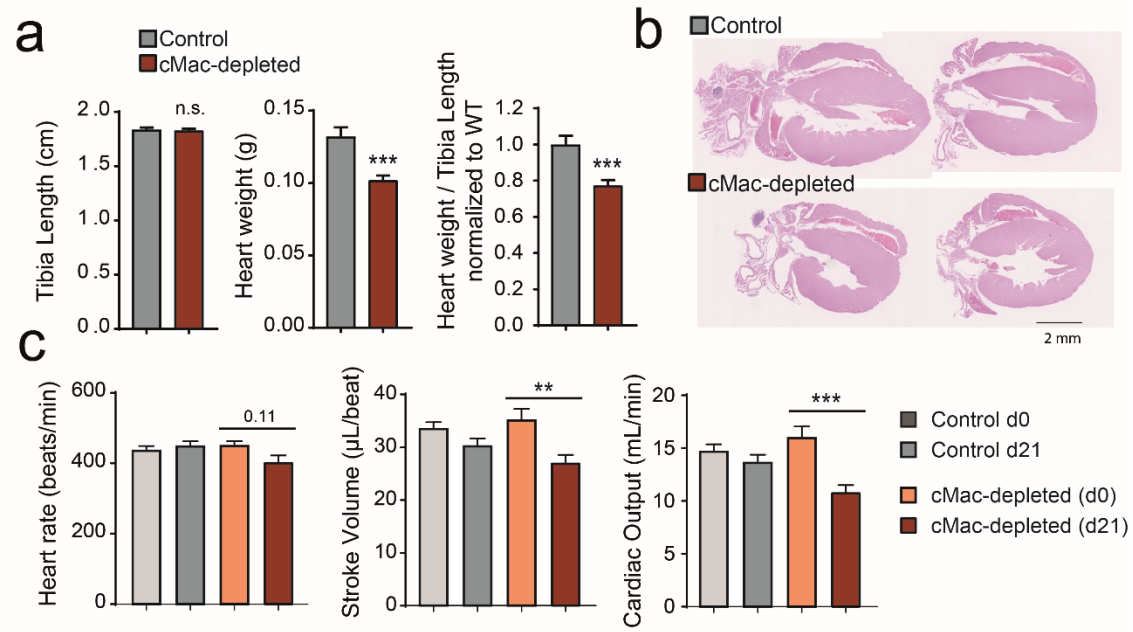

Figure 31. Cardiac mass loss and lower cardiac output in cMac-depleted mice.

Control (WT) and cMac-depleted mice (CD169^{DTR}) treated with DT for 3 weeks were analysed for different parameters. **(a)** Heart weight and tibia length values. Bars show mean ± SEM from 8-10 mice per group. ***, p<0.001; n.s. not significant as determined by unpaired t-test. **(b)** hematoxylin-eosin staining in hearts to show macroscopic changes. Scale bar, 2 mm. **(c)** Heart rate, stroke volume and cardiac output parameters as obtained by echocardiography. Bars show mean ± SEM from 15-21 mice per group. **, p<0.01; ***, p<0.001 as determined by unpaired t-test.

Although we confirmed systolic defects by intra-cardiac hemodynamic analysis, as indicated by lower LV-end systolic pressure (LVESP) and a significant reduction in maximal dP/dt at baseline and after isoproterenol infusion (Fig.32b), no significant changes in LV-ejection fraction (% EF) and fractional shortening (% FS) were found by echocardiography (Fig.30b). Thus, the significant reduction in LVESP could be explained by a lower LV afterload rather than systolic dysfunction, but confirmation of this will require further direct measures of blood pressure. Interestingly, we found significant impairment in diastolic function, characterized a reduction of mitral E to A wave ratios (E/A ratio) during filling of the left ventricle (Fig.30b), suggestive of dysfunctional diastole, which was consistent with the observed reduction in -dP/dt max at baseline and after isoproterenol infusion (Fig.32c).

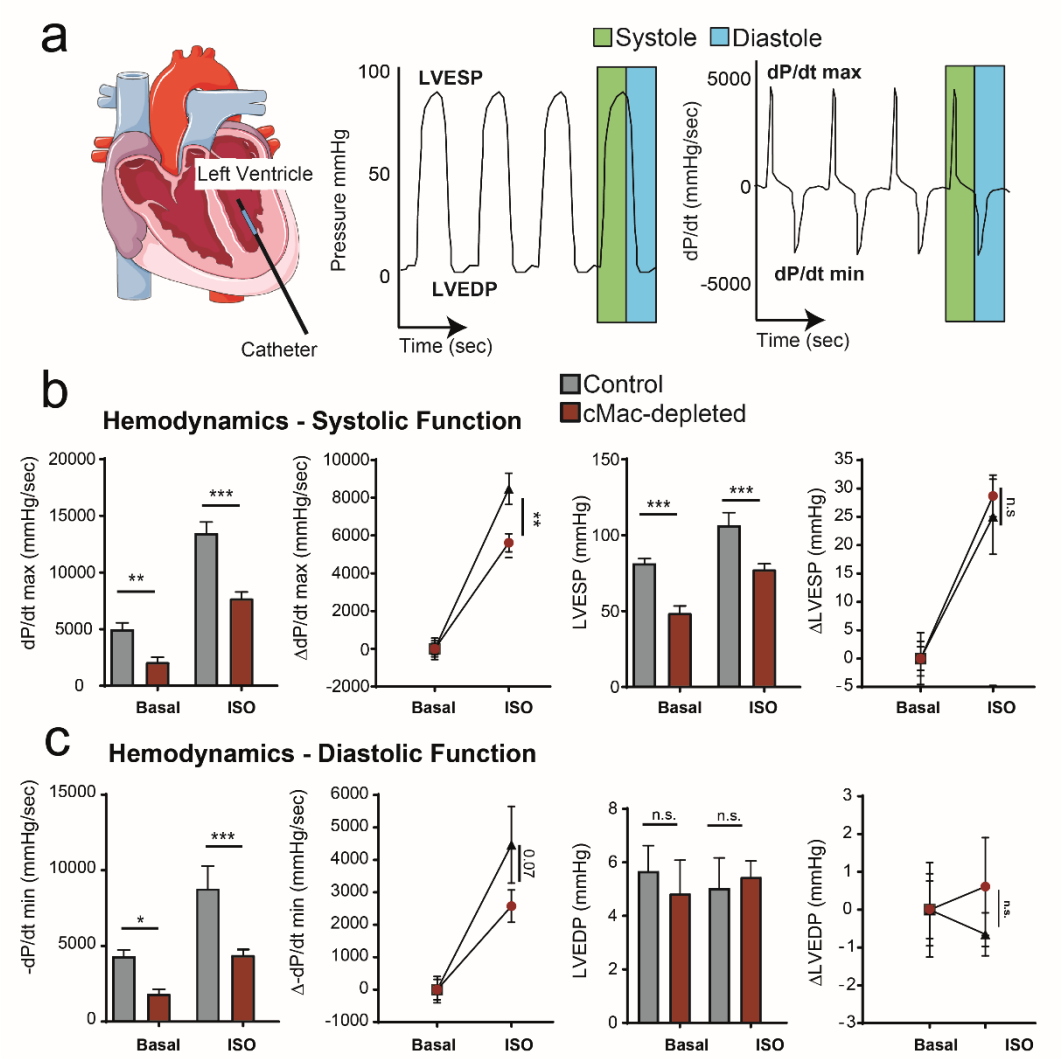

Figure 32. Intracardiac hemodynamics in cMac-depleted mice.

Control (WT) and cMac-depleted mice (CD169^{DTR}) treated with DT for 3 weeks were analysed for different parameters. **(a)** Experimental scheme for intracardiac hemodynamics. A catheter was introduced in the left ventricle (as indicated in methods) and recordings were made for different parameters in basal and 5 minutes after Isoproterenol administration. **(b-c)** Values for those parameters indicative for systolic **(b)**, or diastolic **(c)** function are shown. Parameters represented are Left ventricular end-systolic pressure (LVESP), left ventricle end-diastolic pressure (LVEDP), maximal derivative of LV pressure (dP/dtmax) and minimal derivative of LV pressure (-dP/dtmin). Absolute values are shown in bar graphs as Mean ± SEM, while the difference between basal and isoproterenol is expressed as delta(Δ) vs basal in dot plots. N = 5-6 mice. *, p<0.05; **, p<0.01; ***, p<0.001; n.s. not significant, as determined by two-way ANOVA.

Because the structural changes after depletion of cMacs could cause irreversible alterations in heart function, we examined to what extent these cardiac anomalies could be reverted if cMacs were allowed to repopulate the myocardium. To this end, we treated CD169^{DTR} mice with DT for three weeks, and then ceased treatment and

followed the mice for 10 more weeks (Fig.33a). Concomitant to restoration of cMac numbers (Fig.33b), ventricular volumes and both systolic (cardiac output) and diastolic (E/A ratio) functions returned to stable baseline values (Fig.33c). Interestingly, ventricular mass values remained low after cMac return, suggesting that cMacs support diastolic function independent of other effects on cardiac structure. We conclude that, by supporting the metabolic and structural demands of cardiomyocytes, cMacs sustain the mechanical properties of the myocardium. Although we propose that many of these alterations arise from alterations in autophagy and exopher production in the absence of macrophages, it is likely that cMacs contribute to myocardial stability through additional mechanisms not addressed here.

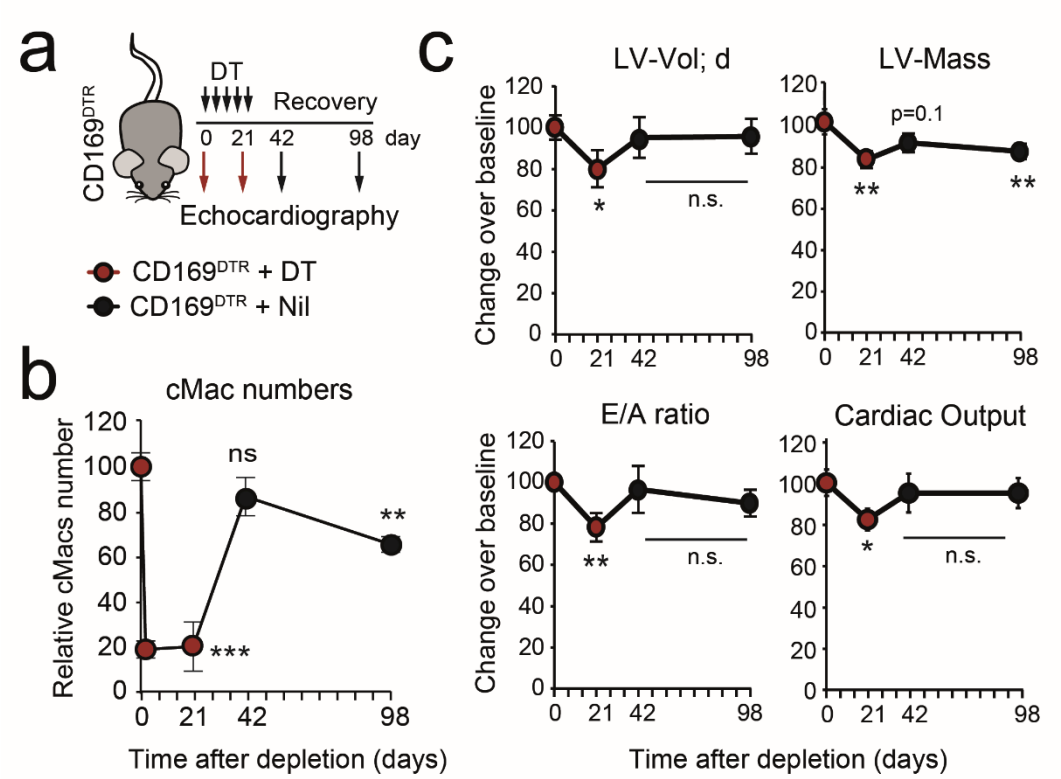

Figure 33. Restoration of cMacs rescue cardiac function

(a) Experimental scheme to analyze cardiac function by echocardiography after cMac recovery. **(b)** Number of cMacs per gram of heart in CD169^{DTR} mice treated with DT for 21 days and then left untreated. Measures were obtained at days 0, 2, 21, 42 (day 21 of recovery) and 98 (day 77 of recovery). Data is shown as mean ± SEM normalized to Day 0, from 3-7 mice per time. **, p<0.01; ***, p<0.001; n.s., not significant as determined by unpaired t-test against day 0. **(c)** Selected cardiac parameters measured by echocardiography in CD169^{DTR} mice treated with DT for 21 days, and then allowed to recover. Measures were obtained at the indicated times in the same mice. Data are mean ± SEM normalized to day 0, from 12mice per group. *, p<0.05; **, p<0.01; n.s., not significant, as determined by Student's t-test analysis against day 0. E/A mitral valve fluxes ratio (E/A ratio), left-ventricle volume (LV-Vol), Cardiac output and left ventricle mass (LV-Mass) are shown.

4.3.5. Inflammasome activation in cMac-depleted hearts

Hearts devoid of macrophages lose function over time, with a decreased autophagy flux and energy production, as shown above. However, the connection between these two factors, autophagy and metabolism, remained unclear. Detailed inspection of hearts from cMacs depleted mice by TEM revealed the presence of dismantled exophers (Fig.34a) and concomitant accumulation of free mitochondria in the extracellular space (Fig.34b). Both intracellular damaged mitochondria (Fig.28 and Fig.29) and mitochondria-derived compounds in the extracellular media are strong activators of the inflammasome pathway (please see section 2.3.4. of the Introduction). Accordingly, western blot analyses of cardiac tissue revealed activation of several inflammasome complexes in CD169^{DTR} mice, even at early time points after depletion (Fig.34c).

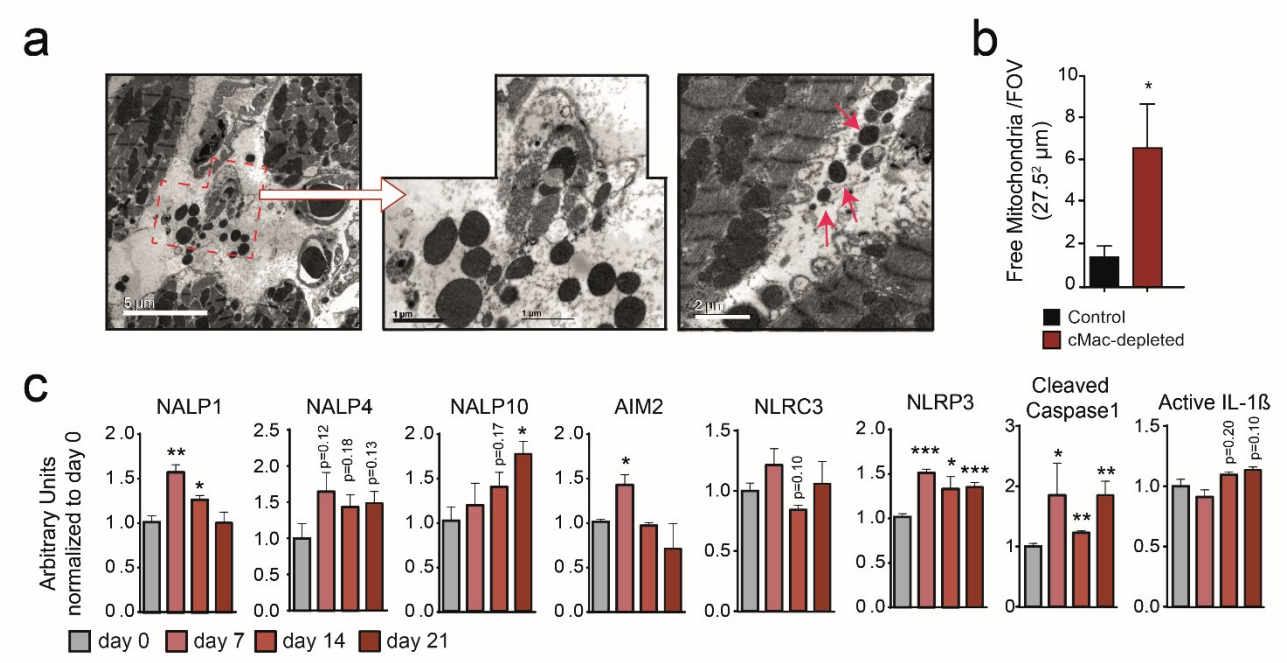

Figure 34. Inflammasome activation in cMac-depleted mice.

(a) TEM images mitochondria released to the extracellular space (red arrows) in Control (WT) and cMac-depleted mice (CD169^{DTR}). Scale bars are 5 µm (left) 1 µm (middle) and 2 µm (right). **(b)** Quantification of free mitochondria per field of view in same animals than in (a). *, p<0.05; as determined by Student's t-test analysis. **(c)** Levels of different inflammasome complexes and related proteins in heart extracts of Control and cMac-depleted mice at the indicated times after DT administration, as measured by western blot. Bar graphs show mean ± SEM protein levels. Data from 3-7 mice per group. *, p<0.05; **, p<0.01; ***, p<0.001 as determined by unpaired t-test.

The inflammasome machinery has been shown to regulate autophagy through cleavage or sequestration of proteins involved in this process (Seveau et al., 2018). This phenomenon may account for the autophagy block and lack of exopher production after long-term cMac depletion (Fig.21a).

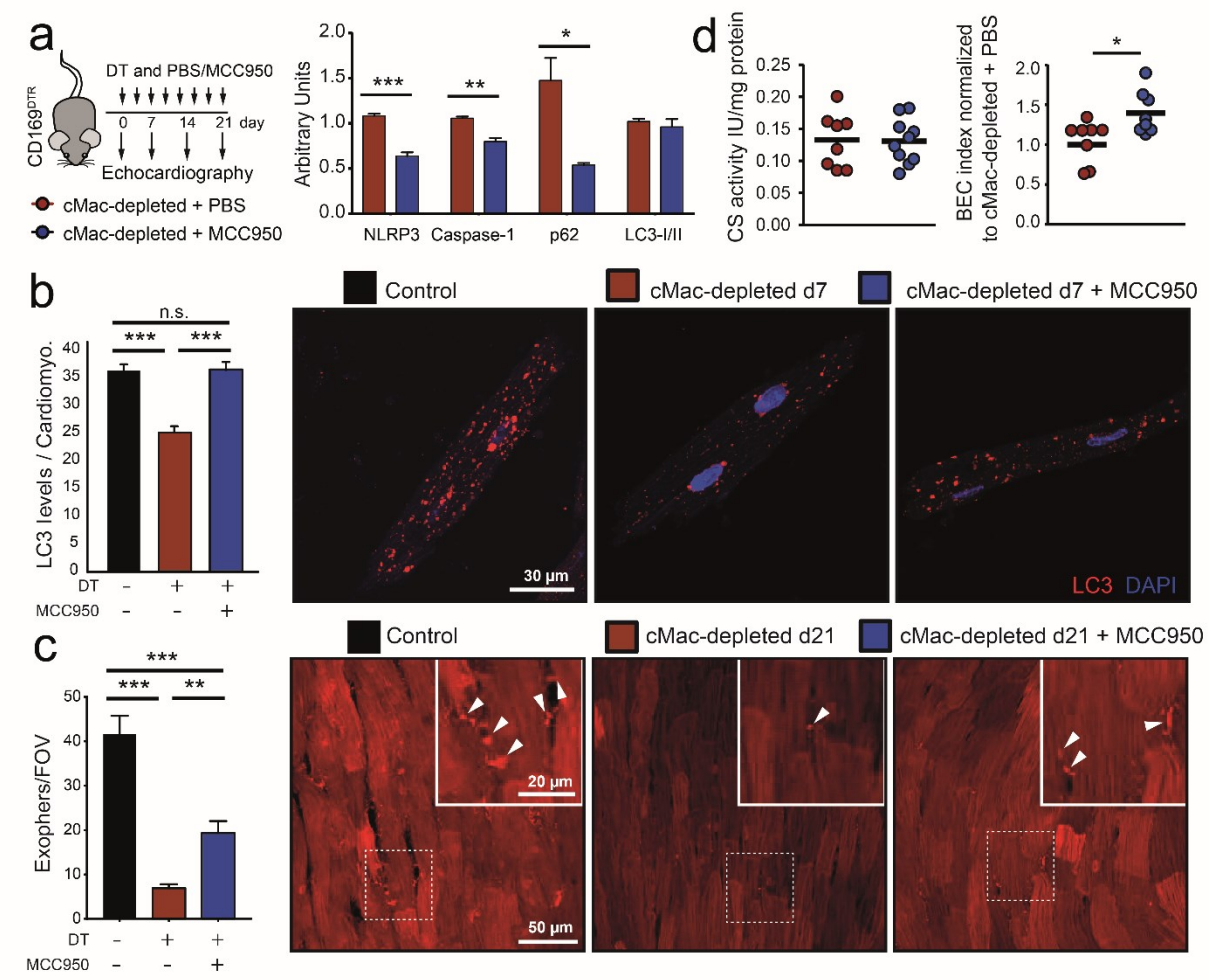

Figure 35. NLRP3 inhibition partially rescues exophers in cMac-depleted mice.

WT (Control) or CD169^{DTR} mice were treated with DT for the indicated times in combination with daily MCC950 or vehicle (PBS). **(a)** (Right) Experimental scheme. (Left) Levels of the indicated proteins, in heart extracts as measured by western blot. Day 21 in treatment. n = 5 mice. **(b)** LC3 levels in isolated cardiomyocytes. Bars show mean ± SEM of LC3+ particles per cardiomyocyte, from 3 mice per group. Scale bar, 20 µm. ***, p<0.001; n.s., not significant, as determined by one-way ANOVA. Day 7 in treatment. **(c)** Representative mircographs (left) and exopher quantification (right). Bars show mean ± SEM exophers per field of view. Data are from 6 mice per group, 2 independent experiments. **, p<0.01; ***, p<0.001; as determined by ANOVA with Tukey´s multiple comparisons test. Day 21 in treatment **(d)** (Left) Graphs shows enzymatic activity per mg of total protein from heart, normalized to the control group. Each dot represents mean for two technical duplicates per mouse, and black lines show means. (Right) Changes in ATPb/GADPH ratios (BEC index) measured by western blot in heart extracts. *, p<0.05 as determined by unpaired t-test. n= 8 mice per group. Day 21 in treatment

Among the inflammasomes analysed, NLRP3 was consistently induced after cMac depletion (Fig.34c). NLRP3 is one of the best studied inflammasome complexes for which a potent pharmacological inhibitor, MCC950, has been developed (Fig.35 and (Coll et al., 2015)). Thus, we assessed the contribution of inflammasome activation towards cardiac alterations by treating cMac-depleted mice with this compound. MCC950 treatment reduced NLRP3 and its target Caspase-1 in cMac-depleted mice. Notably, it also reduced the amount of the autophagy substrate p62 (Fig.35a), a protein that accumulates in cMac-depleted mice (Fig.21d). In line with these findings, MCC950 partially rescued the autophagy flux (Fig.35b), exopher production (Fig.35c), and mitochondrial function in cMac-depleted mice (Fig.35d) suggesting that the autophagy block in cMac-depleted mice is at least in part mediated by inflammasome activation.

Combined, these data establish a regulatory loop involving autophagy, mitochondrial release in exophers and elimination by cMacs. If the latter fails, inflammasome activation blocks autophagy in cardiomyocytes leading to heart dysfunction. Contrasting with this model, however, long-term treatment with MCC950 failed to rescue cardiac function in cMac-depleted mice as assessed by echocardiographic analysis (Fig.36). We conclude that activation of the NLRP3 inflammasome is only partly responsible of the cardiac defects that appear in the absence of cMacs.

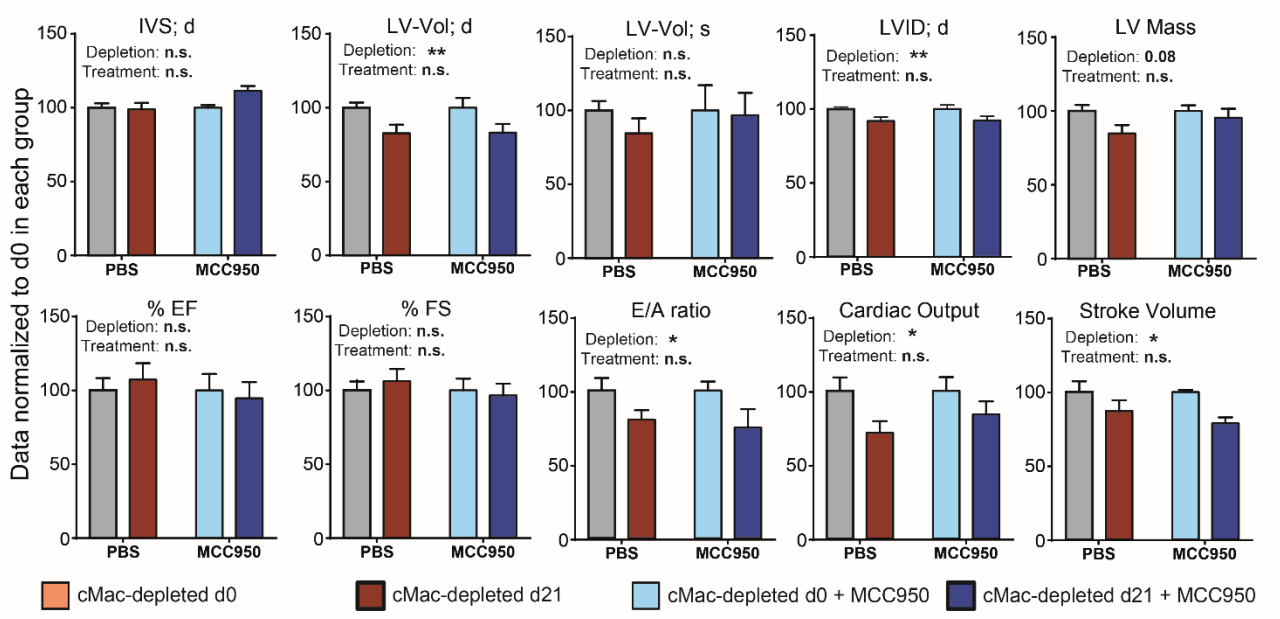

Figure 36. NLRP3 inhibition does not rescue cardiac function in cMac-depleted mice.

Selected cardiac parameters measured by echocardiography in cMac-depleted mice ($CD169^{DTR}$) treated with DT for the indicated times in combination with daily MCC950 or vehicle (PBS). % Fraction shortening (%FS), % Ejection Fraction (%EF), E/A mitral valve fluxes ratio (E/A ratio), interventricular septum thickness (IVS), left-ventricle volume (LV-Vol), left ventricular-internal diameter (LV-ID), left ventricle mass (LV-Mass), Cardiac output and Stroke volume are shown. In some cases, the same parameter is measured at systole (s) and diastole (d). n = 5-10 mice per group.

4.4. Exopher uptake by cardiac macrophages

We finally aimed to better understand the contribution of cMacs in this process. Phagocytosis is not the unique role of macrophages in tissues, they also produce cytokines and participate in organogenesis and repair. Thus, we aimed to identify the pathway(s) used by macrophages to recognize and capture cardiac exophers, as we predicted that this would allow us to interfere with this process while leaving other macrophage functions intact.

4.4.1. Role of Mertk in capture of cardiomyocyte-derived material

Although relatively uncommon, uptake of material from living, functional cells occurs in healthy tissues (a phenomenon of "assisted phagocytosis"; please see part 2.4. of the Introduction). In many of these cases, Mertk, a tyrosine kinase receptor in the surface of phagocytes, mediates recognition of phosphatidylserine (PS) on target cells and allows subsequent internalization (Arandjelovic and Ravichandran, 2015). In addition, Mertk has been further proposed to be important in the heart for debris clearing after myocardial infarction (DeBerge et al., 2017). In addition, Mertk is transcriptionally regulated by LXR nuclear receptors (A-Gonzalez et al., 2009), a signalling pathway that we found altered in our proteome analysis (Fig.26c). Inspection of published databases (Fig.37a from (Pinto et al., 2012)) and qPCR analyses (Fig.37b) confirmed that both Mertk and LXRβ were expressed by heart macrophages. We also confirmed PS exposure by cytometric analyses of isolated exophers, thus demonstrating that exophers are PS+ (Fig.37c). Thus, we considered Mertk a potential candidate to mediate the recognition of cardiac exophers. To assess this directly, we first searched for the presence of PS+ particles in fresh ventricular sections using Annexin V as a probe. We found CX3CR1^{GFP} cMacs localized proximal to PS+ particles (Fig.37c and Movie S9), which supported our contention that Mertk might be a receptor for PS exposed in the surface of exophers.

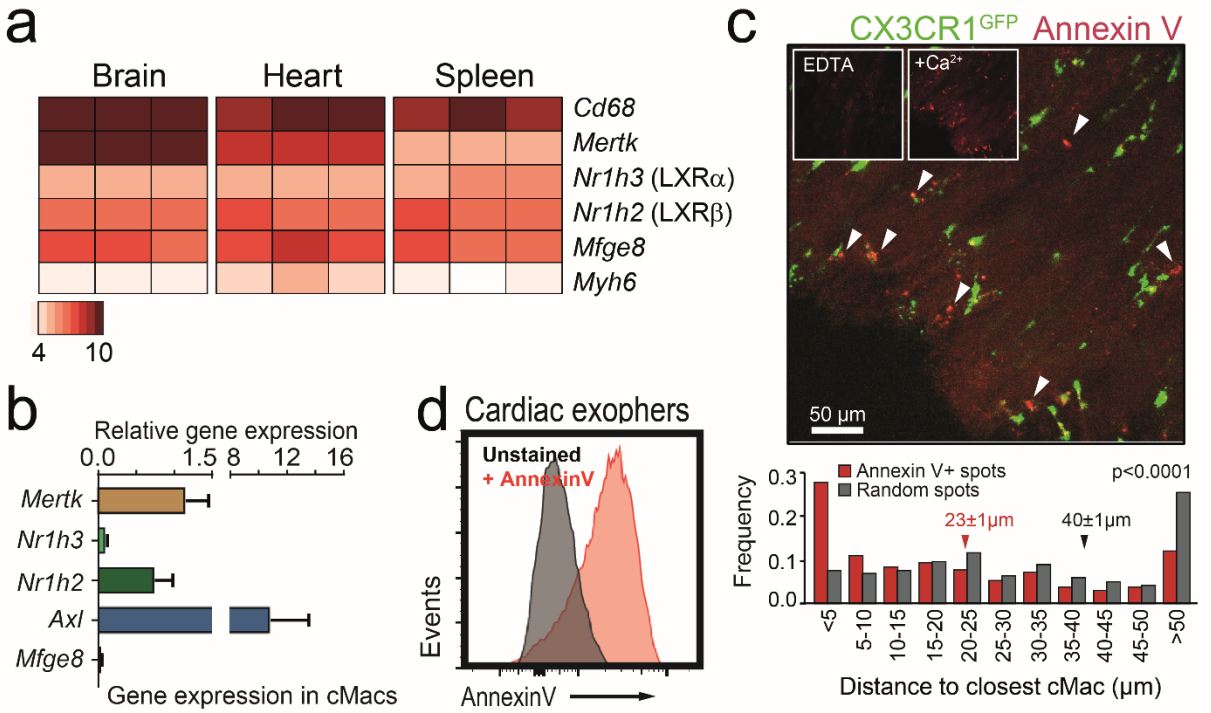

Figure 37. PS exposure in cardiac exophers as a detection signal for cMacs.

(a) Heatmaps showing differential expression of phagocytosis-related genes and Myh6 (negative control) in cMas vs microglia and splenic macrophages. Analyses were performed from public databases (Pinto et al., 2012). **(b)** Expression of genes involved in phagocytosis by qPCR in cMacs. Data normalized to Mertk. Bars show mean ± SEM from 5 mice per group. **(c)** Slices of viable myocardium from CX3CR1^{GFP} mice showing the presence of PS patches (Annexin V; red). Annexin V binding is calcium-dependent (EDTA control), and identifies PS+ patches, which localize proximal to GFP+ cMacs. Bar graph shows distance distribution of Annexin V spots (red) or Random spots (grey) to the closest cMac. Numbers indicate mean ± SEM distances for each group. Data from 16-32 images from 4 mice per group. P value was obtained by nonparametric Mann-Whitney test. See also Movie S9 **(d)** Flow cytometry after AnnexinV staining in exophers of Card^{RED}; LC3^{GFP} mice.

We therefore analysed hearts from LXR- and Mertk-deficient mice. Transfer of cardiomyocyte-derived mitochondria tagged with mt-Keima was severely impaired in mice lacking either Mertk or both LXRα and β receptors (Fig.38a). In addition, we found debris accumulated in the extracellular space of Mertk- and LxR-deficient mice, including large amount of cardiomyocyte-derived mitochondria at levels comparable to cMac-depleted mice (Fig.38b-c), altogether demonstrating that Mertk is an important phagocytic receptor involved in the physiological removal of exophers and mitochondria released into the cardiac milieu.

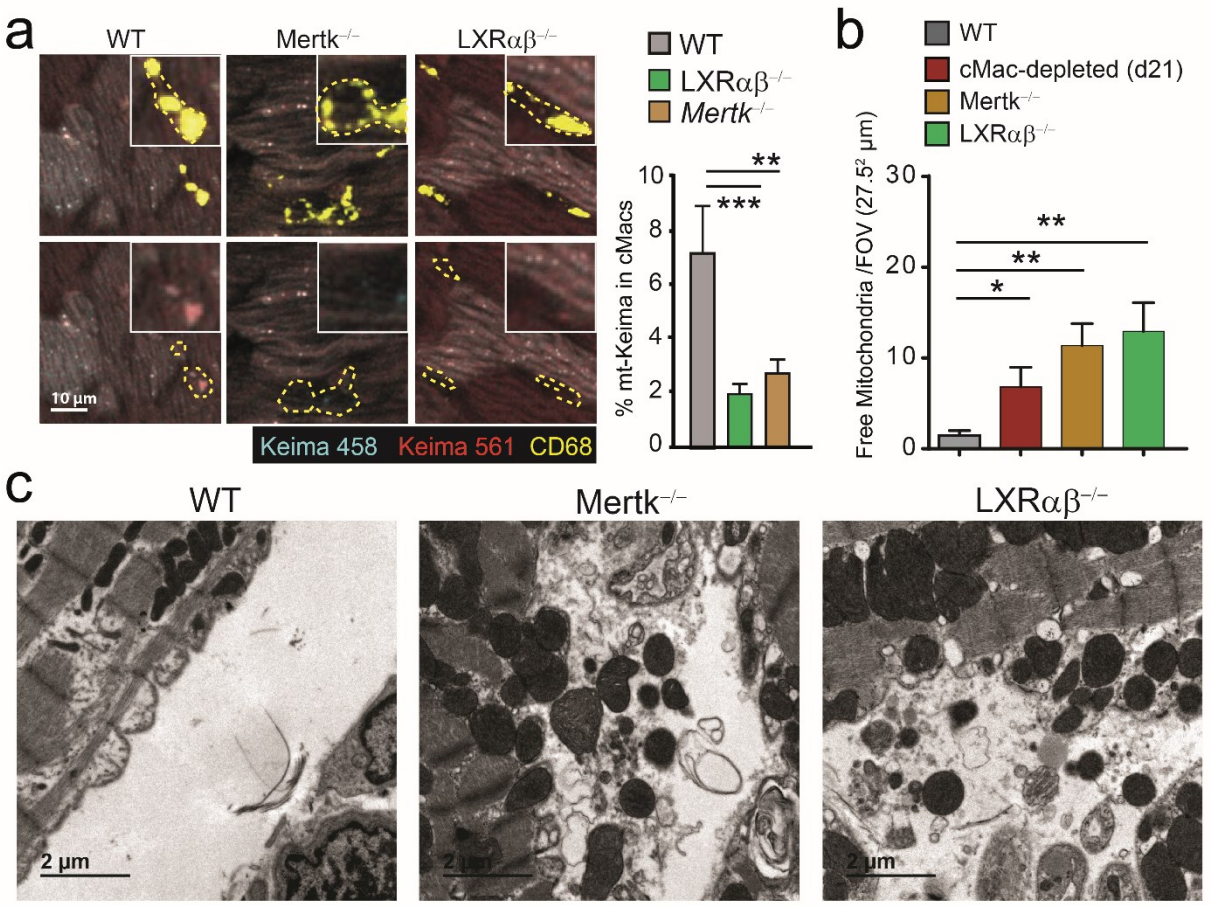

Figure 38. The phagocytic receptor Mertk mediates mitochondria uptake by cMacs.

(a) Bars show the percentage of mt-Keima+ signal inside cMacs in hearts from wild type, *Mertk*$^{-/-}$ and LXRαβ$^{-/-}$ mice infected with AAV9-Keima. Representative micrographs show cMacs (CD68, yellow), and cardiomyocyte-derived mitochondria (mt-Keima; cyan-red). Data are mean ± SEM from 4-5 mice per group. **, p<0.01; ***, p<0.001; n.s., not significant as determined by nonparametric Kruskal-Wallis analysis with Dunn´s multiple comparison test against WT. **(b-c)** Quantification of free mitochondria per field of view by TEM (b) and TEM images of mitochondria released to the extracellular space in wild type, *Mertk*$^{-/-}$ and LXRαβ$^{-/-}$ mice (c). *, p<0.05; **, p<0.01; as determined by nonparametric Kruskal-Wallis analysis with Dunn´s multiple comparison test against WT.

4.4.2. Inflammasome activation and autophagy alterations in Mertk-deficient mice.

Our previous analyses of cMac-depleted hearts revealed activation of the Inflammasome. Indeed, extracellular accumulation of cardiomyocyte-derived mitochondria in hearts from depleted and mutant mice (Fig.38b-c) might represent a common signal for activation of the NLRP3 inflammasome. Consistent with this possibility, western blot analyses of heart tissue from LXR- and Mertk-deficient mice revealed Inflammasome activation (Fig.39a). Similar to $CD169^{DTR}$ mice, inflammasome activation was concomitant to a reduction of the autophagy flux in *Mertk*$^{-/-}$ mice (Fig.39c), suggesting partial blockade in autophagy. Western Blot analysis of autophagy related proteins in mice lacking Mertk or LXR receptors showed higher LC3-II to LC3-I ratios and p62 accumulation (Fig.39b), confirming autophagy blockade in these mice.

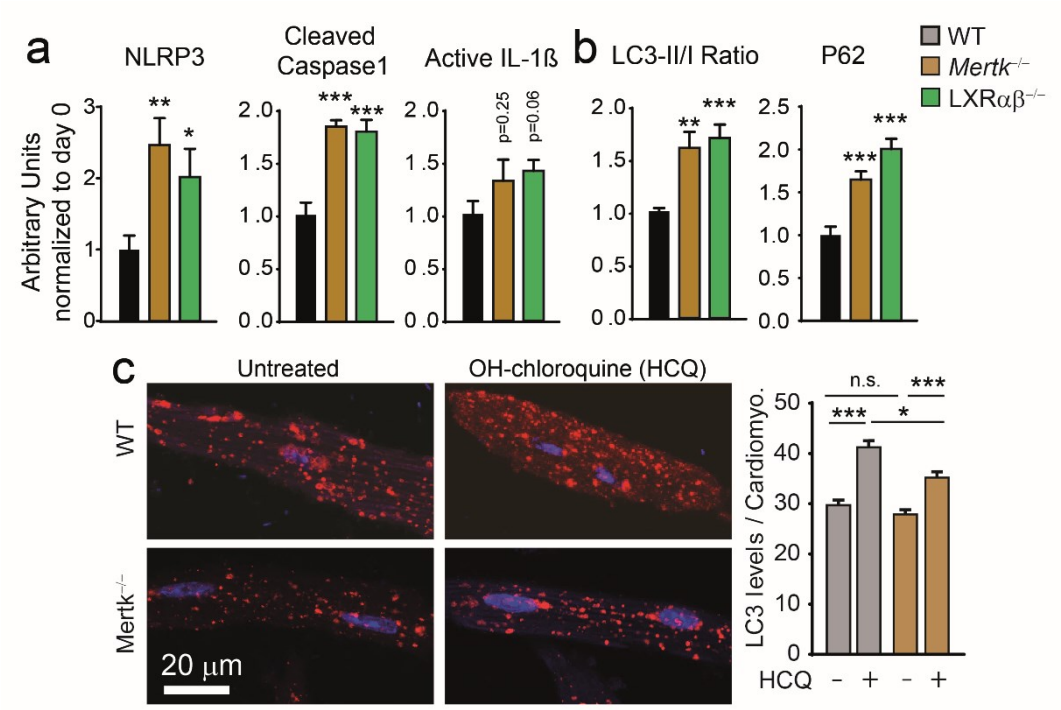

Figure 39. Inflammasome activation and autophagy block in Mertk-deficient mice.

(a-b) Levels of different NLRP3 inflammasome related- (a) or autophagy related-proteins (b) in heart extracts of wild type, *Mertk*$^{-/-}$ and LXRαβ$^{-/-}$ mice, as measured by western blot. Bar graphs show mean ± SEM protein levels. Data from 6-7 mice per group. *, p<0.05; **, p<0.01; ***, p<0.001 as determined by unpaired t-test. **(c)** Autophagy flux in isolated cardiomyocytes from wild type, *Mertk*$^{-/-}$ and LXRαβ$^{-/-}$ mice mice. Fluxes were measured by staining for LC3 (red) and nuclei (DAPI, blue) in basal and Hydroxychloroquine (HCQ)-treated cells. Bars show mean ± SEM of LC3+ particles per cardiomyocyte. n = 3 mice per group. Scale bar, 20 µm. *, p<0.05; ***, p<0.001; n.s., not significant, as determined by ANOVA.

4.4.3. Mertk-deficiency causes progressive alterations in the heart

Through TEM and functional studies we found that cardiomyocytes from Mertk-deficient mice recapitulated some of the defects found in cMac-depleted hearts, including sarcomere shortening (Fig.40a-b), increased number of mitochondria by TEM and Tom20 staining (Fig.40a and Fig40.c), and aberrant mitochondrial morphology and lower crista density (Fig.40d).

Mertk deficiency or mutations in mice or humans (Duncan et al., 2003; Gal et al., 2000) cause retinal alterations that are worsened with age. In line with this, we found a decline in mitochondrial quality in 30 week-old aged *Mertk*$^{-/-}$ mice (Fig.40e-f). Finally, supporting mitochondrial dysfunction in these mice, we found elevated *in vivo* uptake of the glucose analogue 2-deoxy-2-(^{18}F)-fluoro-D-glucose (^{18}F-FDG) by PET-CT imaging, thus revealing a metabolic switch to preferential glucose use in the absence of functional cMacs (Fig.40d). Thus, uptake of cardiomyocyte derived material through Mertk-dependent phagocytosis contributes to maintaining mitochondria quality and metabolic stability in cardiomyocytes. The mechanisms by which Mertk-deficiency affects cardiac structure and function at latter time points should be addressed in future studies.

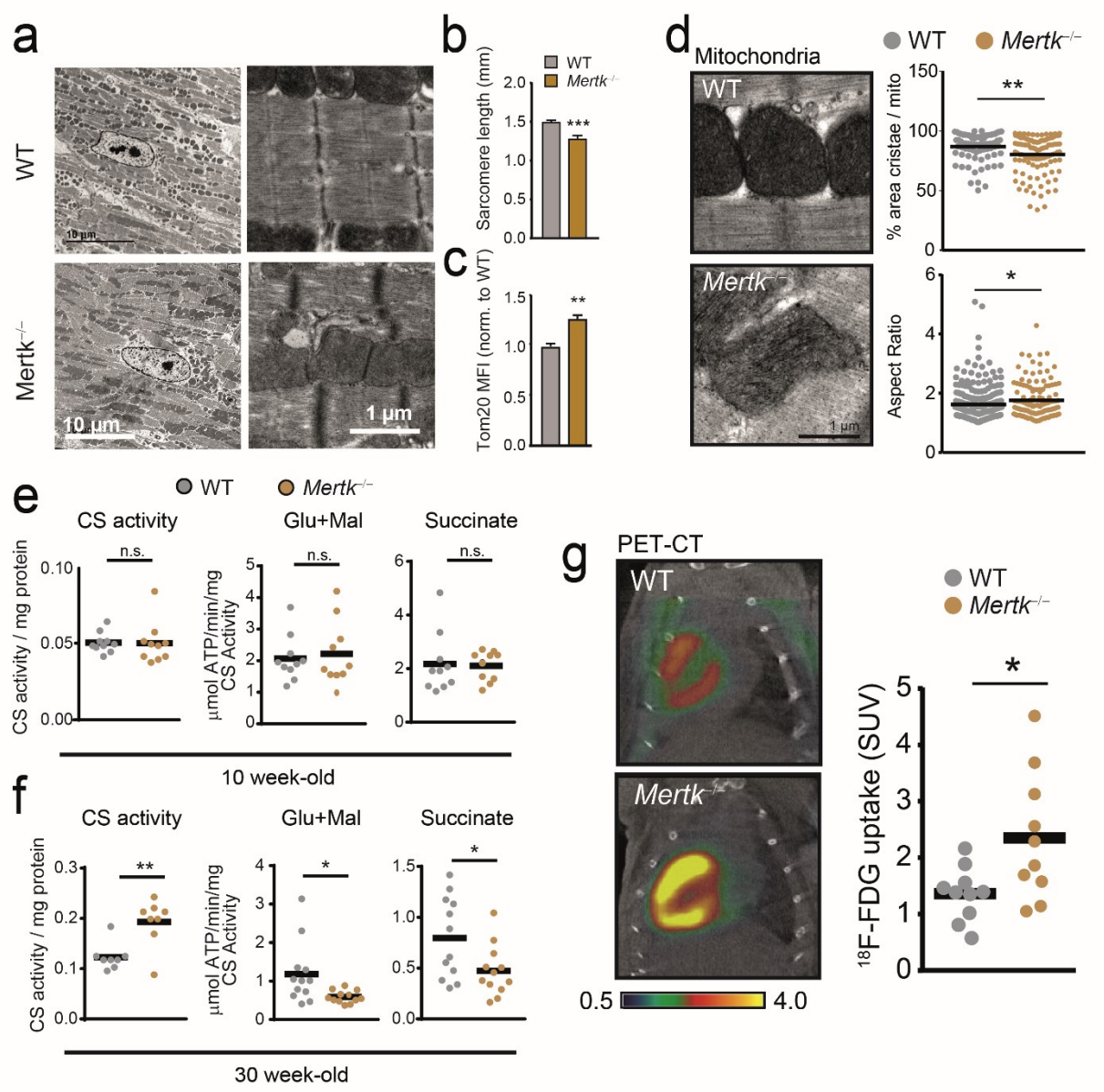

Figure 40. Inflammasome activation and autophagy block in Mertk-deficient mice.

Wild type and *Mertk*$^{-/-}$ mice were analyzed for different parameters. **(a)** Representative TEM images. Scale bars, 10 µm (Left) or 1 µm (Right). **(b-c)** Sarcomere length (b) and mitochondrial content determined by Tom20 immunofluorescence analysis (c). Bars show mean ± SEM from n= 9-10 mice per group; **, p<0.01; ***, p<0.01; as determined by unpaired t-test. **(d)** TEM images (micrographs at left), and morphometric parameters and quantification of mitochondrial area and cristae area per mitochondria. Each dot represents one mitochondria and bars show means, from 15-20 images from 3-4 mice per group. **, p<0.01; *, p<0.05 as determined by nonparametric Mann-Whitney test. **(e-f)** CS activity and Ex vivo ATP production rates in isolated mitochondria in wild-type or *Mertk*$^{-/-}$ mice at different ages in the presence of the indicated substrates (glutamate + malate, or succinate). ATP values are corrected to CS activity and bars represent means; data from 10-12 mice per group. Each dot is the mean for 2 technical duplicates. *, p<0.05; **, p<0.01; n.s, not significant, as determined by unpaired t-test. **(g)** PET-CT images of ^{18}F-FDG uptake. Image quantification is shown in dot plots and given as standard uptake values (SUV) at right, where each dot is one mouse; data from 10 mice per group. *, p<0.05; as determined by unpaired t-test.

5. Discussion

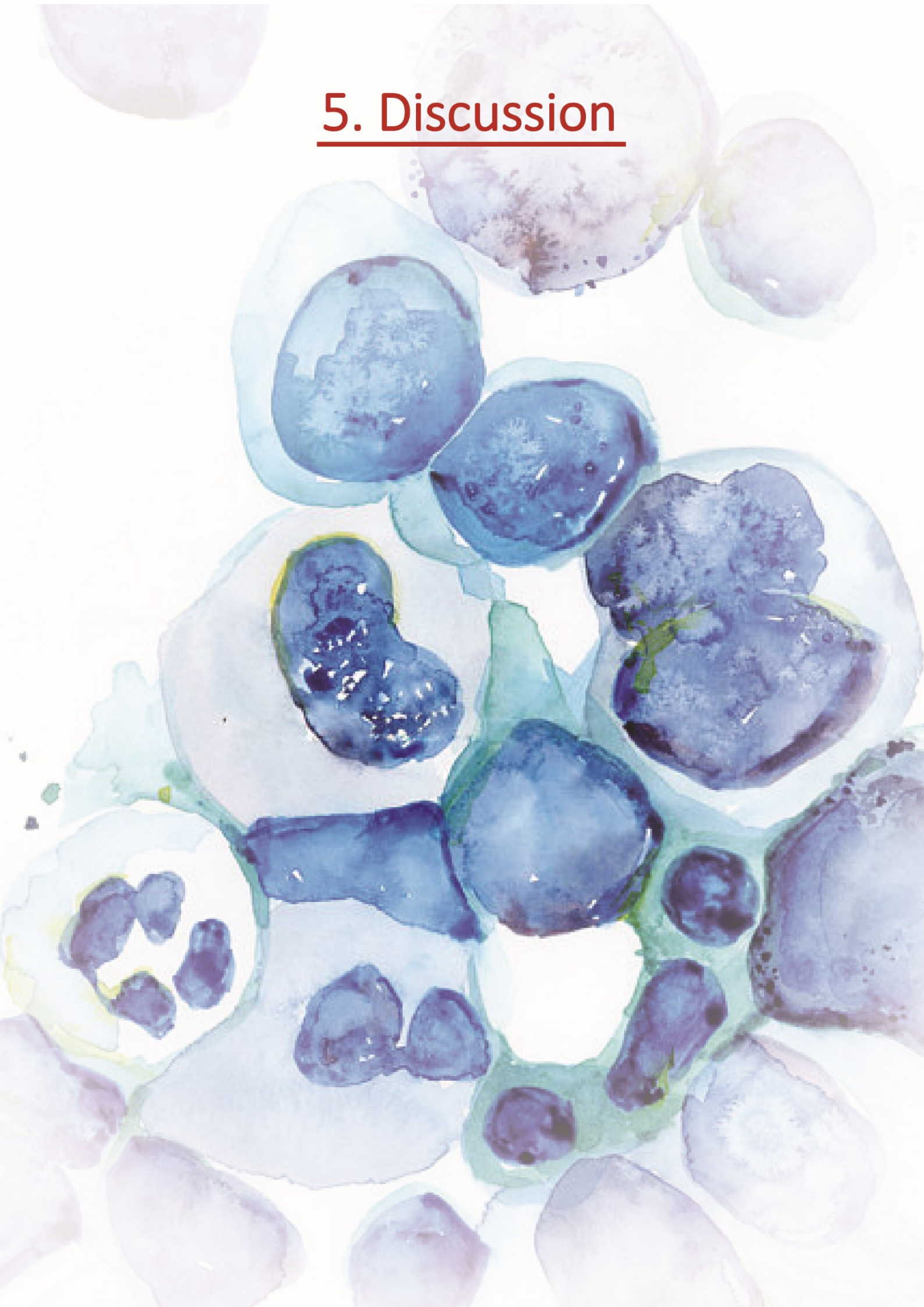

5. Discussion

In the present thesis, we have defined several aspects of the biology of cardiac-resident macrophages (cMacs). More importantly, we uncover a new mechanism by which cMacs help cardiomyocytes to get rid of unwanted cellular debris, including damaged mitochondria.

Virtually every tissue in the body contains resident macrophages and in many instances various phenotypically distinct subsets are evident in discrete micro-anatomical niches of the same tissue. Those cells fulfill tissue-specific and niche-specific functions critical to maintain homeostasis in a wide number of organs (Davies et al., 2013). Accordingly, this thesis demonstrates that macrophages are important for cardiomyocyte homeostasis and heart physiology, since elimination of cMacs or interference in their phagocytic ability with various genetic tools results in cardiac dysfunction with time.

From a broader perspective, identification of active phagocytosis of cardiomyocyte-derived organelles by cMacs establishes a paradigm for how resident phagocytes contribute to tissue homeostasis. It also predicts that idiopathic cardiac pathologies may, in some instances, emanate from defects in these support leukocytes, rather than in cardiomyocytes.

A central conclusion of this PhD thesis is that cMacs are a key component of the cardiac tissue, and that they provide a type of support for cardiac function that was previously unknown.

5.1. cMacs are an important component of the Heart

The discovery of cMacs is quite recent (Pinto et al., 2012), and thus many aspects of those cells are poorly understood. Using a combination of flow cytometry and imaging techniques, my thesis work demonstrates that macrophages are highly abundant in the healthy adult mouse heart, and display an even distribution in the organ (Fig1-3). On average, each cMac establish contacts with 5 different cardiomyocyte and vice versa, creating a highly interconnected partnership with those cells (Fig.4). However, cMacs have been reported to be increased and display a pro-inflammatory phenotype in aged mice (Hulsmans et al., 2017; Pinto et al., 2014) but also display unique dynamics of recruitment during the postnatal period (Lavine et al., 2014). It is unclear how changes in the number and phenotype of cMacs from embryonic stages (Epelman et al., 2014a) to old age influences cardiac function.

We have found heterogeneity in the expression of certain markers (Fig.1) and micro-anatomical location of cMacs (Fig.3), both observations are of unknown significance. In particular, my work has focused in cMacs imbricated between cardiomyocytes, however other cMacs are specifically located in perivascular regions and the pericardium (Fig.3). Perivascular cMacs may have similar roles to perivascular populations of macrophages in other issues like preservation of blood-tissue barriers, immune defense against blood-borne pathogens, control of inflammatory responses or prevention of fibrosis (Chakarov et al., 2019; Lapenna et al., 2018). Also intriguing is the presence of a barrier of macrophages in the pericardium. A recent report proposed anti-fibrotic responses for these cells after myocardial infarction, which display a transcriptional profile closer to peritoneal and pleural macrophages than to other macrophages in the heart (Deniset et al., 2019). Importantly, a previous study reported increased cMacs density in the atrio-ventricular node. Conditional deletion of connexin 43 in macrophages or macrophage depletion demonstrated a role for this population of macrophages in atrioventricular conduction. This was the first description of a homeostatic role for cMacs, thereby establishing a role for these cells in basal cardiac function (Hulsmans et al., 2017). Contrasting with this report, we did not find accumulation of macrophages in this or any other micro-anatomical region (Fig.3) even if the same reporter mice model ($Cx3cr1^{GFP}$)

was used in both studies. While these discrepancies may be explained by differences in the imaging protocol and age of the mice used, the observation of large numbers of macrophages populating multiple regions of the healthy heart, including the ventricular myocardium, suggests broader homeostatic functions for heart-resident macrophages than previously anticipated. In this regard, our data shows that cMacs are actively phagocytic in the heart, contributing to the elimination of material originating from different sources, including infiltrating leukocytes, endothelial cells and cardiomyocytes (Fig.5).

Thus, my work has identified cMacs endowed with phagocytic activity as a functional component of the healthy myocardium, a finding that reinforces the notion that phagocytosis optimizes tissue function (Gordon, 2016).

5.2. Cardiac exophers: a mechanism of surrogated autophagy.

My thesis work has identified an alternative route for elimination of proteins and mitochondria from healthy or stressed cardiomyocytes that is driven by components of the autophagy machinery, but uniquely relies in previously unidentified, membranous structures (cardiac exophers), and ultimately relies on cMacs for efficient elimination. Our findings have a number of potential implications: first, they reveal that autophagy in a mammalian heart can be completed by the exchange of material between cells. Second, it predicts the existence of dedicated biochemical mediators in cardiomyocytes that sort unfit mitochondria between intracellular autophagosomes and exophers for ejection outside the cell.

5.2.1. Cardiac exophers: A mechanism for transcellular degradation of cardiomyocyte material.

Based on the observation that macrophages were able to incorporate fluorescent material originated in cardiomyocytes, an assay developed in this thesis (Fig.5), we decided to explore the nature of this process. By imaging the hearts of mice with fluorescent cardiomyocytes we identify subcellular particles (Fig.6) that we termed "cardiac exophers". We used this terminology because cardiac exophers present an average diameter of 3.5 µm (Fig.6), very close to the 4 µm diameter reported in similar structures in neurons (Melentijevic et al., 2017). These particles are big enough to contain several organelles at once (Fig.7 and (Melentijevic et al., 2017)) and should not be confounded with exosomes, which are 100 times smaller (typically ~ 40 to 100 nm in diameter (Maas et al., 2017)). Actually, the size of an exopher is closer to apoptotic bodies (1–5 µm diameter), which are subcellular fragments produced during apoptotic cell disassembly and are considered the largest type of vesicle in the extracellular vesicle family (Atkin-Smith and Poon, 2017). However, contrary to apoptotic bodies, exophers are produced by live viable cells and may thus be endowed with unique biological functions.

Adult mammalian cardiomyocytes present extremely long lifespans and low renewal rates. With an estimated annual turnover of 0.3-1% for adult humans, this implies that less than 50% of cardiomyocytes are exchanged during a normal lifespan (Bergmann et al., 2009). Thus, transfer of cardiomyocyte-derived material to cMacs due to cardiomyocyte apoptosis may be very low in steady-state conditions. Counterintuitively, however, we found cardiac exophers in the extracellular space, many of which located close to, or inside, cMacs (Fig.6). This data suggested that transfer of cellular material between cardiomyocytes and cMacs, as also observed by flow cytometry (Fig.5), occurs through these particles.

Examination of cardiac exophers by TEM and proteomics analyses revealed specific enrichment in mitochondria-borne proteins, when compared to total cardiac tissue (Fig.7 and Fig.9-10). In addition, we demonstrate the transference of cardiomyocyte-derived mitochondrial protein (mt-Keima) (Fig.13) and mtDNA to neighboring cMacs (Fig.12). Recent reports show that mitochondria can be transferred between cells to contribute with positive roles, such as mesenchymal stem cells via tunneling nanotubes (Rodriguez et al., 2018) and astrocytes to neurons in a stroke model (Hayakawa et al., 2016). However, we find that most mitochondria in cardiac exophers are damaged (Fig.15) and they are degraded after uptake by cMacs (Fig.14), uncovering a previously underappreciated option for mitochondrial quality control in cardiomyocytes: mitochondrial expulsion for surrogated elimination by neighboring cMacs (Fig.41, see below). Our results, along with a previous report in ganglionar neurons of the retina (Davis et al., 2014), constitute the only examples to our knowledge of transcellular degradation of mitochondria (or “transmitophagy”).

In summary, we identify a new subcellular entity produced by cardiomyocytes, the cardiac exophers. Those particles are enriched in damaged mitochondria and constitute a newly-identified type of mechanism of quality control, by which cardiomyocytes transfer damaged cellular material to surrounding macrophages.

5.2.2. The connection between cardiac exophers and autophagy

Similar to neural exophers in *C. elegans* (Melentijevic et al., 2017), cardiac exophers accumulated varied cargo: mitochondria, sarcomere fragments, protein aggregates…etc (Fig.7-10), thus identifying exopher formation and transfer as a general quality control mechanism.

Interestingly, TEM and immunofluorescence analysis of exophers showed heterogeneity in the cargo between exophers, for example some transported sarcomeric proteins while others did not (Fig.7 and Fig.10). Another important finding was that exopher production could be modulated by stress, such as administration of isoproterenol or myocardial infarction (Fig.22-24). Thus, we propose that exopher numbers and content may vary depending on what cardiomyocytes need in each context. An open question is to determine whether and how exopher content varies under different physiological or pathological conditions, such as those induced upon mitochondrial stress (e.g., by treatment with Isoproterenol or Paraquat) or protein aggregation seen in certain cardiomyopathies (Dorsch et al., 2019).

Here, by using autophagy-inducing drugs (Fig.17) or genetic models (*Atg7* deficiency) (Fig.16 and Fig.18-19), we demonstrate a functional connection between exopher formation and autophagy. Autophagy is an ancient mechanism dedicated to maintaining cellular homeostasis through the degradation of damaged cytoplasmic components and organelles (Rubinsztein et al., 2011). Conventionally, this occurs through fusion of autophagosomes with lysosomes inside the cell. In contrast to degradative autophagy, it has been shown that the autophagic machinery, through shared but partially divergent pathways, may lead to secretion of cytoplasmic constituents instead of their degradation in a process termed “secretory autophagy” (Ponpuak et al., 2015). Either way, both mechanisms allow cells to get rid of cytoplasmic material, but the biological functions and consequences may be entirely different, as further discussed in the next section.

Are then cardiac exophers a type of ejected autophagosomes? Both cardiac exophers and autophagosomes recruit LC3 (Fig.16), a molecule with roles in autophagosome

formation and substrate selection, and their formation is regulated by Atg7 (Fig.19) (Rubinsztein et al., 2011). At present, however, we cannot discriminate whether exophers are a type of autophagosome. In one hand it may be that, in some instances, the outer membrane of autophagosomes fuse with the plasma membrane instead of lysosomes (Ponpuak et al., 2015), thus releasing their content to the extracellular space surrounded by the autophagosome´s inner membrane. Alternatively, exophers may constitute a previously unrecognized type of quality control mechanism that share molecular mediators with autophagy (Discussion Figure 1).

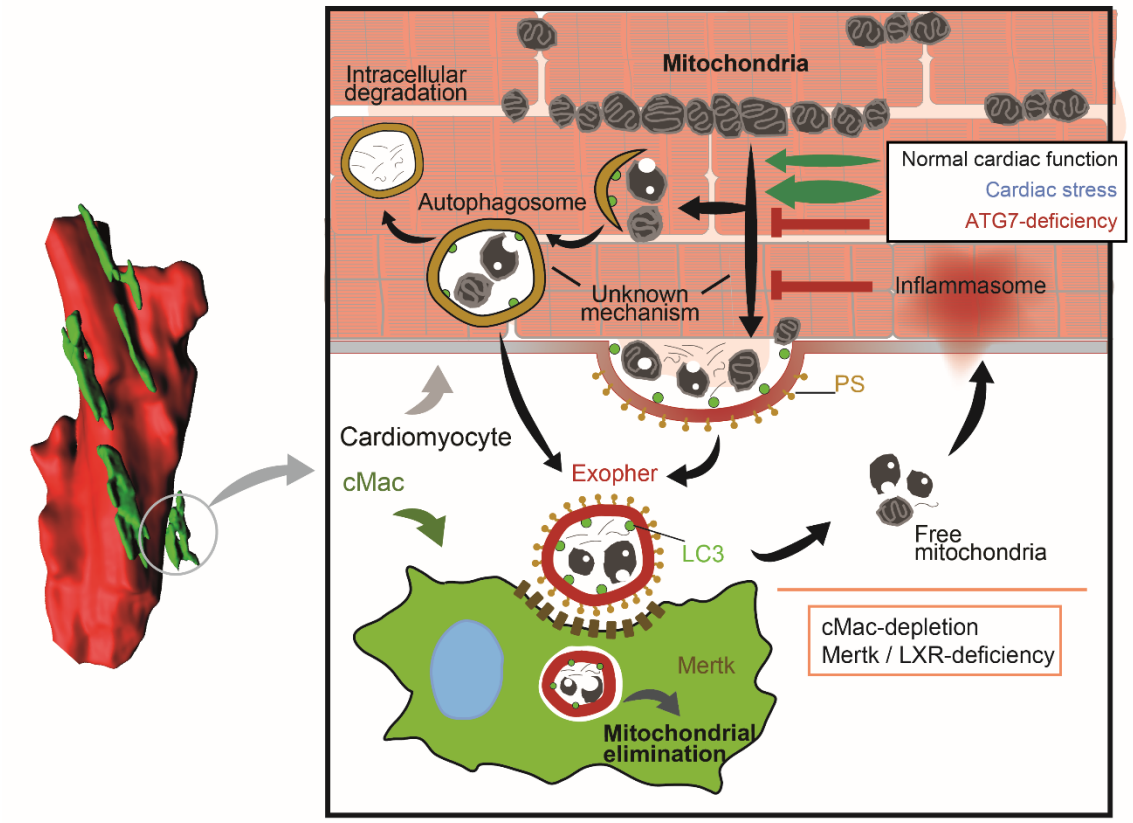

Discussion Figure 1. Model of mitochondrial elimination through cardiac exophers.

Model of the mechanism reported here. Mitochondria are damaged due to the normal function of cardiomyocytes and higher abundance of damaged mitochondria can be detected in the border of the cell. Part of these mitochondria are intracellularly degraded while others are packed and released inside exophers into the extracellular space. The process is driven by the cardiomyocyte's autophagy machinery, is stimulated by stress (e.g., isoproterenol treatment) and inhibited by deficiency in Atg7. Ejected exophers are phagocytosed by neighbouring cMacs through the receptor Mertk. In the absence of cMacs or Mertk, mitochondria and other material are released to the milieu and can activate the inflammasome, which in turn inhibits autophagy and impairs production of new exophers.

Overall, although further experiments are needed to elucidate the detailed mechanisms at play, we probe the connection between the production of cardiac exophers and autophagy. Our results predict that previously unidentified factors are operating in cardiomyocytes to sort unfit mitochondria between intracellular degradation systems (i.e. macroautophagy) and exophers for ejection outside the cell. Mechanistic dissection of this novel facet of proteostasis and mitochondrial homeostasis should be highly informative for a better understanding of cardiomyocytes homeostasis and therapeutic interventions in some forms of myocardial disease.

5.2.3. Functional requirement for cardiac exophers

We find that production of cardiac exophers by cardiomyocytes is a mechanism for clearing out dysfunctional mitochondria and other cellular components that may jeopardize cardiomyocyte homeostasis (Dai et al., 2014a). There are some examples in biology of cells that require this form of "assisted" phagocytosis for the elimination of cellular waste. For example, in some neurons trough structures that resemble exophers (Davis et al., 2014) and photoreceptors, which depend on neighboring cells for the elimination of damaged photoreceptor discs. When this assisted phagocytosis fails (by deficiency in certain receptors) the cells die thereby causing blindness, as seen in both mice and humans (Gal et al., 2000; Kim et al., 2013). Indeed, we find remarkable similarities between the removal of cardiac mitochondria and naturally damaged photoreceptors in the retina: both are essential for organ function, are surrogated by highly specialized parenchymal cells, and rely on the PS receptor Mertk for the capture of the eliminated material.

Just like in dedicated photosensing cells, cardiomyocytes are very specialized with about one third of their volume occupied by mitochondria (Schaper et al., 1985), which is a reflect of the enormous energetic demands of these cells with uninterrupted function throughout the organism's lifetime (Piquereau and Ventura-Clapier, 2018). Thus, assisted degradation of mitochondria by neighboring cMacs may ensure persistent cardiomyocyte fitness. Consistent with this notion, our results in cMac-depleted (Fig.26-

29) or Phagocytic-deficient mice (Fig.39-40) show that in both cases cardiomyocytes accumulate debris and damaged organelles with time, thus failing to maintain mitochondria quality and proteostasis in the absence of cMac support.

Conceivably, if only detrimental material (i.e., trash) is eliminated through cardiac exophers, as our data currently suggest, then exophers should always be beneficial for cells. Hence, what is the true benefit of exopher production for cardiomyocytes and why only some cells in the body seem to adopt a surrogated autophagy strategy? In other words, why do we find exopher production so restricted to cardiac cells? Here are some possible explanations underlying the dependence of cardiomyocytes on exophers:

1) Energetically, autophagy is typically regarded as positive for the cell since it provides amino acids for cellular fueling and protein synthesis. However, cardiomyocytes rely very little in amino acid metabolism at steady-state (Lopaschuk and Ussher, 2016). Additionally, autophagy requires ATP at different steps of the process, including initiation and progression, binding of chaperones to substrates and protein unfolding, but mostly for lysosome production, lysosomal acidification (Settembre et al., 2013; Singh and Cuervo, 2011) and intracellular transport for fusion with autophagosomes (Cordonnier et al., 2001). However, cardiomyocytes must devote most of their energy to sarcomere contraction, with an energy storage pool that only allows for a few seconds of activity (Piquereau and Ventura-Clapier, 2018). Thus, it is likely that it would be advantageous for cardiomyocytes to subrogate the degradation its components to professional adjacent phagocytic cells.

2) Structurally, cardiomyocytes are highly differentiated cells of large dimensions (around 130 um length, 30 um thick (Fig.27)), with a cytoplasm fully packed with mitochondria and sarcomere (Fig.28). We propose that these structural features set important constrains that likely limit the fusion of large autophagosomes with lysosomes in the cytoplasm. These constraints are very evident in neurons, in which mitochondria that are damaged in long axons need to travel to the soma for degradation in lysosomes (Davis and Marsh-Armstrong, 2014). Extrusion through exophers and transmitophagy challenge this model, proposing a more

efficient way for neurons to solve the problem. Therefore cells with major architectural constrains, as seen in neurons and cardiomyocytes, may benefit from the professional help of neighboring phagocytes.

3) A more hypothetical consideration is that neurons and cardiomyocytes acquire a "selfish" behavior typical of long-lived cells. There is evidence suggesting that some oxidized lipids and protein aggregates cannot be degraded by cells. Thus, when long-lived post-mitotic cells fail to degrade their waste products, these accumulate in the form of lipofuscin granules, which have unknown consequences for the cell's health. In their "mitochondrial–lysosomal axis theory of aging", Brunk and Terman propose that lysosomal enzymes are directed towards lipofuscin granules in senescent long-lived cells and, subsequently, they are lost for effective autophagy degradation because lipofuscin remains non-degradable (Brunk and Terman, 2002). This could lead to progressive impairment of autophagy and the gradual accumulation of damaged mitochondria and misfolded proteins, features both that lead to aged-related cardiomyopathy (Rubinsztein et al., 2011) and neurodegeneration (Brunk and Terman, 2002). Since both cardiomyocytes and neurons have very low renewal capacity, exopher production may be a self-defense mechanism for long-lived post-mitotic cells to minimize the accumulation of intracellular lipofuscin aggregates, and this remains an important hypothesis to test in future studies.

4) Although we propose that exophers might be beneficial for every cell, it appears to be restricted to some cell types. We note, however, that it would be challenging for phagocytes to manage the vast debris produced if every single cell released their damaged components to the extracellular milieu. Thus, for the common interest of the organism, exopher production should be limited to a subset of "privileged" cells. Interestingly, some cancer cells opt for a similar secretory strategy, which is referred to as tumor-released autophagosomes (TRAPs). In this case, it has been proposed that TRAPs can co-opt macrophage function for the tumor benefit (Wen et al., 2018). These findings suggest that

exophers may not only be a mechanism for waste elimination, but also a means for communication with macrophages.

In summary, we propose that subrogated elimination of mitochondria to cMacs may be a necessary feature of the heart originating from the unique structural, mechanic, and metabolic demands of cardiomyocytes, a cell of uninterrupted function and a fully packed cytoplasm. We propose that assisted phagocytosis by neighboring cMacs may be key to ensure persistent cardiomyocyte fitness during the animal's lifespan.

5.3. Cardiac phenotype of mice with defective cardiac tissue-resident macrophages

From the observation that cardiomyocytes extrude damaged material in exophers, which are captured and degraded by cMacs, we aimed to assess the functional roles of these cells in global heart function. In this work, we mainly focused in two models: mice in which this population is eliminated (CD169^{DTR} model), and mice mutant for *Mertk* gene, which encodes for a major phagocytic receptor.

cMac depletion in CD169^{DTR} mice (Fig.20) results in a progressive accumulation of debris, including damaged mitochondria, outside cardiomyocytes (Fig.34). It is know that mitochondria-derived components are strong activators of the inflammasome (Weinberg et al., 2015) and that inflammasome activation can inhibit autophagy (Seveau et al., 2018). Accordingly, we found activation of several inflammasomes in hearts of cMac depleted mice (Fig.34), which correlated with blockade of autophagy flux and a reduction in exopher production after long-term depletion (Fig21). Intriguingly, the final consequence of long-term cMac depletion was accumulation of dysfunctional mitochondria inside cardiomyocytes, resulting in compromised ATP production (Fig.28-29 and Fig.41) and organ function (Fig.30-32). Altogether, these results reveal that cMacs are important cells for cardiac homeostasis and function.

cMacs depletion in CD169^{DTR} model is an important improvement over existing methods, as these alternative approaches for studying cMac functions (i.e. Clodronate administration, CD11b^{DTR} or Cx3cr1^{DTR} mouse models) affected other leukocyte populations in the heart, such as monocytes or neutrophils (Dick et al., 2019; Epelman et al., 2014a; Heidt et al., 2014; Hulsmans et al., 2017). Nonetheless, CD169^{DTR} mice are not an infallible model since DT administration depletes macrophages in tissues other than the heart, including liver, spleen or bone marrow (Fig.25 and (Chow et al., 2011; Gupta et al., 2016)). Importantly, we did not find systemic inflammation in CD169^{DTR} mice (Table 1) or mitochondrial alterations in liver mitochondria (Fig.28-29), despite a depletion efficiency in this tissue similar to the heart (Fig.25). Thus, although DT

administration to CD169^{DTR} mice depletes populations of macrophages in other tissues, these results indicate that damage originated to cardiac tissue was tissue-specific.

Considering that macrophages do far more than phagocytosis (Davies et al., 2013), an open question is how much of the cardiac phenotype found in cMac-depleted mice is due to phagocytosis of exophers vs other functions performed by cMacs in the heart. To explore this we used the Mertk-deficient mouse model. Mertk is a membrane receptor, which indirectly binds Phosphatidylserine (PS), a structure common to apoptotic cells (Rothlin et al., 2015) and exophers (Fig.37). Mertk-deficient macrophages have problems in the detection and elimination of apoptotic cells (Rothlin et al., 2015) and we found similar problems in capturing cardiomyocyte-derived mitochondria by macrophages (Fig.38). As a result, Mertk-deficient mice displayed some of the features observed in cMacs-depleted mice: accumulation of extracellular debris and inflammasome activation (Fig.38), reduced autophagy (Fig.39) and poor mitochondrial quality (Fig.40). However, the phenotype of Mertk-deficient mice is evidently milder than that of cMac-depleted mice, and appears to worsen with age, a finding that is intriguing because it recapitulates other pathologies associated with Mertk-deficiency, such as blindness and fertility (Lu et al., 1999; Nandrot et al., 2000)).

While the consequences of Mertk-deficiency at latter stages of life may require further exploration, there are some aspects that should be considered to better understand our results. First, Mertk-deficiency does not block completely the elimination of cardiomyocyte derived mitochondria (Fig.38). There is vast redundancy of ligands and receptors involved in recognition of apoptotic cells, which highlights the importance of this process. In fact, we show that cMacs express at least one other receptor for PS (Axl; Fig.37) at levels higher than Mertk. In addition, another receptor (Timd4) has been identified as a phenotypic marker of a subset of cardiac macrophages (Dick et al., 2019). Second, the binding efficiency of macrophages to target particles depends on the relative affinity of the molecules involved, as well as on their surface density on both leukocyte and target (Rosales and Uribe-Querol, 2017). Third, phagocytosis through Mertk-independent pathways have been reported to be more pro-inflammatory (Birge et al., 2016). Thus, even if Mertk-deficient cMacs are able to

eliminate cardiac exophers through Mertk-independent pathways, the efficiency and, more importantly, their silent (i.e. non-inflammatory) removal may be compromised.

We finally note that the phenotype observed in both CD169^{DTR} and *Mertk*$^{-/-}$ mice, namely autophagy block, accumulation of dysfunctional mitochondria and infammasome activation, closely resembles those found in age-related cardiomyopathy (Rubinsztein et al., 2011). We predict that alterations in cMacs, such as those associated with aging in other macrophage populations (Rawji et al., 2016), may compromise organ function and be a currently unappreciated cause of heart disease.

5.4. Future directions.

Identification of active phagocytosis of cardiomyocyte-derived material by cMacs establishes a novel function for cardiac macrophages and unveils a paradigm for how resident phagocytes contribute to tissue homeostasis. Although further studies will be required, the identification of exophers suggests that cardiomyocytes, neurons and possibly other long-lived cells (i.e. skeletal muscle Fig.12), use this mechanism and depend on neighboring macrophages for effective disposal of cellular components that are the result of a physiological stress. An important future task will be to identify such populations of long-lived cells across the organism.

Currently, we can only speculate how extrusion of mitochondria and other material into exophers may be beneficial for cardiomyocytes instead of intracellular degradation. The identification of biochemical pathways acting in cardiomyocytes to sort mitochondria into these two options will be key to develop strategies to clearly define to what extent the exopher mechanism is important, and to identify new genes that may be altered in heart disease.

It will be also important to determine when this process starts in development and to what extent it is affected by, or influences, organismal aging. This will be key for better understanding the purpose of this mechanism and potential therapeutic implications in age-related cardiomyopathies. Finally, we predict that cardiac dysfunction may, in some instances, emanate from defects in immune cells, rather than from cardiomyocytes, a concept of important consequences for the diagnosis and treatment of heart disease.

6. Conclusions

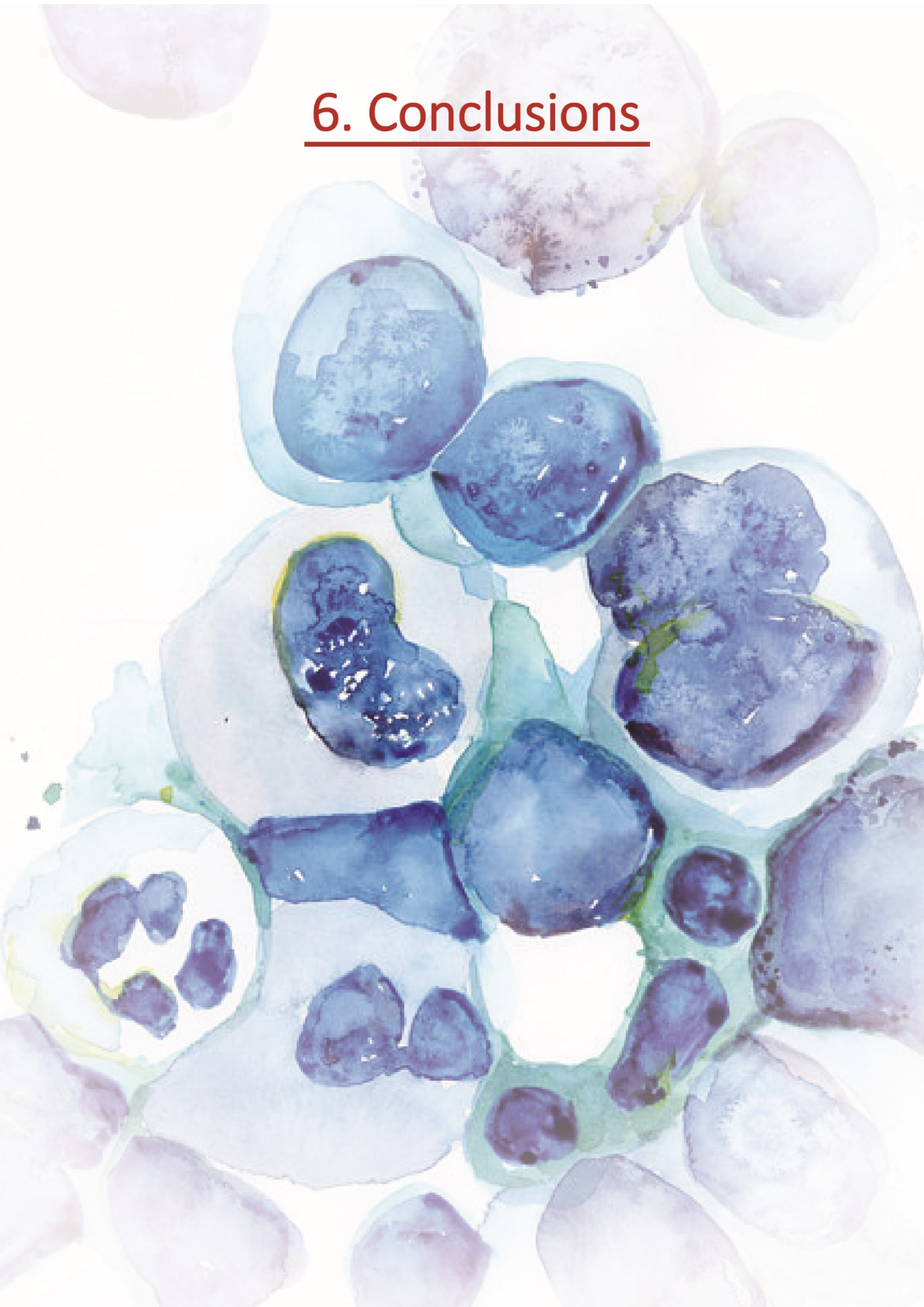

6.1. Conclusions

The main conclusions extracted from this present PhD thesis are listed below:

1. The adult mouse heart hosts an abundant population of tissue resident macrophages (cMacs), which displays broad distribution and close interaction with individual cardiomyocytes.

2. cMacs present high phagocytic activity in the steady-state, incorporating material originated from several cell components of the heart, including cardiomyocytes.

3. Cardiomyocytes shed cardiac exophers, which are subcellular particles of defined size and composition that are released into the extracellular milieu of the healthy myocardium.

4. Cardiac exophers transport multiple material but are highly enriched in damaged mitochondria.

5. A measurable fraction of cardiomyocyte-derived mitochondria is delivered to cMacs for degradation. In fact more than half of the cardiomyocyte's mitochondria are degraded in cMacs.

6. The autophagic machinery of cardiomyocytes control exopher production.

7. Exopher production by cardiomyocytes adapts to stress.

8. cMacs can be efficiently depleted in CD169DTR mice model.

9. Macrophage elimination in CD169DTR mice causes cardiomyopathy, characterized by an autophagy block and accumulation of defective mitochondria inside cardiomyocytes.

10. The phagocytic receptor Mertk mediates the uptake of cardiomyocyte-derived mitochondria by cMacs and deficiency in Mertk causes a cardiomyopathic phenotype similar to that caused by cMac elimination, which worsens with age.

6.2. Conclusiones

Los resultados presentados en este trabajo permiten extraer las siguientes conclusiones:

1. El corazón adulto de ratón alberga una abundante población de macrófagos residentes (cMacs) que se distribuye por todo el órgano y mantiene una estrecha interacción con los cardiomiocitos.

2. Los cMacs presentan una gran actividad fagocitaria en homeostasis, incorporando material procedente de múltiples poblaciones cardíacas, incluyendo a los cardiomiocitos.

3. Los cardiomiocitos extruden exoferas cardíacas, unas partículas sub-celulares con un tamaño y composición específica que son liberadas al medio extracelular en el miocardio sano.

4. Las exoferas cardíacas transportan material diverso, pero están altamente enriquecidas en mitocondrias dañadas.

5. Más de la mitad de las mitocondrias originadas en los cardiomiocitos es degradada en los cMacs.

6. La maquinaria de autofagia presente en los cardiomiocitos controla la producción de las exoferas cardíacas.

7. La producción de las exoferas por los cardiomiocitos se adapta a condiciones de estrés.

8. Los cMacs expresan CD169 y pueden ser eliminados de forma eficiente en el modelo de ratón $CD169^{DTR}$.

9. La eliminación de macrófagos en el ratón $CD169^{DTR}$ causa una cardiomiopatía, caracterizada por un bloqueo de la autofagia y la acumulación de mitocondrias dañadas dentro de los cardiomiocitos.

10. El receptor fagocitario Mertk media la captación por los macrófagos del material liberado por los cardiomiocitos. La ausencia de Mertk mimetiza parte del fenotipo observado en los ratones cuyos macrófagos han sido eliminados, el cual se hace más evidente a medida que los animales envejecen.

7. Materials and Methods

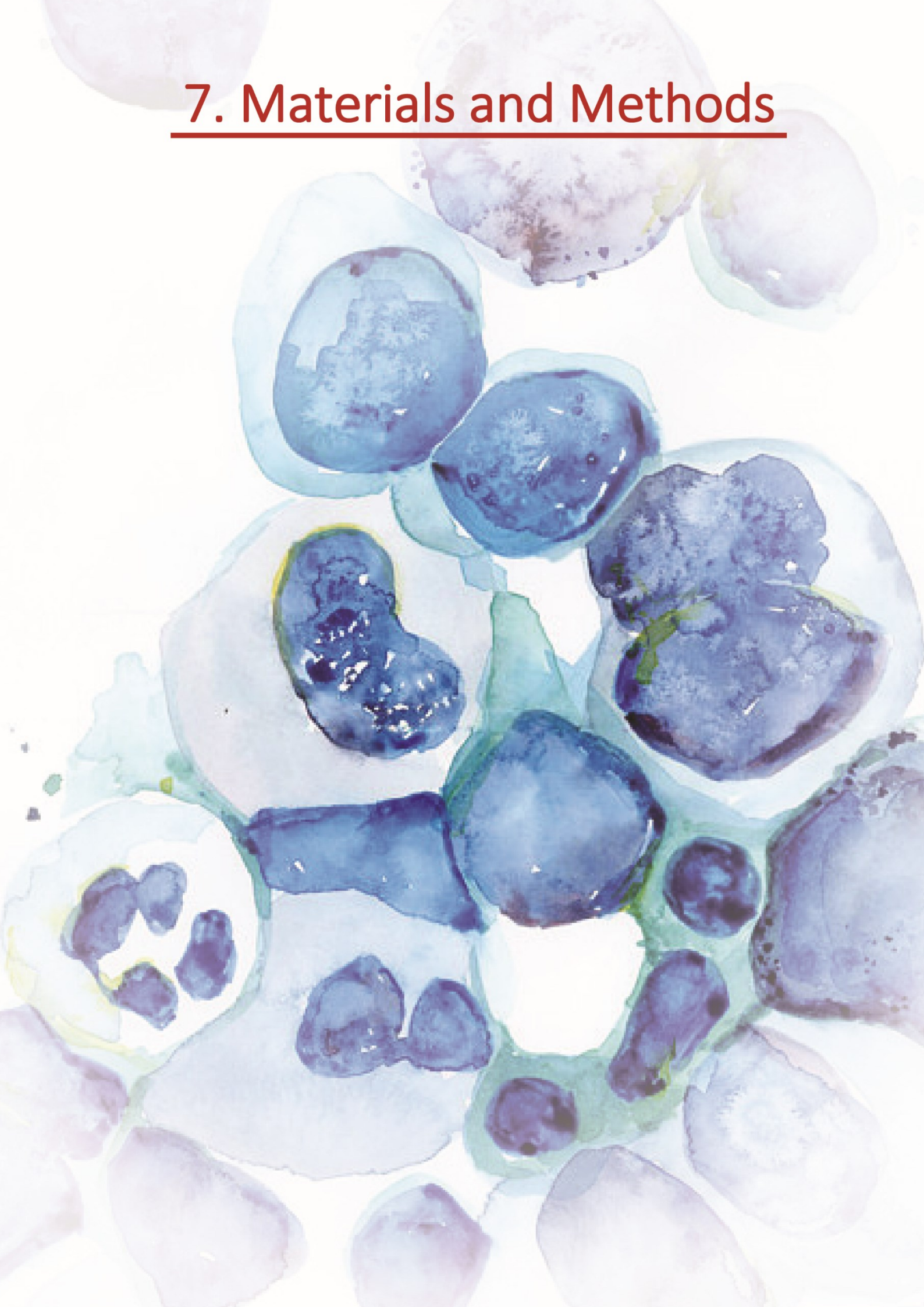

7. Materials and Methods

7.1. Mice and Human samples

EXPERIMENTAL MICE

All experiments were performed in 8- to 18-week-old male mice in a C57BL/6 background, except those were indicated (aging experiments in WT and Mertk-deficient). Mice were housed in a specific pathogen-free facility at Fundación CNIC. Chow and water were available *ad libitum*. All mice were maintained in a 12h light/12h darkness schedule. Experimental procedures were approved by the Animal Care and Ethics Committee of the CNIC and local authorities.

Strain	Phenotype	Reference
WT	Wild Type mice	Charles Rivers
CX3CR1^{GFP}	GFP expression on myeloid lineage	(Jung et al., 2000)
LysM^{GFP}	GFP expression on myeloid lineage	(Faust et al., 2000)
MAFIA	GFP expression on myeloid lineage	(Burnett et al., 2004)
LC3-GFP	GFP fused to LC3 protein allows for autophagosome identification	(Mizushima et al., 2004)
αMHC^{Cre}	Cre recombinase expressed under *αMHC* promotor	(Oka et al., 2006)
αMHC^{CreERT}	Cre recombinase inducible by tamoxifen expressed under *αMHC* promotor	(Sohal et al., 2001)
Cdh5^{CreERT}	Cre recombinase inducible by tamoxifen expressed under *Cdh5* promotor	(Sorensen et al., 2009)
Rosa26^{Tdtom}	STOP codon in tdTomato sequence flanked by loxP sequences	(Madisen et al., 2010)
Atg7^{flox}	*Atg7* sequence flanked by flox sequences	(Komatsu et al., 2005)
WT^{RED}	DsRed expression under beta-actina promoter control	(Vintersten et al., 2004)
CD169^{DTR}	DTR expression in the *Cd169* locus. Allows macrophage depletion upon Diphtheria Toxin (DT) injection	(Miyake et al., 2007)
Mertk$^{-/-}$	Mice deficient in *Mertk*	(A-Gonzalez et al., 2017)
LXRαβ$^{-/-}$	Mice deficient in *Nr1h3* and *Nr1h2*	(A-Gonzalez et al., 2017)
Oma1$^{-/-}$	Mice deficient in *Oma1*	(Quiros et al., 2012)
CD45.1 or BL/6.SJL^{C57}	mouse strain with C57BL/6 background and a diferent isoform of *Ptprc* (which encodes for CD45)	Jackson Laboratories

BL/6^{NZB}	Conplastic mouse strain with the nuclear genome of C57BL/6 but mitochondrial DNA of NZB	(Latorre-Pellicer et al., 2016)

These mice were generated by crossing the different mice strains indicated above:

Name	Strain	Phenotype
Card^{RED}	αMHC^{Cre}; Rosa26^{Tdtom}	TdTomato expression on cardiomyocytes
Card^{RED} LC3-GFP	Card^{RED} LC3-GFP	Combination of Card^{RED} and LC3-GFP
Card^{RED} CD169^{DTR}	αMHC^{Cre}; Rosa26^{Tdtom}; CD169^{DTR}	Combination of Card^{RED} and CD169^{DTR}
Card^{RED} Mertk$^{-/-}$	αMHC^{Cre}; Rosa26^{Tdtom}; Mertk$^{-/-}$	Combination of Card^{RED} and Mertk$^{-/-}$
Cdh5^{CreERT} Rosa26^{Tdtom}	Cdh5^{CreERT}; Rosa26^{Tdtom}	Conditional TdTomato expression on endothelial cells upon tamoxifen injection
αMHC^{CreERT} Rosa26^{Tdtom}	αMHC^{CreERT}; Rosa26^{Tdtom}	Conditional TdTomato expression on cardiomyocytes upon tamoxifen injection
αMHC^{CreERT} Atg7$^{flox/+}$	αMHC^{CreERT} Atg7$^{flox/+}$	Conditional hemizigosity in *Atg7*
αMHC^{Cre} Atg7$^{flox/+}$	αMHC^{Cre} Atg7$^{flox/+}$	Constitutive hemizigosity in *Atg7*

HUMAN SAMPLES

We obtained papillary muscles from the heart of patients undergoing mitral valve replacement. Inclusion criteria for patients that donated cardiac tissue were age older than 18 years and in need of mitral valve replacement. Emergency procedures were the only exclusion criteria. Five patients were included between July and September 2017. Baseline clinical characteristics of patients are described in Data Table 2. Patients were anesthetized as usual following our local protocol. Median sternotomy and aortic and double venous cannulation were standard. Normothermic bypass was initiated after heparinitation. After antegrade cardioplegia the heart was arrested and left atrial was opened. Mitral valve was excised cutting mitral chordes and the head of papillary muscles. A portion of the papillary muscles head was stored in PFA 4% Glutaraldehyde 1% (for electron microscopy) or PFA 2% (for immunofluorescence), following the protocols described below. This study was conducted in accordance with the Helsinki Declaration and approved by the local ethics committee at Hospital Universitario de la Princesa (Madrid). Written informed consent was obtained from every patient.

Table 2. Description of patients that donated cardiac tissue for analysis.

Patient no.	1	2	3	4	5
Age (years)	55	72	74	75	62
Sex	Female	Female	Male	Female	Female
LVEF	Normal	Normal	Normal	Normal	Normal
Indication for surgery	Mitral regurgitation	Mitral regurgitation	Mitral regurgitation	Mitral stenosis	Mitral regurgitation
Bypass time (min)	96	102	80	66	85
Crossclamp time (min)	75	81	60	55	74

LVEF: left ventricle ejection fraction.

7.2. Animal procedures

GENERATION OF BONE MARROW TRANSPLANTED MICE

Recipient WT^{RED} (CD45.2) or $BL/6.SJL^{C57}$ (CD45.1) mice were lethally irradiated (6.5 Gy split doses, 3 h apart), and subsequently received $BL/6.SJL^{C57}$ (CD45.1) or $BL/6^{NZB}$ (CD45.2) bone marrow donor cells, respectively. Donor BM cells were harvested by flushing both femora into RPMI. 10^6 cells were intravenously injected into recipients.

PARABIOSIS

Parabiosis is a surgical procedure that allows for the union of circulatory systems of 2 animals (anastomosis), taking advantage of the natural angiogenic response that takes place after the connection of both animals at the dermis. To generate parabiotic pairs, we followed our previously described procedures (A-Gonzalez et al., 2017). Mice were anesthetized with a mixture of 7.5% ketamine (Imalgene, Merial Laboratorios) 5% xylazine (Rompum, Bayer), inyected intraperitoneallly 10µl/g. Then, animals were shaved at the corresponding lateral aspects and matching skin incisions were made from the olecranon to the knee joint of each mouse, and the subcutaneous fascia was bluntly dissected to create about 0.5 cm of free skin. The olecranon and knee joints were attached by a single 5-0 polypropylene suture and tie, and the dorsal and ventral skins were approximated by continuous suture. A single dose of flunixin meglumine (Schering-Plough) was injected subcutaneously in each partner at the end of the surgical procedure (1 mg/kg). One month after surgery blood samples were obtained from each of the partners to assess leukocyte chimerism.

MYOCARDIAL INFARCT BY PERMANENT CORONARY LIGATION

Myocardial infarction was induced by ligation of the proximal left anterior descending (LAD) coronary artery for 7 days without allowing reperfusion. Mice were anesthetized with a mixture of Atropine, Xylazine and Ketamine and intubated prior to surgery. In order to get access to the heart, skin was opened in a small part of the chest, followed

by removal of the muscle layers at the level of the third rib. Then, this third rib was cut and a small orifice was done in the chest. Using a 8-0 polypropylene suture, a knot was done at the LAD coronary artery level, and the wound was closed with 6-0 sutures. After the surgery, a single dose of flunixin meglumine (Schering-Plough, Segre, France) was injected subcutaneously and animals were kept in a 37ºC chamber for the next 24 hours. At day 7 after surgery, animals were sacrificed and cardiac tissue collected.

HEMODYNAMICS

Ventricular catheterization was performed as previously described (Pacher et al., 2008). Mice were anesthetized (ketamine/xylazine (100/10 mg/kg) and intubated. A skin incision was made to visualize the diaphragm, which was heat cauterized to expose the heart apex. The pericardium was removed gently with forceps. Using a 25–30 gauge needle, a stab wound was made near the heart apex into the left ventricle (LV). The catheter tip (Transonic, NY, USA) was inserted retrogradely into the LV. After allowing the signal to stabilize for 5 min, recordings were made of baseline left ventricular end-systolic pressure (LVESP), left ventricular end-diastolic pressure (LVEDP), maximal derivative of LV pressure (dP/dtmax) and minimal derivative of LV pressure (dP/dtmin). The same parameters were recorded 5 minutes after the injection a single dose of isoproterenol (40ng/kg) through the femoral vein when signal was stable. At the conclusion of the experiment, the catheter was removed by gently pulling it back through the stab wound, and the animal was euthanized.

INDUCTION OF CRE-ERT RECOMBINASE WITH TAMOXIFEN

We use several Inducible Cre strains for different purposes in this work. Fluorescent protein expression in endothelial cells was induced in $Cdh5^{CreERT}$ $Rosa26^{Tdtom}$ mice by intraperitoneal treatment with tamoxifen (1mg/mice) at days 11, 9 and 7 before analysis. In order to obtain single Tdtomato positive cardiomyocytes in αMHC^{CreERT} $Rosa26^{Tdtom}$ mice, we give a single dose of tamoxifen at lower concentration (1µg/mice). Finally, cardiomyocyte-specific deficiency in *Atg7* using αMHC^{CreERT} $Atg7^{flox}$ mice was induced by injecting tamoxifen (1mg/mice) for two consecutive days.

MACROPHAGE DEPLETION

Depletion of cMacs in either $CD169^{DTR}$ or αMHC^{Cre}; $Rosa26^{Tdtom}$; $CD169^{DTR}$ mice was performed by intraperitoneal injection of 10 µg/kg diphtheria toxin (DT; Sigma). A single injection was administered at the indicated times for transient depletion, or three times a week for long-term (21d) depletion. In these experiments, control wild type or αMHC^{Cre} $Rosa26^{Tdtomato}$; $CD169^{WT}$ mice were treated with same doses of DT. Where indicated, $CD169^{DTR}$ mice treated with saline were used as controls.

TREATMENT ADMINISTRATION

For some experiments, animals were treated with **Rapamycin** (4mg/Kg mice in PBS/DMSO in a 50/50% mixture) or vehicle trice per week intraperitoneally for 2 weeks and analyzed at day 14. **Isoproterenol** hydrochloride (ISO; 25 mg/kg/day; Sigma-Aldrich) was chronically administered in mice. Mice were anesthetized with Sevoflurane (2,5-3.5 % and 1 % O2) and osmotic minipumps (Mini-Osmotic Pump, Alzet) were subcutaneously implanted for continuous delivery during 7 consecutive days. Finally, for some experiments animals were administrated daily with **MCC950** (Merck) 7 mg/kg/day for the indicated times.

7.3. Experimental setups

INCORPORATION OF EXOGENOUS MATERIAL BY MACROPHAGES

Phagocytic cMacs were identified based on the incorporation of DsRed or Tomato fluorescence (as shown in Fig.5). Engulfment of material in CD45.1-WT^{RED} bone marrow chimeras was based on DsRed signal acquisition by CD45.1-derived cardiac macrophages in the WT^{RED} transplanted mice. Engulfment of cells in parabionts of CD45.1 with WT^{RED} mice was based on acquisition of DsRed signal by tissue-resident macrophages in the non-fluorescent partner as previously described (A-Gonzalez et al., 2017). Non-parabiotic CD45.1 mice were used as controls to set the appropriate gates. Engulfment of cardiomyocyte- and endothelial cell-derived material in αMHC^{Cre} Rosa26^{Tdtom} and Cdh5^{CreERT} Rosa26^{Tdtom}, respectively, was based on tdTomato signal acquisition by cMacs when comparing with non-fluorescent control mice.

MT-KEIMA REPORTER IN CARDIOMYOCYTES

AAV vectors were all produced by the triple transfection method, using HEK 293A cells as described previously (Xiao et al., 1998). Shuttle plasmid pAAV-mt-Keima was derived from mt-Keima-Red-Mito-7 (a gift from Michael Davidson (Addgene plasmid # 56018)) and from pAcTnT (a gift from B.A. French). The mt-Keima cDNA is a fusion of *Keima* gene in-frame to the matrix import sequence of human Cox8A: MSVLTPLLLRGLTGSARRLPVPRAKIHSLPPEGKLGM. The expression is driven by the cardiac-specific promoter *TnT* (see scheme in Fig.13a). Virus were packaged into AAV-9 capsids by the CNIC Viral Vector Unit using helper plasmids pAdDF6 (providing the three adenoviral helper genes) and pAAV2/9 (providing rep and cap viral genes). Four- to Six-week-old mice were injected with 3-10 x 10^{10} viral genomes encoding mt-Keima and analyzed 2 to 6 weeks later.

DETECTION OF EXOGENOUS mtDNA IN MACROPHAGES

BL/6.SJL^{C57} mice (with C57BL/6 nuclear and C57 mitochondrial DNA) were lethally irradiated and transplanted with BL/6^{NZB} bone marrow (C57BL/6 nuclear and NZB

mitochondrial DNA), as described above. Differential expression of the CD45.1/CD45.2 surface marker on these strains additionally allow cytometric discrimination and sorting. BL/6^{NZB} CD45.2+ transplanted macrophages were isolated from different tissues by cytometric sorting and DNA isolated using NaOH 50mM at 95ºC, and neutralization with TrisHCl pH 7.5. Polymorphic G4276A nucleotide in mt-ND2 mitochondrial gene was used to genotype the samples. This polymorphism in C57 mtDNA forms part of a BamHI restriction site, which is absent in NZB mtDNA (Latorre-Pellicer et al., 2016). Total genomic DNA was PCR amplified using standard conditions with the REDExtract-N-Amp^{TM} PCR ReadyMix^{TM} and the following primers: 5'-AAGCTATCGGGCCCATACCCCG-3'(3862-3884) and 5'-GTTGAGTAGAGTGAGGGATGGG-3' (4503-4525), as follow: 95ºC, 30s; 58ºC, 30s; 72ºC, 45s for 30 cycles. An aliquot of PCR was digested with FastDigest BamHI (New England Biolabs), at 37ºC for 10-15 minutes. After agarose gel electrophoresis, DNA was visualized with a Gel Doc XR+System (Bio-Rad), and band intensities were quantified with Quantity One 1-D Analysis Software. The proportion of C57 mtDNA was calculated by adding the intensities of the 414bp and 250bp BamHI fragments and dividing by the sum of the intensities of all fragments (undigested 664bp fragment from NZB mtDNA, and the 414bp and 250bp BamHI-digested fragments from C57mtDNA).

DEGRADATION OF EXOGENOUS mtDNA AND mt-Keima IN MACROPHAGES

We sorted cMacs from mt-Keima-infected hearts or from BL/6^{NZB}-transplanted BL/6.SJL^{C57} and cultured a maximum of 3x10^5 cardiac macrophages per well in 48w plates. We used a medium with αMEM containing NaPyruvate, L-Glutamine and Penicillin/Streptomycin, plus Essential aminoacids, including 10% FBS and 10 ng/mL M-CSF. Macrophages were cultured for 72h at 37Cº, 5% CO2.

7.4. Flow cytometry and cell sorting

TISSUE PREPARATION

The large intestine (colon) was cut into small pieces and subjected to epithelial separation by incubation with HBSS with 2mM of EDTA for 20 min at 37ºC and subsequently digested in HBSS with liberase (1U/ml, Roche) and DNase I (10 mU/ml, Sigma) for 40 min at 37°C. Bone marrow was flushed and hearts, skeletal muscles, livers, and spleens were minced and digested in HBSS with liberase (1U/ml, Roche) and DNase I (10 mU/ml, Sigma) for 30min at 37ºC. After digestion, single-cell suspensions were obtained by gentle pipetting and mechanical dissociation of the remaining pieces through cell strainers (BD Falcon). Single-cell suspensions were incubated with the indicated antibodies for 15 min at 4°C (see antibody Table below). Samples were acquired in a LSRII Fortessa (BD Biosciences) or Canto HTS (BD) equipped with DIVA software (BD). The FlowJo software (FlowJo LLC, Ashland, OR) was used to analyse the data.

Antibodies	Clone	Source
CD45-PerCP/Cy5.5	30-F11	Biolegend
CD45.1-PerCP/Cy5.5	A20	Tonbo biosciences
CD45.2-FITC	104	Tonbo biosciences
CD45.2-APC/Cy7	104	eBioscience
CD11b-PE	M1/70	Tonbo biosciences
CD11b-Bv510	M1/70	Biolegend
CD11b-APC	M1/70	Tonbo biosciences
F4/80-biotin	BM8	eBioscience

Streptavidin	Label	Source
Streptavidin	eF780	eBioscience
Streptavidin	PE	eBioscience
Streptavidin	DyLight 649	Jackson Immunoresearch

F4/80-APC	BM8	eBioscience
F4/80-PE/Cy7	BM8	Biolegend
MHCII-PE/Cy7	M5/114.15.2	Biolegend
MHCII-Biotin	M5/114.15.2	Biolegend
Ly6C-FITC	HK1.4	Biolegend
CD115-PE	AFS98	Thermofisher
Ly6G-AF647	1A8	eBioscience
CCR2-APC	475301	R&D

ESTIMATION OF CELL NUMBERS

Truecount beads (BD) were prepared at a concentration of 10,000 beads per ml in a buffer containing EDTA 0.5M, FBS 0.5% (PEB) and 0.1 µg/mL DAPI (Life Technologies) in PBS. 500 µl of this PEB/DAPI buffer containing beads were added to single cell suspensions stained for flow cytometry as indicated above. To estimate the absolute number of cells, 500-1000 beads were acquired per tube in order to ensure accuracy. Cell counts per mg of tissue were calculated as follows:

$$\frac{cells}{beads} x \frac{10{,}000\ beads}{ml\ PEB\ buffer} x \frac{0{,}5\ ml\ PEB\ buffer}{fraction\ of\ tissue\ digested} x \frac{1}{weight\ of\ organ\ (mg)} = \frac{cells}{mg}$$

For blood, absolute cell numbers given as cells per ml were obtained using an automated hemocounter (Abacus Junior, Diatron; Holliston, USA).

FLOW CYTOMETRY AND SORTING OF CARDIAC EXOPHERS

The heart was cut into small pieces and subsequently digested in HBSS with liberase (1U/ml, Roche) and DNase I (10 mU/ml, Sigma) for 40 min at 37°C. After digestion, single-cell suspensions were obtained by gentle pipetting. We used a strategy of serial centrifugation forces (Fig.8) at 50g and 300g discarding pellet and keeping supernatant for a final centrifugation at 1000g. Within the pellet of this fraction, we used the endogenous expression of tdTomato in Card^{RED} along with size, antibody (CD31-Bv605;

clone 390 Biolegend) and Draq5 staining (Biolegend) to define cardiac exophers and sort them in an Aria Cell Sorter (BD) equipped with DIVA software (BD). In some experiments, exophers were stained for Mitotracker Deep Red (ThermoFisher), MitoNIR (Abcam) or labelled Annexin V-PE (BD Biosciences). In the case of Annexin V, staining was done in Annexin binding buffer (10mM HEPES/NaOH, pH 7.4; 140 mM NaCl; 2,5 mM $CaCl_2$). This protocol is an adaptation of previously described protocols to obtain samples enriched in apoptotic bodies, which are akin in size to cardiac exophers (4 µm; (Atkin-Smith et al., 2017)). Part of the material obtained in each one of these fractions was subjected to cytospin in a Shandon Cytospin™ 4 Cytocentrifuge (ThermoFisher) at 1000 rpm for 5 minutes, medium velocity. Cells and exophers were then fixed in 4% paraformaldehyde for 5 min, permeabilised with 0.01% TritonX100 in PBS for 15 minutes and blocked 1 hour with 10% BSA and 2% goat serum. For immunofluorescence samples were incubated with rabbit anti-RFP (polyclonal; Rockland), washed thrice in PBS and incubated with secondary antibodies (Goat anti-Rabbit AF546; Molecular Probes).

PROLIFERATION ASSAY USING BRDU

For metabolic labelling with 5-Bromodeoxyuridine, mice were administered BrdU (BD Biosciences) in drinking water (0.5mg/ml) for 4 days, starting from the time of DT injection until tissue collection. Hearts were collected at the indicated times and processed as indicated above to obtain single cell suspensions. Then, cells were stained for CD45, CD11b, F4/80, MHCII and Ly6C, followed by fixation and intracellular labelling of BrdU using an APC-conjugated anti-BrdU antibody, as per manufacturer's instructions (BD Biosciences). Samples were analysed in LSRII Fortessa (BD Biosciences) equipped with DIVA software (BD). The FlowJo software (FlowJo LLC, Ashland, OR) was used to analyse the data.

CYTOMETRIC ANALYSIS OF MITOCHONDRIAL MEMBRANE POTENTIAL

Oligomycin (10 mg/ml; Sigma-Aldrich) was used to promote mitochondrial polarization (ATP synthase inhibition). Carbonyl cyanide-4 (trifluoromethoxy) phenylhydrazone (FCCP, 1uM) uncouples oxygen consumption, collapses the proton

gradient and ablates the mitochondrial membrane potential. Total cardiac leukocyte fraction and cardiac purified exopheres were treated with oligomyocin, FCCP or medium alone for 3 hours at 37ºC. Immortalized mouse adult fibroblasts (MAFs) from C57BL/6 were used as internal control to assess the treatment responsiveness. Mitochondrial membrane potential was measured using the fluorescent probe MitoNIR (Abcam) by FACS according to manufacture's instructions. Cells were incubated in cell culture medium supplemented with 1x MitoNIR for 20 minutes at 37ºC. Data acquisition was performed using the FACSCanto™ II system (BD Biosciences). All experiments were performed in triplicates. Samples were analysed with the BD FACSDiva™ software package and the average of the medians and corresponding standard deviations were calculated using the FlowJo software (v10).

7.5. Imaging Techniques

We used different imaging techniques in this work, each one of them adjusted to different purposes. Optical clearing of tissues and imaging by **light sheet microscopy** allowed us to analyse the global distribution of macrophages in the heart, and to estimate their numbers. This is possible because the field size captured by unit of time is much higher, while resolution tends to be compromised. **Confocal microscopy** allowed us to analyse broad tissue regions at high resolution, necessary to assess the micro anatomical distribution of macrophages, Keima+ mitochondria transfer and exopher numbers. **Transmission electron microscopy** allows a subcellular level of resolution, necessary to explore sarcomere and mitochondria status in cardiomyocytes of the different animal models. We also used **bright field microscopy** for the examination of macrophages and cardiomyocytes isolated from hearts. Finally, we used **Echocardiography** to analyse cardiac function *in vivo*.

OPTICAL CLEARING AND LIGHT SHEET MICROSCOPY OF WHOLE HEARTS

4 week-old heterozygous CX3CR1^{GFP} mice were euthanized and immediately transcardially perfused with 10ml PBS containing 2mM EDTA pH7.4, followed by 10ml of 4% paraformaldehyde (PFA) through the left ventricle. The heart was dissected and fixed in 4% PFA (Sigma) overnight at 4°C, followed by extensive washing with PBS. The fixed hearts were permeabilised with graded methanol solutions from 50%, 70%, 95% and 100%, each incubated for 45minutes, followed by 100% methanol/20%DMSO for 1 hour. Tissue was rehydrated back to PBS with 45 minute incubation at room temperature. Permeabilised sample was blocked overnight in blocking buffer (2.5% goat serum, 2.5% donkey serum, 5% BSA, 0.02% gelatin, 20%DMSO, 0.3% TritonX100 in PBS), washed extensively with PBS and incubated with primary antibodies in dilution buffer (2.5% goat serum, 2.5% donkey serum, 0.2% BSA, 0.02% gelatin, 5%DMSO, 0.3% TritonX100 in PBS) for 48 hours. Chicken anti-GFP (1:300 dilution, Abcam ab13970) and Armenian hamster anti-CD31 antibodies (1:300 dilution; clone 2H8, Merck) were used. Sample was washed 6 times with 3M NaCl+0.3% TritonX100 in PBS, and twice with PBS.

Each wash was for 30 minutes at room temperature. Tissue was incubated with secondary antibodies (anti-chicken Alexa fluor-647, anti-hamster Alexa fluor-750) (Abcam) at 1:300 in dilution buffer for 48 hours, washed as indicated above and taken for tissue clearing. All antibody incubations were carried out at 37°C. Heart tissue was cleared using the BABB (Benzyl alcohol/ Benzyl benzoate) protocol. Samples were dehydrated with methanol as was done for permeabilization, equilibrated with BABB:methanol in a 1:1 ratio for 45 minutes and refractive index matched with BABB (1:2) for 45 minutes until clear. Cleared heart was imaged using the light sheet Ultramicroscope (LaVision BioTec GmbH, Bielefeld, Germany) in BABB with a 2X objective, NA 0.5, using a white light supercontinuum laser. Post-acquisition, high resolution raw data was downsampled and corrected to remove high intensity artifacts arising from uneven light illumination during acquisition, using Imaris 8.0 (Bitplane AG). Image contrast was further improved using the unsharp mask function of FIJI Is Just ImageJ (NIH), and rendered in 3D using Imaris 8.0.

CONFOCAL MICROSCOPY OF CARDIAC TISSUE

Mice were sacrificed with CO_2 and perfused with a saline solution in order to collect the hearts into a 2% PFA solution. Human samples for immunofluorescence fixed in PFA 2% were obtained as indicated above. After 24 hours in fixation solution at 4ºC, samples were cryopreserved with a sucrose gradient, and frozen in OCT Compound (Tissue Tek) using dry ice. Tissues were cut in 12 (most of them) or 30 (for 3D reconstructions) µm sections in a cryostat (Leica CM1850). Macrophage detection by immunofluorescence was carried out in cardiac slices permeabilised with 0.01% TritonX100 in PBS for 15 minutes and blocked 1 hour with 10% BSA and 2% goat serum. For immunofluorescence, mouse tissues were incubated with rat anti-CD68 (clone FA-11; BioRad), rat anti-CD169 (clone 3D6; kindly provided by S.Gordon), rabbit anti-laminin (polyclonal; Sigma), rabbit anti-NDUFS2 (Polyclonal Abcam), rabbit anti-Cytochrome C (clone EPR1327; Abcam), rabbit anti-Tom20 (clone FL-145; Santa Cruz Biotechnology), rabbit anti-Myh7 (clone NOQ7.5.4D; Sigma) or rabbit anti-LAMP1 (polyclonal; Sigma) primary antibodies. Humans samples were incubated with mouse antibodies anti-CD68 (clone PG-M1;

Dako), mouse anti-MYH (clone MF20; DSHB) or rabbit anti-Tom20 (clone FL-145; Santa Cruz Biotechnology). Tissues were washed thrice in PBS and incubated with secondary antibodies (Molecular Probes) or Phalloidine-AF647 (Thermofisher). All the staining steps were conducted in blocking solution for 1 hour at room temperature. Finally, tissues were washed in PBS and nuclei were counterstained with DAPI (Life Technologies) before mounting with Mowiol 4–88 (Sigma-Aldrich).

TRANSMISSION ELECTRON MICROSCOPY (TEM)

For TEM analysis of WT and *Mertk*$^{-/-}$ mice or Human samples, heart pieces were primarily fixed in 1% glutaraldehyde and 4% PFA in PBS overnight. Samples were post fixed in 1% osmium tetroxide for 60 minutes and dehydrated through a series of ethanol solutions (30%, 50%, 70%, 95%, and 100%) and acetone. After the last dehydration step, samples were incubated in a 1:3, 1:1, 3:1 mixture of Durcupan resin and acetone and cured at 60º for 48h. Ultrathin sections (50-60 nm) were obtained using a diamond knife (Diatome) in an ultramicrotome (Leica Reichert ultracut S) and collected in 200-mesh copper grids. The sections were counterstained with 2% uranyl acetate in water from 20 min followed by a lead citrate solution (Reynolds, 1963). Samples were examined with a JEOL JEM1010 electron microscope (Tokyo, Japan) equipped with an Orius SC200 digital camera (Gatan Inc.) at the Transmission Electron Microscopy Laboratory (Interdepartmental Research Service, UAM).

For images of Isoproterenol treated mice we used a different protocol in order to obtain better contrast of mitochondria crista. Samples were primarily fixed as described above but after buffer washes, samples were post-fixed for 1 h at room temperature in a 1:1 solution of 1% osmium tetroxide and 3% aqueous potassium ferrocyanide. Samples were then rinsed in distilled H2O. Tissues were dehydrated through a graded acetone series and embedded in Spurr's low viscosity embedding mixture (Electron Microscopy Sciences). Ultra-thin sections (60 nm) were then mounted on copper grids and stained with lead citrate. Samples were examined on a JEOL 10-10 electron microscope.

BRIGHT FIELD MICROSCOPY

Cardiac macrophages were isolated by FACS and subjected to cytospin in a Shandon Cytospin™ 4 Cytocentrifuge (ThermoFisher) at 800 rpm for 5 minutes, medium velocity. Cells were then fixed in 4% paraformaldehyde for 5 min, stained in eosin for 5 min, washed in dH_2O, stained in hematoxilin for 5 min, and finally washed with dH_2O and mounted with Mowiol. Cardiomyocytes were isolated as indicated below and imaged ex vivo. Microscope used for bright field imaging was a Nikon 90i.

ECHOCARDIOGRAPHY

Echocardiography assessment was blinded and performed by an expert operator in mice under isoflurane anesthesia using a high-frequency ultrasound system with a 30-MHz linear probe (Vevo 2100, Visualsonics Inc., Canada). A base apex electrocardiogram was continuously monitored through 4 leads connected to the ultrasound machine and isoflurane delivery was adjusted to maintain the heart rate in 450±50 bpm. Normothermia was maintained placing mice in a heating platform. Images were recorded and transferred to a computer for posterior blinded analysis using the Vevo 2100 Workstation software. Parasternal standard 2D and MM long and short axis views (LAX and SAX view, respectively) were acquired to assess left ventricle (LV) systolic function and LV dimensions. LV ejection fraction (LV-EF), end-diastolic anterior and posterior wall thickness (LVAW,d and LVPW,d: respectively), end-diastolic and end-systolic LV internal diameter (LVID,d and LVID,s; respectively) were subsequently calculated. A 2D apical view was used to evaluate diastolic dysfunction, using pulsed-wave (PW) Doppler, to estimate mitral valve inflow pattern. Early and late diastolic velocity peak waves (E and A, respectively) were measured and the E/A ratio calculated.

7.6. Image analyses

CARDIAC EXOPHERS BY IMMUNOFLUORESCENCE

Total exophers numbers in the different models and localization of cardiac exophers relative to CD68, CytC, NDUFS2, Tom20, MYH7 and DAPI was done manually, as the tdTomato signal from Card^{RED} cardiomyocytes did not allow segmentation. The criteria for co-localization was the overlapping position of tdTomato signal in the exophers of αMHC^{Cre} Rosa26^{Tdtom} mice and the stained markers, while the percentage of co-localization between cardiac exophers and any other "marker" was quantified as follows:

$$\%\ \text{of exophers co} - \text{localizing with "marker"} = \frac{\text{N. of exopheres colocalizing with "marker"}\ \text{x } 100}{\text{N. of total exopheres}}$$

We measured the distances between macrophages and cardiac exophers using FIJI Is Just ImageJ (NIH), and compared them to the same number of random spots in those images. Random spots were 3.5 µm diameter circles (similar to cardiac exophers) generated by a macro using FIJI Is Just ImageJ (NIH).

MACROPHAGE TO CARDIOMYOCYTE RATIO

The cMacs to cardiomyocytes ratio was analyzed in CX3CR1$^{GFP/+}$ mice. Heart from those mice were fixed and frozen as described in the immunostaining methods. We obtained thick slices (60 µm) from OCT-included samples using a cryostat and subjected them to permeabilization (in PBS + Triton 0.1% solution), blocking (10% BSA, 5% NGS in PBS) and staining steps, all of them performed overnight at 4ºC. We stain the samples with primary rabbit anti-laminin (polyclonal; Sigma) and secondary goat anti-rabbit AF546 antibodies to label cardiomyocytes basal lamina. We performed quantification of cMacs and cardiomyocytes interactions in 30 µm thick optic fields obtained using an SPE microscope (Leica).

For the visualization of individual cardiomyocytes we used tissues of αMHC^{CreERT} Rosa26^{Tdtom} mice. Cardiac tissue was fixed with a 2% PFA solution. After 24 hours in fixation solution at 4ºC, samples were incubated trice with washing buffer (0.05%

tritonX-100 in PBS) 1 hour each and Blocked with 1% BSA in PBS overnight. For immunofluorescence, mouse tissues were incubated with rat anti-CD68 (clone FA-11; BioRad) and rabbit anti-RFP (polyclonal; Rockland) primary antibodies and goat secondary antibodies (Molecular Probes). After immunostaining, tissues were washed trice with washing buffer (0.05% tritonX-100 in PBS) 1 hour each and dehydrated with an ethanol gradient (50%/70%/100% twice) before inclusion in clearing solution (Ethyl cinnamate; SIGMA). A large portion of tissue was imaged using a SP8 microscope (Leica) using resonant scanner and was then reconstructed using Imaris 8.0 (Bitplane AG).

3D RECONSTRUCTION OF CARDIAC EXOPHERS

We measured the 3D features of cardiac exophers and cardiac macrophages using Imaris Software (Bitplane AG, Switzerland). For 3D reconstructions, we used 0.25 µm detail level and a threshold based on absolute intensity. The source channels for the reconstruction of cardiac exopheres and cardiac macrophages were Tomato in αMHC^{Cre} Rosa26^{Tdtom} mice and CD68-FITC, respectively. From the parameters provided by the ImarisCell module we selected Volume, Area and Sphericity. In the case of cardiac exophers, diameter was calculated from Volume considering them as perfect spheres due to their high Sphericity index (0.71±0.01 in exophers vs. 0.37±0.01 in cMacs).

IDENTIFICATION OF ACID VS NEUTRAL PH COMPARTMENTS USING KEIMA

Keima is a fluorescent protein resistant to lysosomal proteases, with an emission spectrum that peaks at 620 nm and a bimodal excitation spectrum peaking at 440 and 586 nm corresponding to the neutral and ionized states of the chromophore's phenolic hydroxyl moiety, respectively. Neutral and ionized states predominate at high and low pHs, respectively, thus allowing measurement of mitophagy in vitro and in vivo (Katayama et al., 2011). We used this property to evaluate mitochondria degradation in macrophages by measuring ratiometric “red-to-green” fluorescence intensities in Keima+ regions co-localizing with macrophages (CD68+) or cardiomyocytes. Imaging was done using an SP5 confocal microscope (Leica) in two channels via two sequential excitations (458 nm for “green”; and 561 nm for “red” excitation), and a 590–650 nm

emission filter in both cases. Laser power was set at the lowest output that would allow clear visualization of the mt-Keima signal. CD68 labelling (for macrophages) was detected using a 488 nm excitation and a 510–550 nm emission filter.

CARDIOMYOCYTES, SARCOMERE AND MITOCHONDRIAL MORPHOLOGY

Cardiomyocytes area, perimeter and shape descriptors where measured by manually definition of cardiomyocytes borders in confocal images from cardiac sections (using laminin staining) and isolated cardiomyocytes (bright field) using ImageJ. Sarcomere length and mitochondria size and shape were obtained by visual inspection and segmentation of these structures in transmission electron microscopy (TEM) images, using ImageJ.

DETECTION OF APOPTOTIC CELLS BY TUNEL STAINING

Terminal deoxynucleotidyl transferase (TdT)-mediated dUTP-biotin nick end labeling (TUNEL) assay was performed using In Situ Cell Death Detection Kit (Roche). Briefly, myocardial sections were permeabilized during 15 minutes with 0.1% TritonX100 in PBS, washed with PBS and then incubated during 30 minutes at 37ºC with a solution containing TdT and biotin-16–deoxyuridine triphosphate (dUTP-biot), followed by incubation with FITC-labelled streptavidin for visualization of apoptotic cells. Quantification of TUNEL+ nuclei was done manually.

MEASUREMENT OF ROS USING DIHYDROETHIDIUM

The redox-sensitive, cell-permeable fluorophore Dihydroethidium (DHE, SigmaAldrich) was used to evaluate the cellular production of ROS. DHE is oxidized by ROS to form a red fluorescent product (ethidium) which intercalates into DNA. Briefly, 12-µm frozen sections were washed with PBS and incubated for 45 minutes at 37ºC with fresh 5mM DHE in DMSO (SigmaAldrich). Nuclei were counterstained with DAPI for quantification of fluorescence intensities, and estimation of ethidium/DAPI signal ratios.

PHOSPHATIDYL-SERINE (PS) STAINING IN LIVE HEART SECTIONS

Hearts from heterozygous CX3CR1^{GFP} mice were collected in excision buffer (HBSS 1x, FBS 5% at pH7.4) and manually cut perpendicular to the ventricular walls to form 1-2 mm thick rings of tissue. Those slices were incubated with Annexin V-PE (BD Biosciences) in Annexin binding buffer (10mM HEPES/NaOH, pH 7.4; 140 mM NaCl; 2,5 mM $CaCl_2$) with or without EDTA 1mM as control, since Annexin-V binding to PS is calcium-dependent. For imaging, slices were placed into glass petri plates containing fresh Annexin binding buffer and immobilized with a coverslip. Images were taken in an SP5 microscope (Leica) maintaining 37 ºC and 5% O_2 pressure. Tissue borders were avoided to exclude areas of dead cardiomyocytes. We measured the distances between macrophages and phosphatidylserine (Annexin V+) patches using FIJI Is Just ImageJ (NIH), and compared them to the same number of random spots in those images. Random spots were 1 µm diameter circles (similar to the phosphatidylserine patches) generated by a macro using FIJI Is Just ImageJ (NIH).

7.7. Mitochondria, inflammasome and autophagy

MITOCHONDRIA ISOLATION AND OXPHOS FUNCTION

Mitochondria were isolated from mouse heart and liver samples as described (Lapuente-Brun et al., 2013) and ATP synthesis was measured by kinetic luminescence assay (Vives-Bauza et al., 2007). Mitochondria were resuspended in 160 µl buffer A (150mM KCl, 25mM Tris-HCl, 2mM EDTA, 0.1% BSA FA, 10mM K-phosphate and 0.1mM $MgCl_2$, pH 7.4) at room temperature and dispensed into the wells of a 96-well luminescence reading plate (Costar). Substrate cocktail and buffer B (0.5M Tris-acetate pH 7.75, 0.8mM luciferine, 20 µg/ml luciferase) were added, and luminescence was measured over 1 min. Substrate cocktails were composed of 6 mM diadenosin pentaphosphate and 6 mM ADP supplemented with glutamate + malate for determination of CI activity, or with succinate for CII activity. ATP production rate is expressed as the amount of ATP produced (nmol/min/mg of protein) relative to controls. Technical duplicates were performed and the average value for each animal was represented.

CITRATE SYNTHASE ACTIVITY

Cytrate synthase activity was determined spectrophotometrically as described (Birch-Machin and Turnbull, 2001). 10 µg of total protein from tissue homogenates were used for the assay. Technical duplicates were performed, as represented. Investigators were not blinded to the group allocation.

$^{31}P/^{1}H$ MAGNETIC RESONANCE SPECTROSCOPY ($^{31}P/^{1}H$-MRS)

Mice were anesthetized with isoflurane during the whole acquisition. Spectroscopy examinations were performed in vivo on a 7T preclinical system (Agilent Varian, Palo Alto, USA) equipped with a DD2 console and an active shielded 115/60 gradient insert coil with 433 mT/m maximum strength. Double-tuned circular transmit/receive coil were used for phosphorus/proton (20 mm), placed over cardiac muscle (Rapid Biomedical GmBH, Rimpar Germany). Proton tissue spectra were acquired by 128

transients with 2048 complex points with a spectral bandwidth of 10 kHz and a repetition time of 1.2 ms. Phosphorus tissue spectra were acquired by 1000 transients with 8192 complex points with a spectral bandwidth of 7 kHz and a repetition time of 800ms. Spectra were acquired with adiabatic radiofrequency pulses to improve sensitivity and minimize spectral distortions with an Ernst flip angle. Chemical shift were expressed relative to phosphocreatine (0 ppm). Signals in nuclear magnetic resonance spectra were determined quantitatively by integration after automatic or manual baseline correction, with fitting of each peak of the spectrum (after phase and baseline correction) to a Lorentzian function using the Mestrenova program (Mestrelab Research, Santiago de Compostela, Spain; released 2015-02-04 version:10.0.1-14719). An exponential line broadening (3 Hz for proton) was applied before Fourier transformation.

BLUE NATIVE ELECTROPHORESIS

Mitochondrial proteins from heart tissue were solubilized with digitonin (4g/g) (Sigma) and run on a 3%–13% gradient Blue Native gel as described (Acin-Perez et al., 2008). Complexes were electroblotted onto PVDF membrane (Merckmillipore) and sequentially probed with antibodies against Complex I (mouse anti-Ndufa9; clone 20C11B11B11), Complex III (rabbit anti-Uqcrc2; polyclonal, Abcam), Complex IV (mouse anti-CoI; clone 1D6E1A8, Invitrogen), and Complex II (mouse anti-Fp70; clone 2E3GC12FB2AE2, Novex by Life Technologies).

WESTERN BLOT ANALYSES

Total heart protein homogenates were separated by 12.5% SDS polyacrylamide gel electrophoresis (SDS PAGE) and electro blotted onto PVDF transfer membrane (BioRad). For protein detection, the following antibodies were used: NLRP3 (clone 25N10E9; ThermoFisher), Caspase-1 (clone 14F468; Santa Cruz), IL-1beta (clone 3A6; Cell signal), LC3 (Polyclonal; Cell Signal), p62 (polyclonal; Cell Signaling), CoI (Complex IV subunit I; clone 1D6E1A8, Invitrogen), βActin (clone EA-53, Sigma Aldrich), CoxIV (Complex IV subunit IV; clone 3F9D3D11AF6, Abcam), PGC1α (Polyclonal; Abcam), TFAM (18G102B2E11), ATPb (ATP Synthase subunit beta; clone 3D5, Abcam) and GADPH

(clone 6C5, Abcam). Quantification of signals arising from near-infrared (NIR) fluorophores conjugated to secondary antibodies was performed by two-channel infrared (IR) scanner (Odyssey v.3.0). Western blot images were quantified by using ImageJ software (National Institutes of Health, Bethesda) and βActin or Ponceau S staining was selected as a loading control, as indicated.

AUTOPHAGY FLUX ANALYSIS

Animals were euthanized and the heart was quickly removed, cannulated through the ascending aorta, and mounted on a Langendorff perfusion apparatus. The heart was then retrogradely perfused for 4 min at room temperature (RT) with pre-filtered Ca2+-free Perfusion-Buffer [NaCl (113 mmol/L); KCl (4.7 mmol/L); KH2PO4 (0.6 mmol/L); Na2HPO4 (0.6 mmol/L); MgSO4·7H2O (1.2 mmol/L); NaHCO3 (12 mmol/L); KHCO3 (10 mmol/L); HEPES (10 mmol/L); taurine (30 mmol/L); glucose (5.5 mmol/L); 2,3-butanedione-monoxime (10 mmol/L), pH 7.4]. Enzymatic digestion was performed with digestion-buffer [perfusion-buffer with Liberase™ (0.2 mg/mL), Trypsin 2.5 % (0,14 mg/mL); CaCl2 (12.5 µmol/L) and Phenol Red (0.032 mmol/L)] for 20 min at 37 °C. At the end of enzymatic digestion, both ventricles were isolated and gently disaggregated in 5 mL of Digestion Buffer. The resulting cell suspension was filtered through a 100-µm sterile mesh (SEFAR-Nitex) and transferred for enzymatic inactivation to a tube with 10 mL of stopping-buffer-1 [perfusion-buffer supplemented with fetal bovine serum (FBS, 10 % v/v) and CaCl2 (12.5 µmol/L)]. After gravity sedimentation for 15 min, cardiomyocytes were resuspended in stopping-buffer-2 containing lower FBS (5 % v/v) for 10 min. Cardiomyocyte Ca2+-reintroduction was performed in stopping-buffer-2 with two progressively increased CaCl2 concentrations (112 µmol/L and 1 mmol/L). Cells were resuspended and allowed to decant for 10 min in each step, contributing to the purification of the cardiomyocyte suspension. The homogeneous suspension of rod-shaped cardiomyocytes was then resuspended in M199 supplemented with l-glutamine, pyruvate, penicillin–streptomycin (1 %), bovine serum albumin (BSA, 2 g/L), blebbistatin (25 µmol/L) and FBS (5 %). Cells were plated in single drops onto 20-mm2 glass bottom microwell dishes (MatTek) precoated with 100 µL of mouse laminin (200 µg/mL) in 900 µL NaCl 0.9% for at least 1 h. For each mouse, 2 dishes were used as a control culture

and 2 dishes were treated with Hydroxycloroquine (30 µM) for 12h to block lysosomal degradation. After culture, cardiomyocytes were fixed overnight at 4°C in 2% paraformaldehyde in PBS. After fixation, immunofluorescence was made following standard procedures: fixation in methanol at 4ºC for 10 min, permeabilized with 0.5% Triton-X 100 and blocked in PBS containing 10% goat serum and 0.1% Triton-X 100. anti-LC3 antibody (clone 5F10 Nanotools) primary antibody was used and Nuclei were co-stained with DAPI. Isolated cardiomyocytes were then imaged with a Leica SP5 confocal microscope using 20×/0.75 dry and 63×/1.30 oil objectives. Quantifications were made by using the macro plugin tool in image J, which automatically detected individual cardiomyocytes and quantified the number of LC3, dots per cell. Autophagy was determined by evaluating autophagic flux, which is achieved by comparing the number of LC3-positive autophagosomes in the absence and presence of hydroxychloroquine.

7.8. Molecular analysis

RNA ISOLATION, REVERSE TRANSCRIPTION AND REAL-TIME PCR

Total RNA was prepared with RNA Extraction RNeasy Plus Micro-kit (QIAGEN) for isolation from macrophages or with Trizol (Sigma) for total tissue RNA. RNA was reverse-transcribed with High- Capacity cDNA Reverse Transcription kit (Applied Biosystems; Carlsbad, CA) according to the manufacturer's protocol. Real-time quantitative PCR (SYBR-green, Applied Biosystems) assays were performed with an Applied Biosystems 7900HT Fast Real-Time PCR System sequencer detector. Expression was normalized to 36b4 expression. Primer sequences are listed below:

Primers	Sequences
36b4_Fw (5′ > 3′)	ACTGGTCTAGGACCCGAGAAG
_Rv (5′ > 3′)	TCCCACCTTGTCTCCAGTCT
Keima_Fw (5′ > 3′)	AGCTTCAGTACGGAAGCATACC
_Rv (5′ > 3′)	TGCTCCTCTCCCATGTATATCC
Tomato_Fw (5′ > 3′)	GCCGACATCCCCGATTACAAGA
_Rv (5′ > 3′)	CGATGGTGTAGTCCTCGTTGTGG
Mertk_Fw (5′ > 3′)	GAGGACTGCTTGGATGAACTGTA
_Rv (5′ > 3′)	AGGTGGGTCGATCCAAGG
LXRα_Fw (5′ > 3′)	CAACAGTGTAACAGGCGCT
_Rv (5′ > 3′)	TGCAATGGGCCAAGGC
LXRβ_Fw (5′ > 3′)	CCCCACAAGTTCTCTGGACACT
_Rv (5′ > 3′)	TGACGTGGCGGAGGTACTG
Axl_Fw (5′ > 3′)	GTGACAGCCTATACCTCGGC
_Rv (5′ > 3′)	GGGGGTTCACTCACCAGATG
Mfge8_Fw (5′ > 3′)	GTGCCCTGTGGGCTACTC
_Rv (5′ > 3′)	GTATTGGGGACGGCTGTG

Abbreviations: Fw, forward primer; Rv, reverse primer

PROTEOMIC ANALYSIS OF MACROPHAGE DEPLETED HEARTS

We used hearts after 0, 14 and 21 days of DT treatment in control WT and CD169^{DTR} mice. Hearts were collected and frozen in liquid nitrogen. The protein extracts were obtained by tissue homogenization with ceramic beads (MagNa Lyser Green Beads, Roche, Germany) in extraction buffer (50 mM Tris-HCl, 1 mM EDTA, 2% SDS, pH 8.5 – 8.8, 50 mM DTT). The protein extract for each time-point from three biological replicate

samples in addition to an internal standard generated as a pool of peptides of all biological conditions were subjected to tryptic digestion and the resulting peptides were labeled with 10-plex isobaric mass tags for relative quantification (TMT, Thermo Scientific). Labeled peptides were subjected to peptide separation into six fractions using a Waters Oasis MCX cartridge (Waters Corp, Milford, MA). The fractionated peptides were analyzed by nano-liquid chromatography-tandem mass spectrometry (nanoLC-MS/MS) using a Q-Exactive mass spectrometer (Termo Scientific). Protein identification was performed using the SEQUEST HT algorithm integrated in Proteome Discoverer 1.4 (Thermo Scientific). MS/MS scans were searched against a mouse reference proteome database (UniProtKB/Swiss-Prot 02_12_2015 Release). Peptides were identified from MS/MS data using the probability ratio method (Martinez-Bartolome et al., 2008) and the False discovery rate (FDR) of peptide identifications was calculated by the refined method (Bonzon-Kulichenko et al., 2015). Quantitative information was extracted from the MS/MS spectra of TMT-labeled peptides using a SQL query from the Thermo Proteome Discoverer file (.msf). Protein abundance changes were analyzed using the WSPP model, and were expressed using the Zq variable, which represents standardized log2 ratio values (Navarro et al., 2014). The validity of the null hypothesis at each one of the levels (spectrum, peptide, protein, and functional category) was carefully checked by plotting the cumulative distributions, as described (Navarro et al., 2014). The proteomics data analysis was performed using the R package Limma v3.32.2 (Ritchie et al., 2015). To test differential expression using the moderated t statistics by Smyth et al (Smyth, 2004), raw and Benjamini-Hochberg adjusted p-values (FDR) were calculated for each of the tests. An adjusted p-value of less than 0.05 was considered statistically significant. The differentially expressed proteins between WT+DT and CD169^{DTR}+DT (d21) were analyzed using Ingenuity Pathway Analysis (IPA, Quiagen, http://www.ingenuity.com). Pathways with adjusted p-values below 0.05 were considered overrepresented.

PROTEOMIC ANALYSIS OF CARDIAC EXOPHERS vs. TOTAL TISSUE

We used hearts form Card^{RED} mice and exophers isolated from the same mice as indicated in Extra Data Figure 2d-e and methods section. Mice were perfused with PBS

and approximately 50 mg of tissue was frozen in liquid nitrogen from each heart, while the rest was used to isolate the corresponding exospheres. The protein extracts were obtained in extraction buffer (50 mM Tris-HCl, 1 mM EDTA, 2% SDS, pH 8.5 – 8.8, 50 mM DTT) by tissue homogenization with ceramic beads (MagNa Lyser Green Beads, Roche, Germany) for total hearts and by heating (5 min at 90ºC), vortexing and centrifugation (10 min at 16100g) for cardiac exophers. Protein lysates from the exospheres and the corresponding heart tissue were boiled in 2x Laemmli sample buffer, subjected to in-gel digestion (Bonzon-Kulichenko et al., 2011) and analyzed using a Proxeon Easy nano-flow HPLC system (Thermo Fisher Scientific, Bremen, Germany) coupled via a nanoelectrospray ion source (Thermo Fisher Scientific) to an Orbitrap Fusion mass spectrometer (Thermo Fisher). C18-based reverse phase separation was used with a 2-cm trap column and a 50-cm analytical column (75 µm I.D, 2 µm particle size, Acclaim PepMap RSLC, 100 C18; Thermo Fisher Scientific) in a continuous acetonitrile gradient consisting of 0-30% A for 120 min, 50-90% B for 3 min (A= 0.1% formic acid; B= 90% acetonitrile, 0.1% formic acid) at a flow rate of 200 nL/min. Mass spectra were acquired in a data-dependent manner, with an automatic switch between MS and MS/MS using a top 15 method and dynamic exclusion. MS spectra in the Orbitrap analyzer were in a mass range of 400–1500 m/z and 120,000 resolution. HCD fragmentation was performed at 33 eV of normalized collision energy and MS/MS spectra were analyzed at 30,000 resolution in the Orbitrap. Protein identification was performed as described above (Proteome Discoverer 2.1; Thermo Scientific) and MS/MS scans were searched against a mouse reference proteome database (UniProtKB/Swiss-Prot April_2018), supplemented with the tdTomato and 116 CRAP proteins (Global Proteome Machine) (16988 sequences in total). Peptide identification from MS/MS data was performed as described above. In order to obtain maximum reliability, we eliminate from the analysis all those proteins that have less than 6 counts within all samples and were not detected at least in 3 samples of the same group (either total cardiac tissue or exophers). We only consider proteins with adjusted p-values below 0.05 as significantly changed between both conditions.

7.9. Statistical analysis

Data are represented as mean values ± standard error of the mean (SEM) or box and whiskers plots. Where applicable, normality was estimated using D'Agostino & Pearson or Shapiro-Wilk normality test. For comparison between 2 groups, paired or unpaired t-test was used when data presented normal distribution and paired or unpaired Mann-Withney when data did not follow normal distribution. For more than 2 groups, data were evaluated by one-way analysis of variance (ANOVA) with Dunnett's multiple comparison when data presented normal distribution and Kruskal-Wallis with Dunn´s multiple comparison when data did not follow normal distribution. Log-rank analysis was used for Mantel-Cox survival curves. Statistically significant outliers were identified using Grubb's test (ESD method). All statistical analyses were performed using Prism v6 (GraphPad Software, California, USA). A p-value below 0.05 was considered statistically significant (*). P-values $p \leq 0{,}01$ (**) and $p \leq 0{,}001$ (***), as well as non-significant differences (n.s.) are indicated.

8. References

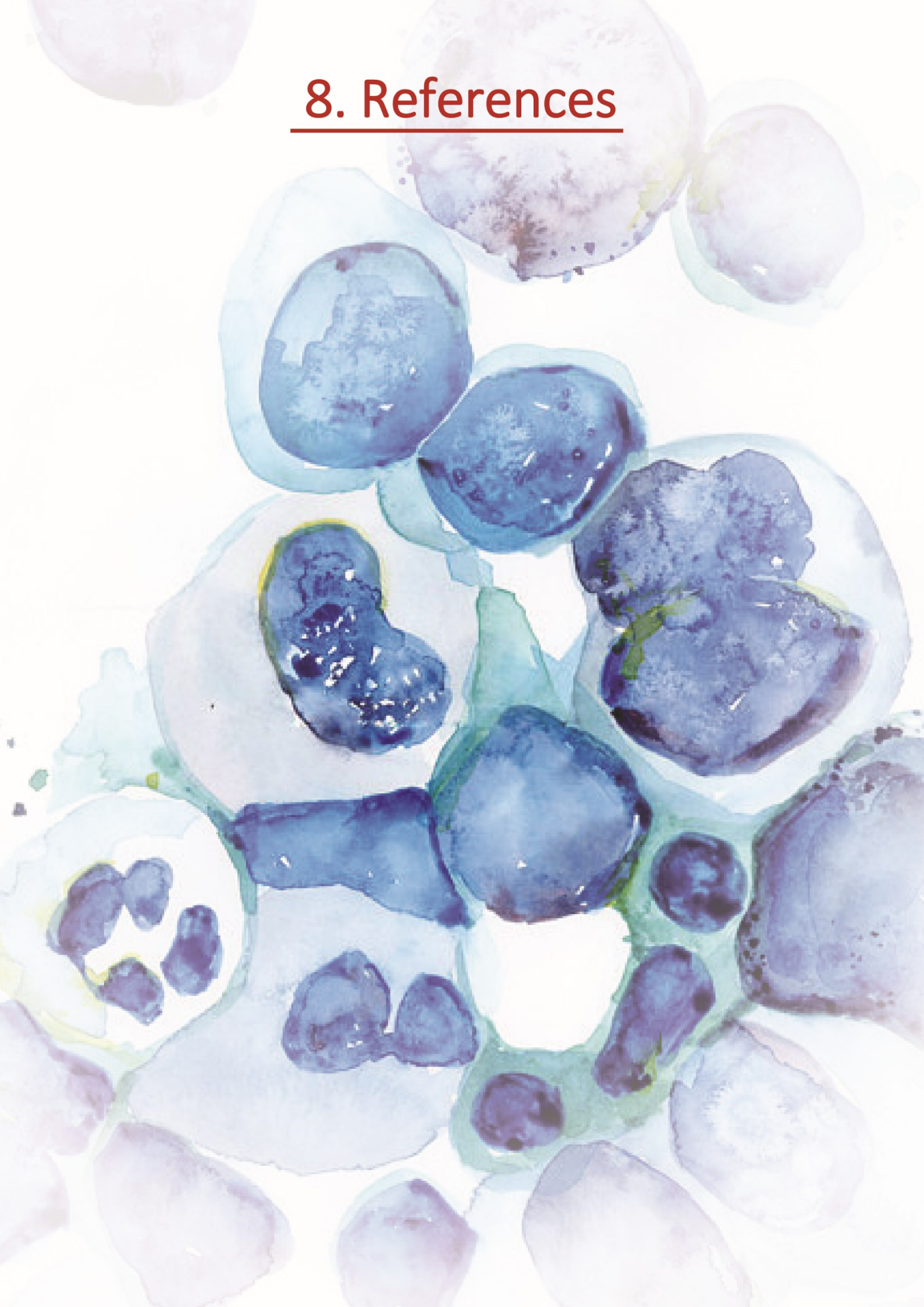

8. References

1. A-Gonzalez, N., Bensinger, S.J., Hong, C., Beceiro, S., Bradley, M.N., Zelcer, N., Deniz, J., Ramirez, C., Diaz, M., Gallardo, G.*, et al.* (2009). Apoptotic cells promote their own clearance and immune tolerance through activation of the nuclear receptor LXR. Immunity *31*, 245-258.
2. A-Gonzalez, N., Quintana, J.A., Garcia-Silva, S., Mazariegos, M., Gonzalez de la Aleja, A., Nicolas-Avila, J.A., Walter, W., Adrover, J.M., Crainiciuc, G., Kuchroo, V.K.*, et al.* (2017). Phagocytosis imprints heterogeneity in tissue-resident macrophages. J Exp Med *214*, 1281-1296.
3. Abbas, A.K., Lichtman, A.H., Pillai, S., Baker, D.L., and Baker, A. Cellular and molecular immunology, Ninth edition. edn.
4. Acin-Perez, R., Fernandez-Silva, P., Peleato, M.L., Perez-Martos, A., and Enriquez, J.A. (2008). Respiratory active mitochondrial supercomplexes. Molecular cell *32*, 529-539.
5. Acin-Perez, R., Lechuga-Vieco, A.V., Del Mar Munoz, M., Nieto-Arellano, R., Torroja, C., Sanchez-Cabo, F., Jimenez, C., Gonzalez-Guerra, A., Carrascoso, I., Beninca, C.*, et al.* (2018). Ablation of the stress protease OMA1 protects against heart failure in mice. Sci Transl Med *10*.
6. Adrover, J.M., Nicolas-Avila, J.A., and Hidalgo, A. (2016). Aging: A Temporal Dimension for Neutrophils. Trends Immunol *37*, 334-345.
7. Ahmad, T., Mukherjee, S., Pattnaik, B., Kumar, M., Singh, S., Rehman, R., Tiwari, B.K., Jha, K.A., Barhanpurkar, A.P., Wani, M.R.*, et al.* (2014). Miro1 regulates intercellular mitochondrial transport & enhances mesenchymal stem cell rescue efficacy. Embo J *33*, 994-1010.
8. Al Rawi, S., Louvet-Vallee, S., Djeddi, A., Sachse, M., Culetto, E., Hajjar, C., Boyd, L., Legouis, R., and Galy, V. (2011). Postfertilization autophagy of sperm organelles prevents paternal mitochondrial DNA transmission. Science *334*, 1144-1147.
9. Anisimov, V.N., Zabezhinski, M.A., Popovich, I.G., Piskunova, T.S., Semenchenko, A.V., Tyndyk, M.L., Yurova, M.N., Rosenfeld, S.V., and Blagosklonny, M.V. (2011). Rapamycin increases lifespan and inhibits spontaneous tumorigenesis in inbred female mice. Cell Cycle *10*, 4230-4236.
10. Aprahamian, T., Takemura, Y., Goukassian, D., and Walsh, K. (2008). Ageing is associated with diminished apoptotic cell clearance in vivo. Clin Exp Immunol *152*, 448-455.
11. Arandjelovic, S., and Ravichandran, K.S. (2015). Phagocytosis of apoptotic cells in homeostasis. Nature immunology *16*, 907-917.
12. Atkin-Smith, G.K., Paone, S., Zanker, D.J., Duan, M., Phan, T.K., Chen, W., Hulett, M.D., and Poon, I.K. (2017). Isolation of cell type-specific apoptotic bodies by fluorescence-activated cell sorting. Sci Rep *7*, 39846.
13. Atkin-Smith, G.K., and Poon, I.K.H. (2017). Disassembly of the Dying: Mechanisms and Functions. Trends Cell Biol *27*, 151-162.
14. Auffray, C., Fogg, D., Garfa, M., Elain, G., Join-Lambert, O., Kayal, S., Sarnacki, S., Cumano, A., Lauvau, G., and Geissmann, F. (2007). Monitoring of blood vessels and tissues by a population of monocytes with patrolling behavior. Science *317*, 666-670.
15. Aumailley, L., Garand, C., Dubois, M.J., Johnson, F.B., Marette, A., and Lebel, M. (2015). Metabolic and Phenotypic Differences between Mice Producing a Werner Syndrome Helicase Mutant Protein and Wrn Null Mice. PLoS One *10*, e0140292.

16. Azzawi, M., Hasleton, P.S., Kan, S.W., Hillier, V.F., Quigley, A., and Hutchinson, I.V. (1997). Distribution of myocardial macrophages in the normal human heart. J Anat *191 (Pt 3)*, 417-423.
17. Bain, C.C., Bravo-Blas, A., Scott, C.L., Perdiguero, E.G., Geissmann, F., Henri, S., Malissen, B., Osborne, L.C., Artis, D., and Mowat, A.M. (2014). Constant replenishment from circulating monocytes maintains the macrophage pool in the intestine of adult mice. Nature immunology *15*, 929-937.
18. Bain, C.C., Scott, C.L., Uronen-Hansson, H., Gudjonsson, S., Jansson, O., Grip, O., Guilliams, M., Malissen, B., Agace, W.W., and Mowat, A.M. (2013). Resident and pro-inflammatory macrophages in the colon represent alternative context-dependent fates of the same Ly6Chi monocyte precursors. Mucosal immunology *6*, 498-510.
19. Bajpai, G., Schneider, C., Wong, N., Bredemeyer, A., Hulsmans, M., Nahrendorf, M., Epelman, S., Kreisel, D., Liu, Y., Itoh, A.*, et al.* (2018). The human heart contains distinct macrophage subsets with divergent origins and functions. Nat Med *24*, 1234-1245.
20. Baylis, D., Bartlett, D.B., Patel, H.P., and Roberts, H.C. (2013). Understanding how we age: insights into inflammaging. Longev Healthspan *2*, 8.
21. Bergmann, O., Bhardwaj, R.D., Bernard, S., Zdunek, S., Barnabe-Heider, F., Walsh, S., Zupicich, J., Alkass, K., Buchholz, B.A., Druid, H.*, et al.* (2009). Evidence for cardiomyocyte renewal in humans. Science *324*, 98-102.
22. Biala, A.K., Dhingra, R., and Kirshenbaum, L.A. (2015). Mitochondrial dynamics: Orchestrating the journey to advanced age. J Mol Cell Cardiol *83*, 37-43.
23. Birch-Machin, M.A., and Turnbull, D.M. (2001). Assaying mitochondrial respiratory complex activity in mitochondria isolated from human cells and tissues. Methods Cell Biol *65*, 97-117.
24. Birge, R.B., Boeltz, S., Kumar, S., Carlson, J., Wanderley, J., Calianese, D., Barcinski, M., Brekken, R.A., Huang, X., Hutchins, J.T.*, et al.* (2016). Phosphatidylserine is a global immunosuppressive signal in efferocytosis, infectious disease, and cancer. Cell Death Differ *23*, 962-978.
25. Blagosklonny, M.V. (2010). Calorie restriction: decelerating mTOR-driven aging from cells to organisms (including humans). Cell Cycle *9*, 683-688.
26. Boengler, K., Schulz, R., and Heusch, G. (2009). Loss of cardioprotection with ageing. Cardiovasc Res *83*, 247-261.
27. Bonzon-Kulichenko, E., Garcia-Marques, F., Trevisan-Herraz, M., and Vazquez, J. (2015). Revisiting peptide identification by high-accuracy mass spectrometry: problems associated with the use of narrow mass precursor windows. J Proteome Res *14*, 700-710.
28. Bonzon-Kulichenko, E., Perez-Hernandez, D., Nunez, E., Martinez-Acedo, P., Navarro, P., Trevisan-Herraz, M., Ramos Mdel, C., Sierra, S., Martinez-Martinez, S., Ruiz-Meana, M.*, et al.* (2011). A robust method for quantitative high-throughput analysis of proteomes by 18O labeling. Mol Cell Proteomics *10*, M110 003335.
29. Bose, J., Gruber, A.D., Helming, L., Schiebe, S., Wegener, I., Hafner, M., Beales, M., Kontgen, F., and Lengeling, A. (2004). The phosphatidylserine receptor has essential functions during embryogenesis but not in apoptotic cell removal. J Biol *3*, 15.
30. Boyer, S.W., Schroeder, A.V., Smith-Berdan, S., and Forsberg, E.C. (2011). All hematopoietic cells develop from hematopoietic stem cells through Flk2/Flt3-positive progenitor cells. Cell Stem Cell *9*, 64-73.
31. Boyle, A.J., Shih, H., Hwang, J., Ye, J., Lee, B., Zhang, Y., Kwon, D., Jun, K., Zheng, D., Sievers, R.*, et al.* (2011). Cardiomyopathy of aging in the mammalian heart is

characterized by myocardial hypertrophy, fibrosis and a predisposition towards cardiomyocyte apoptosis and autophagy. Exp Gerontol *46*, 549-559.

32. Brunk, U.T., and Terman, A. (2002). The mitochondrial-lysosomal axis theory of aging: accumulation of damaged mitochondria as a result of imperfect autophagocytosis. Eur J Biochem *269*, 1996-2002.
33. Burnett, S.H., Kershen, E.J., Zhang, J., Zeng, L., Straley, S.C., Kaplan, A.M., and Cohen, D.A. (2004). Conditional macrophage ablation in transgenic mice expressing a Fas-based suicide gene. J Leukoc Biol *75*, 612-623.
34. Cai, X., Chiu, Y.H., and Chen, Z.J. (2014). The cGAS-cGAMP-STING pathway of cytosolic DNA sensing and signaling. Mol Cell *54*, 289-296.
35. Carey, B., and Trapnell, B.C. (2010). The molecular basis of pulmonary alveolar proteinosis. Clin Immunol *135*, 223-235.
36. Carr, I., Clegg, E.J., and Meek, G.A. (1968). Sertoli cells as phagocytes: an electron microscopic study. J Anat *102*, 501-509.
37. Casanova-Acebes, M., Nicolas-Avila, J.A., Li, J.L., Garcia-Silva, S., Balachander, A., Rubio-Ponce, A., Weiss, L.A., Adrover, J.M., Burrows, K., N, A.G.*, et al.* (2018). Neutrophils instruct homeostatic and pathological states in naive tissues. J Exp Med *215*, 2778-2795.
38. Casanova-Acebes, M., Pitaval, C., Weiss, L.A., Nombela-Arrieta, C., Chevre, R., N, A.G., Kunisaki, Y., Zhang, D., van Rooijen, N., Silberstein, L.E.*, et al.* (2013). Rhythmic modulation of the hematopoietic niche through neutrophil clearance. Cell *153*, 1025-1035.
39. Chakarov, S., Lim, H.Y., Tan, L., Lim, S.Y., See, P., Lum, J., Zhang, X.M., Foo, S., Nakamizo, S., Duan, K.*, et al.* (2019). Two distinct interstitial macrophage populations coexist across tissues in specific subtissular niches. Science *363*.
40. Chasis, J.A., and Mohandas, N. (2008). Erythroblastic islands: niches for erythropoiesis. Blood *112*, 470-478.
41. Chen, G., Zhuchenko, O., and Kuspa, A. (2007). Immune-like phagocyte activity in the social amoeba. Science *317*, 678-681.
42. Chen, Q., Ross, T., Hu, Y., and Lesnefsky, E.J. (2012). Blockade of electron transport at the onset of reperfusion decreases cardiac injury in aged hearts by protecting the inner mitochondrial membrane. J Aging Res *2012*, 753949.
43. Chovatiya, R., and Medzhitov, R. (2014). Stress, inflammation, and defense of homeostasis. Molecular cell *54*, 281-288.
44. Chow, A., Huggins, M., Ahmed, J., Hashimoto, D., Lucas, D., Kunisaki, Y., Pinho, S., Leboeuf, M., Noizat, C., van Rooijen, N.*, et al.* (2013). CD169(+) macrophages provide a niche promoting erythropoiesis under homeostasis and stress. Nature medicine *19*, 429-436.
45. Chow, A., Lucas, D., Hidalgo, A., Mendez-Ferrer, S., Hashimoto, D., Scheiermann, C., Battista, M., Leboeuf, M., Prophete, C., van Rooijen, N.*, et al.* (2011). Bone marrow CD169+ macrophages promote the retention of hematopoietic stem and progenitor cells in the mesenchymal stem cell niche. J Exp Med *208*, 261-271.
46. Chung, W.S., and Barres, B.A. (2012). The role of glial cells in synapse elimination. Curr Opin Neurobiol *22*, 438-445.
47. Chung, W.S., Clarke, L.E., Wang, G.X., Stafford, B.K., Sher, A., Chakraborty, C., Joung, J., Foo, L.C., Thompson, A., Chen, C.*, et al.* (2013). Astrocytes mediate synapse elimination through MEGF10 and MERTK pathways. Nature *504*, 394-400.
48. Coll, R.C., Robertson, A.A., Chae, J.J., Higgins, S.C., Munoz-Planillo, R., Inserra, M.C., Vetter, I., Dungan, L.S., Monks, B.G., Stutz, A.*, et al.* (2015). A small-molecule

inhibitor of the NLRP3 inflammasome for the treatment of inflammatory diseases. Nature medicine *21*, 248-255.

49. Collins, L.V., Hajizadeh, S., Holme, E., Jonsson, I.M., and Tarkowski, A. (2004). Endogenously oxidized mitochondrial DNA induces in vivo and in vitro inflammatory responses. J Leukoc Biol *75*, 995-1000.
50. Colman, R.J., Anderson, R.M., Johnson, S.C., Kastman, E.K., Kosmatka, K.J., Beasley, T.M., Allison, D.B., Cruzen, C., Simmons, H.A., Kemnitz, J.W.*, et al.* (2009). Caloric restriction delays disease onset and mortality in rhesus monkeys. Science *325*, 201-204.
51. Cooper, M.D., and Alder, M.N. (2006). The evolution of adaptive immune systems. Cell *124*, 815-822.
52. Cordonnier, M.N., Dauzonne, D., Louvard, D., and Coudrier, E. (2001). Actin filaments and myosin I alpha cooperate with microtubules for the movement of lysosomes. Mol Biol Cell *12*, 4013-4029.
53. Cuervo, A.M. (2008). Autophagy and aging: keeping that old broom working. Trends Genet *24*, 604-612.
54. Cuervo, A.M., Bergamini, E., Brunk, U.T., Droge, W., Ffrench, M., and Terman, A. (2005). Autophagy and aging: the importance of maintaining "clean" cells. Autophagy *1*, 131-140.
55. Cuervo, A.M., and Dice, J.F. (2000). Age-related decline in chaperone-mediated autophagy. J Biol Chem *275*, 31505-31513.
56. Cuezva, J.M., Chen, G., Alonso, A.M., Isidoro, A., Misek, D.E., Hanash, S.M., and Beer, D.G. (2004). The bioenergetic signature of lung adenocarcinomas is a molecular marker of cancer diagnosis and prognosis. Carcinogenesis *25*, 1157-1163.
57. Culemann, S., Gruneboom, A., Nicolas-Avila, J.A., Weidner, D., Lammle, K.F., Rothe, T., Quintana, J.A., Kirchner, P., Krljanac, B., Eberhardt, M.*, et al.* (2019). Locally renewing resident synovial macrophages provide a protective barrier for the joint. Nature *572*, 670-675.
58. Dai, D.F., Chiao, Y.A., Marcinek, D.J., Szeto, H.H., and Rabinovitch, P.S. (2014a). Mitochondrial oxidative stress in aging and healthspan. Longev Healthspan *3*, 6.
59. Dai, D.F., Karunadharma, P.P., Chiao, Y.A., Basisty, N., Crispin, D., Hsieh, E.J., Chen, T., Gu, H., Djukovic, D., Raftery, D.*, et al.* (2014b). Altered proteome turnover and remodeling by short-term caloric restriction or rapamycin rejuvenate the aging heart. Aging Cell *13*, 529-539.
60. Dalli, J., Jones, C.P., Cavalcanti, D.M., Farsky, S.H., Perretti, M., and Rankin, S.M. (2012). Annexin A1 regulates neutrophil clearance by macrophages in the mouse bone marrow. Faseb J *26*, 387-396.
61. Das, K.C., and Muniyappa, H. (2013). Age-dependent mitochondrial energy dynamics in the mice heart: role of superoxide dismutase-2. Exp Gerontol *48*, 947-959.
62. Davies, L.C., Jenkins, S.J., Allen, J.E., and Taylor, P.R. (2013). Tissue-resident macrophages. Nat Immunol *14*, 986-995.
63. Davies, L.C., and Taylor, P.R. (2015). Tissue-resident macrophages: then and now. Immunology *144*, 541-548.
64. Davis, C.H., Kim, K.Y., Bushong, E.A., Mills, E.A., Boassa, D., Shih, T., Kinebuchi, M., Phan, S., Zhou, Y., Bihlmeyer, N.A.*, et al.* (2014). Transcellular degradation of axonal mitochondria. Proc Natl Acad Sci U S A *111*, 9633-9638.
65. Davis, C.H., and Marsh-Armstrong, N. (2014). Discovery and implications of transcellular mitophagy. Autophagy *10*, 2383-2384.
66. De La Fuente, M. (1985). Changes in the macrophage function with aging. Comp Biochem Physiol A Comp Physiol *81*, 935-938.

67. DeBerge, M., Yeap, X.Y., Dehn, S., Zhang, S., Grigoryeva, L., Misener, S., Procissi, D., Zhou, X., Lee, D.C., Muller, W.A., *et al.* (2017). MerTK Cleavage on Resident Cardiac Macrophages Compromises Repair After Myocardial Ischemia Reperfusion Injury. Circ Res *121*, 930-940.

68. DeFalco, T., Potter, S.J., Williams, A.V., Waller, B., Kan, M.J., and Capel, B. (2015). Macrophages Contribute to the Spermatogonial Niche in the Adult Testis. Cell Rep *12*, 1107-1119.

69. Delbridge, L.M.D., Mellor, K.M., Taylor, D.J., and Gottlieb, R.A. (2017). Myocardial stress and autophagy: mechanisms and potential therapies. Nat Rev Cardiol *14*, 412-425.

70. Deniset, J.F., Belke, D., Lee, W.Y., Jorch, S.K., Deppermann, C., Hassanabad, A.F., Turnbull, J.D., Teng, G., Rozich, I., Hudspeth, K., *et al.* (2019). Gata6(+) Pericardial Cavity Macrophages Relocate to the Injured Heart and Prevent Cardiac Fibrosis. Immunity *51*, 131-140 e135.

71. Dey, A., Allen, J., and Hankey-Giblin, P.A. (2014). Ontogeny and polarization of macrophages in inflammation: blood monocytes versus tissue macrophages. Front Immunol *5*, 683.

72. Dhahbi, J.M., Tsuchiya, T., Kim, H.J., Mote, P.L., and Spindler, S.R. (2006). Gene expression and physiologic responses of the heart to the initiation and withdrawal of caloric restriction. J Gerontol A Biol Sci Med Sci *61*, 218-231.

73. Dick, S.A., Macklin, J.A., Nejat, S., Momen, A., Clemente-Casares, X., Althagafi, M.G., Chen, J., Kantores, C., Hosseinzadeh, S., Aronoff, L., *et al.* (2019). Self-renewing resident cardiac macrophages limit adverse remodeling following myocardial infarction. Nature immunology *20*, 29-39.

74. Dockrell, D.H., Lee, M., Lynch, D.H., and Read, R.C. (2001). Immune-mediated phagocytosis and killing of Streptococcus pneumoniae are associated with direct and bystander macrophage apoptosis. J Infect Dis *184*, 713-722.

75. Dorn, G.W., 2nd, Clark, C.F., Eschenbacher, W.H., Kang, M.Y., Engelhard, J.T., Warner, S.J., Matkovich, S.J., and Jowdy, C.C. (2011). MARF and Opa1 control mitochondrial and cardiac function in Drosophila. Circ Res *108*, 12-17.

76. Dorsch, L.M., Schuldt, M., Knezevic, D., Wiersma, M., Kuster, D.W.D., van der Velden, J., and Brundel, B. (2019). Untying the knot: protein quality control in inherited cardiomyopathies. Pflugers Arch *471*, 795-806.

77. Duncan, J.L., LaVail, M.M., Yasumura, D., Matthes, M.T., Yang, H., Trautmann, N., Chappelow, A.V., Feng, W., Earp, H.S., Matsushima, G.K., *et al.* (2003). An RCS-like retinal dystrophy phenotype in mer knockout mice. Invest Ophthalmol Vis Sci *44*, 826-838.

78. Duvezin-Caubet, S., Jagasia, R., Wagener, J., Hofmann, S., Trifunovic, A., Hansson, A., Chomyn, A., Bauer, M.F., Attardi, G., Larsson, N.G., *et al.* (2006). Proteolytic processing of OPA1 links mitochondrial dysfunction to alterations in mitochondrial morphology. J Biol Chem *281*, 37972-37979.

79. Edwards, J.R., and Mundy, G.R. (2011). Advances in osteoclast biology: old findings and new insights from mouse models. Nature reviews Rheumatology *7*, 235-243.

80. Ema, H., Morita, Y., and Suda, T. (2014). Heterogeneity and hierarchy of hematopoietic stem cells. Exp Hematol *42*, 74-82 e72.

81. Epelman, S., Lavine, K.J., Beaudin, A.E., Sojka, D.K., Carrero, J.A., Calderon, B., Brija, T., Gautier, E.L., Ivanov, S., Satpathy, A.T., *et al.* (2014a). Embryonic and adult-derived resident cardiac macrophages are maintained through distinct mechanisms at steady state and during inflammation. Immunity *40*, 91-104.

82. Epelman, S., Lavine, K.J., and Randolph, G.J. (2014b). Origin and functions of tissue macrophages. Immunity *41*, 21-35.

83. Evrard, M., Chong, S.Z., Devi, S., Chew, W.K., Lee, B., Poidinger, M., Ginhoux, F., Tan, S.M., and Ng, L.G. (2015). Visualization of bone marrow monocyte mobilization using Cx3cr1gfp/+Flt3L-/- reporter mouse by multiphoton intravital microscopy. J Leukoc Biol *97*, 611-619.

84. Fabriek, B.O., Polfliet, M.M., Vloet, R.P., van der Schors, R.C., Ligtenberg, A.J., Weaver, L.K., Geest, C., Matsuno, K., Moestrup, S.K., Dijkstra, C.D.*, et al.* (2007). The macrophage CD163 surface glycoprotein is an erythroblast adhesion receptor. Blood *109*, 5223-5229.

85. Fadok, V.A., Bratton, D.L., Konowal, A., Freed, P.W., Westcott, J.Y., and Henson, P.M. (1998). Macrophages that have ingested apoptotic cells in vitro inhibit proinflammatory cytokine production through autocrine/paracrine mechanisms involving TGF-beta, PGE2, and PAF. The Journal of clinical investigation *101*, 890-898.

86. Fadok, V.A., Voelker, D.R., Campbell, P.A., Cohen, J.J., Bratton, D.L., and Henson, P.M. (1992). Exposure of phosphatidylserine on the surface of apoptotic lymphocytes triggers specific recognition and removal by macrophages. Journal of immunology *148*, 2207-2216.

87. Faust, N., Varas, F., Kelly, L.M., Heck, S., and Graf, T. (2000). Insertion of enhanced green fluorescent protein into the lysozyme gene creates mice with green fluorescent granulocytes and macrophages. Blood *96*, 719-726.

88. Feng, W., Yasumura, D., Matthes, M.T., LaVail, M.M., and Vollrath, D. (2002). Mertk triggers uptake of photoreceptor outer segments during phagocytosis by cultured retinal pigment epithelial cells. J Biol Chem *277*, 17016-17022.

89. Flynn, J.M., O'Leary, M.N., Zambataro, C.A., Academia, E.C., Presley, M.P., Garrett, B.J., Zykovich, A., Mooney, S.D., Strong, R., Rosen, C.J.*, et al.* (2013). Late-life rapamycin treatment reverses age-related heart dysfunction. Aging Cell *12*, 851-862.

90. Gal, A., Li, Y., Thompson, D.A., Weir, J., Orth, U., Jacobson, S.G., Apfelstedt-Sylla, E., and Vollrath, D. (2000). Mutations in MERTK, the human orthologue of the RCS rat retinal dystrophy gene, cause retinitis pigmentosa. Nat Genet *26*, 270-271.

91. Ganz, T. (2012). Macrophages and systemic iron homeostasis. Journal of innate immunity *4*, 446-453.

92. Garcia-Prat, L., Martinez-Vicente, M., Perdiguero, E., Ortet, L., Rodriguez-Ubreva, J., Rebollo, E., Ruiz-Bonilla, V., Gutarra, S., Ballestar, E., Serrano, A.L.*, et al.* (2016). Autophagy maintains stemness by preventing senescence. Nature *529*, 37-42.

93. Gautier, E.L., Chow, A., Spanbroek, R., Marcelin, G., Greter, M., Jakubzick, C., Bogunovic, M., Leboeuf, M., van Rooijen, N., Habenicht, A.J.*, et al.* (2012). Systemic analysis of PPARgamma in mouse macrophage populations reveals marked diversity in expression with critical roles in resolution of inflammation and airway immunity. J Immunol *189*, 2614-2624.

94. Geissmann, F., Jung, S., and Littman, D.R. (2003). Blood monocytes consist of two principal subsets with distinct migratory properties. Immunity *19*, 71-82.

95. Ginhoux, F., Greter, M., Leboeuf, M., Nandi, S., See, P., Gokhan, S., Mehler, M.F., Conway, S.J., Ng, L.G., Stanley, E.R.*, et al.* (2010). Fate mapping analysis reveals that adult microglia derive from primitive macrophages. Science *330*, 841-845.

96. Goffart, S., von Kleist-Retzow, J.C., and Wiesner, R.J. (2004). Regulation of mitochondrial proliferation in the heart: power-plant failure contributes to cardiac failure in hypertrophy. Cardiovasc Res *64*, 198-207.

97. Goldberg, E.L., and Dixit, V.D. (2015). Drivers of age-related inflammation and strategies for healthspan extension. Immunol Rev *265*, 63-74.

98. Gordon, S. (2016). Phagocytosis: An Immunobiologic Process. Immunity *44*, 463-475.

99. Gordon, S., Pluddemann, A., and Martinez Estrada, F. (2014). Macrophage heterogeneity in tissues: phenotypic diversity and functions. Immunological reviews *262*, 36-55.

100. Gosselin, D., Link, V.M., Romanoski, C.E., Fonseca, G.J., Eichenfield, D.Z., Spann, N.J., Stender, J.D., Chun, H.B., Garner, H., Geissmann, F.*, et al.* (2014). Environment drives selection and function of enhancers controlling tissue-specific macrophage identities. Cell *159*, 1327-1340.

101. Gray, E.E., and Cyster, J.G. (2012). Lymph node macrophages. Journal of innate immunity *4*, 424-436.

102. Gredilla, R., Sanz, A., Lopez-Torres, M., and Barja, G. (2001). Caloric restriction decreases mitochondrial free radical generation at complex I and lowers oxidative damage to mitochondrial DNA in the rat heart. FASEB journal : official publication of the Federation of American Societies for Experimental Biology *15*, 1589-1591.

103. Green, D.R., and Kroemer, G. (2004). The pathophysiology of mitochondrial cell death. Science *305*, 626-629.

104. Griffith, T.S., and Ferguson, T.A. (2011). Cell death in the maintenance and abrogation of tolerance: the five Ws of dying cells. Immunity *35*, 456-466.

105. Guaras, A., Perales-Clemente, E., Calvo, E., Acin-Perez, R., Loureiro-Lopez, M., Pujol, C., Martinez-Carrascoso, I., Nunez, E., Garcia-Marques, F., Rodriguez-Hernandez, M.A.*, et al.* (2016). The CoQH2/CoQ Ratio Serves as a Sensor of Respiratory Chain Efficiency. Cell reports *15*, 197-209.

106. Gupta, P., Lai, S.M., Sheng, J., Tetlak, P., Balachander, A., Claser, C., Renia, L., Karjalainen, K., and Ruedl, C. (2016). Tissue-Resident CD169(+) Macrophages Form a Crucial Front Line against Plasmodium Infection. Cell Rep *16*, 1749-1761.

107. Gyorffy, B.A., Kun, J., Torok, G., Bulyaki, E., Borhegyi, Z., Gulyassy, P., Kis, V., Szocsics, P., Micsonai, A., Matko, J.*, et al.* (2018). Local apoptotic-like mechanisms underlie complement-mediated synaptic pruning. Proc Natl Acad Sci U S A *115*, 6303-6308.

108. Han, X., Turdi, S., Hu, N., Guo, R., Zhang, Y., and Ren, J. (2012). Influence of long-term caloric restriction on myocardial and cardiomyocyte contractile function and autophagy in mice. J Nutr Biochem *23*, 1592-1599.

109. Hanayama, R., Tanaka, M., Miyasaka, K., Aozasa, K., Koike, M., Uchiyama, Y., and Nagata, S. (2004). Autoimmune disease and impaired uptake of apoptotic cells in MFG-E8-deficient mice. Science *304*, 1147-1150.

110. Hariharan, N., Zhai, P., and Sadoshima, J. (2011). Oxidative stress stimulates autophagic flux during ischemia/reperfusion. Antioxid Redox Signal *14*, 2179-2190.

111. Harrison, D.E., Strong, R., Sharp, Z.D., Nelson, J.F., Astle, C.M., Flurkey, K., Nadon, N.L., Wilkinson, J.E., Frenkel, K., Carter, C.S.*, et al.* (2009). Rapamycin fed late in life extends lifespan in genetically heterogeneous mice. Nature *460*, 392-395.

112. Hashimoto, D., Chow, A., Noizat, C., Teo, P., Beasley, M.B., Leboeuf, M., Becker, C.D., See, P., Price, J., Lucas, D.*, et al.* (2013). Tissue-resident macrophages self-maintain locally throughout adult life with minimal contribution from circulating monocytes. Immunity *38*, 792-804.

113. Hashimoto, D., Miller, J., and Merad, M. (2011). Dendritic cell and macrophage heterogeneity in vivo. Immunity *35*, 323-335.

114. Hayakawa, K., Esposito, E., Wang, X., Terasaki, Y., Liu, Y., Xing, C., Ji, X., and Lo, E.H. (2016). Transfer of mitochondria from astrocytes to neurons after stroke. Nature *535*, 551-555.

115. Heidt, T., Courties, G., Dutta, P., Sager, H.B., Sebas, M., Iwamoto, Y., Sun, Y., Da Silva, N., Panizzi, P., van der Laan, A.M.*, et al.* (2014). Differential contribution of monocytes to heart macrophages in steady-state and after myocardial infarction. Circ Res *115*, 284-295.

116. Henson, P.M., and Hume, D.A. (2006). Apoptotic cell removal in development and tissue homeostasis. Trends Immunol *27*, 244-250.

117. Herbers, E., Kekalainen, N.J., Hangas, A., Pohjoismaki, J.L., and Goffart, S. (2019). Tissue specific differences in mitochondrial DNA maintenance and expression. Mitochondrion *44*, 85-92.

118. Hochreiter-Hufford, A., and Ravichandran, K.S. (2013). Clearing the dead: apoptotic cell sensing, recognition, engulfment, and digestion. Cold Spring Harbor perspectives in biology *5*, a008748.

119. Hoeffel, G., and Ginhoux, F. (2018). Fetal monocytes and the origins of tissue-resident macrophages. Cell Immunol *330*, 5-15.

120. Hoeffel, G., Wang, Y., Greter, M., See, P., Teo, P., Malleret, B., Leboeuf, M., Low, D., Oller, G., Almeida, F.*, et al.* (2012). Adult Langerhans cells derive predominantly from embryonic fetal liver monocytes with a minor contribution of yolk sac-derived macrophages. J Exp Med *209*, 1167-1181.

121. Hoeksema, M.A., and Glass, C.K. (2019). Nature and nurture of tissue-specific macrophage phenotypes. Atherosclerosis *281*, 159-167.

122. Howangyin, K.Y., Zlatanova, I., Pinto, C., Ngkelo, A., Cochain, C., Rouanet, M., Vilar, J., Lemitre, M., Stockmann, C., Fleischmann, B.K.*, et al.* (2016). Myeloid-Epithelial-Reproductive Receptor Tyrosine Kinase and Milk Fat Globule Epidermal Growth Factor 8 Coordinately Improve Remodeling After Myocardial Infarction via Local Delivery of Vascular Endothelial Growth Factor. Circulation *133*, 826-839.

123. Hua, Y., Zhang, Y., Ceylan-Isik, A.F., Wold, L.E., Nunn, J.M., and Ren, J. (2011). Chronic Akt activation accentuates aging-induced cardiac hypertrophy and myocardial contractile dysfunction: role of autophagy. Basic Res Cardiol *106*, 1173-1191.

124. Hue, L., and Taegtmeyer, H. (2009). The Randle cycle revisited: a new head for an old hat. Am J Physiol Endocrinol Metab *297*, E578-591.

125. Hulsmans, M., Clauss, S., Xiao, L., Aguirre, A.D., King, K.R., Hanley, A., Hucker, W.J., Wulfers, E.M., Seemann, G., Courties, G.*, et al.* (2017). Macrophages Facilitate Electrical Conduction in the Heart. Cell *169*, 510-522 e520.

126. Huynh, M.L., Fadok, V.A., and Henson, P.M. (2002). Phosphatidylserine-dependent ingestion of apoptotic cells promotes TGF-beta1 secretion and the resolution of inflammation. The Journal of clinical investigation *109*, 41-50.

127. Ikeda, Y., Sciarretta, S., Nagarajan, N., Rubattu, S., Volpe, M., Frati, G., and Sadoshima, J. (2014). New insights into the role of mitochondrial dynamics and autophagy during oxidative stress and aging in the heart. Oxid Med Cell Longev *2014*, 210934.

128. Ikeda, Y., Shirakabe, A., Maejima, Y., Zhai, P., Sciarretta, S., Toli, J., Nomura, M., Mihara, K., Egashira, K., Ohishi, M.*, et al.* (2015). Endogenous Drp1 mediates mitochondrial autophagy and protects the heart against energy stress. Circ Res *116*, 264-278.

129. Islam, M.N., Das, S.R., Emin, M.T., Wei, M., Sun, L., Westphalen, K., Rowlands, D.J., Quadri, S.K., Bhattacharya, S., and Bhattacharya, J. (2012). Mitochondrial transfer from

bone-marrow-derived stromal cells to pulmonary alveoli protects against acute lung injury. Nature medicine *18*, 759-765.

130. Janeway, C. (2005). Immunobiology : the immune system in health and disease, 6th edn (New York, Garland Science).
131. Janeway, C.A., Jr. (1989). Approaching the asymptote? Evolution and revolution in immunology. Cold Spring Harbor symposia on quantitative biology *54 Pt 1*, 1-13.
132. Joza, N., Susin, S.A., Daugas, E., Stanford, W.L., Cho, S.K., Li, C.Y., Sasaki, T., Elia, A.J., Cheng, H.Y., Ravagnan, L.*, et al.* (2001). Essential role of the mitochondrial apoptosis-inducing factor in programmed cell death. Nature *410*, 549-554.
133. Judge, S., Jang, Y.M., Smith, A., Hagen, T., and Leeuwenburgh, C. (2005). Age-associated increases in oxidative stress and antioxidant enzyme activities in cardiac interfibrillar mitochondria: implications for the mitochondrial theory of aging. FASEB journal : official publication of the Federation of American Societies for Experimental Biology *19*, 419-421.
134. Jung, S., Aliberti, J., Graemmel, P., Sunshine, M.J., Kreutzberg, G.W., Sher, A., and Littman, D.R. (2000). Analysis of fractalkine receptor CX(3)CR1 function by targeted deletion and green fluorescent protein reporter gene insertion. Mol Cell Biol *20*, 4106-4114.
135. Katayama, H., Kogure, T., Mizushima, N., Yoshimori, T., and Miyawaki, A. (2011). A sensitive and quantitative technique for detecting autophagic events based on lysosomal delivery. Chem Biol *18*, 1042-1052.
136. Kaufman, J. (2010). Evolution and immunity. Immunology *130*, 459-462.
137. Khaidakov, M., Heflich, R.H., Manjanatha, M.G., Myers, M.B., and Aidoo, A. (2003). Accumulation of point mutations in mitochondrial DNA of aging mice. Mutat Res *526*, 1-7.
138. Kierdorf, K., Erny, D., Goldmann, T., Sander, V., Schulz, C., Perdiguero, E.G., Wieghofer, P., Heinrich, A., Riemke, P., Holscher, C.*, et al.* (2013). Microglia emerge from erythromyeloid precursors via Pu.1- and Irf8-dependent pathways. Nature neuroscience *16*, 273-280.
139. Kim, I., Rodriguez-Enriquez, S., and Lemasters, J.J. (2007). Selective degradation of mitochondria by mitophagy. Arch Biochem Biophys *462*, 245-253.
140. Kim, J.Y., Zhao, H., Martinez, J., Doggett, T.A., Kolesnikov, A.V., Tang, P.H., Ablonczy, Z., Chan, C.C., Zhou, Z., Green, D.R.*, et al.* (2013). Noncanonical autophagy promotes the visual cycle. Cell *154*, 365-376.
141. Kingsley, P.D., Malik, J., Fantauzzo, K.A., and Palis, J. (2004). Yolk sac-derived primitive erythroblasts enucleate during mammalian embryogenesis. Blood *104*, 19-25.
142. Klein, I., Cornejo, J.C., Polakos, N.K., John, B., Wuensch, S.A., Topham, D.J., Pierce, R.H., and Crispe, I.N. (2007). Kupffer cell heterogeneity: functional properties of bone marrow derived and sessile hepatic macrophages. Blood *110*, 4077-4085.
143. Klionsky, D.J., Abdelmohsen, K., Abe, A., Abedin, M.J., Abeliovich, H., Acevedo Arozena, A., Adachi, H., Adams, C.M., Adams, P.D., Adeli, K.*, et al.* (2016). Guidelines for the use and interpretation of assays for monitoring autophagy (3rd edition). Autophagy *12*, 1-222.
144. Kohyama, M., Ise, W., Edelson, B.T., Wilker, P.R., Hildner, K., Mejia, C., Frazier, W.A., Murphy, T.L., and Murphy, K.M. (2009). Role for Spi-C in the development of red pulp macrophages and splenic iron homeostasis. Nature *457*, 318-321.
145. Komatsu, M., Waguri, S., Ueno, T., Iwata, J., Murata, S., Tanida, I., Ezaki, J., Mizushima, N., Ohsumi, Y., Uchiyama, Y.*, et al.* (2005). Impairment of starvation-induced and constitutive autophagy in Atg7-deficient mice. The Journal of cell biology *169*, 425-434.

146. Kosmider, B., Messier, E.M., Janssen, W.J., Nahreini, P., Wang, J., Hartshorn, K.L., and Mason, R.J. (2012). Nrf2 protects human alveolar epithelial cells against injury induced by influenza A virus. Respir Res *13*, 43.

147. Krombach, F., Munzing, S., Allmeling, A.M., Gerlach, J.T., Behr, J., and Dorger, M. (1997). Cell size of alveolar macrophages: an interspecies comparison. Environ Health Perspect *105 Suppl 5*, 1261-1263.

148. Krysko, D.V., Agostinis, P., Krysko, O., Garg, A.D., Bachert, C., Lambrecht, B.N., and Vandenabeele, P. (2011). Emerging role of damage-associated molecular patterns derived from mitochondria in inflammation. Trends Immunol *32*, 157-164.

149. Lapenna, A., De Palma, M., and Lewis, C.E. (2018). Perivascular macrophages in health and disease. Nature reviews Immunology *18*, 689-702.

150. Lapuente-Brun, E., Moreno-Loshuertos, R., Acin-Perez, R., Latorre-Pellicer, A., Colas, C., Balsa, E., Perales-Clemente, E., Quiros, P.M., Calvo, E., Rodriguez-Hernandez, M.A.*, et al.* (2013). Supercomplex assembly determines electron flux in the mitochondrial electron transport chain. Science *340*, 1567-1570.

151. Latorre-Pellicer, A., Moreno-Loshuertos, R., Lechuga-Vieco, A.V., Sanchez-Cabo, F., Torroja, C., Acin-Perez, R., Calvo, E., Aix, E., Gonzalez-Guerra, A., Logan, A.*, et al.* (2016). Mitochondrial and nuclear DNA matching shapes metabolism and healthy ageing. Nature *535*, 561-565.

152. Lavine, K.J., Epelman, S., Uchida, K., Weber, K.J., Nichols, C.G., Schilling, J.D., Ornitz, D.M., Randolph, G.J., and Mann, D.L. (2014). Distinct macrophage lineages contribute to disparate patterns of cardiac recovery and remodeling in the neonatal and adult heart. Proc Natl Acad Sci U S A *111*, 16029-16034.

153. Leid, J., Carrelha, J., Boukarabila, H., Epelman, S., Jacobsen, S.E., and Lavine, K.J. (2016). Primitive Embryonic Macrophages are Required for Coronary Development and Maturation. Circ Res *118*, 1498-1511.

154. Lemke, G. (2013). Biology of the TAM receptors. Cold Spring Harbor perspectives in biology *5*, a009076.

155. Levine, B., and Kroemer, G. (2008). Autophagy in the pathogenesis of disease. Cell *132*, 27-42.

156. Li-Harms, X., Milasta, S., Lynch, J., Wright, C., Joshi, A., Iyengar, R., Neale, G., Wang, X., Wang, Y.D., Prolla, T.A.*, et al.* (2015). Mito-protective autophagy is impaired in erythroid cells of aged mtDNA-mutator mice. Blood *125*, 162-174.

157. Li, Y., Ma, Y., Song, L., Yu, L., Zhang, L., Zhang, Y., Xing, Y., Yin, Y., and Ma, H. (2018). SIRT3 deficiency exacerbates p53/Parkinmediated mitophagy inhibition and promotes mitochondrial dysfunction: Implication for aged hearts. Int J Mol Med *41*, 3517-3526.

158. Linehan, E., Dombrowski, Y., Snoddy, R., Fallon, P.G., Kissenpfennig, A., and Fitzgerald, D.C. (2014). Aging impairs peritoneal but not bone marrow-derived macrophage phagocytosis. Aging Cell *13*, 699-708.

159. Linton, P.J., Gurney, M., Sengstock, D., Mentzer, R.M., Jr., and Gottlieb, R.A. (2015). This old heart: Cardiac aging and autophagy. J Mol Cell Cardiol *83*, 44-54.

160. Little, J.P., Simtchouk, S., Schindler, S.M., Villanueva, E.B., Gill, N.E., Walker, D.G., Wolthers, K.R., and Klegeris, A. (2014). Mitochondrial transcription factor A (Tfam) is a pro-inflammatory extracellular signaling molecule recognized by brain microglia. Mol Cell Neurosci *60*, 88-96.

161. London, A., Cohen, M., and Schwartz, M. (2013). Microglia and monocyte-derived macrophages: functionally distinct populations that act in concert in CNS plasticity and repair. Frontiers in cellular neuroscience *7*, 34.

162. Lopaschuk, G.D., and Jaswal, J.S. (2010). Energy metabolic phenotype of the cardiomyocyte during development, differentiation, and postnatal maturation. J Cardiovasc Pharmacol *56*, 130-140.

163. Lopaschuk, G.D., and Ussher, J.R. (2016). Evolving Concepts of Myocardial Energy Metabolism: More Than Just Fats and Carbohydrates. Circ Res *119*, 1173-1176.

164. Lu, Q., Gore, M., Zhang, Q., Camenisch, T., Boast, S., Casagranda, F., Lai, C., Skinner, M.K., Klein, R., Matsushima, G.K., *et al.* (1999). Tyro-3 family receptors are essential regulators of mammalian spermatogenesis. Nature *398*, 723-728.

165. Maas, S.L.N., Breakefield, X.O., and Weaver, A.M. (2017). Extracellular Vesicles: Unique Intercellular Delivery Vehicles. Trends Cell Biol *27*, 172-188.

166. MacLennan, I.C. (1994). Germinal centers. Annual review of immunology *12*, 117-139.

167. Madisen, L., Zwingman, T.A., Sunkin, S.M., Oh, S.W., Zariwala, H.A., Gu, H., Ng, L.L., Palmiter, R.D., Hawrylycz, M.J., Jones, A.R., *et al.* (2010). A robust and high-throughput Cre reporting and characterization system for the whole mouse brain. Nature neuroscience *13*, 133-140.

168. Maeda, H., Gleiser, C.A., Masoro, E.J., Murata, I., McMahan, C.A., and Yu, B.P. (1985). Nutritional influences on aging of Fischer 344 rats: II. Pathology. J Gerontol *40*, 671-688.

169. Mai, S., Klinkenberg, M., Auburger, G., Bereiter-Hahn, J., and Jendrach, M. (2010). Decreased expression of Drp1 and Fis1 mediates mitochondrial elongation in senescent cells and enhances resistance to oxidative stress through PINK1. J Cell Sci *123*, 917-926.

170. Martin, C.J., Booty, M.G., Rosebrock, T.R., Nunes-Alves, C., Desjardins, D.M., Keren, I., Fortune, S.M., Remold, H.G., and Behar, S.M. (2012). Efferocytosis is an innate antibacterial mechanism. Cell Host Microbe *12*, 289-300.

171. Martinez-Bartolome, S., Navarro, P., Martin-Maroto, F., Lopez-Ferrer, D., Ramos-Fernandez, A., Villar, M., Garcia-Ruiz, J.P., and Vazquez, J. (2008). Properties of average score distributions of SEQUEST: the probability ratio method. Mol Cell Proteomics *7*, 1135-1145.

172. Mechnikov, I.I. (1892). Leçons sur la Pathologie Comparée de l´Inflammation. In Masson Paris.

173. Medzhitov, R. (2008). Origin and physiological roles of inflammation. Nature *454*, 428-435.

174. Melentijevic, I., Toth, M.L., Arnold, M.L., Guasp, R.J., Harinath, G., Nguyen, K.C., Taub, D., Parker, J.A., Neri, C., Gabel, C.V., *et al.* (2017). C. elegans neurons jettison protein aggregates and mitochondria under neurotoxic stress. Nature *542*, 367-371.

175. Miyake, Y., Asano, K., Kaise, H., Uemura, M., Nakayama, M., and Tanaka, M. (2007). Critical role of macrophages in the marginal zone in the suppression of immune responses to apoptotic cell-associated antigens. The Journal of clinical investigation *117*, 2268-2278.

176. Miyanishi, M., Tada, K., Koike, M., Uchiyama, Y., Kitamura, T., and Nagata, S. (2007). Identification of Tim4 as a phosphatidylserine receptor. Nature *450*, 435-439.

177. Mizushima, N., Yamamoto, A., Matsui, M., Yoshimori, T., and Ohsumi, Y. (2004). In vivo analysis of autophagy in response to nutrient starvation using transgenic mice expressing a fluorescent autophagosome marker. Mol Biol Cell *15*, 1101-1111.

178. Molawi, K., Wolf, Y., Kandalla, P.K., Favret, J., Hagemeyer, N., Frenzel, K., Pinto, A.R., Klapproth, K., Henri, S., Malissen, B., *et al.* (2014). Progressive replacement of embryo-derived cardiac macrophages with age. J Exp Med *211*, 2151-2158.

179. Moschoi, R., Imbert, V., Nebout, M., Chiche, J., Mary, D., Prebet, T., Saland, E., Castellano, R., Pouyet, L., Collette, Y., *et al.* (2016). Protective mitochondrial transfer from bone marrow stromal cells to acute myeloid leukemic cells during chemotherapy. Blood *128*, 253-264.

180. Mozaffarian, D., Benjamin, E.J., Go, A.S., Arnett, D.K., Blaha, M.J., Cushman, M., Das, S.R., de Ferranti, S., Despres, J.P., Fullerton, H.J., *et al.* (2016). Heart Disease and Stroke Statistics-2016 Update: A Report From the American Heart Association. Circulation *133*, e38-360.

181. Mukundan, L., Odegaard, J.I., Morel, C.R., Heredia, J.E., Mwangi, J.W., Ricardo-Gonzalez, R.R., Goh, Y.P., Eagle, A.R., Dunn, S.E., Awakuni, J.U., *et al.* (2009). PPAR-delta senses and orchestrates clearance of apoptotic cells to promote tolerance. Nature medicine *15*, 1266-1272.

182. Murray, P.J., and Wynn, T.A. (2011). Protective and pathogenic functions of macrophage subsets. Nature reviews Immunology *11*, 723-737.

183. Mylonas, K.J., Jenkins, S.J., Castellan, R.F., Ruckerl, D., McGregor, K., Phythian-Adams, A.T., Hewitson, J.P., Campbell, S.M., MacDonald, A.S., Allen, J.E., *et al.* (2015). The adult murine heart has a sparse, phagocytically active macrophage population that expands through monocyte recruitment and adopts an 'M2' phenotype in response to Th2 immunologic challenge. Immunobiology *220*, 924-933.

184. Nagata, S. (2007). Autoimmune diseases caused by defects in clearing dead cells and nuclei expelled from erythroid precursors. Immunological reviews *220*, 237-250.

185. Nahrendorf, M., and Swirski, F.K. (2013). Monocyte and macrophage heterogeneity in the heart. Circ Res *112*, 1624-1633.

186. Nahrendorf, M., Swirski, F.K., Aikawa, E., Stangenberg, L., Wurdinger, T., Figueiredo, J.L., Libby, P., Weissleder, R., and Pittet, M.J. (2007). The healing myocardium sequentially mobilizes two monocyte subsets with divergent and complementary functions. J Exp Med *204*, 3037-3047.

187. Nakahira, K., Haspel, J.A., Rathinam, V.A., Lee, S.J., Dolinay, T., Lam, H.C., Englert, J.A., Rabinovitch, M., Cernadas, M., Kim, H.P., *et al.* (2011). Autophagy proteins regulate innate immune responses by inhibiting the release of mitochondrial DNA mediated by the NALP3 inflammasome. Nature immunology *12*, 222-230.

188. Nakai, A., Yamaguchi, O., Takeda, T., Higuchi, Y., Hikoso, S., Taniike, M., Omiya, S., Mizote, I., Matsumura, Y., Asahi, M., *et al.* (2007). The role of autophagy in cardiomyocytes in the basal state and in response to hemodynamic stress. Nature medicine *13*, 619-624.

189. Nandrot, E., Dufour, E.M., Provost, A.C., Pequignot, M.O., Bonnel, S., Gogat, K., Marchant, D., Rouillac, C., Sepulchre de Conde, B., Bihoreau, M.T., *et al.* (2000). Homozygous deletion in the coding sequence of the c-mer gene in RCS rats unravels general mechanisms of physiological cell adhesion and apoptosis. Neurobiol Dis *7*, 586-599.

190. Nathan, C., and Ding, A. (2010). Nonresolving inflammation. Cell *140*, 871-882.

191. Navarro, P., Trevisan-Herraz, M., Bonzon-Kulichenko, E., Nunez, E., Martinez-Acedo, P., Perez-Hernandez, D., Jorge, I., Mesa, R., Calvo, E., Carrascal, M., *et al.* (2014). General statistical framework for quantitative proteomics by stable isotope labeling. J Proteome Res *13*, 1234-1247.

192. Neubauer, S. (2007). The failing heart--an engine out of fuel. N Engl J Med *356*, 1140-1151.

193. Nguyen, K.D., Qiu, Y., Cui, X., Goh, Y.P., Mwangi, J., David, T., Mukundan, L., Brombacher, F., Locksley, R.M., and Chawla, A. (2011). Alternatively activated

macrophages produce catecholamines to sustain adaptive thermogenesis. Nature *480*, 104-108.

194. Nicolas-Avila, J.A., Adrover, J.M., and Hidalgo, A. (2017). Neutrophils in Homeostasis, Immunity, and Cancer. Immunity *46*, 15-28.
195. Nicolas-Avila, J.A., Hidalgo, A., and Ballesteros, I. (2018). Specialized functions of resident macrophages in brain and heart. J Leukoc Biol *104*, 743-756.
196. Niemann, B., Chen, Y., Issa, H., Silber, R.E., and Rohrbach, S. (2010). Caloric restriction delays cardiac ageing in rats: role of mitochondria. Cardiovasc Res *88*, 267-276.
197. Notley, C.A., Brown, M.A., McGovern, J.L., Jordan, C.K., and Ehrenstein, M.R. (2015). Engulfment of activated apoptotic cells abolishes TGF-beta-mediated immunoregulation via the induction of IL-6. Journal of immunology *194*, 1621-1627.
198. Odegaard, J.I., and Chawla, A. (2008). Mechanisms of macrophage activation in obesity-induced insulin resistance. Nature clinical practice Endocrinology & metabolism *4*, 619-626.
199. Odegaard, J.I., Ricardo-Gonzalez, R.R., Goforth, M.H., Morel, C.R., Subramanian, V., Mukundan, L., Red Eagle, A., Vats, D., Brombacher, F., Ferrante, A.W.*, et al.* (2007). Macrophage-specific PPARgamma controls alternative activation and improves insulin resistance. Nature *447*, 1116-1120.
200. Oka, T., Hikoso, S., Yamaguchi, O., Taneike, M., Takeda, T., Tamai, T., Oyabu, J., Murakawa, T., Nakayama, H., Nishida, K.*, et al.* (2012). Mitochondrial DNA that escapes from autophagy causes inflammation and heart failure. Nature *485*, 251-255.
201. Oka, T., Maillet, M., Watt, A.J., Schwartz, R.J., Aronow, B.J., Duncan, S.A., and Molkentin, J.D. (2006). Cardiac-specific deletion of Gata4 reveals its requirement for hypertrophy, compensation, and myocyte viability. Circ Res *98*, 837-845.
202. Ovchinnikov, D.A. (2008). Macrophages in the embryo and beyond: much more than just giant phagocytes. Genesis *46*, 447-462.
203. Pacher, P., Nagayama, T., Mukhopadhyay, P., Batkai, S., and Kass, D.A. (2008). Measurement of cardiac function using pressure-volume conductance catheter technique in mice and rats. Nat Protoc *3*, 1422-1434.
204. Paolicelli, R.C., Bolasco, G., Pagani, F., Maggi, L., Scianni, M., Panzanelli, P., Giustetto, M., Ferreira, T.A., Guiducci, E., Dumas, L.*, et al.* (2011). Synaptic pruning by microglia is necessary for normal brain development. Science *333*, 1456-1458.
205. Pavillard, L.E., Canadas-Lozano, D., Alcocer-Gomez, E., Marin-Aguilar, F., Pereira, S., Robertson, A.A.B., Muntane, J., Ryffel, B., Cooper, M.A., Quiles, J.L.*, et al.* (2017). NLRP3-inflammasome inhibition prevents high fat and high sugar diets-induced heart damage through autophagy induction. Oncotarget *8*, 99740-99756.
206. Perdiguero, E.G., Klapproth, K., Schulz, C., Busch, K., de Bruijn, M., Rodewald, H.R., and Geissmann, F. (2015). The Origin of Tissue-Resident Macrophages: When an Erythro-myeloid Progenitor Is an Erythro-myeloid Progenitor. Immunity *43*, 1023-1024.
207. Perez, V.I., Bokov, A., Van Remmen, H., Mele, J., Ran, Q., Ikeno, Y., and Richardson, A. (2009). Is the oxidative stress theory of aging dead? Biochim Biophys Acta *1790*, 1005-1014.
208. Phinney, D.G., Di Giuseppe, M., Njah, J., Sala, E., Shiva, S., St Croix, C.M., Stolz, D.B., Watkins, S.C., Di, Y.P., Leikauf, G.D.*, et al.* (2015). Mesenchymal stem cells use extracellular vesicles to outsource mitophagy and shuttle microRNAs. Nat Commun *6*, 8472.

209. Picca, A., Lezza, A.M.S., Leeuwenburgh, C., Pesce, V., Calvani, R., Landi, F., Bernabei, R., and Marzetti, E. (2017). Fueling Inflamm-Aging through Mitochondrial Dysfunction: Mechanisms and Molecular Targets. Int J Mol Sci *18*.

210. Piko, L., Hougham, A.J., and Bulpitt, K.J. (1988). Studies of sequence heterogeneity of mitochondrial DNA from rat and mouse tissues: evidence for an increased frequency of deletions/additions with aging. Mech Ageing Dev *43*, 279-293.

211. Pillay, J., den Braber, I., Vrisekoop, N., Kwast, L.M., de Boer, R.J., Borghans, J.A., Tesselaar, K., and Koenderman, L. (2010). In vivo labeling with 2H2O reveals a human neutrophil lifespan of 5.4 days. Blood *116*, 625-627.

212. Pinto, A.R., Godwin, J.W., Chandran, A., Hersey, L., Ilinykh, A., Debuque, R., Wang, L., and Rosenthal, N.A. (2014). Age-related changes in tissue macrophages precede cardiac functional impairment. Aging (Albany NY) *6*, 399-413.

213. Pinto, A.R., Ilinykh, A., Ivey, M.J., Kuwabara, J.T., D'Antoni, M.L., Debuque, R., Chandran, A., Wang, L., Arora, K., Rosenthal, N.A*., et al.* (2016). Revisiting Cardiac Cellular Composition. Circ Res *118*, 400-409.

214. Pinto, A.R., Paolicelli, R., Salimova, E., Gospocic, J., Slonimsky, E., Bilbao-Cortes, D., Godwin, J.W., and Rosenthal, N.A. (2012). An abundant tissue macrophage population in the adult murine heart with a distinct alternatively-activated macrophage profile. PLoS One *7*, e36814.

215. Piquereau, J., and Ventura-Clapier, R. (2018). Maturation of Cardiac Energy Metabolism During Perinatal Development. Front Physiol *9*, 959.

216. Pollard, J.W. (2009). Trophic macrophages in development and disease. Nature reviews Immunology *9*, 259-270.

217. Ponpuak, M., Mandell, M.A., Kimura, T., Chauhan, S., Cleyrat, C., and Deretic, V. (2015). Secretory autophagy. Curr Opin Cell Biol *35*, 106-116.

218. Pyo, J.O., Yoo, S.M., Ahn, H.H., Nah, J., Hong, S.H., Kam, T.I., Jung, S., and Jung, Y.K. (2013). Overexpression of Atg5 in mice activates autophagy and extends lifespan. Nat Commun *4*, 2300.

219. Quiros, P.M., Ramsay, A.J., Sala, D., Fernandez-Vizarra, E., Rodriguez, F., Peinado, J.R., Fernandez-Garcia, M.S., Vega, J.A., Enriquez, J.A., Zorzano, A*., et al.* (2012). Loss of mitochondrial protease OMA1 alters processing of the GTPase OPA1 and causes obesity and defective thermogenesis in mice. Embo J *31*, 2117-2133.

220. Rawji, K.S., Mishra, M.K., Michaels, N.J., Rivest, S., Stys, P.K., and Yong, V.W. (2016). Immunosenescence of microglia and macrophages: impact on the ageing central nervous system. Brain *139*, 653-661.

221. Reynolds, E.S. (1963). The use of lead citrate at high pH as an electron-opaque stain in electron microscopy. The Journal of cell biology *17*, 208-212.

222. Ritchie, M.E., Phipson, B., Wu, D., Hu, Y., Law, C.W., Shi, W., and Smyth, G.K. (2015). limma powers differential expression analyses for RNA-sequencing and microarray studies. Nucleic Acids Res *43*, e47.

223. Rodriguez, A.M., Nakhle, J., Griessinger, E., and Vignais, M.L. (2018). Intercellular mitochondria trafficking highlighting the dual role of mesenchymal stem cells as both sensors and rescuers of tissue injury. Cell Cycle *17*, 712-721.

224. Rosales, C., and Uribe-Querol, E. (2017). Phagocytosis: A Fundamental Process in Immunity. Biomed Res Int *2017*, 9042851.

225. Roszer, T., Menendez-Gutierrez, M.P., Lefterova, M.I., Alameda, D., Nunez, V., Lazar, M.A., Fischer, T., and Ricote, M. (2011). Autoimmune kidney disease and impaired engulfment of apoptotic cells in mice with macrophage peroxisome proliferator-activated receptor gamma or retinoid X receptor alpha deficiency. Journal of immunology *186*, 621-631.

226. Rothlin, C.V., Carrera-Silva, E.A., Bosurgi, L., and Ghosh, S. (2015). TAM receptor signaling in immune homeostasis. Annual review of immunology *33*, 355-391.

227. Rubinsztein, D.C., Marino, G., and Kroemer, G. (2011). Autophagy and aging. Cell *146*, 682-695.

228. Ruggiero, L., Connor, M.P., Chen, J., Langen, R., and Finnemann, S.C. (2012). Diurnal, localized exposure of phosphatidylserine by rod outer segment tips in wild-type but not Itgb5-/- or Mfge8-/- mouse retina. Proc Natl Acad Sci U S A *109*, 8145-8148.

229. Saddik, M., and Lopaschuk, G.D. (1991). Myocardial triglyceride turnover and contribution to energy substrate utilization in isolated working rat hearts. J Biol Chem *266*, 8162-8170.

230. Saelens, X., Festjens, N., Vande Walle, L., van Gurp, M., van Loo, G., and Vandenabeele, P. (2004). Toxic proteins released from mitochondria in cell death. Oncogene *23*, 2861-2874.

231. Salminen, A., Kaarniranta, K., and Kauppinen, A. (2012). Inflammaging: disturbed interplay between autophagy and inflammasomes. Aging (Albany NY) *4*, 166-175.

232. Sato, M., and Sato, K. (2011). Degradation of paternal mitochondria by fertilization-triggered autophagy in C. elegans embryos. Science *334*, 1141-1144.

233. Schaper, J., Meiser, E., and Stammler, G. (1985). Ultrastructural morphometric analysis of myocardium from dogs, rats, hamsters, mice, and from human hearts. Circulation research *56*, 377-391.

234. Scherz-Shouval, R., Shvets, E., Fass, E., Shorer, H., Gil, L., and Elazar, Z. (2007). Reactive oxygen species are essential for autophagy and specifically regulate the activity of Atg4. Embo J *26*, 1749-1760.

235. Schiwon, M., Weisheit, C., Franken, L., Gutweiler, S., Dixit, A., Meyer-Schwesinger, C., Pohl, J.M., Maurice, N.J., Thiebes, S., Lorenz, K.*, et al.* (2014). Crosstalk between sentinel and helper macrophages permits neutrophil migration into infected uroepithelium. Cell *156*, 456-468.

236. Schulz, C., Gomez Perdiguero, E., Chorro, L., Szabo-Rogers, H., Cagnard, N., Kierdorf, K., Prinz, M., Wu, B., Jacobsen, S.E., Pollard, J.W.*, et al.* (2012). A lineage of myeloid cells independent of Myb and hematopoietic stem cells. Science *336*, 86-90.

237. Sciarretta, S., Zhai, P., Shao, D., Zablocki, D., Nagarajan, N., Terada, L.S., Volpe, M., and Sadoshima, J. (2013). Activation of NADPH oxidase 4 in the endoplasmic reticulum promotes cardiomyocyte autophagy and survival during energy stress through the protein kinase RNA-activated-like endoplasmic reticulum kinase/eukaryotic initiation factor 2alpha/activating transcription factor 4 pathway. Circ Res *113*, 1253-1264.

238. Scott, R.S., McMahon, E.J., Pop, S.M., Reap, E.A., Caricchio, R., Cohen, P.L., Earp, H.S., and Matsushima, G.K. (2001). Phagocytosis and clearance of apoptotic cells is mediated by MER. Nature *411*, 207-211.

239. Sebastian, D., Sorianello, E., Segales, J., Irazoki, A., Ruiz-Bonilla, V., Sala, D., Planet, E., Berenguer-Llergo, A., Munoz, J.P., Sanchez-Feutrie, M.*, et al.* (2016). Mfn2 deficiency links age-related sarcopenia and impaired autophagy to activation of an adaptive mitophagy pathway. Embo J *35*, 1677-1693.

240. Senyo, S.E., Lee, R.T., and Kuhn, B. (2014). Cardiac regeneration based on mechanisms of cardiomyocyte proliferation and differentiation. Stem Cell Res *13*, 532-541.

241. Serhan, C.N., Chiang, N., and Van Dyke, T.E. (2008). Resolving inflammation: dual anti-inflammatory and pro-resolution lipid mediators. Nature reviews Immunology *8*, 349-361.

242. Settembre, C., Fraldi, A., Medina, D.L., and Ballabio, A. (2013). Signals from the lysosome: a control centre for cellular clearance and energy metabolism. Nat Rev Mol Cell Biol *14*, 283-296.

243. Seveau, S., Turner, J., Gavrilin, M.A., Torrelles, J.B., Hall-Stoodley, L., Yount, J.S., and Amer, A.O. (2018). Checks and Balances between Autophagy and Inflammasomes during Infection. J Mol Biol *430*, 174-192.

244. Shigeta, A., Huang, V., Zuo, J., Besada, R., Nakashima, Y., Lu, Y., Ding, Y., Pellegrini, M., Kulkarni, R.P., Hsiai, T.*, et al.* (2019). Endocardially Derived Macrophages Are Essential for Valvular Remodeling. Dev Cell *48*, 617-630 e613.

245. Shimada, K., Crother, T.R., Karlin, J., Dagvadorj, J., Chiba, N., Chen, S., Ramanujan, V.K., Wolf, A.J., Vergnes, L., Ojcius, D.M.*, et al.* (2012). Oxidized mitochondrial DNA activates the NLRP3 inflammasome during apoptosis. Immunity *36*, 401-414.

246. Shinmura, K., Tamaki, K., Sano, M., Murata, M., Yamakawa, H., Ishida, H., and Fukuda, K. (2011). Impact of long-term caloric restriction on cardiac senescence: caloric restriction ameliorates cardiac diastolic dysfunction associated with aging. J Mol Cell Cardiol *50*, 117-127.

247. Shirakabe, A., Ikeda, Y., Sciarretta, S., Zablocki, D.K., and Sadoshima, J. (2016). Aging and Autophagy in the Heart. Circulation research *118*, 1563-1576.

248. Singh, R., and Cuervo, A.M. (2011). Autophagy in the cellular energetic balance. Cell Metab *13*, 495-504.

249. Skelly, D.A., Squiers, G.T., McLellan, M.A., Bolisetty, M.T., Robson, P., Rosenthal, N.A., and Pinto, A.R. (2018). Single-Cell Transcriptional Profiling Reveals Cellular Diversity and Intercommunication in the Mouse Heart. Cell Rep *22*, 600-610.

250. Smyth, G.K. (2004). Linear models and empirical bayes methods for assessing differential expression in microarray experiments. Statistical applications in genetics and molecular biology *3*, Article3.

251. Soehnlein, O., and Lindbom, L. (2010). Phagocyte partnership during the onset and resolution of inflammation. Nature reviews Immunology *10*, 427-439.

252. Sohal, D.S., Nghiem, M., Crackower, M.A., Witt, S.A., Kimball, T.R., Tymitz, K.M., Penninger, J.M., and Molkentin, J.D. (2001). Temporally regulated and tissue-specific gene manipulations in the adult and embryonic heart using a tamoxifen-inducible Cre protein. Circ Res *89*, 20-25.

253. Song, M., Chen, Y., Gong, G., Murphy, E., Rabinovitch, P.S., and Dorn, G.W., 2nd (2014). Super-suppression of mitochondrial reactive oxygen species signaling impairs compensatory autophagy in primary mitophagic cardiomyopathy. Circulation research *115*, 348-353.

254. Soni, S., Bala, S., Gwynn, B., Sahr, K.E., Peters, L.L., and Hanspal, M. (2006). Absence of erythroblast macrophage protein (Emp) leads to failure of erythroblast nuclear extrusion. J Biol Chem *281*, 20181-20189.

255. Sorensen, I., Adams, R.H., and Gossler, A. (2009). DLL1-mediated Notch activation regulates endothelial identity in mouse fetal arteries. Blood *113*, 5680-5688.

256. Spaulding, C.C., Walford, R.L., and Effros, R.B. (1997). Calorie restriction inhibits the age-related dysregulation of the cytokines TNF-alpha and IL-6 in C3B10RF1 mice. Mech Ageing Dev *93*, 87-94.

257. Spits, H., and Di Santo, J.P. (2011). The expanding family of innate lymphoid cells: regulators and effectors of immunity and tissue remodeling. Nature immunology *12*, 21-27.

258. Stepanov, V., Mateo, P., Gillet, B., Beloeil, J.C., Lechene, P., and Hoerter, J.A. (1997). Kinetics of creatine kinase in an experimental model of low phosphocreatine and ATP in the normoxic heart. Am J Physiol *273*, C1397-1408.

259. Stevens, S.M., von Gise, A., VanDusen, N., Zhou, B., and Pu, W.T. (2016). Epicardium is required for cardiac seeding by yolk sac macrophages, precursors of resident macrophages of the adult heart. Dev Biol *413*, 153-159.

260. Stotland, A., and Gottlieb, R.A. (2016). alpha-MHC MitoTimer mouse: In vivo mitochondrial turnover model reveals remarkable mitochondrial heterogeneity in the heart. Journal of molecular and cellular cardiology *90*, 53-58.

261. Sugiura, A., McLelland, G.L., Fon, E.A., and McBride, H.M. (2014). A new pathway for mitochondrial quality control: mitochondrial-derived vesicles. Embo J *33*, 2142-2156.

262. Sun, B., Qi, N., Shang, T., Wu, H., Deng, T., and Han, D. (2010). Sertoli cell-initiated testicular innate immune response through toll-like receptor-3 activation is negatively regulated by Tyro3, Axl, and mer receptors. Endocrinology *151*, 2886-2897.

263. Sun, N., Yun, J., Liu, J., Malide, D., Liu, C., Rovira, II, Holmstrom, K.M., Fergusson, M.M., Yoo, Y.H., Combs, C.A*., et al.* (2015). Measuring In Vivo Mitophagy. Mol Cell *60*, 685-696.

264. Taffet, G.E., Pham, T.T., and Hartley, C.J. (1997). The age-associated alterations in late diastolic function in mice are improved by caloric restriction. J Gerontol A Biol Sci Med Sci *52*, B285-290.

265. Tak, T., Tesselaar, K., Pillay, J., Borghans, J.A., and Koenderman, L. (2013). What's your age again? Determination of human neutrophil half-lives revisited. J Leukoc Biol *94*, 595-601.

266. Tan, A.S., Baty, J.W., Dong, L.F., Bezawork-Geleta, A., Endaya, B., Goodwin, J., Bajzikova, M., Kovarova, J., Peterka, M., Yan, B*., et al.* (2015). Mitochondrial genome acquisition restores respiratory function and tumorigenic potential of cancer cells without mitochondrial DNA. Cell Metab *21*, 81-94.

267. Taneike, M., Yamaguchi, O., Nakai, A., Hikoso, S., Takeda, T., Mizote, I., Oka, T., Tamai, T., Oyabu, J., Murakawa, T*., et al.* (2010). Inhibition of autophagy in the heart induces age-related cardiomyopathy. Autophagy *6*, 600-606.

268. Terman, A., Dalen, H., Eaton, J.W., Neuzil, J., and Brunk, U.T. (2003). Mitochondrial recycling and aging of cardiac myocytes: the role of autophagocytosis. Exp Gerontol *38*, 863-876.

269. Toda, S., Segawa, K., and Nagata, S. (2014). MerTK-mediated engulfment of pyrenocytes by central macrophages in erythroblastic islands. Blood *123*, 3963-3971.

270. Tomczyk, M., Kraszewska, I., Szade, K., Bukowska-Strakova, K., Meloni, M., Jozkowicz, A., Dulak, J., and Jazwa, A. (2017). Splenic Ly6C(hi) monocytes contribute to adverse late post-ischemic left ventricular remodeling in heme oxygenase-1 deficient mice. Basic Res Cardiol *112*, 39.

271. Torralba, D., Baixauli, F., and Sanchez-Madrid, F. (2016). Mitochondria Know No Boundaries: Mechanisms and Functions of Intercellular Mitochondrial Transfer. Front Cell Dev Biol *4*, 107.

272. Tschopp, J. (2011). Mitochondria: Sovereign of inflammation? Eur J Immunol *41*, 1196-1202.

273. Verhoven, B., Schlegel, R.A., and Williamson, P. (1995). Mechanisms of phosphatidylserine exposure, a phagocyte recognition signal, on apoptotic T lymphocytes. J Exp Med *182*, 1597-1601.

274. Vintersten, K., Monetti, C., Gertsenstein, M., Zhang, P., Laszlo, L., Biechele, S., and Nagy, A. (2004). Mouse in red: red fluorescent protein expression in mouse ES cells, embryos, and adult animals. Genesis *40*, 241-246.

275. Vives-Bauza, C., Yang, L., and Manfredi, G. (2007). Assay of mitochondrial ATP synthesis in animal cells and tissues. Methods Cell Biol *80*, 155-171.

276. Wan, E., Yeap, X.Y., Dehn, S., Terry, R., Novak, M., Zhang, S., Iwata, S., Han, X., Homma, S., Drosatos, K., *et al.* (2013). Enhanced efferocytosis of apoptotic cardiomyocytes through myeloid-epithelial-reproductive tyrosine kinase links acute inflammation resolution to cardiac repair after infarction. Circ Res *113*, 1004-1012.

277. Wanagat, J., Wolff, M.R., and Aiken, J.M. (2002). Age-associated changes in function, structure and mitochondrial genetic and enzymatic abnormalities in the Fischer 344 x Brown Norway F(1) hybrid rat heart. Journal of molecular and cellular cardiology *34*, 17-28.

278. Wang, M., and Shah, A.M. (2015). Age-associated pro-inflammatory remodeling and functional phenotype in the heart and large arteries. Journal of molecular and cellular cardiology *83*, 101-111.

279. Wang, X., Su, H., and Ranek, M.J. (2008). Protein quality control and degradation in cardiomyocytes. J Mol Cell Cardiol *45*, 11-27.

280. Watanabe, S., Alexander, M., Misharin, A.V., and Budinger, G.R.S. (2019). The role of macrophages in the resolution of inflammation. The Journal of clinical investigation *130*.

281. Weinberg, S.E., Sena, L.A., and Chandel, N.S. (2015). Mitochondria in the regulation of innate and adaptive immunity. Immunity *42*, 406-417.

282. Wen, Z.F., Liu, H., Gao, R., Zhou, M., Ma, J., Zhang, Y., Zhao, J., Chen, Y., Zhang, T., Huang, F., *et al.* (2018). Tumor cell-released autophagosomes (TRAPs) promote immunosuppression through induction of M2-like macrophages with increased expression of PD-L1. J Immunother Cancer *6*, 151.

283. Wohlgemuth, S.E., Julian, D., Akin, D.E., Fried, J., Toscano, K., Leeuwenburgh, C., and Dunn, W.A., Jr. (2007). Autophagy in the heart and liver during normal aging and calorie restriction. Rejuvenation Res *10*, 281-292.

284. Wu, J.J., Liu, J., Chen, E.B., Wang, J.J., Cao, L., Narayan, N., Fergusson, M.M., Rovira, II, Allen, M., Springer, D.A., *et al.* (2013). Increased mammalian lifespan and a segmental and tissue-specific slowing of aging after genetic reduction of mTOR expression. Cell Rep *4*, 913-920.

285. Xiao, X., Li, J., and Samulski, R.J. (1998). Production of high-titer recombinant adeno-associated virus vectors in the absence of helper adenovirus. J Virol *72*, 2224-2232.

286. Yamaguchi, O., and Otsu, K. (2012). Role of autophagy in aging. J Cardiovasc Pharmacol *60*, 242-247.

287. Yona, S., Kim, K.W., Wolf, Y., Mildner, A., Varol, D., Breker, M., Strauss-Ayali, D., Viukov, S., Guilliams, M., Misharin, A., *et al.* (2013). Fate mapping reveals origins and dynamics of monocytes and tissue macrophages under homeostasis. Immunity *38*, 79-91.

288. Yoshida, H., Hayashi, S., Kunisada, T., Ogawa, M., Nishikawa, S., Okamura, H., Sudo, T., and Shultz, L.D. (1990). The murine mutation osteopetrosis is in the coding region of the macrophage colony stimulating factor gene. Nature *345*, 442-444.

289. Yoshida, H., Kawane, K., Koike, M., Mori, Y., Uchiyama, Y., and Nagata, S. (2005). Phosphatidylserine-dependent engulfment by macrophages of nuclei from erythroid precursor cells. Nature *437*, 754-758.

290. Yu, J., Nagasu, H., Murakami, T., Hoang, H., Broderick, L., Hoffman, H.M., and Horng, T. (2014). Inflammasome activation leads to Caspase-1-dependent mitochondrial damage and block of mitophagy. Proc Natl Acad Sci U S A *111*, 15514-15519.

291. Zhao, L., Zou, X., Feng, Z., Luo, C., Liu, J., Li, H., Chang, L., Wang, H., Li, Y., Long, J., *et al.* (2014). Evidence for association of mitochondrial metabolism alteration with lipid accumulation in aging rats. Exp Gerontol *56*, 3-12.

292. Zhou, J., Chong, S.Y., Lim, A., Singh, B.K., Sinha, R.A., Salmon, A.B., and Yen, P.M. (2017). Changes in macroautophagy, chaperone-mediated autophagy, and mitochondrial metabolism in murine skeletal and cardiac muscle during aging. Aging (Albany NY) *9*, 583-599.

293. Zhou, R., Yazdi, A.S., Menu, P., and Tschopp, J. (2011). A role for mitochondria in NLRP3 inflammasome activation. Nature *469*, 221-225.

294. Ziegler-Heitbrock, L. (2007). The CD14+ CD16+ blood monocytes: their role in infection and inflammation. J Leukoc Biol *81*, 584-592.

295. Zigmond, E., and Jung, S. (2013). Intestinal macrophages: well educated exceptions from the rule. Trends Immunol *34*, 162-168.

9. Annexes

9. Annexes

9.1. Abbreviations

αMHC	Alpha Myosin Heavy Chain
^{18}F-FDG	Radiolabelled Fluoro-deoxyglucose (^{18}F)
%EF	% Ejection Fraction
%FS	% Fractional Shortening
AAV9	Adeno-associated virus serotype 9
AMP	Adenosine Monophosphate
ANOVA	Analysis Of Variance
Atg (5/7/9)	Autophagy related gene (5/7/9)
ATP	Adenosine Triphosphate
ATPb	ATP synthase subunit beta
BABB	Benzyl-Alcohol Benzyl-Benzoate
BEC index	Bioenergetic Cellular index
BM	Bone Marrow
BrdU	Bromodeoxyuridine
BSA	Bovine Serum Albumin
CCR2	C-C chemokine Receptor type 2
Cdh5	Cadherin 5
CD(n)	Cluster of Differentiation (Protein number)
cGAMP	Cyclic Guanosine–Adenosine Monophosphate
cGAS	Cyclic Guanosine–Adenosine Monophosphate Synthase
cMacs	Cardiac-resident Macrophages
CM	Cardiomyocyte
CMP	Common Myeloid Progenitor
CNS	Central Nervous System
CoI	Cytochrome c oxidase subunit I
CoxIV	Cytochrome c oxidase subunit IV
CS	Citrate Synthase

Csf1r	Colony stimulating factor 1 receptor
CX3CL1	Chemokine (C-X3-C motif) Ligand 1
CX3CR1	CX3C chemokine Receptor 1
CYTC	Cytochrome C
DAMPs	Damage-Associated Molecular Patterns
DAPI	4’,6-Diamidino-2-Phenylindole
DCs	Dendritic Cells
DHE	Dihydroethidium
DMSO	Dimethyl Sulfoxide
DNA	Deoxyribonucleic Acid
Draq5	Deep Red Anthraquinone 5
DsRed	Discosoma-derived Red fluorescent protein
DT	Diphteria Toxin
DTR	Diphteria Toxin Receptor
DTT	Dithiothreitol
dUTP	2´-Deoxyuridine, 5´-Triphosphate
ECM	Extracellular Matrix
EDTA	Ethylenediaminetetraacetic acid
Emp	Extracellular matrix protein-binding protein emp
EMPs	Erythro-Myeloid Progenitors
FACS	Fluorescence Activated Cell Sorting
FAD	Flavin Adenine Dinucleotide
FCCP	Carbonyl Cyanide-4-(trifluoromethoxy)Phenylhydrazone
FDR	False Discovery Rate
FIS1	Mitochondrial Fission 1
FLT3	Fms Like Tyrosine kinase 3
FOV	Field Of View
FP70	Flavoprotein 70 kDa
FSC	Forward Scatter
G-CSF	Granulocyte Colony-Stimulating Factor
GAPDH	Glyceraldehyde 3-Phosphate Dehydrogenase

Gas6	Growth arrest-specific 6
GFP	Green Fluorescent Protein
GM-CSF	Granulocyte-Macrophage Colony-Stimulating Factor
HBSS	Hank's Balanced Salt Solution
HCQ	Hydroxychloroquine
HEPES	4-(2-Hydroxyethyl)-1-Piperazineethanesulfonic acid
HSC	Hematopoietic Stem Cell
IL1β	Interleukin 1β
IL10	Interleukin 10
ISO	Isoproterenol
i.p. injection	Intraperitoneal injection
i.v. injection	Intravenous injection
IVS	Interventricular Septum
KO	Knockout
LAD artery	Left Anterior Descending Artery
LAMP1	Lysosomal-Associated Membrane Protein 1
LAX	Long Axis
LC3	Microtubule-associated protein 1A/1B Light Chain 3B
LPC	Lysophosphatidylcholine
LV	Left Ventricle
LVEDP	Left Ventricle End Diastolic Pressure
LVESP	Left Ventricle End Systolic Pressure
LV-Vol	Left Ventricle Volume
LVID	Left Ventricle Internal Diameter
Ly6C	Lymphocyte antigen 6C
Ly6G	Lymphocyte antigen 6G
LysM	Lysozyme M
Lyve-1	Lymphatic vessel endothelial hyaluronic acid receptor 1
LxR	Liver X Receptor
MAFIA	Macrophage Fas-Induced Apoptosis (reporter mouse)
MAFs	Mouse Adult Fibroblasts

M-CSF	Macrophage Colony-Stimulating Factor
Mfge(8/10)	Milk Fat Globule-EGF Factor (8/10)
MFI	Mean/Median Fluorescence Intensity (as indicated)
MHCII	Major Histocompatibility Complex class II
mRNA	Messenger RNA
MS	Mass Spectrometry
MyHC	Myosin heavy chain
MYH6/7	Myosin heavy chain (6/7)
MPs	Myeloid Progenitors
MRS	Magnetic Resonance Spectroscopy
MSCs	Mesenchymal Stem Cells
mtDNA	Mitochondrial DNA
mTOR	mammalian Target Of Rapamycin
nDNA	Nuclear DNA
NADH	Nicotinamide adenine dinucleotide
ND	Not Detected
NDUFA9	NADH dehydrogenase [ubiquinone] 1 alpha subcomplex subunit 9
NDUFS2	NADH dehydrogenase [ubiquinone] iron-sulfur protein 2
NETs	Neutrophil extra-cellular traps
NK cell	Natural Killer cell
NLRP3	NACHT, LRR and PYD domains-containing protein 3
NLRs	NOD-Like Receptors
OCT	Optimal Cutting Temperature Compound
OXPHOS	Mitochondrial Oxidative Phosphorylation System
PAMPs	Pathogen-Associated Molecular Pattern
PBS	Phosphate Buffered Saline
PCr	Phosphocreatine
PCR	Polymerase Chain Reaction
PET-CT	Positron Emission Tomography–Computed Tomography
PFA	Paraformaldehyde
PGC1α	Peroxisome proliferator activated receptor gamma coactivator 1 alpha

PRRs	Pattern Recognition Receptors
PS	Phosphatidylserine
qPCR	Quantitative Polymerase Chain Reaction
RBCs	Red Blood Cells
RFP	Red Fluorescent Protein
RNA	Ribonucleic acid
ROS	Reactive Oxygen Species
Runx1	Runt-related transcription factor 1
S1P	Sphingosine-1-phosphate
SAX	Short Axis
SDS	Sodium Dodecyl Sulfate
SEM	Standard Error of the Mean
SC	Supercomplex
SSC	Side Scatter
STING	Stimulator of interferon genes
TCA cycle	Tricarboxylic Acid cycle
TEM	Transmission Electron Microscopy
TFAM	Transcription Factor A, Mitochondrial
TGFβ	Transforming growth factor beta
TLR	Toll-Like Receptor
TNFα	Tumour necrosis factor alpha
Tnn2	Cardiac muscle troponin T
TOM20	Translocase of outer (mitochondrial) membrane 20
TRAPs	Tumour Released Autophagosomes
TUNEL	Terminal deoxynucleotidyl transferase dUTP Nick-End Labeling
WT	Wild Type
UQCR2	Ubiquinol-cytochrome-C Reductase complex core protein 2

9.2. Collaboration of the PhD student in additional projects

In the course of this thesis, I have participated in other projects resulting in the publication of scientific articles in peer-reviewed journals. A brief explanation of this work and the articles related to it are described below.

Hematopoietic niche regulation by neutrophils in tissues.

Initially postulated as a side-project of this thesis. In this Project, I have performed experiments in parabiont mice finding that circulating neutrophils infiltrate most tissues in healthy mice. Interestingly, this process occurs following either continuous or circadian pattern, depending on the tissue. We found that neutrophils are degraded by macrophages in the intestine and an impaired migration of neutrophils to this tissue causes a down-regulation of cytokines involved in distant bone marrow niche regulation (i.e. G-CSF). In other tissues like Lungs, the circadian infiltration of neutrophils regulates the expression of genes related with metastasis. Part of my work in this project has been published recently in (Casanova-Acebes et al., 2018).

Characterization of neutrophil heterogeneity.

Our observation of neutrophils infiltrating tissues in the steady-state (Casanova-Acebes et al., 2018) raised the possibility that heterogeneous populations of neutrophils existed in different tissues, similar to what has been reported for resident macrophages. I performed bulk RNAseq on isolated neutrophils from different tissues including blood, bone marrow, spleen, lung, intestine and skin finding clear differences in the transcriptional profile of those cells. We are now repeating experiments at the single cell level to better characterize the source and magnitude of this heterogeneity. Although this project is still ongoing, I have participated in the elaboration of two reviews, which summarize the field of neutrophil heterogeneity, and their functions in different tissues (Adrover et al., 2016; Nicolas-Avila et al., 2017).

Macrophage functions in other tissues.

Through a collaboration with Dr. Kronke's group in Erlangen, I have participated in a project focused in studyng the composition, origin and differentiation of subsets of macrophages within healthy and inflamed joints (rheumatoid arthritis model). We found a barrier-forming population of macrophages in the synovium, which maintained their numbers through a pool of locally proliferating mononuclear cells embedded in the synovial tissue. These lining macrophages restrict inflammatory reactions by providing a tight-junction-mediated shield for intra-articular structures (Culemann et al., 2019).

I also collaborated in a project focused in determining the phagocytic activity of different tissue-resident macrophage populations, and the consequences that phagocytosis have in the transcriptional activity of macrophages (A-Gonzalez et al., 2017).

Finally, I co-wrote a review focused in the origin and function of cardiac- and brain-resident macrophages (Nicolas-Avila et al., 2018).

9.3. Publications

1. Culemann, S., Grüneboom, A., **Nicolas-Avila, J.A.,** Weidner, D., Lämmle, K.F., Rothe, T., Quintana, J.A., Kirchner, P., Krljanac, B., Eberhardt, M., Ferrazzi, F., *et al.* (2019). Locally renewing resident synovial macrophages provide a protective barrier for the joint. **Nature**, 572, 670-675.

2. **Nicolas-Avila, J.A.**, Hidalgo, A., and Ballesteros, I. (2018). Specialized functions of resident macrophages in brain and heart. **J Leukoc Biol** 104, 743-756.

3. Casanova-Acebes, M.* **Nicolas-Avila, J.A.***, Li, J.L.*, Garcia-Silva, S., Balachander, A., Rubio-Ponce, A., Weiss, L.A., Adrover, J.M., Burrows, K., A-Gonzalez, N.*, et al.* (2018). Neutrophils instruct homeostatic and pathological states in naive tissues. **J Exp Med** 215, 2778-2795. Co-first authorship*

4. **Nicolas-Avila, J.A.**, Adrover, J.M., and Hidalgo, A. (2017). Neutrophils in Homeostasis, Immunity, and Cancer. **Immunity** 46, 15-28.

5. A-Gonzalez, N., Quintana, J.A., Garcia-Silva, S., Mazariegos, M., Gonzalez de la Aleja, A., **Nicolas-Avila, J.A**., Walter, W., Adrover, J.M., Crainiciuc, G., Kuchroo, V.K.*, et al.* (2017). Phagocytosis imprints heterogeneity in tissue-resident macrophages. **J Exp Med** 214, 1281-1296.

6. Adrover, J.M., **Nicolas-Avila, J.A.**, and Hidalgo, A. (2016). Aging: A Temporal Dimension for Neutrophils. **Trends Immunol** 37, 334-345.

Most of the data presented in this thesis is part of a manuscript currently under review in *Nature*.

7. **Nicolás-Ávila, J.A.***, Lechuga-Vieco, A.V.*, Esteban-Martínez, L., Sanchez-Díaz, M., Díaz, E., Santiago, D.J., Rubio-Ponce, A., Li, J.L., Balachander, A., Quintana, J.A., *et al*. (2019) Surrogated elimination of mitochondria in the heart. **Under review in Nature.** Co-first authorship*

Two additional studies in which the author of this thesis has collaborated are currently under revision in other journals.